Screening genetic variation for photosynthetic capacity and efficiency in wheat

A thesis submitted for the degree of

Doctor of Philosophy

of

The Australian National University

by

M.C. Viridiana Silva Pérez

May 2016

Australian National University

Statement of authorship

All work presented in this thesis is my own, unless otherwise stated. Cooperative work and specific contributions by others are referred to in the acknowledgements. The material presented in this thesis does not contain work used for the award of any other degree or diploma.

Viridiana Silva Pérez

Abstract

The world population is rising, placing increasing demands on food production. One way to contribute to food security is by improving yields of staple crops like wheat. Yield can be calculated from the product of plant biomass and harvest index (the ratio of grain yield to above ground biomass). Since harvest index of wheat has already reached its maximum biological limit in some environments, attention is now focused on increasing crop biomass. Efficient interception of photosynthetically active radiation and effective photosynthetic sugar production underpin yield, however, little breeding has been done for photosynthetic performance. Exploiting existing genetic variation for important photosynthetic traits such as photosynthetic capacity (P_c) and photosynthetic efficiency (P_{eff}) will help to improve wheat yield. CO_2 assimilation rate, which is a commonly measured parameter for assessing photosynthetic performance, is found to vary across wheat genotypes. Two additionally important parameters are Rubisco activity (V_{cmax}) and electron transport rate (J). There is much less information reported regarding genetic variation of these two latter parameters because measurements of CO_2 response curves with gas exchange used to derive V_{cmax} and J are slow and unsuitable for rapid screening of many genotypes in the field. The two main objectives of this project were firstly, to find out if there is genetic variation for these important photosynthetic traits in wheat, and secondly, to develop a rapid method for screening photosynthetic and leaf attributes in different wheat genotypes. To deal with variable leaf temperatures in the field and accurately estimate V_{cmax} and J, improved values for the temperature dependence of several Rubisco kinetic parameters were needed. These temperature-dependencies were derived from measurements made under controlled conditions. A method for rapidly estimating variation in P_c components V_{cmax} and J and in other photosynthetic traits was developed based on calibration of leaf reflectance spectra against photosynthetic parameters derived using conventional gas exchange, morphological (leaf mass per unit area, LMA) and chemical (nitrogen and chlorophyll per unit area) measurements of 76 wheat genotypes screened in several different environments. When observed data were compared against predictions from reflectance spectra, correlation coefficients (R^2 values) of 0.62 for V_{cmax25}, 0.71 (J), 0.89 (LMA) and 0.93 (N_{area}), were obtained. Reflectance spectra from an additional 458 elite and landrace wheat genotypes were measured to further assess variation in photosynthetic traits. There were significant differences between wheat genotypes in V_{cmax25} per unit N, which is a good measure of P_{eff}. Environment presented interaction with genotypes for P_c and P_{eff} when measurements performed in glasshouse & field or in

Australia & Mexico were compared. In future, linking genotypic variation for photosynthetic traits to DNA-based genetic markers will permit even faster selection of genotypes in breeding. Reflectance spectra should be a good tool to accelerate identification and selection of wheat genotypes and detection of important genomic regions for photosynthetic capacity and efficiency in wheat.

Acknowledgements

I am deeply grateful to my three supervisors, Dr John R. Evans, Dr Robert T. Furbank and Dr. Anthony G. Condon for their patience, approachability, support and guidance through my PhD. Thank you for making this journey pleasant and for giving me the tools to continue in the future.

John, I really appreciate the time that you spent explaining the Biochemical Model of leaf photosynthesis, reading my thesis, discussing new topics, making me think more and teaching me to see further than I use to. Thank you very much for your kindness, the coffees and the nice conversations during lunch.

Bob, I really value your enthusiasm, your contagious optimism to overcome difficulties and your passion to elaborate projects. Thanks to you I have learnt to see the whole system together, joining the elements from biochemistry, molecular biology, plant physiology crop sciences, phenomics… and to get out from my crop sciences universe.

Tony, I am very grateful for your patience organizing my experiments in the glasshouse and in the field at CSIRO. Thank you for your advice to work in the field, for your support and suggestions in the project. Thanks for teaching me Australian slang and giving me the opportunity to continue my project.

The collaboration with ANU comes from CIMMYT, in particularly with Dr Matthew Reynolds. I am very happy that I met him in Mexico. I had the opportunity to expand my knowledge at ANU because of his collaborations Mexico and overseas. I really admire all the effort and energy that he has spent letting me know the importance of increasing wheat yield and putting together numerous teams in the world.

When I arrived in Canberra I discovered that I was in the right place. I had the great opportunity to meet important physiologists in photosynthesis, crop scientists and breeders. I am so grateful for all the valuable advices from Tony Fischer, Richard Richards, Susanne von Caemmerer and José Jiménez-Berni that contribute in my thinking during my experiments, analysing data and writing.

I am particularly grateful to the sceptical Tony Fischer. Your scepticism and multiple questions forced me to be better prepared and alert about both life and sciences. Thank you for caring for me, for sharing your knowledge, for cheering me on and for your wise answers when I asked for advice.

> *Learn from yesterday, live for today, hope for tomorrow.*
>
> *The important thing is not to stop questioning.*
>
> *Albert Einstein*

Table of contents

List of abbreviations

Symbol	Description	Units
A	CO_2 assimilation rate per unit leaf area at 400 inlet $\mu mol\ CO_2\ mol^{-1}$.	$\mu mol\ CO_2\ m^{-2}\ s^{-1}$
A_{800}	CO_2 assimilation rate measured at 800 inlet $\mu mol\ CO_2\ mol^{-1}$.	$\mu mol\ CO_2\ m^{-2}\ s^{-1}$
ANOVA	Analysis of Variance	
BMF	Biomass at flowering	$Mg\ ha^{-1}$
BMM	Biomass at maturity	$Mg\ ha^{-1}$
CABP	^{14}C- labelled carboxy arabinitol-1,5-bisphosphate	
BW	Bread wheat	
C_c	Chloroplastic CO_2 partial pressure	μbar
$C_{c,800}$	Chloroplastic CO_2 partial pressure calculated from measurements made with an inlet CO_2 concentration of 800 $\mu mol\ CO_2\ mol^{-1}$.	μbar
C_i	Intercellular airspace CO_2 partial pressure	μbar
$C_{i,800}$	Intercellular CO_2 partial pressure measured with an inlet CO_2 concentration of 800 $\mu mol\ CO_2\ mol^{-1}$	μbar
C_i/C_a	Ratio of internal to atmospheric CO_2 concentration	$\mu mol\ CO_2\ mol\ air^{-1}$
CIMMYT	International Maize and Wheat Improvement Center	
CSIRO	Commonwealth Scientific and Industrial Research Organisation	
CO_2	Carbon dioxide	
CV	Coefficient of variation percentage	$\%$
DAE	Days after emergence	Days
DF	Degrees of freedom	
DTF	Days to flowering	Days
DTM	Number of days after seedlings emergence to physiological maturity	Days
DW	Durum wheat	
E	Activation energy	$kJ\ mol^{-1}$
Env	Environment	
F'	Steady state of fluorescence in the light	
$F_{m'}$	Maximal chlorophyll fluorescence during a saturating light pulse of a leaf in the light	
Γ	CO_2 compensation point	μbar
Γ_*	CO_2 photocompensation point. Chloroplastic CO_2 partial pressure at which the rate of carboxylation equals the rate of photorespiratory CO_2 release	μbar
G×E	Interaction genotype by environment	
G×N	Interaction genotype by fertilizer treatment	
GR	Growth Rate	

Symbol	Description	Units
g_s	Stomatal conductance	mol H_2O m^{-2} s^{-1}
GS	Growth stages of wheat (Zadoks *et al.*, 1974)	
g_m	Mesophyll conductance	mol CO_2 m^{-2} s^{-1} bar^{-1}
HI	Harvest Index	
J	Electron transport rate	μmol e^- m^{-2} s^{-1}
J_{800}	Electron transport rate measured with an inlet CO_2 concentration of 800 μmol CO_2 mol^{-1}	
J_g	Electron transport rate calculated from gas exchange	
J_f	Electron transport rate calculated from fluorescence	
K_c	Michaelis-Menten constant for CO_2	μbar
k_{catc}	Catalytic turnover rate of Rubisco carboxylation	mol CO_2(mol sites)$^{-1}$$s^{-1}$
K_o	Michaelis-Menten constant for O_2	mbar
LMA	Leaf dry mass per area	g m^{-2}
N_{area}	Leaf nitrogen per unit area	N g m^{-2}
-N	Low nitrogen treatment	
+N	High nitrogen treatment	
O	O_2 partial pressure	mbar
O_2	Oxygen	
PGF	Percentage of grain filling	%
P_c	Photosynthetic capacity	
P_{eff}	Photosynthetic efficiency	
PLSR	Partial Least Squares Regression	
QTL	Quantitative Trait Loci	
R	Universal gas constant 8.314	J mol^{-1} K^{-1}
R_d	Mitochondrial respiration	μmol CO_2 m^{-2} s^{-1}
Rubisco	Ribulose-1,5-bisphosphate carboxylase-oxygenase	
RuBP	Ribulose-1,5-bisphosphate	
RUE	Radiation Use Efficiency	G MJ^{-1}
SE	Standard Error	
SPAD	Chlorophyll meter SPAD Minolta units	SPAD Units
$S_{c/o}$	Rubisco specificity factor	
T	Leaf temperature	°C
V_{cmax}	Velocity of carboxylation	μmol CO_2 m^{-2} s^{-1}
V_{cmax25}	Velocity of carboxylation at 25 °C	μmol CO_2 m^{-2} s^{-1}
V_{cmax25}/N_{area}	Velocity of carboxylation per leaf nitrogen or photosynthetic efficiency	μmol m^{-2} s^{-1}(gN^{-1})
V_{omax}	Velocity of oxygenation	μmol O_2 m^{-2} s^{-1}
value25	Value at 25 °C	

Summary of experiments and set of genotypes

Symbol	Description	Chapter
	SET OF GENOTYPES	
EVA	Early vigour set (Table 3.2).	3
BYPB	Best and Unreleased Yield Potential measured before anthesis (Table 3.2).	3
CIMCOG	CIMMYT Core Germplasm Subset II (Table 3.3).	3
CA	CIMCOG set measured at anthesis.	
CB	CIMCOG set measured before anthesis (Table 3.3).	6
CC	Elite wheat genotypes, Candidates to CIMCOG II (A 14).	6
L	Group of Landraces wheat genotypes (A 15).	
	EXPERIMENTS	
Aus1	Glasshouse experiment at CSIRO Black Mountain, Australia using **EVA** set (Table 3.1).	3
Aus2	Glasshouse experiment at CSIRO Black Mountain, Australia using **BYPB** set (Table 3.1).	3
Aus3	Field experiment at Ginninderra Experimental Station in Australia (Table 3.1) using **BYPB**, **EVA** and **CA** set of genotypes.	3
Aus3T	V45, V57, V62 and V66 genotypes measured from **Aus3** for the Temperature experiment.	2
Cabinet	Temperature experiment carried out in a temperature controlled cabinet at ANU with four genotypes V25, V27, V32, V34.	2
Mex	Field experiment at Norman E. Borlaug Experimental Station in Obregon, Mexico (Table 3.1) using **CA** and **CB** set of genotypes.	3
Mex2	Field experiment at Norman E. Borlaug Experimental Station in Obregon, Mexico using **CC** and **L** set of genotypes.	6

CHAPTER 1

General Introduction

Centro Experimental Norman E. Borlaug, Cd. Obregón, Mexico. 2013.

1.1 FOOD SECURITY AND WHEAT YIELD

At present, the world human population is approximately 7.3 billion, growing by an additional 83 million people per year. It is projected to reach 8.5 billion by 2030 and 9.7 billion by 2050, and during this time the poorest countries will be the most susceptible to economic inequality and malnutrition (U.N., 2015). The increment in world population will increase the demand of basic commodities; people will need food, clothing, and different sources of energy to improve or maintain the living standard that this era provides. Usually higher demand is associated with higher prices if the product is limited, and third world consumers have limited resources to cope with increased food prices. Similarly, if the yield of staple crops is affected negatively, it will be more difficult to afford them. Scenarios for 2050, without considering climate change, predict that the demand in cereals in the world will increase between 42 to 59% and prices will rise between 13 to 30% (Reynolds, 2011; Fischer *et al.*, 2014).

One option to avoid a crisis in production of staple crops is to increment supply by increasing crop yield. Wheat (*Triticum* spp.) is a staple crop, widely consumed as bread, pasta, cereal, among other products, and it provides one-fifth of the total calories of the world's population (FAO, 2010). To cope with increasing demand, farm yield (FY) needs to increase by 1.3% per annum (p.a.) to nearly double the current annual progress of ~0.6% p.a. Wheat FY can vary from 1.8 to 8.6 t ha^{-1}, but wheat potential yield (PY), yield obtained with good management (irrigation, fertilizers, pest and disease control) is much higher than FY and can vary from 2.6 to 10.9 t ha^{-1} (Fischer *et al.*, 2014). Wheat yields can be improved by, narrowing the gap between FY and PY, and increasing PY *per se*. For example, the Yaqui Valley in Mexico (megaenvironment that is representative of more than 40% of wheat production in developing countries) has a yield gap of 2.6 t ha^{-1}, which can be improved with crop management. PY has been around 8±1 t ha^{-1} for 30 years (Figure 1.1). By contrast, in Western Australia PY is only 2.6 8±1 t ha^{-1} (Fischer *et al.*, 2014) as production is limited by low rainfall. Therefore, to cope with the increasing food demand, research is needed to enable greater increase in PY.

Figure 1.1 Yield gap for wheat in the Yaqui Valley, Mexico between potential yield (PY) and farm yield (FY). The linear increment in PY from 1980-2010 is 28 kg ha^{-1}year^{-1}. FY plotted against year, and PY plotted against year of release. Modified from Fischer et al., 2014.

1.2 POTENTIAL YIELD

In order to accelerate progress towards increasing wheat PY, research to increase both photosynthetic capacity and grain sink capacity is vital in breeding programs (Foulkes *et al.*, 2011). Potential Yield (PY), under optimal conditions, can be factored into three components: light interception (LI), radiation use efficiency (RUE) and harvest index (HI) (Reynolds *et al.*, 2009; Reynolds *et al.*, 2012b) (Equation 1.1):

$$PY = LI \times RUE \times HI \tag{1.1}$$

LI is the sum of daily photosynthetically active radiation (PAR) intercepted by green tissue (MJ m^{-2}), and RUE is the conversion of that radiation into biomass (g MJ^{-1}) (Fischer *et al.*, 2014). Both variables are useful to describe how plants harvest light energy for the photosynthetic process and convert carbon dioxide into biomass.

HI is the ratio of grain dry mass to total plant dry mass (above-ground biomass), and it has been closely associated with wheat yield improvement since the 1950's (Austin *et al.*, 1980; Hay, 1995). HI measured in varieties released between 1950 and 1987 in Australia, Canada and England increased from 0.2 to 0.54 (Evans, 1993; Hay, 1995). In parallel, spring wheat yield progress from cultivars released from 1960 to 1990 increased ~0.88% p.a, which was correlated with increased kernel number per square meter. The main explanation for this is the introduction of the major Norin10 dwarfing genes via the introgression of the *Rht1* and *Rht2* genes (Hay, 1995; Sayre *et al.*, 1997).

Some recent figures have shown that as wheat HI reached a maximum of 0.55, yield progress has slowed to ~0.6% p.a. (Fischer *et al.*, 2014). Wheat HI of 0.5 has been reported to be the optimal ideotype for wheat to yield 16 t ha^{-1} (Berry *et al.*, 2006). The physiological explanation for this is that plant structure constrains a balance between the weight of the grain versus the stems required to prevent lodging and to also support enough leaf area for photosynthesis. In this sense, it is has been suggested that to increase yield further, biomass also needs to be increased.

CO_2 enrichment experiments have shown that wheat yield can be increased by growth in higher CO_2 concentrations (Ainsworth and Long, 2005). In addition, experimental manipulation of sources and sinks indicates that there are empty florets that can contribute to increase HI, but there is insufficient photosynthesis to form more fertile florets (Parry *et al.*, 2011). Thus future research to increase PY needs to be focused on increasing crop biomass while maintaining HI (Hay, 1995).

1.3   SOURCE AND SINK

The source is the tissues where assimilates are generated as result of photosynthesis. The main sources of assimilate are leaves and some contribution of green stems and floral organs (Gifford and Evans, 1981). The flag leaf and the wheat ear are the main sources in wheat during grain filling (Sanchez-Bragado *et al.*, 2014).

The sink are tissues that demand assimilates from the source. The sink maybe be growing meristems, organ elongation or for storage organs such as the grain. The storage sink can be sucrose, carbohydrates, proteins or lipids (Gifford and Evans, 1981). The economic sink in wheat is the grain. The relationship between source and sink is essential for the formation of grain yield and to determine ways of increase it.

Sink (growing organs) and source (photosynthetic tissues) work in unison with each other. It has been observed that crops may be either source or sink limited during grain filling (Rawson *et al.*, 1976; Reynolds *et al.*, 2005). The source and sink limitation may vary between species and with stage of development. In wheat crops source limitation is likely to occur during the period after flowering. At this time stems are elongating, spikes are growing and grain number is determined (Fischer, 1985). A source limitation also occurs during grain filling when conditions are unfavourable. Once grain number has been determined and conditions are favourable then crops may be sink limited if they have sufficient leaf area and photosynthesis to fill the grains (Borrás *et al.*, 2004).

Transport of assimilates and interaction of source and sink is complex. Sinks can induce feedback or product-inhibition via signalling pathways (Patrick and Offler, 2001). The complexity of the sink-source relationship can be also be affected by environmental conditions that can modify leaf area, relative growth rate and will vary depending on whether plants are single or grown in a canopy (Gifford and Evans, 1981).

The photosynthetic machinery must be considered during the entire life cycle and even the demand for carbon may vary during the lifecycle. For example, when florets in wheat start to develop, there are signals that determine the grain number in the spike (Foulkes *et al.*, 2011). This is when the photosynthetic machinery and the developing sink work in unison to determine yield potential via grain number as well as grain size. Therefore, photosynthesis, assimilate availability and allocation, phloem translocation of assimilates and water, spike photosynthesis, sink strength and floret fertility all need to be explored together to increase wheat yield (Patrick and Offler, 2001; Borrás *et al.*, 2004; Foulkes *et al.*, 2011; Sanchez-Bragado *et al.*, 2014).

To meet future global food demand, there is a worldwide effort to increase yield potential in wheat. A key player in research for food security in wheat is The International Maize and Wheat Improvement Centre, known by its Spanish acronym, CIMMYT®. It is a not-for-profit research and training organization with partners in over 100 countries. The centre works to sustainably increase the productivity of maize and wheat systems and thus ensure global food security and reduce poverty (www.cimmyt.org).

In 2009, researchers in CIMMYT and collaborators around the world started a project to improve wheat yield (Reynolds *et al.*, 2011b). The project was divided in three main themes 1) increasing photosynthetic performance in wheat, 2) optimizing partitioning to grain yield while maintaining lodging resistance, and 3) breeding to accumulate yield potential traits in wheat. Results have been presented each year and published in proceedings papers (Reynolds *et al.*, 2011b; Reynolds *et al.*, 2012a; Reynolds and Braun, 2013; Reynolds *et al.*, 2014; Reynolds *et al.*, 2015). This project is part of Theme 1.

1.4 PHOTOSYNTHETIC IMPROVEMENT

Photosynthesis is the process by which green plants use solar energy to produce carbohydrates from CO_2. The main enzyme of the process is Rubisco (ribulose-1,5-bisphosphate carboxylase-oxygenase). Some of the carbohydrates are expected to be oxidized through dark respiration to yield CO_2 and energy, while much of the carbon is converted into biomass. Net photosynthesis is the difference between gross photosynthesis

and the sum of the rates of two respiratory processes: photorespiration and dark respiration (Olivier, 1998).

Natural selection have been working over millions of years improving physiological traits such as photosynthetic capacity and efficiency in plants, and it is unlikely that artificial mutations in Rubisco increase photosynthesis without a trade-off, or that eliminating photorespiration in C_3 plants could be trade-off-free (Denison, 2009). However, whereas the unit of selection is normally and individual plant during evolution, for crops it is the community of plants which is important and the way in which the community of plants can be as resource efficient as possible. A major challenge will therefore be to identify physiological processes which are robust at the crop level.

C_3 plants like wheat waste energy during photorespiration because the oxygenase reaction catalysed by Rubisco forms phosphoglycolate and metabolic effort is required to recycle the carbon skeleton (Peterhansel and Maurino, 2011). Photorespiration is reduced under elevated CO_2 or in plants that use the C_4 photosynthetic pathway. Consequently, C_3 plants grown at high CO_2 concentrations and C_4 plants have a greater photosynthetic performance, biomass and yield than C_3 plants grown at ambient CO_2 (~380 ppm) (Ainsworth and Long, 2005). However, not all C_3 plants evaluated responded similarly and it has been shown that the effect of CO_2 fertilization can vary depending on environmental conditions (Slattery *et al.*, 2013).

In the last decade numerous approaches have been suggested to improve C_3 photosynthesis (Parry *et al.*, 2011; Furbank *et al.*, 2015; Ort *et al.*, 2015). These approaches can be divided into two groups: 1) carbon uptake in the Calvin Cycle where Rubisco, CO_2 concentrating mechanism and photorespiration are the main targets for improvement, and 2) light harvesting, that involves the interception of light at the canopy level, the use of photons for electron transport, leaf photoprotection when light interception exceeds the rate of utilisation and canopy architecture (Table 1.1).

Many teams are working with genetic engineering to improve the two main steps of photosynthesis: carboxylation and light reactions. Even if these projects have a high impact when they are finished, they will require many years to deliver a crop ready to be implemented in the agriculture system.

Table 1.1 Summary of the main targets and approaches to improve C$_3$ photosynthesis.

Target	Main approaches
Carbon dioxide uptake	
Rubisco	▪ Rubisco affinity for CO$_2$ and catalytic efficiency (Parry *et al.*, 2011; Parry *et al.*, 2013) ▪ Rubisco chaperones (Whitney *et al.*, 2015) ▪ Rubisco thermotolerance (Kumar *et al.*, 2009; Scafaro *et al.*, 2012) ▪ Rubisco kinetics diversity (Galmés *et al.*, 2014)
CO$_2$ concentrating mechanisms (CCMs)	▪ Cyanobacterial bicarbonate transporters of carboxysomes in C$_3$ plants and aquaporin activity (Price *et al.*, 2011) ▪ Biochemical C$_4$ pathways into C$_3$ pathways (von Caemmerer *et al.*, 2012; Furbank *et al.*, 2015)
Photorespiration	▪ Peroxisomes (Maurino and Peterhansel, 2010) ▪ Genes that affect the normal photorespiratory cycle (Peterhansel *et al.*, 2012) ▪ Bacterial enzymes that recycle the photorespiratory products (Peterhansel and Maurino, 2011)
Calvin cycle	▪ Sedoheptulose-1,7- bisphosphatase to increase photosynthetic rate (Lefebvre *et al.*, 2005) ▪ Fructose 1,6-bisphosphate aldolase reduced photosynthetic rate and plant growth (Haake *et al.*, 1999)
Light harvesting	
Chlorophylls and photoprotection	▪ Chlorophyll *d* and *f* (Chen and Blankenship, 2011) ▪ The xanthophyll cycle (Niyogi *et al.*, 1998)
Light interception	▪ Leaf erectness and leaf angle in wheat (Isidro *et al.*, 2012) ▪ Canopy architecture (Deery *et al.*, 2014) ▪ Stay green (Derkx *et al.*, 2012) ▪ Biomass, RUE, LI and PAR (Reynolds *et al.*, 2009; Reynolds *et al.*, 2011a)

A good example of scaling up is the low impact of increasing Rubisco RNA abundance in soybean by 50% but it only results in a 6% improvement in estimated grain yield when growing with fertilizer and a loss of 6% of estimated grain yield without additional nitrogen source (Sinclair *et al.*, 2004). Possible trade-offs in photosynthesis must be taken into account when assessing the likely impact of higher photosynthesis on biomass and yield as

it depends on numerous factors, from sink-source interactions in plants to water and nutrient availability (Sadras and Richards, 2014). Furthermore, gains in plant energy conversion efficiency can be reduced by biotic and abiotic factors and crop management. Elevated $[O_3]$, water stress, temperature stress, and foliar damage reduce yields and limit the closure of the yield gap (Slattery *et al.*, 2013).

Scaling up from molecular biology to crop yield is a big jump as it depends on both a rational understanding of the process and visualising the big picture (Passioura, 1979). However, there have been many cases of scaling up from basic knowledge to an impact in agriculture (Sinclair *et al.*, 2004). For example, the release to farmers of wheat genotypes with better water use efficiency selected using stable carbon isotope discrimination (Condon *et al.*, 1987; Condon *et al.*, 2002) or selection of durum wheat more resistant to salinity (Munns *et al.*, 2003; Munns and Tester, 2008). Scaling up from leaf photosynthetic attributes to yield is complex as it depends on the sink-source relationship, environmental conditions, species dependent variation, limitations of measurements made in a single tissue, plant and crop factors.

Not surprisingly, given the issues discussed above, some experiments with modern cultivars have often shown either tenuous or no correlation between CO_2 assimilation rate and yield (Brinkman and Frey, 1978; Hart *et al.*, 1978; Murthy and Singh, 1979; Gifford and Evans, 1981; Evans, 1993; Sadras *et al.*, 2012). However, improvements in yield are theoretically possible by increasing photosynthesis (Richards, 2000; Zhu *et al.*, 2010). For example, soybean yield has been related to stomatal conductance and photosynthesis (Morrison *et al.*, 1999; Jin *et al.*, 2010). Rice yield potential was related to crop growth rate during late reproductive period and canopy photosynthesis (Takai *et al.*, 2006), rice yield has also been related with canopy diffusive conductance (Horie *et al.*, 2006) and yield showed a positive correlation with CO_2 assimilation rate in cytochrome b_6/f complex transgenic rice lines (Yamori *et al.*, 2016). According to field and glasshouse experiments, increases in wheat yield across the years have been associated with improvements in RUE, CO_2 assimilation rate and stomatal conductance in the flag leaf (Shimshi and Ephrat, 1975; Reynolds *et al.*, 1994; Watanabe *et al.*, 1994; Fischer *et al.*, 1998b; Gutierrez-Rodriguez *et al.*, 2000; Reynolds *et al.*, 2000; Shearman *et al.*, 2005; Sadras and Lawson, 2011).

The evidence that photosynthetic traits have increased in modern genotypes provides incentives for further research to understand leaf-level photosynthesis and diversity in elite and landraces wheats. Part of this project focuses on detection of natural diversity, for CO_2 assimilation rate and other related traits. In this case Rubisco activity (V_{cmax}) and RuBP

regeneration rate (J) have been analysed through a knowledge of the stoichiometry in photosynthetic carbon reduction and they can be measured in the field (Farquhar *et al.*, 1980; von Caemmerer, 2000). However, few papers have been published analysing genetic variation for V_{cmax} and J in wheat (Driever *et al.*, 2014; Jahan *et al.*, 2014) and there is no published data for wheat measuring V_{cmax} and J diversity in the field. If we intend to use such derived traits for selecting wheat varieties with high RUE, it is necessary to compile more information about the genotypic variation for V_{cmax} and J and have a better understanding of these traits.

1.5 GAS EXCHANGE TO ASSESS PHOTOSYNTHETIC PERFORMANCE IN PLANTS

1.5.1 *A:C_i* curves and *A:C_c* curves

Gas exchange can be used to understand the underlying physiology of photosynthesis in plants. Instruments such as the LI-6400XT Portable Photosynthesis system (LI-COR Inc., Lincoln, NE, USA) measure fluxes of CO_2 and H_2O diffusion through leaf stomata. CO_2 is the main substrate for Rubisco in the Calvin Cycle. The difference between CO_2 concentration entering and exiting a chamber where the leaf is placed permits calculation of the CO_2 assimilation rate by the leaf (A). The LI-COR is able to regulate different CO_2 concentrations around the leaf so that CO_2 response curves can be measured.

Knowing stomatal conductance (g_s), the intercellular CO_2 concentration (C_i) can be calculated such that *A:Ci* curves can be constructed (Figure 1.2). Since Rubisco carboxylation rate depends on the partial pressure of CO_2 inside the chloroplast (C_c), one also needs to know the mesophyll conductance (g_m) in leaves. This allows the construction of *A:C_c* curves (Figure 1.2). C_c takes into account the resistance to diffusion that CO_2 encounters between the intercellular airspaces and the chloroplast stroma as it diffuses through the cell wall membranes and aqueous phase to Rubisco.

Figure 1.2 CO_2 assimilation rate, *A*, as a function of intercellular CO_2, *C_i*, (diamonds) and chloroplastic CO_2, *C_c* (circles) at 21% Oxygen, 25 °C. Model curves fitted to *A* are shown. Data from one flag leaf of *Triticum aestivum* cv. Mace. Flow rate 500 µmol s^{-1}, irradiance 1800 µmol quanta m^{-2} s^{-1}. g_m was assumed to be 0.55 mol m^{-2} s^{-1} bar^{-1}. Transition from *V_{cmax}* to *J* limited curves occurred at *A*=28.5 µmol CO_2 m^{-2} s^{-1} (horizontal arrow) and *C_c*=252 µbar and *C_i*=324 µbar (vertical arrows).

The response curves can be used to estimate the velocity of carboxylation of Rubisco (*V_{cmax}*) and the RuBP regeneration or electron transport rate (*J*) based on the C$_3$ biochemical model (Farquhar *et al.*, 1980). When net photosynthesis is positive, the intercellular CO_2 partial pressure (*C_i*) is greater than that in the chloroplast (*C_c*). Using *A:C_c* curves to calculate *V_{cmax}* means that the initial slope is steeper than in *A:C_i* curves, which changes the range where Rubisco activity or RuBP regeneration are the rate limitation. It is expected that the estimation of *V_{cmax}* and *J* in the leaf will be more realistic by using *C_c* (Figure 1.2.).

A is a commonly measured parameter for assessing photosynthetic performance; it is found to vary among wheat genotypes and has been related to wheat yield (Reynolds *et al.*, 1994; Fischer *et al.*, 1998b; Gutierrez-Rodriguez *et al.*, 2000; Reynolds *et al.*, 2000). However, *A* is strongly dependent upon g$_s$ (Condon *et al.*, 2004). *A* can be high because the genotype has high biochemical capacity or because it has high g$_s$ or a leaf can have high capacity but be measured when g$_s$ was low (Figure 1.3). For this reason, *V_{cmax}* and *J* are more robust traits than *A* to study photosynthetic capacity in plants.

Figure 1.3 CO_2 assimilation rate, *A*, depends on stomatal conductance, g_s, for a leaf with a certain V_{cmax} and *J*. Point (a) has the same *A* as (b) but with a lower g_s and requires a higher V_{cmax} and *J* capacity.

1.5.2   Meaning of V_{cmax} and *J*

Calculations and detailed stoichiometry of V_{cmax} and *J* have been widely described in the biochemical model of leaf photosynthesis for C_3 plants (Farquhar *et al.*, 1980; von Caemmerer, 2000). The model is based on the Calvin cycle and the electron transport chain taking into account photorespiration and Rubisco kinetics using the Michaelis-Menten equation.

The biochemical model assumes stoichiometries for carboxylation, oxygenation and electron transport. During carboxylation, one molecule of RuBP yields two molecules of 3-phosphoglycerate (PGA). For oxygenation, one molecule of RuBP produces one molecule of PGA and one molecule of 2-phosphoglycolate, which is recycled in the photorespiratory cycle to produce 0.5 molecules of PGA. During thylakoid electron transport, the reduction of $NADP^+$ to $NADPH + H^+$ requires the transfer of two electrons, which in turn requires four photons, two to each photosystem (von Caemmerer, 2000).

In the C_3 biochemical model of leaf photosynthesis two main equations describe the process: one, the maximum velocity of Rubisco (ribulose-1,5-bisphosphate carboxylase-oxygenase) carboxylation (V_{cmax}) and two, the electron transport rate (*J*) needed for RuBP (ribulose-1,5-bisphosphate) regeneration. The response of *A* at different CO_2 partial pressures (*C*) is used to derive values for the variables V_{cmax}, *J* and R_d by assuming values for several Rubisco kinetic parameters (Equations 1.2 and 1.3).

$$A = \frac{V_{cmax}(C-\Gamma_*)}{C+K_c\left(1+\frac{O}{K_O}\right)} - R_d \tag{1.2}$$

$$A = \frac{J(C-\Gamma_*)}{4C+8\Gamma_*} - R_d \tag{1.3}$$

The equations are based on the Michaelis-Menten equation. For plant leaves it is necessary to consider carboxylation and oxygenation, which requires the O_2 partial pressure, O, the Michaelis-Menten constants for CO_2 and O_2, K_c and K_o respectively, and Γ^* that is the chloroplastic CO_2 partial pressure at which the rate of carboxylation equals the rate of photorespiratory CO_2 release. Because instruments routinely measure net assimilation of CO_2, non-photorespiratory CO_2 release by mitochondrial respiration (R_d) is also needed.

V_{cmax} and J are key photosynthetic traits for a leaf. In biological terms, V_{cmax} represents the maximum rate of carboxylation by Rubisco. Figuratively, V_{cmax} has been compared to the power of a car engine; a car with more cylinders will have a higher capacity and more power.

In the case of J, in biological terms, it represents the rate at which energy from the sun is used by the leaf for photosynthesis. J is the electron transport rate which enables the regeneration of RuBP. Sunlight captured by the leaf pigments is converted into chemical energy in the chloroplast splitting H_2O molecules which generate electrons that flow through photosystem II and I to produce NADPH and ATP that are used in the regeneration of RuBP in the Calvin Cycle. Continuing the alternative analogue, J can be seen as petrol for a car, the energy that makes the engine to work.

Photosynthetic measurements are extensively used to calculate V_{cmax} and J in plant physiology and ecophysiology. However, a tool that allows a greater number of individuals to be measured for photosynthetic performance is still needed.

1.6 LEAF REFLECTANCE TO ASSESS PHOTOSYNTHETIC PERFORMANCE IN PLANTS

Reflection is 'the redirection of a beam of radiation when it encounters a boundary'. The beam can be reflected coherently as happens with a mirror or can be scattered by unequal surfaces. The beam is electromagnetic radiation, which because of the time spent travelling in magnetic and electric fields can be seen as electromagnetic waves. A wavelength measured in meters is the distance between adjacent wave crests from the electromagnetic wave, and frequency measured in cycles is the number of waves that go across a certain

point in one second. Electromagnetic waves from all frequencies form the electromagnetic spectrum (Jones and Vaughan, 2010). Some regions of the spectrum are: Far (vacuum) ultraviolet (UV) (10-180 nm), Near UV (180-350 nm), visible (VIS) (350-770 nm) (Ingle and Crouch, 1988). Photosynthetically Active Radiation is defined from 400 to 700 nm (McCree, 1971).

Reflectance from the first part of the electromagnetic spectrum has been related to xanthophylls, chlorophylls, and water in plants (Figure 1.4.a), and the red edge in the derivative of reflectance is commonly related to photosynthesis (Figure 1.4.b) (Peñuelas and Filella, 1998).

The IR region is commonly divided in to three bands: near infrared (770-1300), short wave infrared 1 (SWIR1) region (1300-1900 nm), and short wave infrared 2 (SWIR2) region (1900-2500 nm). Research in this part of the spectrum has increased because hyperspectral cameras and radiometers can more easily measure the full spectrum, 350-2500 nm and secondly because the information has been useful. IR spectra measured in leaves have been correlated with photosynthetic parameters (V_{cmax} and J) (Serbin *et al.*, 2012), and have been used to predict carbon, nitrogen and phosphorus in leaf extracts (Gillon *et al.*, 1999). Other uses are in imaging, for example vision at night (Figure 1.5).
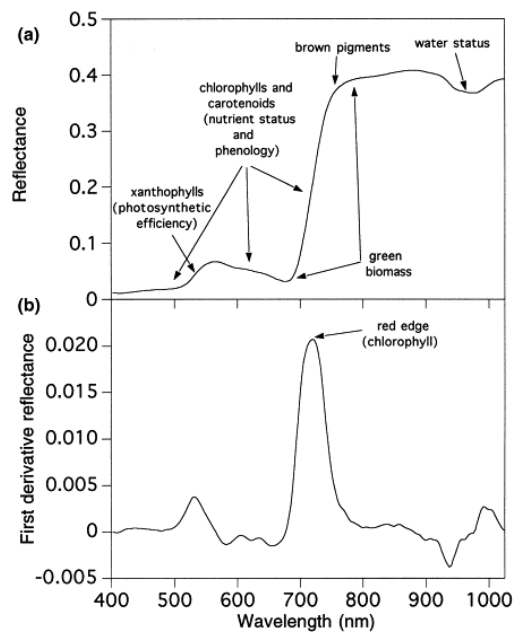
Figure 1.4 Reflectance (a) and the first derivative of reflectance (b) spectra for typical healthy leaves. The main wavelengths used in physiological reflectance indices are indicated: 430 and 445 nm for carotenoids; 531 and 570 nm for xanthophylls; 550–680 nm and `red-edge' position for chlorophyll; 700–800 nm for brown pigments; 800 and 900 nm as structural reference wavelengths; 970 nm for water; and 800–900 nm and 680 nm for green biomass' (Peñuelas and Filella, 1998).

Figure 1.5 The same photo taken during the night using (a) a normal camera (b) using a SWIR camera. http://www.sensorsinc.com/gallery/images.

1.6.1 Measuring reflectance from a canopy

Reflection from vegetation has been measured with radiometers and images from satellites for global vegetation programs which began in 1972 with the multi-spectral satellite LANDSAT 1. Reflectance has been used to estimate terrestrial photosynthesis and light use efficiency from vegetation because it is the source of primary production on the planet (Grace *et al.*, 2007). Numerous vegetation indices (VI) using the visible and infrared region of the spectrum have been proposed to measure chlorophyll in vegetation (Zarco-Tejada *et al.*, 2001). The most successful are the photochemical reflectance index (PRI) and the normalized difference vegetation index (NDVI). PRI is correlated with the xanthophyll cycle which protects plants from photodamage, and uses reflectance from the visible region at 531 and 570 nm (Gamon *et al.*, 1992). NDVI is used to track active photosynthesis in the biomass of a plant canopy using reflectance in the visible and infrared region of the electromagnetic spectrum (Tucker, 1979).

More recently, measurements of the full spectrum from 350-1000 nm or 350-2500 nm depending on the instrument have been used to estimate leaf chemical properties and leaf dry mass per area (LMA). For instance, high spectral resolution remote sensing from Airborne Visible Infrared Imaging Spectrometer (AVIRIS) has successfully predicted leaf chemical properties and leaf mass per area (LMA) from a tropical forest using the partial least square regression (PLSR) (Asner and Martin, 2008; Asner *et al.*, 2009; Asner *et al.*, 2011a; Asner *et al.*, 2011b). Leaf nitrogen, chlorophyll *a* and *b*, carotenoids, LMA and assimilation of CO_2 have also been predicted from spectral reflectance at canopy level. Correlations of predictions varied from R^2=0.49 for A_{max} to R^2=0.9 for LMA (Doughty *et al.*, 2011).

1.6.2   Measuring reflectance from a leaf

One advantage of measuring leaf reflectance is that the spectra are not too contaminated by reflectance from the soil and the atmosphere. Both of these factors can complicate the usefulness of canopy reflectance spectra. Leaf measurements are important because they have allowed scaling up to canopy level and provide a link to biochemical measurements in the laboratory.

Reflectance measurements of leaves have been reported since 1929. In 1961, a colorimeter with a reflectance attachment was used to measure the percentage of 625 nm light that was reflected. This value showed a high correlation with chlorophyll content in soybean and Valencia orange leaves, thus providing a useful indicator of chlorophyll content in leaves (Benedict and Swidler, 1961). A chlorophyll-meter based on transmittance of 670 and 750 nm, correlated strongly (0.998) with chlorophyll content. Consequently, this method was developed for estimating the deepness of green colour and the chlorophyll content per unit area of the leaves (Inada, 1963). Nowadays, there are several portable leaf chlorophyll meters available in the market, such as the Minolta SPAD chlorophyll meter. SPAD measures the chlorophyll content via light transmittance through absorbance of red light at 650 nm and infrared light 940 nm, it is hand-held battery portable and there is a model that permit to save the information and download in the computer (Mullan and Mullan, 2012).

Following from the success of remote sensing at the canopy level, hyperspectral reflectance has been developed for predicting physiological and biochemical leaf parameters at leaf level. Successful predictions of photosynthetic parameters have been obtained for tropical trees, aspen, cotton and soybean (Doughty *et al.*, 2011; Serbin *et al.*, 2012; Ainsworth *et al.*, 2014), and nitrogen content and LMA in wheat (Ecarnot *et al.*, 2013). These examples show the potential of using hyperspectral reflectance (350-2500 nm) to screen wheat for photosynthetic parameters.

1.7   THESIS AIM AND OUTLINE

It is now possible to calculate Rubisco activity (V_{cmax}) and electron transport rate (J) and these can serve as main traits to study photosynthetic diversity in wheat. The first objective was to determine variation in photosynthetic parameters using panels of elite wheat lines. Secondly, as the determination of these parameters is slow, the second objective was to develop a new method using hyperspectral reflectance to predict multiple traits.

This thesis is composed of conventional methods and hyperspectral reflectance to study and understand photosynthetic diversity in wheat. The first part is based on the

biochemical model of leaf photosynthesis for C_3 plants and gas exchange measurements. In Chapter 2, the kinetic constants that are used in the biochemical model were adapted for wheat. In Chapter 3 further understanding of V_{cmax} and Rubisco content measured *in vitro* were considered to analyse diversity of V_{cmax} in four sets of wheat genotypes: two experiments in the glasshouse in Australia, one experiment in the field in Mexico and other experiment in the field in Australia. Among others traits, J, leaf dry mass per unit area and leaf nitrogen were considered in each experiment. Statistical comparisons across wheat genotypes, environments and plant stage were used to understand diversity of the traits measured.

The second part of the thesis explores hyperspectral reflectance as a rapid tool to measure photosynthetic traits. Chapter 4 presents the methodology used to measure reflectance in wheat and the analysis of the partial least square regression (PLSR). Validation of the method for V_{cmax}, J, LMA, N_{area}, SPAD (as surrogate of chlorophyll content) and chlorophylls is shown in Chapter 5. Chapter 6 gives two examples where the models derived in the validations are used to predict J, LMA and N_{area} in two new set of elite and landrace wheat genotypes. Finally, Chapter 7 presents a synthesis of the main findings of the thesis and possibilities for future research.

CHAPTER 2

Biochemical model of C₃ photosynthesis applied to wheat at different temperatures

Temperature controlled cabinet. Research School of Biology. ANU. Canberra, Australia, 2014

2.1 ABSTRACT

In this study, the effect of temperature on estimating V_{cmax25} with the C_3 photosynthesis model is analysed for wheat. Plants were evaluated under controlled conditions in a growth cabinet and in the field at different temperatures. In the cabinet, measurements were made in 2 and 21 % O_2 to constrain the fitting. The fitting of observed CO_2 response curves measured in the cabinet began by assuming some of the kinetic constants. The activation energy (E) for R_d from tobacco was assumed and corroborated from observed data. Then, the initial slope from the CO_2 response curve was used to calculate the CO_2 compensation point (Γ), from which Γ_* was predicted. E for V_{cmax} for wheat was assumed from the literature. Values for K_c and K_o at 25 °C were assumed from tobacco. Values of E for K_c, K_o and V_{omax} were found along with values for V_{cmax} and R_d at 25 °C which minimised two variances, namely Γ_* and the assimilation rates measured at low CO_2 concentrations across all temperatures and both oxygen concentrations. Several new kinetic constants are proposed for wheat. These constants were tested on CO_2 response curves measured on wheat genotypes in the field at different temperatures during the course of a day. The new kinetics constants improved the fitting of curves measured at different temperatures.

2.2 INTRODUCTION

The biochemical model of leaf photosynthesis for C_3 plants is widely used in plant physiology to calculate the maximum velocity of Rubisco (ribulose-1,5-bisphosphate carboxylase-oxygenase) carboxylation *in vivo* (V_{cmax}) and electron transport rate (J) or rate of RuBP (ribulose-1,5-bisphosphate) regeneration (Equations 2.1 and 2.2). The model using kinetic parameters derived from tobacco (*Nicotiana tabacum*) has been applied to many species measured at 25 °C. To adjust the kinetic parameters to different leaf temperatures, the Arrhenius equation (Equation 2.9) has been used. As CO_2 response curves measured in the field for this project were obtained at different leaf temperatures (Figure 2.1), it was deemed necessary to verify that this did not bias the estimated values of V_{cmax} and J.

The temperature range for good photosynthetic performance for cold adapted plants is from 0 to 30 °C and for warm adapted plants between 15 and 45 °C (Sage and Kubien, 2007). At the beginning of this project, it was assumed that V_{cmax25} could be calculated with the Arrhenius equation from measurements of wheat measured in the field between 20 and 34 °C. However, it became apparent when analysing repeated measurements on the same leaf through a day that this was not the case.
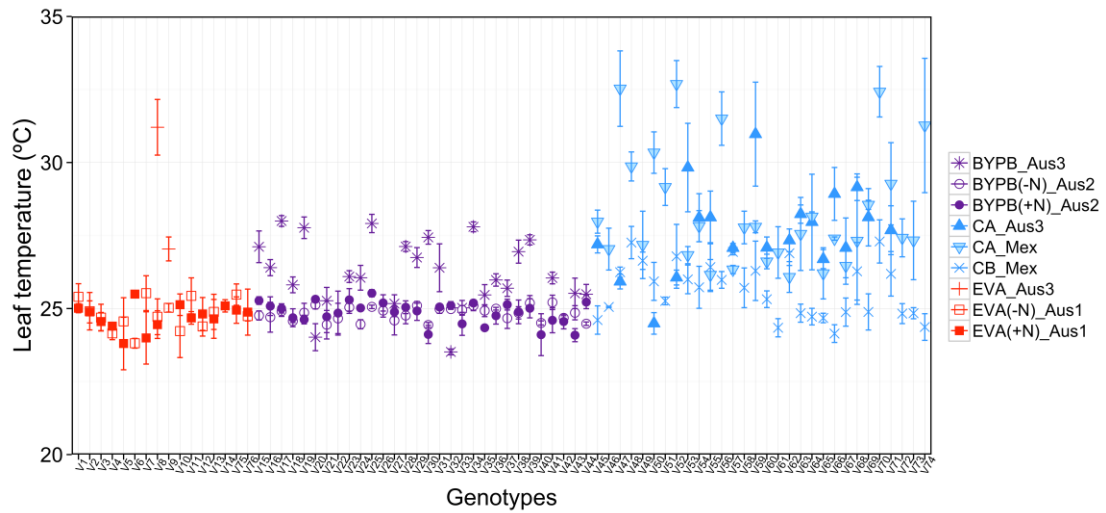
Figure 2.1 Leaf temperature for wheat plants measured in the glasshouse (Aus1 and Aus2) and in the field (Aus3 and Mex). Genotype details are given in Chapter 3. Symbols are the average of the repetitions, and error bars represent the standard error from the same repetitions.

Temperature affects plant performance and photosynthesis in a variety of ways. High temperatures can affect Rubisco, Rubisco activase, Rubisco activation state and membrane fluidity. It has been shown that the catalytic turnover of Rubisco (k_{cat}) from C₃ plants increases at least 6 times from 16 to 40 °C, while the affinity for CO_2 decreases (Sage, 2002).

When deriving estimates of V_{cmax} from gas exchange measurements, one requires the kinetic parameters K_c and K_o which are the Michaelis-Menten constants for carboxylation and oxygenation respectively, and V_{omax} that is the maximum velocity of oxygenation (von Caemmerer, 2000). To account for different leaf temperatures, activation energies for each parameter are also required. Using values and activation energies for V_{omax}, K_c and K_o from tobacco and *Atriplex glabriuscula,* predictions of CO_2 assimilation rate for *Chenopodium album* were higher than the observed data, particularly at high CO_2 concentrations (Sage, 2002). This suggests that the kinetic constants for *C. album* may differ from those of tobacco. Therefore, it was concluded that activation energies for Rubisco kinetic constants needed to be derived in order to calculate V_{cmax25} from the field measurements of wheat carried out here.

Rubisco is a bifunctional enzyme catalysing reactions with both CO_2 and O_2. In order to assess the oxygenase parameters, CO_2 response curves were measured under two O_2 concentrations and a range of temperatures for each leaf. Analysis of curves obtained under low O_2 (2%) permits us to derive K_c, while curves measured at ambient O_2 (21%) reflect the

apparent affinity when oxygen is competitively inhibiting the carboxylase (von Caemmerer, 2000). By making measurements under two O_2 concentrations, it is possible to derive the temperature responses of both K_c and K_o. Although studies using photosynthetic kinetic parameters have been reported for wheat (Table 2.1), no study provides a complete set of information such as available for tobacco (Bernacchi *et al.*, 2001; Bernacchi *et al.*, 2002). The activation energy for V_{cmax} in tobacco has been shown to be between 64.8 (Badger and Collatz, 1977) and 65.33 kJ mol⁻¹ (Bernacchi *et al.*, 2001). For wheat, a value of 63 kJ mol⁻¹ was obtained (Evans, 1986) and has been assumed here. The activation energy for respiration in tobacco is 46.39 kJ mol⁻¹ (Bernacchi *et al.*, 2001). However, it is likely that this varies between species (Atkin and Tjoelker, 2003). Consequently, some experiments were carried out to corroborate this value for wheat.

Table 2.1 *In vitro* Michaelis-Menten constants for Rubisco in wheat, triticale, tobacco and rice.

Species	K_c Value at 25°C (μbar)	K_o Value at 25°C (μbar)	Reference
Triticum aestivum	335±24	304±30	(Makino *et al.*, 1988)
	291±10	194±30	(Cousins *et al.*, 2010)
	326±27	271±26	(Carmo-Silva *et al.*, 2010)
	308.4±3	328.6±6	(Galmés *et al.*, 2014)
	488±12	343±10	(Prins *et al.*, 2016)
Triticale	482±72	305±4	(Prins *et al.*, 2016)
Nicotiana	272.38	165.82	(Bernacchi *et al.*, 2002)
tabacum	259	179	(von Caemmerer *et al.*, 1994)
Oryza sativa	239	266	(Makino *et al.*, 1988)

E: Activation Energy. Solubility for CO_2 of 0.0334 mol (L bar⁻¹) and for O_2 of 0.00126 mol (L bar)⁻¹ were used to convert K_c and K_o values from concentrations to partial pressures.

Temperature can also affect the fluidity of membranes and the functioning of protein complexes within them (Sage and Kubien, 2007). The temperature dependence of mesophyll conductance (g_m) should also be considered in the calculations of V_{cmax} and J (Sage and Kubien, 2007). Unlike for tobacco, the temperature response of g_m for wheat is modest from 15 ºC to 40 ºC (Equation 2.5) (von Caemmerer and Evans, 2015).

Since *in vitro* Rubisco measurements are laborious, kinetics constants have been derived *in vivo* using CO_2 response curves for tobacco (von Caemmerer *et al.*, 1994; Bernacchi *et al.*, 2001). It was decided to pursue the same approach for wheat measuring CO_2 response curves at different temperatures and different O_2 concentrations.

The main purpose of this chapter is to derive a set of kinetic constants for wheat Rubisco that can be used to fit Equation 2.1 to provide more accurate calculations of V_{cmax25} from measurements made under variable temperatures.

2.3 MATERIALS AND METHODS

2.3.1 Experiments and gas exchange measurements

Results are organised in two experiments described below: **Cabinet** and **Aus3T**. For these experiments, gas exchange was measured on the flag leaf of wheat using a LI-6400XT Portable Photosynthesis system (LI-COR Inc., Lincoln, NE, USA). The air flow rate was 500 µmol s⁻¹ with an irradiance of 1800 µmol quanta m⁻² s⁻¹. The CO_2 concentration used refers to the inlet gas.

   a) Cabinet

For the **Cabinet** experiment, three wheat genotypes (**Merinda, Espada** and **Mace**) and one triticale genotype (**Hawkeye**) were chosen from previous experiments where they represented the entire range of variability in photosynthetic efficiency for the genotypes measured (see section 3.4.2.2).

The four genotypes were sown on August 11th, 2014. Each genotype was sown in three pots of 5 L with 75:25 loam:vermiculite soil mix containing basal fertilizer and grown in a glasshouse with temperature 25/15 °C (day/night) at CSIRO Black Mountain, Canberra, Australia (-35.271875, 149.113982). Plants emerged on August 18th, 2014 and were thinned to two plants per pot about one week later.

Gas exchange was measured on flag leaves from September 25th to October 15th, 2014 when the plants were close to anthesis, GS59-60 (Zadoks *et al.*, 1974). On the morning of the measurement, they were transferred from the glasshouse to a controlled environment cabinet (Thermoline Scientific Model-TRIL/SL) and light intensity 200 µmol quanta m⁻² s⁻¹ in the facilities of the Research School of Biology in the Australian National University (ANU), Canberra (-35.277078, 149.116686). Plants were well irrigated before and through the experiment to avoid water stress. Temperature required for each measurement was adjusted in the cabinet and in the leaf temperature mode of the LI-COR that was used to measure CO_2 response curves. The initial conditions were 21% O_2 concentration, 15 °C leaf temperature and 400 µmol CO_2 mol⁻¹. When 2% O_2 was used, it was obtained by mixing N_2 and O_2 using mass flow controllers (Omega Engineering Inc. Stamfort, CT,

USA). The LI-COR prompt was set to 2% O_2 in order to obtain correct gas exchange calculations.

Six plants of **Merinda (V34)** were measured at 51, 52 and 53 DAE with leaf temperatures of 15, 25, 30, 35 °C. At each temperature, CO_2 response curves were measured at 21% and then 2 % O_2 using 50, 100, 150, 200, 250 and 400 µmol CO_2 mol^{-1}. The lights on the LI-COR chamber were turned off after the last CO_2 response curve was measured, and dark respiration was recorded 30 minutes later. For two plants, respiration was recorded at decreasing temperatures of 35, 30 and 25 °C. In four plants, it was recorded at decreasing temperatures of 35, 30, 25, 20, 15°C and then at increasing temperatures of 15, 20, 25, 30 and 35 °C at 400 µmol CO_2 mol^{-1} and 21 % O_2.

Two plants of **Espada (V25)** were measured at 39 and another plant at 50 DAE with increasing leaf temperatures of 15, 30, 35 °C. At each temperature, CO_2 response curves were measured at 21% and then 2 % O_2 using 50, 100, 150, 200, 250 and 400 µmol CO_2 mol^{-1}. For two plants, dark respiration was recorded after 30 minutes at decreasing temperatures of 35, 25 and 15 °C at 400 µmol CO_2 mol^{-1} and 21 %O_2.

Five plants of **Mace (V32)** were measured at 57 and 59 DAE and four plants of **Hawkeye (V27)** were measured at 58 and 59 DAE. For each leaf, CO_2 response curves were measured at leaf temperatures of 15, 20, 25, 30 and 35 °C in 21% O_2 and 50, 100, 150, 200, 250, 400, 600, 800, 1000 and 1200 µmol CO_2 mol^{-1}. After the last curve, the lights on the LI-COR chamber were turned off, and dark respiration was recorded 30 minutes later at decreasing temperatures of 35, 30 and 25 °C at 400 µmol CO_2 mol^{-1} and 21 % O_2.

b) Field (Aus3T)

Field experiment **Aus3** is described in detail in Chapter 3 section 3.3.1 and Table 3.1. In experiment **Aus3T**, four wheat genotypes: **V45, V57, V62** and **V66** (Table 3.3) from **Aus3** were selected to measure temperature responses of leaf gas exchange on December 17th, 2013 when plants were 75 DAE, and flowering nearly completed, approximately at GS69. The measurements were made on three different plants from one plot of each genotype. Field air temperature was recorded with the head of the LI-COR opened. Block temperature was set to approximate the field air temperature; resulting leaf temperature and block temperature were recorded during the experiment (A1). For each leaf, CO_2 response curves were measured using 150, 250, 400, 600, 800 and 1200 µmol CO_2 mol^{-1}.

2.3.2 Calculations of V_{cmax}, J and mesophyll conductance

Results from the **Cabinet** experiment were used to derive Rubisco kinetic constants. Therefore, calculations for the g_m and adjustments to calculate Rubisco activity (V_{cmax}) and the electron transport rate (J) will be described during the chapter.

For experiment **Aus3T**, the maximum Rubisco activity at 25 °C (V_{cmax25}) and J were calculated using the kinetic constants obtained in this chapter (Table 2.2) and the leaf biochemical model of photosynthesis (Farquhar *et al.*, 1980). The average rate of CO_2 assimilation (A) of all genotypes (Experiments: **Aus1**, **Aus2**, **Aus3** and **Mex** from Chapter 3) was 25 µmol CO_2 m⁻² s⁻¹, with a mean intercellular CO_2 (C_i) of 260 µmol CO_2 mol⁻¹ (A_{260}) when measured under ambient CO_2. A_{260} was interpolated from the line relating CO_2 assimilation rate to intercellular CO_2 concentrations between 50 and 400 µmol CO_2 mol⁻¹ for each leaf and subsequently used to estimate g_m (Equation 2.4).

2.3.3 Equations

CO_2 assimilation rate (A, µmol CO_2 m⁻² s⁻¹) and the chloroplastic CO_2 partial pressure, µmol mol⁻¹ (C_c) are used to build the CO_2 response curve (Chapter 1, Figure 1.2). The velocity of carboxylation (V_{cmax}, µmol CO_2 m⁻² s⁻¹), is derived from the initial slope which depends on the Michaelis-Menten constants for CO_2 and O_2 (K_c and K_o µbar and mbar, respectively), the O_2 partial pressure (O, 197 mbar) and the chloroplastic CO_2 partial pressure at which the rate of carboxylation equals the rate of photorespiratory CO_2 release (Γ^*, µbar). Rubisco limited CO_2 assimilation rate is expressed as

$$A = \frac{V_{cmax}(C_c - \Gamma_*)}{C_c + K_c\left(1 + \frac{O}{K_o}\right)} - R_d \qquad (2.1)$$

where R_d is the mitochondrial respiration (µmol CO_2 m⁻² s⁻¹) (von Caemmerer, 2000).

The second part of the CO_2 response curve is used to infer the electron transport rate (J, µmol e⁻ m⁻² s⁻¹), expressed as

$$A = \frac{J(C_c - \Gamma_*)}{4C_c + 8\Gamma_*} - R_d \qquad (2.2)$$

The chloroplastic CO_2 partial pressure (C_c, µmol) used in equations (2.1 and 2.2) is derived from the intercellular CO_2 partial pressure (C_i, µbar), A and the mesophyll conductance (g_m, mol m⁻² s⁻¹ bar⁻¹) from the following equation (2.3)

$$C_c = C_i - \frac{A}{g_m} \qquad (2.3)$$

To a first approximation, g_m varies in direct proportion to photosynthetic capacity (von Caemmerer and Evans, 1991). Therefore, the value assumed for g_m for each leaf was derived by linear scaling to the rate of CO_2 assimilation at a common C_i of 260 µmol mol^{-1} (A_{260}) using the following equation:

$$g_m = g_{m,avg} * \frac{A_{260}}{25} \tag{2.4}$$

Where $g_{m,avg}$, (0.55 mol m^{-2} s^{-1} bar^{-1}) was based on the average of six different plants of triticale variety Hawkeye measured with carbon isotope techniques that combine tunable diode laser spectroscopy and gas exchange (Evans and von Caemmerer, 2013) at CSIRO Black Mountain (0.55 mol m^{-2} s^{-1} bar^{-1}, Estavillo *et al.,* – unpublished data). This is similar to other values for wheat (Tazoe *et al.*, 2011; von Caemmerer and Evans, 2015). The value of 25 (µmol CO_2 m^{-2} s^{-1}) on the denominator was the average A from all genotypes at 25 °C.

CO_2 response curves were measured at different leaf temperatures. A linear response of g_m to leaf temperature (von Caemmerer and Evans, 2015) is given by equation 2.5:

$$g_{mT} = g_{m,25} (0.0094T + 0.786) \tag{2.5}$$

The chloroplastic CO_2 partial pressure at which the rate of carboxylation equals the rate of photorespiratory CO_2 release (Γ^*, µbar) depends on the ratio of the velocities of oxygenation (V_{omax}, µmol O_2 m^{-2} s^{-1}) and carboxylation (V_{cmax}).

$$\Gamma_* = \frac{V_{omax} K_c O}{2 V_{cmax} K_o} \tag{2.6}$$

A value of 0.22 was assumed for the ratio V_{omax}/V_{cmax} at 25 °C as has been used in tobacco and wheat (von Caemmerer, 2000; Cousins *et al.*, 2010).

The observed CO_2 compensation point (Γ) was calculated from a line fitted to the measurements made in 50 and 100 µmol mol^{-1} inlet CO_2 concentrations:

$$\Gamma = C_{c50} - A_{50} \frac{(C_{c100} - C_{c50})}{(A_{100} - A_{50})} \tag{2.7}$$

This value was used to calculate a value for observed Γ_* ($\Gamma_{*,obs}$) as follows (von Caemmerer *et al.*, 1994):

$$\Gamma_{*,obs} = \Gamma \left(1 - \frac{R_d}{V_{cmax}}\right) - \left[\frac{K_c\left(1 + \frac{O}{K_o}\right) R_d}{V_{cmax}}\right] \tag{2.8}$$

The temperature response function used for K_c, K_o, V_{cmax}, V_{omax}, R_d, and Γ_* is given by:

$$P = P_{25}\, e^{\left(\frac{E(T-25)}{R \cdot 298 \cdot (T+273.15)}\right)}$$

(2.9)

where P is the parameter value at leaf temperature T (°C), P_{25} is the value of the parameter at 25 °C, E is the activation energy (kJ mol⁻¹) and R is the universal gas constant 8.314 J mol⁻¹ K⁻¹.

To fit observed data with equation 2.1, six main parameters were used: R_d, Γ_*, V_{cmax}, K_c, K_o and V_{omax}. The photosynthetic model requires a value at 25 °C (value25) and an activation energy (E) for each parameter. Several values were assumed from the literature: E for R_d 46.39 kJ mol⁻¹ (section 2.4.1.1), value25 for Γ_* (Bernacchi *et al.*, 2002), E for V_{cmax} in wheat of 63 kJ mol⁻¹ (Evans, 1986), value25 for K_c and K_o from tobacco (Bernacchi *et al.*, 2001; Bernacchi *et al.*, 2002) and V_{omax}/V_{cmax} at 25 °C of 0.22 (von Caemmerer, 2000; Cousins *et al.*, 2010). The value of $\Gamma_{*,obs}$ from Eq. 2.8 provided an additional constraint for the fitting routine by comparing it to Γ_{*new} calculated using Equation 2.6 at each temperature and oxygen condition with K_c, K_o, V_{omax} and V_{cmax} adjusted to each temperature with Equation 2.9. During the fitting for each leaf, the value25 of Rubisco capacity (V_{cmax25}) and respiration (R_d) together with E for K_c and K_o were found.

2.4   RESULTS

CO_2 response curves at different temperatures were measured under two different O_2 concentrations to enable the derivation of Rubisco kinetic parameters for wheat. The first group of experiments was carried out in controlled conditions from which a new set of kinetic constants for wheat was obtained. The second group of experiments were used to validate the kinetic constants using CO_2 response curves measured at different temperatures in the field.

2.4.1   Leaf model prediction of *in vivo* photosynthesis in wheat

In order to understand the effect of temperature on the calculations of V_{cmax}, experiments in the **cabinet** at 21 and 2% O_2 were performed, focused on the initial slope of CO_2 response curves. Values of V_{cmax} and J derived from gas exchange measurements and the model fitted to them depend on photosynthetic kinetic constants that have been assumed in the model. The most frequent kinetic constants used to fit the photosynthetic model have been derived from *Atriplex glabriuscula* and *Nicotiana tabacum* (Table 2.2.a and 2.2.b). However, using these kinetic constants, the modelled response did not describe the wheat CO_2 response curve observed at different temperatures and oxygen concentrations (Figure

2.2.a and 2.2.b.). The observed *A* measured *in vivo* with gas exchange did not correspond to predictions made using the model (Equation 2.1 and 2.2) with kinetic constants from Table 2.2.a. Using kinetic constants obtained by Bernacchi, 2001 & 2002 derived from tobacco (Table 2.2.b, Figure 2.2.b), improved the fitting but there were still inconsistences, especially at 2% O₂. The fitting was substantially improved by deriving new activation energies (Table 2.2.c, Figure 2.2.c).

Table 2.2 The kinetic constants used to model CO₂ assimilation rate in Figure 2.2 a, b & c.

Kinetic constants/Specie		(a) *N. tabacum*[2,4] *A. glabriuscula*[1]	(b) *N. tabacum*	(c) New constants for wheat
K_c	Value at 25°C (µbar)	259[2]	272.38[4]	272[4]
	E (kJ mol⁻¹)	59.4[1]	80.99[4]	***93.72±2.5[6]***
K_o	Value at 25°C (mbar)	179[2]	165.82[4]	166
	E (kJ mol⁻¹)	36[1]	23.72[4]	***33.6±5.9[6]***
Γ_*	Value at 25°C (µbar)	37.43[4]	37.43[4]	*37.74[6]*
	E (kJ mol⁻¹)	24.46[4]	24.46[4]	*24.42[6]*
V_{cmax}	Value at 25°C (µmol m⁻² s⁻¹)	134	113.9	117.5
	E (kJ mol⁻¹)	64.8[1]	65.3[3]	63[5]
V_{omax}	E (kJ mol⁻¹)	65.86	32.58[+]	***27.1±4.8[6]***
R_d	Value at 25°C (µmol m⁻² s⁻¹)	1.37	1.27	1.14
	E (kJ mol⁻¹)	46.39[3]	46.39[3]	46.39[3]
References		[1](Badger and Collatz, 1977) [2](von Caemmerer *et al.*, 1994)	[3](Bernacchi *et al.*, 2001) [4](Bernacchi *et al.*, 2002)	[5](Evans, 1986) [6]This report, n=6

E: Activation Energy; [+]V_{omax} calculated from Bernacchi et al. (2002) constants. V_{cmax} and R_d values at 25 °C belong to each plot.
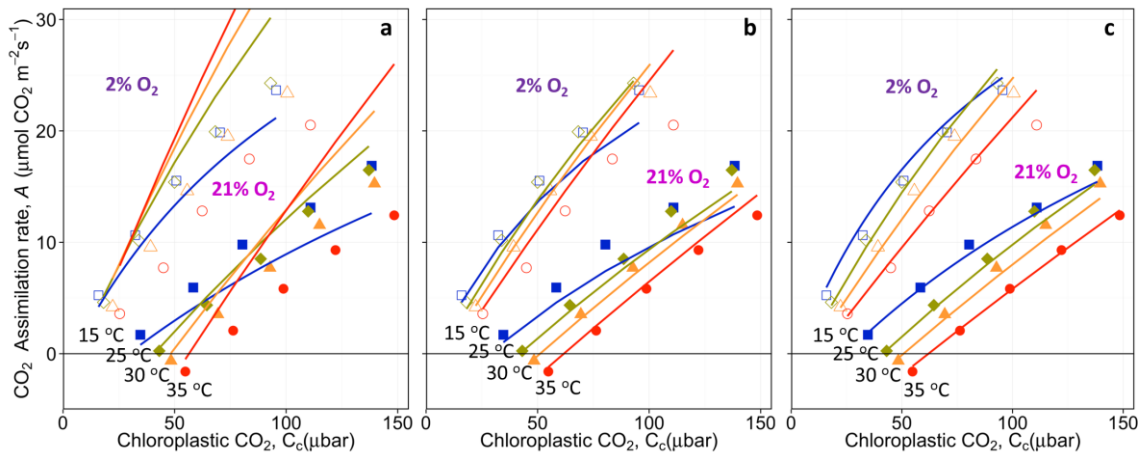
Figure 2.2 CO₂ assimilation rate, *A*, as a function of chloroplastic CO₂, *Cc*, at two different O₂ concentrations (Open symbols, 2% O₂; Closed symbols 21% O₂) and four temperatures (square 15 °C, diamond 25 °C, triangle 30 °C, circle 35 °C). Symbols are the observed *A* from one leaf of *Triticum aestivum* cv. Merinda. Lines are the predicted *A* using each column of kinetic constants from table 2.2. *Cc* was calculated from Equation 2.3, the assumed value of mesophyll conductance, gₘ, from Equation 2.4 and the temperature dependence of gₘ,₂₅ from Equation 2.5. Flow rate 500 µmol s⁻¹, irradiance 1800 µmol quanta m⁻² s⁻¹ and 50, 100, 150, 200 and 250 µmol CO₂ mol⁻¹ of CO₂ reference.

2.4.1.1 Kinetic constants for respiration

From the literature a similar value of E for R_d has been observed in tobacco and wheat (Evans, 1986; Bernacchi *et al.*, 2001). In order to confirm this, dark respiration (R_{dark}) in leaves of wheat was measured at 15, 20, 25, 30 & 35 °C and fitted using E= 46.39 kJ mol⁻¹ (Table 2.2). This activation energy derived from Tobacco matches that observed here for wheat dark respiration (Figure 2.3). The temperature response was similar whether obtained with increasing or decreasing temperatures (not shown). We assume the temperature dependency for R_d is the same as that for dark respiration.
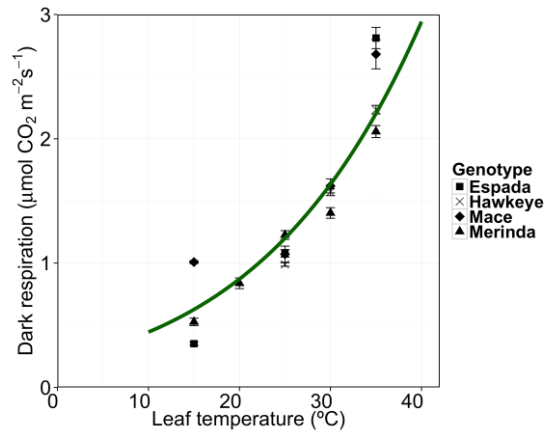
Figure 2.3 The temperature response of dark respiration, R_{dark}, for flag leaves of *Triticum aestivum* cv. Espada, Hawkeye, Mace and Merinda. Each point is the mean of three to six leaves. The error bars are the standard error from the leaves measured. Each leaf was measured after a CO_2 response curve and 30 minutes of darkness, at five temperatures from 15 °C to 35 °C. The line is the predicted respiration from 10 °C to 40 °C using Equation 2.9, E=46.39 kJ mol⁻¹, R=8.314 J mol⁻¹ K⁻¹, $R_{dark(25\,°C)}$ = 1.2 µmol CO_2 m⁻² s⁻¹. Flow rate of 500 µmol s⁻¹ and at 400 µmol CO_2 mol⁻¹ for inlet CO_2.

2.4.1.2 Kinetic constants for the compensation point

Two important points can be extracted from the initial slope of the CO_2 response curve: Γ, where the curve crosses the x axis ($A = 0$), and Γ_*, the CO_2 partial pressure on the curve when $A = -R_d$ (von Caemmerer, 2000). From the observed CO_2 response curves measured on Merinda, at 15 °C, 25 °C, 30 °C and 35 °C, at 21 and 2 % O_2 (Figure 2.2.), a line fitted to the first two points was used to calculate Γ (Equation 2.7), and then Γ_* observed (Γ_{*obs}) using Equation 2.8, assuming that E of V_{cmax} in wheat is 63 kJ mol⁻¹ (Evans, 1986), E of R_d is 46.39 kJ mol⁻¹ (section 2.4.1.1), and value25 for K_c and K_o from Bernacchi et al. (2001, 2002).

Under 21% O_2, the observed CO_2 compensation point, Γ, closely matched that observed for tobacco (Figure 2.4.a). However, under 2% O_2 the observed Γ was slightly less than that predicted using tobacco Rubisco kinetic parameter values.
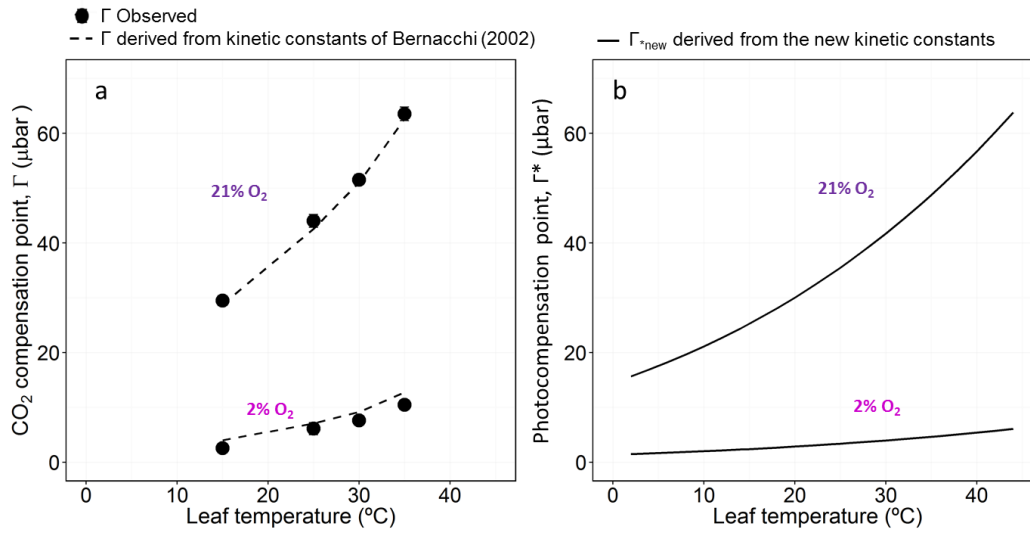
Figure 2.4 Temperature dependence of the CO₂ compensation point in 2 and 21% O₂.
a) CO₂ compensation point when *A*=0. Circles are the observed Γ derived from six *A:Ci*
curves from flag leaves of *Triticum aestivum* cv. Merinda (Equation 2.8). Dashed lines are
Γ calculated with kinetic constants from Bernacchi et al. 2002 (Equation 2.7).
b) CO₂ photocompensation point when *A*= -R$_d$, the solid lines are Γ$_{*new}$ calculated from the
new kinetic constants.

The average value for the CO₂ photocompensation point, Γ$_{*new,}$ from six plants of Merinda measured at 21 % O₂ and 25 °C was 35.4±0.41 µbar using an atmospheric partial pressure for Canberra of 938 mbar. When adjusted to sea level (oxygen partial pressure 210 mbar), this equates to 37.74 µbar. The value of *E* for Γ$_*$ was obtained by summing *E* for V_{omax} and K_c, and subtracting *E* for V_{cmax} and K_o after the fitting (24.4 kJ mol^{-1}, Table 2.2.c). This value is similar to that reported for tobacco (Table 2.2.b). Thus, the value and temperature dependence of the CO₂ photocompensation point appears to be similar between wheat and tobacco.

2.4.1.3 Fitting observed values in the model

Minimising the variance between Γ$_{*obs}$ and Γ$_{*new}$ helped to constrain the solution of the fitting which also tried to minimise the variance between *A* observed and predicted at each temperature and both oxygen concentrations using Equation 2.1. This procedure was repeated for six different plants of Merinda. The average activation energies for K_c and K_o obtained from Merinda (Table 2.2.c) were then used to fit data collected from other genotypes (Mace, Hawkeye and Espada) at different temperatures in the cabinet to assess their general validity.
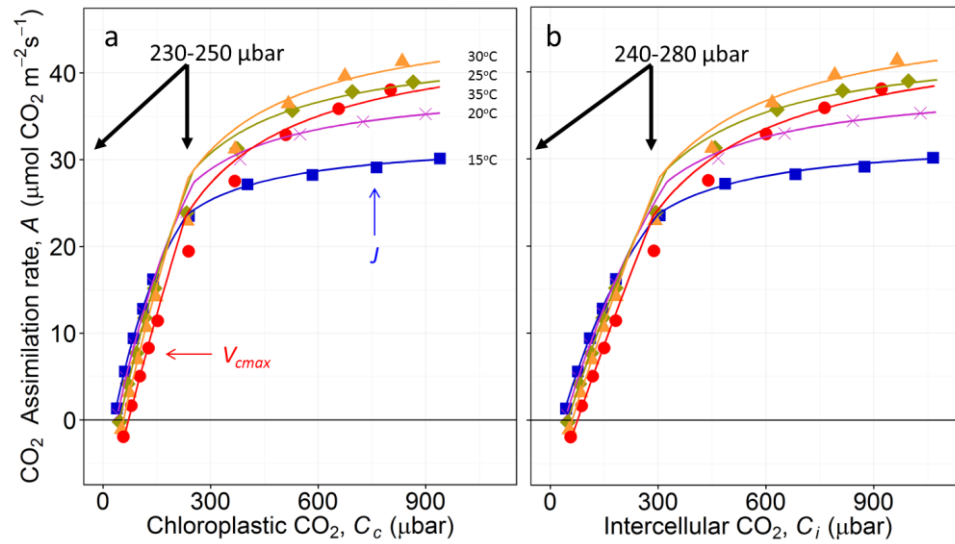
Figure 2.5 CO₂ assimilation rate, *A*, as a function of chloroplastic CO₂, *C_c* a) and intercellular CO₂, *C_i* b), in 21% oxygen at five different leaf temperatures (Square 15 °C, cross 20 °C, diamond 25 °C, triangle 30 °C, circle 35 °C). Model curves are *A* predicted with the new kinetic constants in Table 2.2.c. Symbols are the observed *A* of one flag leaf from *Triticum aestivum* cv. Mace. Flow rate 500 μmol s⁻¹, irradiance 1800 μmol quanta m⁻² s⁻¹. *C_c* was calculated from Equation 2.3.

The ability of the new constants to fit CO₂ response curves is illustrated in Figure 2.5. Two versions are shown. The fundamental data obtained from the LI6400 (*A:C_i*) are shown in panel **b)**, whereas *A:C_c* curves are shown in panel **a)** because it was necessary to include g_m when fitting Equations 2.1, 2.2, 2.3, 2.4 and 2.5. The initial slope of the CO₂ response curves is used to derive V_{cmax}, which increases at higher temperatures. For example, from *A:C_c* curves, V_{cmax} was 50, 78, 121, 184 and 277 μmol CO₂ m⁻² s⁻¹ at 15, 20, 25, 30, 35 °C respectively (Figure 2.5). As temperatures increase, the affinity of Rubisco for CO₂ decreases such that the initial slope changes little. The increase in respiration rate also contributes to the increase in Γ at higher temperatures. At high CO₂ partial pressures, the RuBP regeneration limited rate increased by 30% from 15 to 30 °C before declining at 35 °C. The transition from a Rubisco to an RuBP regeneration limitation happens at a lower chloroplastic CO₂ partial pressure (230 to 250 μbar) compared to intercellular CO₂ partial pressure (240 to 280 μbar), but did not vary greatly with temperature.

2.4.2   Assessing the new kinetics constants for wheat in the field

The new parameters (Table 2.2.c) were used to fit *A:C_c* curves obtained in the field (**Aus2T**). The model curves could be fitted well to the observed data (one example shown in Figure 2.6).
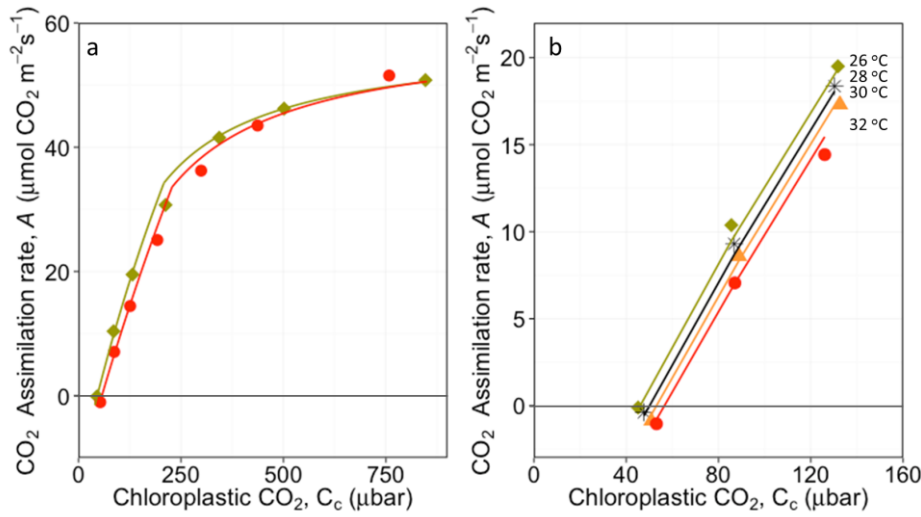
Figure 2.6 CO₂ assimilation rate, *A*, of a wheat leaf (V45) measured in the field as a function of chloroplastic CO₂, *C_c*; a) Full *A*:*C_c* curve at 26 and 32 °C; b) Initial slope at different temperatures (diamond 26 °C, asterisk 28 °C, triangle 30 °C, circle 32 °C). The lines predict *A* with the new kinetic constants of Table 2.2.c. Flow rate 500 µmol s⁻¹, irradiance 1800 µmol quanta m⁻² s⁻¹ and 21% O₂.

2.4.2.1 V_{cmax} trends for wheat in the field and in controlled conditions

Genotypes measured in **Aus3T** and in the **cabinet** were used to assess the validity in estimating V_{cmax} at 21% oxygen at different temperatures.

First, values for V_{cmax} and R_d were sought that minimised variance between observed and modelled rates predicted using Equation 2.1 with the new kinetic parameters. V_{cmax25} was calculated using Equation 2.9 from each curve measured at different leaf temperatures. To avoid possible effects of declining Rubisco activation at temperatures higher than 30 °C, only values derived from leaf temperatures up to 30 °C were used (15 to 30 °C in the cabinet and 25 to 30 °C in **Aus3T**) to calculate the baseline of 100%.

Second, two ways of calculating V_{cmax} were used and compared:

1. V_{cmax} fitted using measurements from multiple temperatures and the new kinetic constants:

Values for V_{cmax25} and R_d were sought by fitting the model at each temperature (15, 20, 25, 30 and 35 °C) using the new kinetic constants (Table 2.2.c), which will be called $V_{cmax(new)}$.

2. V_{cmax} fitted at each temperature using Bernacchi constants:

Values for V_{cmax25} and R_d were sought by fitting the model at each temperature (15, 20, 25, 30 and 35 °C) using tobacco kinetic constants (Table 2.2.b), which will be called $V_{cmax(Bernacchi)}$.
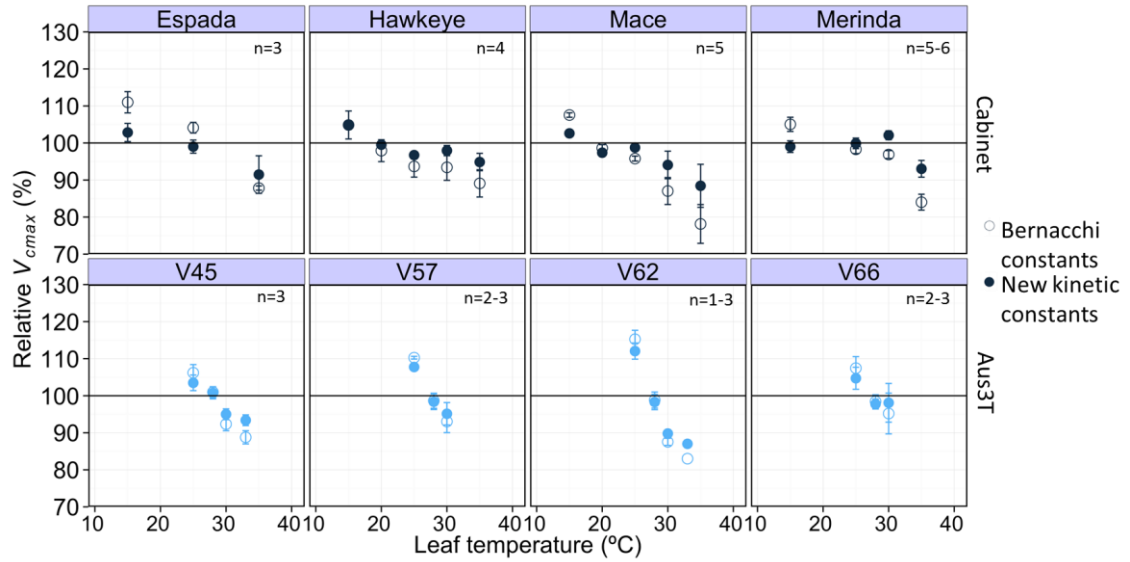
Figure 2.7 Assessing the stability of V_{cmax25} estimated for a leaf measured at multiple temperatures either under controlled conditions (cabinet) or the field (Aus3T). Values of V_{cmax} were derived using the new kinetic constants (closed symbols) or tobacco kinetic constants (Bernacchi *et al.*, 2001; Bernacchi *et al.*, 2002) (open symbols) at each temperature and then converted to V_{cmax25} using equation 2.9. Error bars are the standard error from repetitions, which are described in Materials and Methods.

Ideally one should obtain the same value for V_{cmax25} regardless of the temperature used during the measurement. The baseline of 100% represented the mean value from curves measured up to and including 30°C. Relative values of $V_{cmax(new)}$ and $V_{cmax(Bernacchi)}$ are shown in Figure 2.7. In both cases, the estimate of V_{cmax25} tended to decline as measurement temperature increases. However, $V_{cmax(new)}$ shows less deviation with temperature than $V_{cmax(Bernacchi)}$ (generally ±5% and ±20%, respectively). The deviations appear to be greater when measured in the field (**Aus3T)** compared to measurements made in controlled conditions **(cabinet)**. The decreased variation in V_{cmax25} using the new constants should improve estimation of V_{cmax} from field data that in some cases was obtained at leaf temperatures greater than 25 °C.

2.4.2.2   Changes in *A, Vcmax* and *J* at different temperatures

Leaf temperature affects *A*, V_{cmax} and *J* differently. In the cabinet, *A* showed a broad peak with a maximum near 20 °C (Figure 2.8.a). By contrast, values for V_{cmax} and *J* obtained from *A:Cc* curves with the new constants show quite strong temperature responses (Figure 2.8.c). *J* increased from 15 to 30 °C and then decreased, while V_{cmax} increased up to the maximum temperature measurement, 32 °C in the field and 35 °C in the cabinet. In the field and in the cabinet *J* and V_{cmax} crossed over at 30 °C.
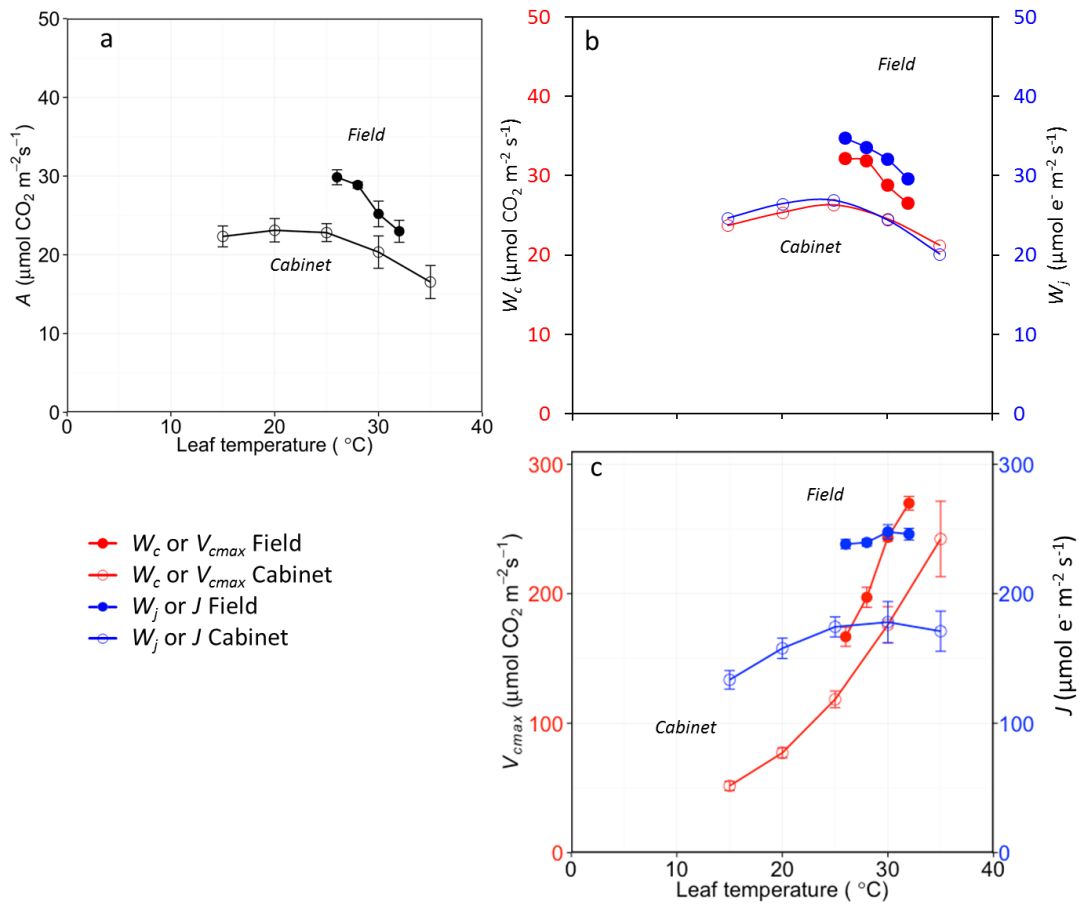
Figure 2.8 Temperature response of a) CO₂ assimilation rate, *A*, b) *A* predicted from *V_{cmax}* (*W_c*), Equation 2.1, or *J* (*W_j*), Equation 2.2, c) Rubisco carboxylation rate, *V_{cmax}* (red) and electron transport rate, *J*, (blue) calculated with the new constants. Mean of three flag leaves from different plants of *Triticum aestivum* V45 measured in Aus3T through a day with leaf temperature increasing from 26 to 32 °C (closed symbols). Mean of five flag leaves measured in the cabinet from different plants of *T. aestivum* cv. Mace with leaf temperature increasing from 15 to 35 °C (open symbols). a) measured when inlet CO₂ was 400 μmol CO₂ mol⁻¹, b) predicted from chloroplastic CO₂ and Equations 2.1 or 2.2, with g_m calculated from Equation 2.4, c) *V_{cmax}* and *J* derived from CO₂ response curves (Figure 2.5 and 2.6) were used to predict *A* (*W_c and W_j*, respectively).

The predicted assimilation rates from *A:C_c* curves assuming Rubisco or RuBP regeneration limitation (Equations 2.1 and 2.2, respectively) were remarkably similar (Figure 2.8.b), but apparently cross from being Rubisco limited below 30 °C to being RuBP regeneration limited above 30 °C in the cabinet. In the field, *A* was apparently Rubisco limited between 26 and 32 °C in part because of a reduction in chloroplastic CO₂. Both *V_{cmax}* and *J* were greater for field-grown leaves than for leaves from plants grown in the glasshouse for the cabinet measurements. The modelled values for *A* predicted in Figure 2.8 reflect the observed rates (Figure 2.8.a.) reasonably well.

2.5 DISCUSSION

The estimate of V_{cmax} from CO_2 response curves depends on the values assumed for the kinetic parameters of Rubisco. As there are few complete sets of values, it is common to assume those determined for tobacco (Bernacchi *et al.*, 2001; Bernacchi *et al.*, 2002). However, it became apparent that using these values from tobacco to analyse wheat measured at different temperatures was problematic. Consequently a detailed characterisation of CO_2 response curves measured under a range of temperatures and two oxygen concentrations was undertaken.

This chapter highlights the importance of adjusting the biochemical model by using kinetic parameters derived for wheat. The new parameters were compared against repeated photosynthetic measurements across a range of leaf temperatures measured in the field or growth cabinet. The new parameter values improved the ability to derive an estimate of V_{cmax} from A:C_i curves measured in the field at leaf temperatures other than 25 °C compared to when activation energies from tobacco were assumed.

2.5.1 Rubisco kinetic constants for wheat

Some kinetic constants from tobacco calculated *in vivo* helped to fit observed data for wheat *in vivo*. *In vitro* value25 for K_c and K_o in wheat differ from those obtained *in vivo* in tobacco, mainly for K_o. *In vitro* K_o for wheat is reported as 304 µbar (Makino *et al.*, 1988) and 328 µbar (Galmés *et al.*, 2014) while value25 of K_c for tobacco is half lower than *in vitro* values (166 µbar). Reports for K_c and K_o measured *in vitro* for different species, make it difficult to select the set of value25 and E that should be used in the fittings, and an inadequate choice could result in poor predictions (Table 2.2.a). A common way to derive V_{cmax} and J is with a published spreadsheet in excel (Sharkey *et al.*, 2007) which uses kinetic constants obtained *in vivo* from tobacco (Bernacchi *et al.*, 2001; Bernacchi *et al.*, 2002). Previously, value25 had been reported for K_c, K_o, Γ_* and k_{cat} based on analysis of CO_2 response curves of transgenic tobacco which had reduced Rubisco content (von Caemmerer *et al.*, 1994). The spreadsheet with that set of kinetic constants has been used in most of the higher plants, assuming that all the plants have the same mechanism for CO_2 assimilation. In part it is true, since prediction of A at 25, 30 and 35 ºC were acceptable when the kinetic constants from Bernacchi et al., 2001 & 2002 were used to predict observed data from wheat (Table 2.2.b). However, there were some inconsistencies in the fitting that were fixed for wheat. The new E of K_c and K_o for wheat increased and V_{omax} decreased in comparison with tobacco. We fixed the value of E for V_{cmax} for wheat at 63 kJ

mol^{-1} (Evans, 1986) which is slightly less than that for tobacco, 65.3 kJ mol^{-1} (Bernacchi *et al.*, 2001). Perhaps these differences are normal since it has been reported that *E* for *k*$_{catc}$ *in vitro* varies from 48 to 72 kJ mol^{-1} across crops (soybean, rice, cotton, tobacco, tomato, spinach, wheat) and *E* of *k*$_{catc}$ *in vitro* for wheat is higher than for tobacco (Galmes *et al.*, 2015). As well, *E* of *k*$_{catc}$ *in vitro* from land plants showed a positive correlation with the optimum growth temperature and Rubisco specificity factor (S$_{c/o}$) (Galmes *et al.*, 2015). Tobacco is from warmer environments than wheat and the temperature required for optimal growth is higher (25 and 20 ºC, respectively), which could relate to the differences in *E* of *K*$_{c}$ and *K*$_{o}$ obtained in this experiment.

It is also reported that the specificity factor (S$_{c/o}$) *in vitro* for tobacco is 82 and 107 mol mol^{-1} for wheat (Parry *et al.*, 1989; Whitney *et al.*, 2009). Interestingly, the assumed value25 for *K*$_{c}$ and *K*$_{o}$ helped to solve the rest of the kinetic parameters in wheat where Γ$_*$ resulted in almost similar values (Table 2.2). Γ$_*$ reflects S$_{c/o}$ *in vivo*. The discrepancy of S$_{c/o}$ *in vitro* and *in vivo* need more work to understand the two different answers.

2.5.2 Effect of temperature on estimating *V*$_{cmax25}$

V$_{cmax}$ calculated with the new constants for wheat varied at increasing temperature (15, 20, **25**, 30, 35 ºC, *V*$_{cmax}$ of 50, 78, **121**, 184, 277 µmol CO$_2$ m^{-2} s^{-1} respectively, Figure 2.5) and during the day temperatures can vary from 23 to 34 ºC (Figure 2.1), for this reason conversion to value25 (*V*$_{cmax}$) is important analysing Rubisco activity for field measurements. However, measurements at temperature higher than 30 ºC should be reconsidered in wheat because the wheat growth and Rubisco could be affected. The optimum growth temperature in wheat during anthesis and grain filling is 20 ºC and the maximum cardinal temperature (when wheat can recover) is 31 ºC at anthesis and 35.4 ºC during grain filling (Porter and Gawith, 1999). Measuring in the field (experiments **Aus3** and **Mex**) the highest temperatures were during anthesis and grain filling between noon and early afternoon. Short periods of heat may not detrimentally affect wheat plants when grown under good management and with irrigation. Thus it should be possible to obtain *V*$_{cmax25}$ from *V*$_{cmax}$ derived at higher temperatures from plants when they are grown under yield potential conditions. However, when high temperatures are expected in the field, it would be better to restrict gas exchange measurements to the morning.

In the case of Rubisco, activation state can be affected by CO$_2$ concentrations and temperature. In fitting the model for C$_3$ photosynthesis to calculate *V*$_{cmax}$, a full Rubisco activation state was assumed. However, in sweet potato, it has been shown that the

Rubisco activation state varies depending on CO_2 concentration. It is higher at low CO_2 (C_i=140 μbar) and lower at high CO_2 concentrations (C_i=500 μbar). Rubisco activation state also decreased at temperatures above 30 ℃. When measured at ambient CO_2 (C_i=250 μbar), activation state decreased from the highest value of 85 % at 30 ℃ to 65 % at 40 ℃ (Sage and Kubien, 2007). Two ideas can be extracted from this information. First, we may have underestimated V_{cmax} if Rubisco was not fully activated. Second, plants growing in the field are subjected to variation in temperature. If this altered the activation state of Rubisco, then V_{cmax} derived from field surveys could be confounded by temperature.

For wheat, g_m did not increase greatly at higher temperatures (von Caemmerer and Evans, 2015), but the ability of Rubisco to select CO_2 over O_2 decreases such that photorespiration increases from 25 to 35 ℃ (Figure 2.3). It was possible to fit CO_2 response curves at 35 ℃ to calculate V_{cmax25} in wheat and by making measurements under both 2% and 21% O_2, we were able to untangle the changes in carboxylation and oxygenation as temperature varied. Nevertheless, measurements from plants that have been exposed to 30 to 35 ℃ for a long time need to be used with caution and one needs to be aware that when deriving Rubisco activity, certain assumptions are required.

2.5.3   Effect of temperature in respiration

Respiration occurs in the mitochondria, and it is the process by which plants consume O_2 and release CO_2. Respiration increases with increasing temperature. At temperatures around 5 °C, enzymes have lower maximum catalytic activity and membranes are less flexible, both of which could reduce respiratory flux. At 25°C, enzymatic performance and availability of substrates both increase compared to that at 5°C and membranes are more flexible. These changes help to increase the flux through respiration. However, at higher temperatures, membranes became very fluid, the activity of some enzymes decrease and substrates may become limited, all of which affect the respiration flux (Atkin and Tjoelker, 2003). In Figure 2.3, dark respiration rate per unit leaf area increased with increasing temperature almost doubling from 25 to 35 ℃. Increasing respiration has also been observed for *Spinacia oleracea* L. cv. Torai grown at 15/10 °C and 30/25 °C (Yamori *et al.*, 2005).

2.6   CONCLUSIONS

V_{cmax} and J are valuable traits to be considered when comparing photosynthetic performance between wheat lines. In this chapter, Rubisco kinetic constants from tobacco were combined with several new kinetic constants appropriate for wheat in order to

calculate V_{cmax} from CO_2 response curves measured in the field at different temperatures. The new constants will be useful to reduce environmental error when calculating V_{cmax} for leaf temperatures ranging from 15 to 35 °C. However, data from plants grown for long periods of heat should be considered separately because Rubisco activation state can decline at high temperature. The new kinetic parameters derived in this chapter provide appropriate values for wheat such that analysis will no longer need to assume values derived from tobacco.

CHAPTER 3

Genetic variation for photosynthetic capacity and efficiency in wheat

Centro Experimental Norman E. Borlaug, Cd. Obregón, Mexico. 2013.

3.1 ABSTRACT

This study uses basic physiological mechanisms to understand photosynthetic capacity (V_{cmax25} and J) and efficiency (V_{cmax25}/N_{area}) in wheat to analyse genotypic diversity in relation to fertilizer, plant stage and environment. Four experiments (**Aus1**, **Aus2**, **Aus3** and **Mex**) were carried out to investigate genetic variation for V_{cmax25}, J, and V_{cmax25}/N_{area} in wheat with complementary traits (A, g_s, C_i/C_a, LMA and N_{area}). Genotypes for **Aus1** and **Aus2** were grown in the glasshouse with two fertilizer levels. Genotypes for **Aus3** and **Mex** experiments were measured in the field in Australia and Mexico respectively; **Mex** genotypes were measured at two plant stages. Results showed that V_{cmax25} and J are robust parameters to assess photosynthetic capacity since they did not depend on g_s or grain filling and V_{cmax25} was positively correlated with Rubisco measured *in vitro*. The main nitrogen effect and development stage did not influence the ranking of genotypes for V_{cmax25}, J and V_{cmax25}/N_{area}. However, growing conditions and geographical location affected ranking of the genotypes. There was significant genotypic variation in most of the experiments for V_{cmax25}, J and V_{cmax25}/N_{area}, except for genotypes measured in Mexico.

3.2 INTRODUCTION

The efficiency of crop production has been defined in thermodynamic terms as the ratio of energy output (carbohydrate) to energy input (solar radiation), which is given by the slope of the relationship between dry matter production and intercepted radiation (g MJ^{-1}) (Monteith, 1977). This parameter is also termed radiation use efficiency (RUE) and its importance is evident in the link with biomass and yield (Equation 1.1). Evidence from modelling and CO_2 enrichment suggests that RUE of wheat could be increased ~50% with improvement in photosynthetic traits (Reynolds *et al.*, 2012b). In the past, assimilation rate (A) has been used to assess photosynthesis in wheat. Some studies have shown diversity in A across wheat genotypes and a positive, minimum or no correlation with yield or with modern wheat genotypes (Murthy *et al.*, 1979; Reynolds *et al.*, 1994; Fischer *et al.*, 1998b; Gutierrez-Rodriguez *et al.*, 2000; Reynolds *et al.*, 2000; Sadras *et al.*, 2012).

Two additionally important parameters to assess photosynthetic performance are Rubisco activity (V_{cmax}) and electron transport rate (J). These parameters can be extracted by modelling the physiological response of leaves to CO_2 and light (Farquhar *et al.*, 1980). While these parameters require more than a single point measurement of A, they have proven to be robust traits to assess photosynthetic capacity in C$_3$ plants since they do not depend on stomatal conductance (g_s) as is the case for simple measurements of A (Condon *et al.*, 2004). In the last 20 years V_{cmax} and J have become common parameters used in plant

physiology and ecophysiology, probably because of the availability of portable tools to assess A in the field (Long *et al.*, 1996) . However, few papers have been published analysing genetic variation for V_{cmax} and J in wheat (Driever *et al.*, 2014; Jahan *et al.*, 2014) and these measurements were done in isolation from other important leaf parameters. If we intend to use such derived traits for selecting wheat varieties with high RUE, it is necessary to compile more information about the genotypic variation for V_{cmax} and J and have a better understanding of these traits. At present there is no published data for wheat analysing genotypic variation for photosynthetic capacity and efficiency using V_{cmax} and J measured in the field.

Leaf nitrogen is also relevant to the study photosynthetic performance because around 30% of leaf nitrogen from a C_3 sun plant is invested in CO_2 fixation and 23% directly in Rubisco protein (Evans and Seemann, 1989). It has also been observed that while A is positively correlated with leaf nitrogen, there is variation in A for a given leaf nitrogen content (Evans, 1989). These data indicate that higher leaf nitrogen does not always indicate higher photosynthetic capacity. Carboxylation efficiency (carboxylase activity per unit of leaf nitrogen) has been used to detect variation in photosynthetic performance between two *Triticum* species (Evans and Seemann, 1984). Therefore, it will be useful to analyse V_{cmax} an indicator of Rubisco activity, as a function on leaf nitrogen per unit area (V_{cmax}/N_{area}), which is termed photosynthetic efficiency in this study.

This chapter analyses photosynthetic capacity (P_c) defined as the amount of investment in photosynthetic machinery per unit leaf area (i.e. V_{cmax} and J) when photosynthesis is not limited by water, light or nitrogen, and photosynthetic efficiency (P_{eff}) as the photosynthetic carbon gain in the leaf per unit of nitrogen invested per unit leaf area. The chapter analyses genotypic variation for these metrics of photosynthetic performance from two perspectives. Firstly, analysing photosynthesis from plant physiological and biochemical mechanisms and secondly assessing photosynthetic diversity under different conditions.

Determining the physiological mechanisms underlying variation in photosynthetic traits will permit us to understand the relationship between leaf biochemistry and leaf anatomy; in this case by measuring leaf dry mass per unit area (LMA). LMA is the ratio between leaf dry mass and leaf area, and correlates with the leaf lamina thickness. LMA comprises different leaf compounds from non-structural and structural carbohydrates, proteins, lignin, lipids, minerals, organic acids, and the density of epidermal cells and mesophyll cells which contain a large number of chloroplasts. High LMA can be due to a thick leaf and/or high leaf density, and a higher chloroplast area (Poorter *et al.*, 2009).

Assessing photosynthetic diversity under different conditions will help to understand P_c and P_{eff} in relation to genotypic variation, plant stage and environment. Complementary measurements such as g_s and the ratio of internal to atmospheric CO_2 concentration (C_i/C_a) are used here to assess the water exchange in leaves (Evans and von Caemmerer, 1996; Condon *et al.*, 2004). SPAD is used as a rapidly measured non-destructive surrogate for chlorophyll content (Konica Minolta, 2009-2013). In some cases yield component traits were measured to have a better understanding of plant life cycle and phenology as longer duration of photosynthetic activity can also be related to prolonged demand for grain filling (Evans, 1993).

The objectives of this chapter are to analyse photosynthetic variation between elite wheat genotypes at the leaf level. V_{cmax} and J will be evaluated to assess P_c considering A as conventional trait to assess photosynthesis. V_{cmax}/N_{area} as a trait to assess P_{eff} will be explored and analysed across different wheat genotypes. Environmental conditions will be tested to understand the factors that influence P_c and P_{eff} across the elite wheat genotypes.

3.3   MATERIALS AND METHODS

3.3.1   Experiments

Results were organised in four experiments (Table 3.1). Experiment **Aus1** was set up in a glasshouse at CSIRO Black Mountain, Canberra (-35.271875, 149.113982), from March 31st to June 30th 2012, artificial light was used in June to extend the photoperiod to 16 h and temperature was controlled to 25/15 °C (day/night). Two seeds were sown in cylindrical pots of 1.06 L (15 × 5cm) with 75:25 loam:vermiculite containing basal fertilizer, and one plant per pot was kept for the experiment which was organized in a randomized block design, three blocks representing each repetition for the high nitrogen treatment (+N) and other three blocks for the low nitrogen treatment (-N). Extra fertilizer Thrive (~300 mL per pot of 1.77g L^{-1}N:27%, P:5.5%, K:9%) was applied each week for +N treatment until 83 DAE. A severe low nitrogen treatment was obtained irrigating the pots with water without fertilizer 1.5 month before measurements. Plant emergence was on April 8th. 23 days after emergence (DAE) and the flag leaf was measured at anthesis (GS58-69) from 73 to 83 DAE. The collection of plants used in this experiment is called the "early vigour set" and it was measured at anthesis so the acronym used for these data is EVA ("early vigour anthesis"); further information is described in the germplasm section. Six to seven genotypes per day at similar plant stage with three repetitions were measured and sampled. Details of traits are in section 3.3.4.

Table 3.1 Details of experiments

Set of genotypes	Description	Key measurements	
		Stage	**Traits**
Aus1 = Glasshouse experiment. CSIRO Black Mountain, Australia (2012)			
EVA(-N),(+N)	16 genotypes	Anthesis	A, V_{cmax25}, J
	3 repetitions	73-83 DAE	SPAD, N_{area}
	Low/high N		
Aus2 = Glasshouse experiment. CSIRO Black Mountain, Australia (2012)			
BYPB(-N),(+N)	30 genotypes	Pre-anthesis	A, V_{cmax25}, J
	2 repetitions	48-56 DAE	SPAD, N_{area}
	Low/high N		
Aus3 = Field experiment. GES-CSIRO, Australia (2013)			
BYPB	28 genotypes	Pre-anthesis	A, V_{cmax25}, J
	4 repetitions	46-54 DAE	SPAD, N_{area}
EVA	2 genotypes	Anthesis	A, V_{cmax25}, J
	4 repetitions	62-67 DAE	SPAD, N_{area}
CA	21 genotypes	Anthesis	A, V_{cmax25}, J
	4 repetitions	60-67 DAE	SPAD, N_{area}
Mex = Field experiment. CENEB-CIMMYT, Mexico (2012-2013)			
CB	30 genotypes	Pre-anthesis	A, V_{cmax25}, J_g, J_f
	3 repetitions	67-82 DAE	SPAD, N_{mass}
CA	30 genotypes	Anthesis	A, V_{cmax25}, J_g, J_f
	3 repetitions	88-103DAE	SPAD, N_{mass}, N_{area}

EV= Early vigour set; BYP= BUNYIP set; C= CIMCOG set. B= before anthesis (pre-anthesis); A= anthesis.   DAE= Days after emergence. See text for traits abbreviations.

Experiment **Aus2** was carried out in a glasshouse at CSIRO Black Mountain, Canberra (-35.271875, 149.113982), from October 12th to December 11th 2012, and temperature was controlled to 25/15 °C (day/night). Three seeds were sown in pots of 5 L with 75:25 loam:vermiculite soil mix containing basal fertilizer, and two plants per pot were kept for the experiment which was organized in a randomized block design, two blocks representing each repetition for the high nitrogen treatment (+N) and one block for the low nitrogen treatment (-N). For the +N treatments extra fertilizer Aquasol (~300 mL per pot of 1.77g L^{-1}N:23%, P:4%, K:18%) was applied every three days from 41 days after emergence (DAE) to 56 DAE. Treatment –N was less severe than **Aus1**, it was obtained irrigating the plants with water without fertilizer 10 days before measurements. Plant emergence was on October 17th and the flag leaf was measured before anthesis (GS49-57) from 48 to 56 DAE. Measurements were done in one plant per pot for +N and in the two plants per for –N. The collection of plants used in this experiment is called BUNYIP and it was measured before anthesis so the acronym used is BYPB. Details of germplasm used

are below in section 3.3.2. Six to ten genotypes per day at similar plant stage with two repetitions were measured and sampled.

Experiment **Aus3** was carried out in the field at CSIRO Experimental Station at Ginninderra (GES), Australia (-35.199837, 149.090898) from September 25th to December 17th, 2013. The emergence of plants was on October 4th, 2013. From 1 to 75 DAE the average maximum from daily temperature (Figure 3.1) was 22.4 °C and the minimum 7.7 °C, in total 142 mm of rain and an accumulative thermal time of 1,126.8 °C. CA and EVA subsets of wheat genotypes were sown in the same experimental design of two randomized blocks. Each block was subdivided into 30 plots (5 × 6). Next to this experimental design, another experimental design of two randomized blocks for the BYPB collection was sown. In this case, each block was subdivided into 42 plots (7 × 6). Each plot for both experimental designs was 5 m × 1.8 m. It contained a single genotype sown in 10 rows, 18 cm apart, and approximately 200 plants m^{-2}. Plots were fertilized and irrigated optimally in all conditions. The BYPB subset of wheat genotypes was measured in the flag leaf before anthesis (GS40-55) from 46-54 DAE where the maximum temperature reached was 28.3 °C and the minimum 5.4 °C. When EVA (GS69, 62-67 DAE) and CA (GS56-69, 60-67 DAE) subset of wheat genotypes were measured, the maximum temperature reached was 32.2 °C and the minimum 4.3 °C. Measurements and sampling were done twice in two plots, resulting in 4 repetitions for 4 to 5 genotypes per day that were at similar plant stage. In this experiment many plants were at the same stage at the same time and fewer wheat genotypes could be measured: 2 wheat genotypes from EVA, 20 wheat genotypes and 6 triticale genotypes from BYPB, and 22 wheat genotypes from CA. They are marked with asterisk in tables 3.2 and 3.3. Details of germplasm used are in section 3.3.2.

Experiment **Mex** was carried out in the field at *Centro Experimental Norman E. Borlaug* (CENEB) research station, located in the Yaqui Valley, Sonora, Mexico (27.370837, -109.930362) for a winter-spring cycle. The sowing was on November 23rd, 2012 and the harvest on April 30th and May 2nd 2013 (150 and 152 DAE respectively). Plant emergence was on 2nd, December, 2012. From the 1 to 138 DAE, the average maximum temperature from daily temperature (Figure 3.1) was 26 °C and the minimum 8.3 °C, in total 15.38 mm of rain and an accumulative thermal time of 2,364.6 °C. Plants were organised in a randomised 5 × 6 lattice experimental design with three repetitions. Each repetition (10 × 3 plots) enclosed two subdivisions of 5 × 3 plots. Each plot (2.4 m × 8.5 m) contained a single genotype sown in 6 rows, two beds in the middle with two rows each and two beds in the edges with one row of the same genotype, the second row in the edges corresponded

to the next genotype or a filling genotype. Beds followed the system 56-24, where 56 cm is the furrow width and 24 cm is the raised bed width. Plants were grown under optimal management in the field. There were in total five auxiliary irrigations, the total 500 mm of water applied. First fertilization was at soil preparation with 50 kg ha^{-1} of N and 50 kg ha^{-1} of P and a second fertilization in the first irrigation of 150 kg ha^{-1} of N. The CB subset of wheat genotypes was measured in the flag leaf before anthesis (GS49-57) from 67 to 82 DAE, where the maximum temperature reached was 29.7 °C and the minimum 1.5 °C. The CA subset of wheat genotypes was measured in the flag leaf at anthesis (GS60-69) from 88 to 103 DAE, where the maximum temperature reached was 32.1 °C and the minimum 2.5 °C. Measurements and sampling were done in one plant per plot; 3 to 6 genotypes per day were measured at similar plant stage with 3 repetitions.
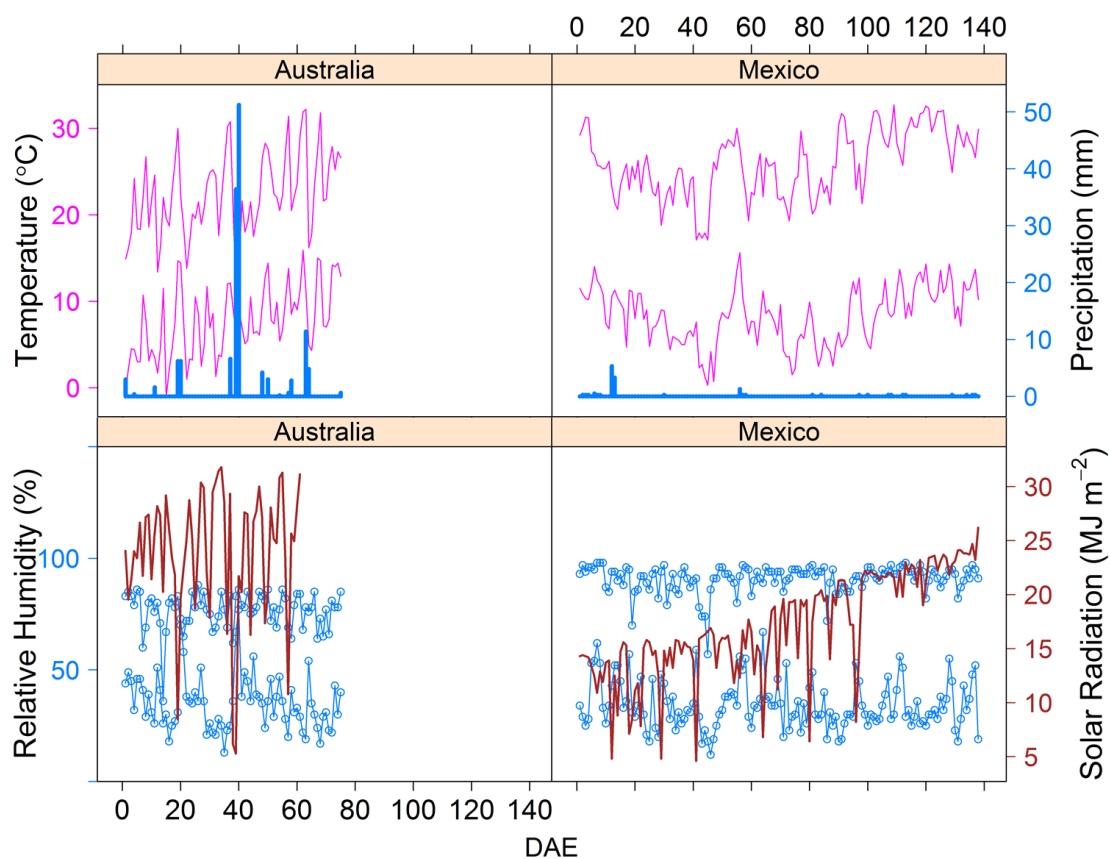
Figure 3.1 Meteorological conditions in Obregon, Mexico and Ginninderra, Australia. Daily observations from days after emergence (DAE) during measurements in Australia (1-75 DAE) and in Mexico (1-38 DAE). Minimum and high temperature in pink, precipitation in blue bars, minimum and maximum humidity (white circles) and solar radiation in red.

3.3.2 Germplasm

As described three sets of wheat/triticale genotypes were used in these experiments (Table 3.2).

Table 3.2 List of wheat genotypes used for early vigour and BUNYIP set.

Early Vigour (EV)			BUNYIP (BYP)					
Gen	**Name**	**Type**	**Gen**	**Name**	**Type**	**Gen**	**Name**	**Type**
V1	Bencubbin	BW	*V15	Abacus	T	*V31	Kosciusko	T
V2	Halberd	BW	*V16	Axe	BW	*V32	Mace	BW
V3	K1056	BW	*V17	Bogong	T	*V33	Magenta	BW
V4	Nacozari	BW	*V18	Bolac	BW	*V34	Merinda	BW
V5	Oasis	BW	*V19	Canobolas	T	*V35	Pastor	BW
V6	Sunstar	BW	*V20	Caparoi	DW	*V36	Scout	BW
V7	W010311	BW	*V21	Chopper	T	*V37	Speedee	T
*V8	W020308	BW	*V22	Derrimut	BW	*V38	Spitfire	BW
*V9	W100104	BW	*V23	Drysdale	BW	*V39	Super Seri	BW
V10	W130114	BW	*V24	Emu Rock	BW	*V40	Tahara	T
V11	W170316	BW	*V25	Espada	BW	*V41	Weebil	BW
V12	W210308	BW	V26	H45	BW	V42	Yenda	BW
V13	W610501	BW	*V27	Hawkeye	T	V43	Zebu	BW
V14	W650208	BW	*V28	Hunter	BW	V44	Zulu	DW
V75	Quarrion	BW	*V29	Hyperno	DW			
V76	Pitic	BW	*V30	Jaywick	T			

T, Triticale genotypes. DW, Durum wheat. BW, Bread wheat. *Genotypes measured in the field in Australia (Aus3).

(1) Early Vigour (EV) set consisted of 16 wheat genotypes from CSIRO in Australia. Genotypes from V1 to V6, V75 and V76 have shown differences in photosynthesis in previous experiments and genotypes from V7 to V14 are characterized to have greater embryo, fast leaf area development and low leaf mass area. **(2) A subset of the Best and Unreleased Yield Potential (BUNYIP)** that contains 21 wheat genotypes and 9 triticale genotypes with high yield in Australia. **(3) CIMMYT Core Germplasm (CIMCOG) Subset II** has 30 wheat genotypes selected at CIMMYT (International Maize and Wheat Improvement Center) for high yield (Table 3.3). Acronym for BUNYIP will be '**BYP**', for CIMCOG will be '**C**' and for Early Vigour will be '**EV**'. An additional letter will be added to each acronym, '**B**' meaning before anthesis, and '**A**' meaning anthesis.

Table 3.3 List of wheat genotypes used for CIMCOG Subset II.

		CIMCOG Subset II (C)
Gen	**Type**	**Name**
*V45	BW	BABAX/LR42//BABAX/3/VORB
V46	BW	BACANORA T 88
*V47	BW	BCN/RIALTO
V48	BW	BECARD/KACHU
V49	BW	BRBT1*2/KIRITATI
*V50	BW	SAUAL/4/CROC_1/AE.SQUARROSA (205)//KAUZ/3/ATTILA/5/SAUAL
V51	BW	SAUAL/WHEAR//SAUAL
*V52	BW	CMH79A.955/4/AGA/3/4*SN64/CNO67//INIA66/5/NAC/6/RIALTO
*V53	WD	CIRNO C 2008
*V54	BW	CNO79//PF70354/MUS/3/PASTOR/4/BAV92*2/5/FH6-1-7
*V55	BW	CROC_1/AE.SQUARROSA(205)//BORL95/3/PRL/SARA//TSI/VEE#5/4/FRET2
V56	BW	KINGBIRD #1//INQALAB 91*2/TUKURU
*V57	BW	MILAN/KAUZ//PRINIA/3/BAV92
V58	BW	PAVON F 76
*V59	BW	PBW343*2/KUKUNA*2//FRTL/PIFED
*V60	BW	PFAU/SERI.1B//AMAD/3/WAXWING
*V61	BW	SERI M 82
*V62	BW	SIETE CERROS T66
*V63	BW	SOKOLL//PBW343*2/KUKUNA/3/ATTILA/PASTOR
*V64	BW	TACUPETO F2001/SAUAL/4/BABAX/LR42//BABAX*2/3/KURUKU
*V65	BW	TACUPETO F2001/BRAMBLING*2//KACHU
*V66	BW	TC870344/GUI//TEMPORALERA M 87/AGR/3/2*WBLL1
*V67	BW	TRAP#1/BOW/3/VEE/PJN//2*TUI/4/BAV92/RAYON/5/KACHU
*V68	BW	UP2338*2/4/SNI/TRAP#1/3/KAUZ*2/TRAP//KAUZ/5/MILAN/KAUZ//CHIL/CHUM18/6/UP2338*2/4/SNI/TRAP#1/3/KAUZ*2/TRAP//KAUZ
*V69	BW	BECARD
V70	BW	WBLL1*2/KURUKU*2/5/REH/HARE//2*BCN/3/CROC_1/AE.SQUARROSA(213)//PGO/4/HUITES
*V71	BW	YAV_3/SCO//JO69/CRA/3/YAV79/4/AE.SQUARROSA(498)/5/LINE1073/6/KAUZ*2/4/CAR//KAL/BB/3/NAC/5/KAUZ/7/KRONSTAD F2004/8/KAUZ/PASTOR//PBW343
*V72	BW	BECARD
*V73	BW	KFA/3/PFAU/WEAVER//BRAMBLING/4/PFAU/WEAVER*2//BRAMBLING
V74	BW	WBLL1*2/4/BABAX/LR42//BABAX/3/BABAX/LR42//BABAX

T, Triticale genotypes. DW, Durum wheat. BW, Bread wheat. *Genotypes measured in Australia (Aus3).

3.3.3   Developmental stages

The Zadoks scale was used to describe the growth stages (GS) of wheat (Zadoks *et al.*, 1974). The first day after emergence (DAE) is considered at GS10, when at least 50% of the seedlings showed the first lamina in the soil surface. Here, before anthesis (B) or pre-anthesis refers to booting and heading stage between GS41-57. After anthesis (A) refers to Anthesis +7 days sampling, this stage is important because the spike reaches the maximum dry weight, the grain weight is insignificant and the water soluble carbohydrate reserves in stem are at their peak (Pask, 2012). In some cases measurements at anthesis were done at

the end of heading and up to 10 days after anthesis between GS56-69. In the experiments section, GS details are specified for each experiment.

3.3.4 Traits measured

Gas exchange was measured with a LICOR LI-6400XT infrared gas analyser (LI-COR Inc., Lincoln, NE, USA); the 6 cm^2 rectangular head was used for experiments **Aus1**, **Aus2** and **Aus3**, and the 2 cm^2 circular head from the fluorescence head (Li-6400-40; LI-COR Inc.) for the **Mex** experiment. Gas exchange was used to measure the photosynthetic rate at 400 inlet µmol CO_2 mol^{-1} (A), stomatal conductance (g_s), the of internal to atmospheric CO_2 concentration (C_i/C_a) and CO_2 response curves to obtain the maximum Rubisco activity at 25 ºC (V_{cmax25}) and the electron transport rate (J or J_g). V_{cmax25} and J were calculated, using the kinetic constants obtained in Chapter 2 and the leaf biochemical model of photosynthesis (Farquhar *et al.*, 1980). In **Mex** experiments, electron transport rate (J_f) was measured with the fluorescence chamber at 400 inlet µmol CO_2 mol^{-1}. SPAD-502 chlorophyll meter (Minolta Camera Co., Ltd, Japan) was used as a surrogate for chlorophyll content (Mullan and Mullan, 2012) to measure flag leaves.

Flag leaves measured for gas exchange experiments **Aus1**, **Aus2** and **Aus3** were sampled three centimetres up and down from the chamber to determine leaf mass area and nitrogen content. Area of the leaf samples was calculated from a digital photo using the program ImageJ 1.47v. Samples were dried then for 48h at 70°C and weighed to obtain leaf mass area (LMA, g m^{-2}). Nitrogen concentration, N_{mass} (N mg g^{-1}) was determined on the same samples by flow injection analysis (QuikChem® Method, Lachat Instruments, CO. USA) after the Kjeldahl digestion of leaves at the Australian National University (ANU). For **Mex** experiments, a complete flag leaf was measured using a leaf area meter (LI3050A/4; LICOR, Lincoln, NE), then, dried for 48h at 70°C and weighed to obtain leaf mass area (LMA, g m^{-2}). Nitrogen concentration, N_{mass} (N mg g^{-1}) was determined at CIMMYT Batan, Mexico with the Technicon AutoAnalyzer II method, where samples are digested and analysed in the Technicon AutoAnalyzer (Galicia *et al.*, 2008). N_{mass} and LMA were used to calculate nitrogen per leaf area N_{area} (N g m^{-2}).

Rubisco content *in vitro* was measured for genotypes Espada, Merinda, Mace, Drysdale and Hawkeye measured in the **cabinet** (see Chapter 2), **Aus2** and **Aus3** experiments. Immediately following gas exchange measurements, the piece of leaf that was in the LI-6400XT chamber was frozen in liquid nitrogen and stored at -80 °C for later determination of Rubisco content. Rubisco content *in vitro* was quantified from frozen leaf samples. About 0.25 cm^2 of leaf tissue was ground in a Ten Broek homogenizer in 1 mL of ice-cold

extraction buffer (50mM Epps-NaOH pH 8.0, 1mM EDTA, 1%(w/v) PVPP, 10mM MgCl$_2$, 10mM NaHCO$_3$, 10mM 1M DTT, 0.01% Triton) with 5µL of plant protease inhibitor cocktail Sigma, and centrifuged at 17,000g for 5 min at 4 °C. 25µL of the supernatant liquid plus 75µL extraction buffer were mixed and incubated with 1µL ^{14}C-labelled carboxy arabinitol-1,5-bisphosphate (CABP) at room temperature. After more than 30 min, [^{14}C]CABP bound to Rubisco was separated from free [^{14}C]CABP using gel filtration through 0.7 × 27 cm columns of Sephadex G-50 fine, equilibrated with 20 mM Bicine-NaOH buffer, pH 8, containing 75 mM NaCl. Fractions with Rubisco-CABP complexes were collected and [^{14}C]CABP was determined by liquid scintillation using a Liquid Scintillation Analyzer, Tri-Carb 2800TR from Perkin Elmer.

V_{cmax25}/N$_{area}$ was used to represent photosynthetic efficiency (P_{eff}). A, V_{cmax25} and J were used to represent photosynthetic capacity (P_c). LMA, N$_{mass}$, N$_{area}$ and SPAD were used to understand leaf structure.

3.3.5 Gas exchange measurements details

The flow rate in the CO$_2$ chamber of the Li-Cor was set at 500 µmol s^{-1} for the 6 cm^2 head and 350 µmol s^{-1} for the 2 cm^2 head, irradiance at 1800 µmol quanta m^{-2} s^{-1}, and block temperature at 25 °C. However, at high temperatures, it was difficult to control temperature resulting in higher leaf temperature. Full CO$_2$ response curves were measured in all experiments. The inlet CO$_2$ was modified each experiment depending on the place and conditions of measurements, since there was a trade-off of time and the number of points to use to increase the accuracy of the fitting. In some cases a higher inlet CO$_2$ was used to get saturation levels. The inlet CO$_2$ for each experiment is underline below:

- o **EVA-Aus1:** 50, 100, 250, 400, 800 µmol CO$_2$ mol^{-1}.
- o **BYPB-Aus2:** 50, 100, 250, 400, 800 µmol CO$_2$ mol^{-1}.
- o **CB-Mex**: 50, 150, 400, 800 µmol CO$_2$ mol^{-1}.
- o **CA-Mex:** 50, 100, 250, 400, 600, 800 µmol CO$_2$ mol^{-1}.
- o **BYPB-Aus3**: 50, 100, 250, 400, 800 µmol CO$_2$ mol^{-1}.
- o **EVA and CA-Field-Aus3:** 50, 150, 250, 400, 600, 800, 1200 µmol CO$_2$ mol^{-1}.

Mesophyll conductance (g$_m$) was based on the average of 6 different plants from the triticale Hawkeye measured with carbon isotope techniques that combine tunable diode laser spectroscopy and gas exchange at CSIRO Black Mountain, resulting in 0.55 mol m^{-2} s^{-1} bar^{-1} (Estavillo *et al.,* – unpublished data). This value also agrees with measurements done in wheat genotypes (von Caemmerer and Evans, 2014). 0.55 mol m^{-2} s^{-1} bar^{-1} was divided

by the average of assimilation rate of all genotypes measured in all experiments (**Aus1**, **Aus2**, **Aus3** and **Mex**), A=25 µmol CO_2 m^{-2} s^{-1}, which corresponded to C_i = 260 µmol CO_2 mol^{-1} and to the 400 inlet µmol CO_2 mol^{-1}. In order to know A at intracellular CO_2 (C_i) of 260 µmol CO_2 mol^{-1} (A_{260}) for each CO_2 response curve a linear regression from 50 to 400 inlet µmol CO_2 mol^{-1} for was used. The final formula used is: g_m= $(0.55/25)*A_{260}$ (Details in Chapter 2).

3.3.6 Yield components

Yield components were measured in the experiment **Mex** after wheat physiological maturity following CIMMYT protocols (Pietragalla and Pask, 2012). Yield (Mg ha^{-1}) was calculated from a subsample of grain harvested in 4.8 m^2 and dried. Harvest Index, HI is the ratio of grain dry weight from 100 spikes and the total plant dry weight. Biomass at maturity BMM (Mg ha^{-1}) was calculated from HI/Yield. Biomass at flowering, BMF (Mg ha^{-1}) was obtained from dry biomass sampled in 4.8 m^2 when plants were flowering, GS61-62.

Growth Rate, GR (g m^{-2} day^{-1}) is calculated as the difference between the dry biomass after anthesis (GS61+7 days) and the dry biomass before anthesis (GS41), divided by the days from this period, because gas exchange measurements were made during this period. Biomass was sampled using plants from 50 cm transects from four furrows of two beds in the middle of the plot (0.8 m^2).

Days to flowering (DTF) are the number of days after seedlings emergence at flowering, GS61-62. Percentage Grain Filling, PGF (%) = (DTM-DTF)/DTM *100. DTM is he number of days after seedlings emergence to physiological maturity. Physiological maturity is considered at GS87 when the grain reaches the maximum dry weight and it becomes viable.

3.3.7 Statistical analysis

The analysis of variance (ANOVA), Tukey's HSD test and the Pearson correlations for phenotypic correlations were carried out with the package *Agricolae* in R statistical software, version 3.1.3 (2015-03-09) (de Mendiburu, 2015). Pearson correlations were calculated from the mean of each genotype (Tables 3.9, 3.11, A6, A8, A10).

3.4 RESULTS

3.4.1 Experimental overview

This section shows the ranges of traits measured in four experiments, **Aus1**, **Aus2**, **Aus3** and **Mex** (Figure 3.2, Figures A2-A3, see section 3.3.1). The data will be used to analyse photosynthetic capacity and efficiency, starting with the basic leaf mechanisms in photosynthesis, and then analysing leaf-photosynthetic diversity for each set of wheat genotypes, EVA, BUNYIP and CIMCOG.
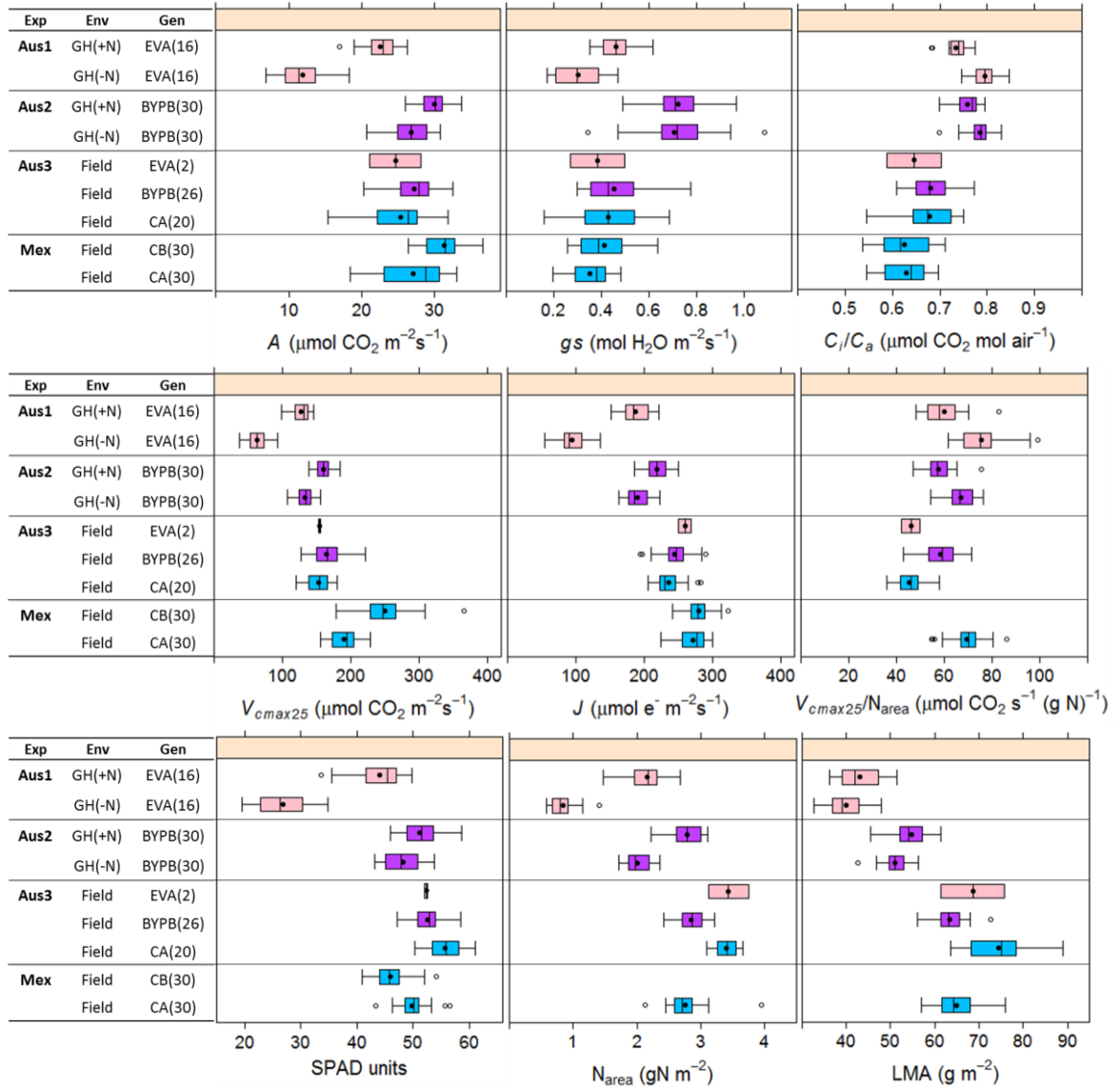
Figure 3.2 Experimental overview. *A*, g$_s$, *C$_i$/C$_a$*, *V$_{cmax25}$*, *J*, *V$_{cmax25}$*/N$_{area}$, SPAD, N$_{area}$ and LMA in Early vigour set, EV (pink); BUNYIP set, BYP (purple); and CIMCOG set, C (blue) grown in different environments and measured at different stages as described in Table 3.1. Boxplots represent the distribution of the data. The coloured section is the interquartile range (IQR), representing 50% of the data. The lower IQR edge is the point at 25% of the data. The middle black point is the mean and the line the median. The upper IQR edge is the 75% point. The whiskers are 1.5 times IQR, showing the minimum and maximum data. Blue circles are outliers.

3.4.2 Mechanistic understanding of photosynthesis in wheat

The velocity of carboxylation (V_{cmax}) represents Rubisco activity *in vivo* inferred from non-destructive measurements on living plants, but it can also be measured *in vitro* from leaf samples. Rubisco is present in leaves as an abundant component of chloroplasts and chloroplast and Rubisco account for a high percentage of leaf nitrogen. Anatomical parameters such as leaf mass per unit dry area (LMA) can reflect high leaf density/thickness and higher chloroplast area. For this reason, in this section Rubisco *in vivo* and Rubisco *in vitro* are analysed as a function of LMA and nitrogen per leaf area (N_{area}).

3.4.2.1 Rubisco in vivo

When LMA and V_{cmax25} were compared across genotypes, a large range for V_{cmax25} was observed over a relatively small range of LMA (Figure 3.3.a). Plants grown with low nitrogen (**EVA -N_Aus1**) seemed to have similar leaf density/thickness as the high nitrogen treatment (**EVA +N_Aus1**). Similar behaviour was observed for **BYPB -N_Aus2** and **BYPB +N_Aus2**. These observations raise the question of whether Rubisco measured *in vitro* behaves similarly at high and low fertilizer treatment.
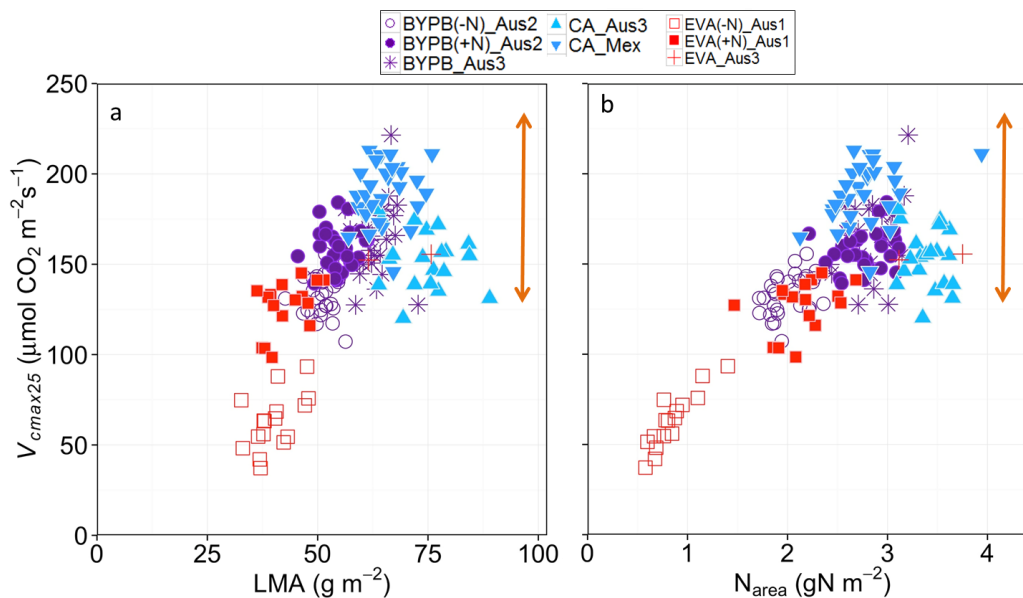
Figure 3.3 V_{cmax25} as a function of a) leaf mass area (LMA), and b) nitrogen (N_{area}) for wheat genotypes grown in different environments and measured at different stages as described in Table 3.1. Symbols represent means of each genotype. The arrow represents the diversity of V_{cmax25} for a given LMA or N_{area}.

At low leaf N, there was a positive correlation between V_{cmax25} and N_{area}, but at higher nitrogen content the correlation was low, which suggests that there is significant variability in V_{cmax25} for a given nitrogen investment at high leaf nitrogen contents per unit leaf area (Figure 3.3.b). Potentially, this parameter, V_{cmax25}/N_{area}, could be used to uncouple measurements of V_{cmax25} from leaf nitrogen, and this trait is used to explore photosynthetic efficiency (P_{eff}) across wheat genotypes.

3.4.2.2 Rubisco in vitro

Four wheat genotypes and one triticale genotype from the BYPB set were selected based on P_{eff} (V_{cmax25}/N_{area}) to measure leaf Rubisco *in vitro* (by the CABP binding assay). Genotypes from EVA and BYPB were ranked based on the mean of repetitions. For the BYPB set, the means were considered from genotypes measured in the glasshouse (**Aus2**) and field (**Aus3**) (Figure 3.4).
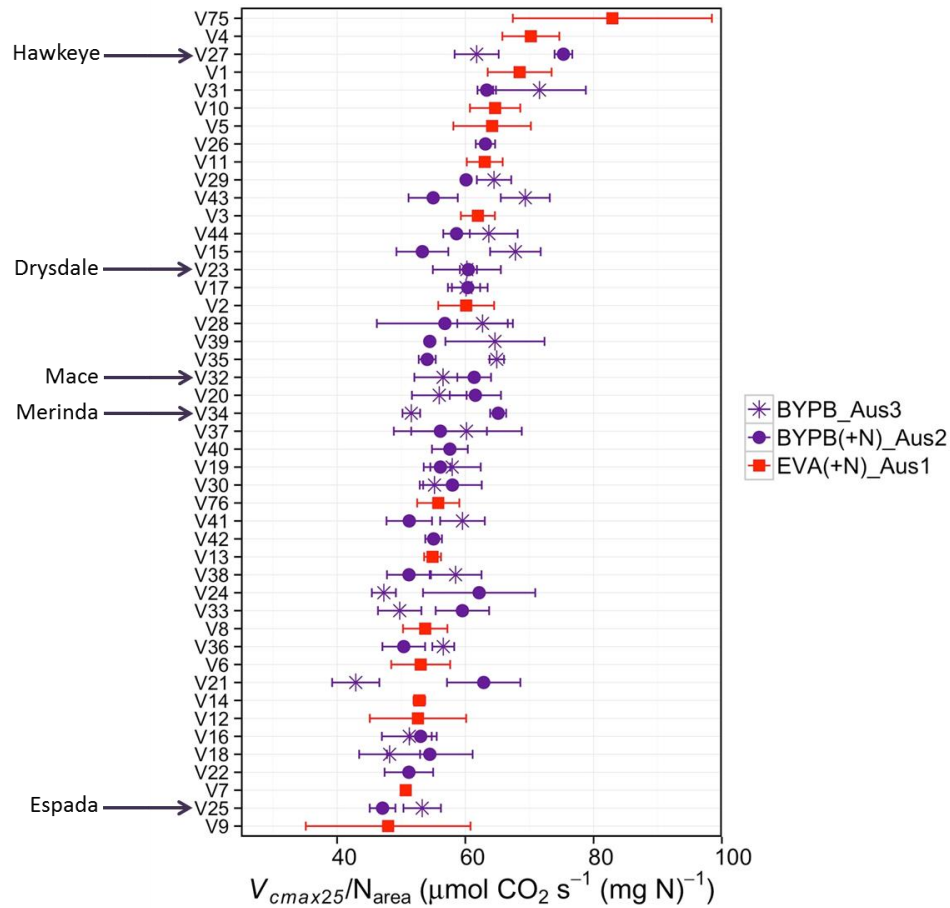
Figure 3.4 Diversity of photosynthetic efficiency represented by V_{cmax25}/N_{area} of the early vigour set (EVA +N_Aus1) and BUNYIP Set measured in the glasshouse (BYPB +N_Aus2) and in the field (BYPB_Aus3). Genotypes labelled were selected for Rubisco *in vitro* measurements of Rubisco. Genotypes were ranked based on the mean of repetitions. For the BYPB set, the means were considered from genotypes measured in the glasshouse (Aus2) and field (Aus3).

The BYPB set was measured in the **cabinet** (see Chapter 2), in the glasshouse with two levels of nitrogen (**Aus2**), and in the field (**Aus3**) so genotypes from this set were chosen to measure leaf Rubisco *in vitro*. The genotypes (Espada, Merinda, Mace, Drysdale and Hawkeye) were selected to cover the range between EVA and BYPB, from lower to higher V_{cmax25}/N_{area} (Figure 3.4).

Measurements of Rubisco *in vitro* (CABP binding) were compared to Rubisco *in vivo* (V_{cmax25}) and related to LMA and N_{area} using leaf samples from genotypes measured in the growth cabinet**,** glasshouse, and field.

V_{cmax25} showed a positive relationship with Rubisco *in vitro* although it was not directly proportional. Consequently, V_{cmax25} per Rubisco declined as Rubisco content per unit leaf area increased (Figure 3.5).

Results of this experiment show that LMA did not correlate with the Rubisco content *in vitro*. Rubisco content varied almost threefold while LMA varied between 45.8 to 65 g m^{-2} (Figure 3.6.a). This confirms the relationship within a given experiment already shown in Figure 3.3.a. Leaf nitrogen showed a positive correlation with Rubisco *in vitro* and diversity for a given N_{area} (Figure 3.6.b), in general similar to V_{cmax25} (Figure 3.3.b).
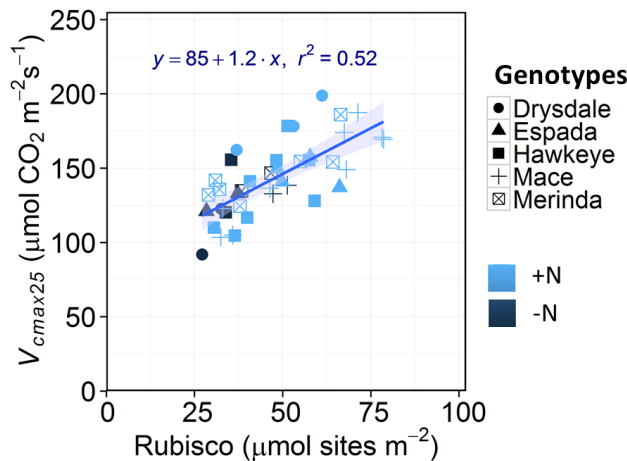
Figure 3.5 Maximum carboxylation rate *in-vivo* (V_{cmax25}) as a function of leaf Rubisco content. Genotypes sampled in the cabinet, glasshouse and field, n=41. The shaded band indicates the level of uncertainty of the regression line.
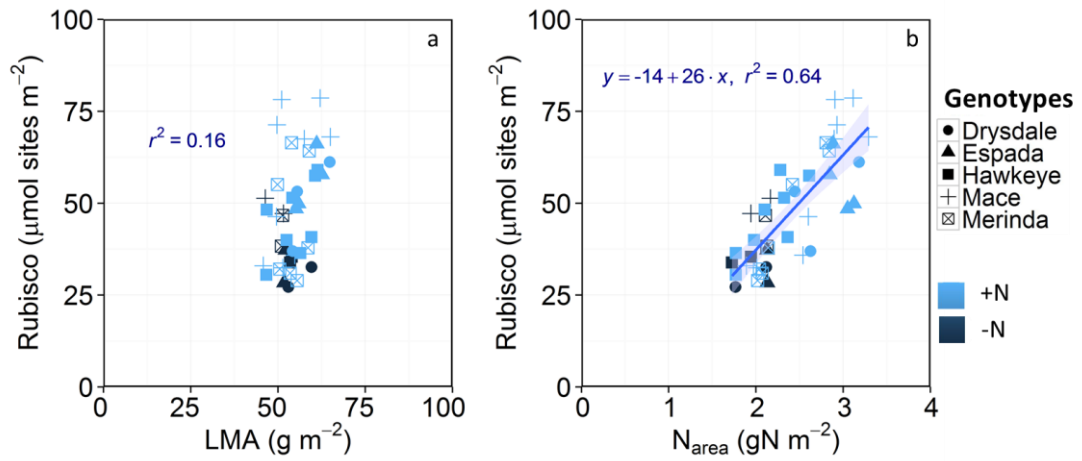
Figure 3.6 Leaf Rubisco content as a function of a. leaf mass area (LMA), b. leaf nitrogen per area (N_{area}). Data from four wheat genotypes and a triticale measured and sampled in the cabinet, glasshouse and field, n=41.

From V_{cmax25}, representing the carboxylation of Rubisco *in vivo*, and Rubisco catalytic sites *in vitro* representing Rubisco content, it is possible to calculate the catalytic turnover rate for Rubisco carboxylation (k_{catc}). This is shown for each genotype in relation to the leaf nitrogen content (Figure 3.7). Even if these five genotypes represent the extremes from EVA and BYPB set, it was difficult to distinguish genetic diversity for k_{catc}. Overall, k_{catc} was not affected by fertilizer treatment. However, k_{catc} was reduced in Espada samples from fertilized compared to unfertilized plants and when comparing k_{catc} in relation to leaf nitrogen, Espada, Mace and Merinda showed a tendency for k_{catc} to decrease at higher N_{area}. Drysdale and Hawkeye showed no trend with N_{area}.
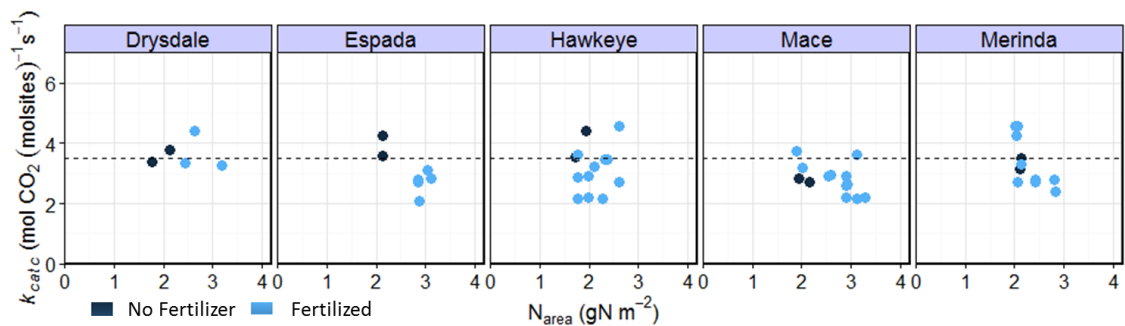
Figure 3.7 Catalytic turnover rate of Rubisco carboxylation (k_{catc}) as a function of nitrogen per leaf area (N_{area}) in four wheat genotypes and a triticale (Hawkeye). Black dot are plants without fertilizer. Blue dots are plants with fertilizer. Samples from plants grown in the glasshouse or in the field are not differentiated. Dotted line is tobacco k_{catc} 3.5 mol $CO_2(molsites)^{-1}s^{-1}$ at 25 °C *in vivo* (von Caemmerer, 2000).

In summary both *in vivo* and *in vitro* measurements of Rubisco showed that Rubisco is not correlated with LMA. This indicates that anatomical constraints have flexibility to enable significant variation in Rubisco content. Regardless of whether Rubisco was derived from gas exchange measurements (Figure 3.3.b) or quantified *in vitro* (Figure 3.6.b). Rubisco is strongly related with leaf nitrogen. It seems that there is variation in Rubisco activity per unit leaf nitrogen V_{cmax25}/N_{area} that can be exploited. V_{cmax25}/N_{area} can be used as one measure of photosynthetic efficiency. However, no evident differences in k_{catc} were detected across 5 genotypes selected on the basis variation in V_{cmax25}/N_{area}.

3.4.3 Genetic diversity in wheat photosynthesis

This section evaluate genetic diversity in wheat photosynthesis at leaf level and the factors (plant stage, nitrogen, and environment) that influence photosynthetic diversity across genotypes. Because the focus of this project was to analyse genetic variation for photosynthetic performance, this section is divided by the sets of genotypes measured: Early Vigour set, BUNYIP and then CIMCOG.

3.4.3.1 Early vigour set wheat genotypes (EVA)

Half of this germplasm set are wheat genotypes selected for early vigour and the other half are elite wheat genotypes. In this section we are interested in determining if there is diversity in photosynthetic traits across early vigour genotypes and elite genotypes, and if strong fertilizer treatment in the glasshouse affects photosynthetic performance.

Nitrogen treatment had a highly significant effect on all variables measured (Table 3.4). The unfertilized treatment reduced A, g_s, V_{cmax25}, J, N_{area}, SPAD and LMA while V_{cmax25}/N_{area} and C_i/C_a increased. Most of the traits were significantly different across genotypes in the ANOVA, and they were also analysed with Tukey's HSD test (A5). Interaction G × N was not significant for gas exchange derived traits, but G × E was significant for LMA, N_{area} and SPAD (Table 3.4).

For experiment **Aus1**, A correlated positively with g_s, V_{cmax25}, J, N_{area}, SPAD and LMA , so that genotypes with high photosynthetic rates had a high maximum velocity of carboxylation, electron transport rate, nitrogen content, chlorophyll content and leaf mass area. Numerous positive correlations were observed among them e.g. V_{cmax25} correlated positively with J, N_{area}, SPAD and LMA (A6).

Table 3.4 EVA set, experiment Aus1. Means from 16 wheat genotypes and 3 repetitions per nitrogen treatment, ANOVA residual standard error (SE) with DF=15. Coefficient of variation percentage (CV%).

Traits	Means		SE	CV%	ANOVA *P-value*		
	-N	+N			Genotype	Nitrogen	G × N
A (μmol CO_2 m^{-2} s^{-1})	11.8	22.6	4	23	0.04	≤0.001	0.3
g_s (mol H_2O m^{-2} s^{-1})	0.3	0.46	0.12	32	0.04	≤0.001	0.4
C_i/C_a (μmol CO_2 mol air^{-1})	0.8	0.74	0.04	4.6	0.06	≤0.001	0.2
V_{cmax25} (μmol CO_2 m^{-2} s^{-1})	62	127	20.6	21.6	0.03	≤0.001	0.4
J (μmol e$^-$ m^{-2} s^{-1})	94	188	28.7	20.3	0.04	≤0.001	0.1
V_{cmax25}/N_{area} (μmol m^{-2} s^{-1}(gN^{-1}))	74.6	60.2	13	19.3	0.02	≤0.001	0.8
N_{area} (N g m^{-2})	0.84	2.1	0.25	16.7	≤0.001	≤0.001	0.05
SPAD	26.6	43.9	4.8	13.7	0.002	≤0.001	0.005
LMA (g m^{-2})	39.9	42.9	4.4	10.6	≤0.001	0.002	0.08

3.4.3.2 BUNYIP wheat genotypes (BYPB)

BUNYIP wheat genotypes are characterized by very high yield in Australia, but some genotypes have not been released as varieties due to other deleterious traits. The objective of this experiment is to find out if there is variation in photosynthetic traits and related traits to photosynthesis in elite wheat genotypes for Australia. In this case BYPB was evaluated twice: one with a fertilizer treatment in the glasshouse, and second measurements from high fertilizer treatment in the glasshouse were compared with the same genotypes grown in the field.

3.4.3.2.1 Effect of fertilizer in BYPB genotypes

–N and +N treatments were less radical than with the **Aus1** experiment in order to generate a medium range of photosynthetic and related parameters. Significant effects of fertilizer treatment on genotypes were still detected in all variables except for g_s (Table 3.5). –N treatment reduced A, V_{cmax25}, J, N_{area}, SPAD and LMA, and increased V_{cmax25}/N_{area}. C_i/C_a was similar in both nitrogen treatments. Interaction of G × N was not significant for any trait.

As with **Aus1**, A correlated positively with g_s, V_{cmax25} and J, so that genotypes with high photosynthetic rate had a high maximum velocity of carboxylation and electron transport rate. J was positively correlated with N_{area} and V_{cmax25} (A8).

Table 3.5 BYPB set, experiment Aus2. Means from 21 wheat and 9 triticale genotypes with 2 repetitions per nitrogen treatment with standard deviation (SD) and coefficient of variation percentage (CV%). ANOVA degrees of freedom =29.

Traits	Means				ANOVA P-value		
	-N	+N	SE	CV%	Genotype	Nitrogen	G × N
A (μmol CO_2 m^{-2} s^{-1})	26.7	30	2.24	7.9	0.003	≤0.001	0.1
g_s (mol H_2O m^{-2} s^{-1})	0.71	0.72	0.16	22	0.09	0.5	0.3
C_i/C_a (μmol CO_2 mol air^{-1})	0.78	0.76	0.03	4.6	0.2	≤0.001	0.5
V_{cmax25} (μmol CO_2 m^{-2} s^{-1})	133	160	14.2	9.7	0.04	≤0.001	0.5
J (μmol e$^-$ m^{-2} s^{-1})	190	219	15.3	7.5	≤0.001	≤0.001	0.2
V_{cmax25}/N_{area} (μmol m^{-2} s^{-1}(gN^{-1}))	67	58	5.6	9	≤0.001	≤0.001	0.2
N_{area} (N g m^{-2})	2	2.8	0.18	7.7	≤0.001	≤0.001	0.1
SPAD	48.2	51.3	2.7	5.5	≤0.001	≤0.001	0.9
LMA (g m^{-2})	51	54.7	2.9	5.4	≤0.001	≤0.001	0.1

3.4.3.2.2 Comparison of BYPB genotypes measured in glasshouse and field

Experiments in the field are important since they are close to the real world environment for wheat production, in a canopy with unconstrained root growth. In order to compare the effect on plant behaviour growing in pots in a glasshouse and in the field, the BUNYIP set was measured in the field (**Aus3**) and compared with the same wheat genotypes grown and measured in the glasshouse (**+N Aus2**). Significant differences in the effects of growing environment were detected for most of the variables. J and LMA were higher in the field than in the glasshouse. A, g_s and C_i/C_a were lower in the field. V_{cmax25}, V_{cmax25}/N_{area}, N_{area} and SPAD were similar in both environments (Table 3.6.). All traits showed significant differences across genotypes, when analysed with Tukey's HSD test (A9). G × E interaction was significant for g_s, C_i/C_a , V_{cmax25}, J, V_{cmax25}/N_{area} and LMA.

Table 3.6 BYPB set measured in glasshouse (+N_Aus2) and in the field (Aus3). Means from 17 wheat and 9 triticale genotypes, 2 repetitions in +N_Aus2 and 4 repetitions in Aus3. ANOVA residual standard error (SE) with DF=25. Coefficient of variation (CV%).

Traits	Means				ANOVA *P-value*		
	+N_Aus2	Aus3	SE	CV%	Genotype	Env	G × E
A (μmol CO_2 m^{-2} s^{-1})	30.1	27.3	2.6	9	≤0.001	≤0.001	0.1
g_s (mol H_2O m^{-2} s^{-1})	0.72	0.46	0.14	25.8	0.05	≤0.001	0.003
C_i/C_a (μmol CO_2 mol air^{-1})	0.76	0.68	0.05	6.5	0.05	≤0.001	0.001
V_{cmax25} (μmol CO_2 m^{-2} s^{-1})	161	165	16	9.7	≤0.001	0.15	0.004
J (μmol e$^-$ m^{-2} s^{-1})	221	246	17.3	7.3	≤0.001	≤0.001	0.004
V_{cmax25}/N_{area} (μmol m^{-2} s^{-1}(gN^{-1}))	57.8	58.3	7	12.2	≤0.001	0.7	0.002
N_{area} (N g m^{-2})	2.8	2.9	0.25	8.9	≤0.001	0.26	0.2
SPAD	51.4	52.4	2.65	5	≤0.001	0.01	0.4
LMA (g m^{-2})	55	63.4	3.7	6	≤0.001	≤0.001	0.004

When there is a significant G × E interaction, it is important to make one correlation for each environment to see if any trait has a different behaviour at given environment. Despite G × E being significantly different, one correlation including measurements in glasshouse and field could explain the trend of correlations between traits. *A* correlated positively with g_s, C_i/C_a , V_{cmax25}, *J* and N_{area}, so genotypes with high photosynthetic rate had high g_s, intercellular CO_2, velocity of carboxylation, electron transport rate and nitrogen content. V_{cmax25} and *J* correlated positively with N_{area} (A10).

3.4.3.3   CIMCOG wheat genotypes (C)

CIMCOG wheat genotypes are elite genotypes from CIMMYT. Two experiments were carried out to evaluate photosynthetic diversity for the CIMCOG set. One analysed the plant stages, before anthesis (CB) and at anthesis (CA) from genotypes grown in the field in Mexico. The second analysed the same genotypes grown in the field in Mexico and in Australia at anthesis. Because usually there is interest in the relationship between photosynthetic traits and yield components, some yield components traits were included in the former experiment.

3.4.3.3.1   Effect of development stage from CIMCOG genotypes

The CIMCOG subset of wheat genotypes were compared when measured in the field before anthesis (**CB_Mex**) and at anthesis (**CA_Mex**). Plant stage had a significant effect on *A*, g_s, V_{cmax25} and SPAD. *A*, g_s, V_{cmax25} and J_g had higher values before anthesis than at anthesis. In contrast, SPAD values were lower before anthesis than at anthesis. C_i/C_a, J_g (electron transport rate from gas exchange), J_f (electron transport rate from fluorescence) and N_{mass} were similar in the two plant stages. Unfortunately, LMA data are missing in this experiment so V_{cmax25}/N_{area} was not calculated. There were highly significant differences across genotypes for *A*, g_s, C_i/C_a, J_g, SPAD and for the yield components. However, V_{cmax25}, J_f, and N_{mass} were not significant (Table 3.7). Significant traits between genotypes in the ANOVA test were analysed with Tukey's HSD test (A11). G × E interaction was not significant for any trait.

The CIMCOG panel is the only set of wheat genotypes where growing traits and yield components were measured. The analysis of variance showed that there were significant differences across genotypes for all the traits (Table 3.8). The Tukey's HSD test show the ranking of genotypes (A11 and A12).

Table 3.7 CIMCOG set measured before anthesis (CB_ Mex) and after anthesis (CA_Mex). The mean is calculated from 30 wheat genotypes and 3 repetitions. ANOVA-Lattice residual standard error (SE) with DF=29. Coefficient of variation (CV%).

Traits	Mean				P-value		
	CB	CA	SE	CV%	Gen	Stage	G × S
A (μmol CO_2 m^{-2} s^{-1})	31.5	27.5	3.7	12.8	≤0.001	≤0.001	0.3
g_s (mol H_2O m^{-2} s^{-1})	0.42	0.36	0.1	28.0	≤0.001	0.003	0.6
C_i/C_a (μmol CO_2 mol air^{-1})	0.6	0.6	0.06	9.3	≤0.001	0.8	0.6
V_{cmax25} (μmol CO_2 m^{-2} s^{-1})	249	189	41.5	18.9	0.4	≤0.001	0.8
J_g (μmol e$^-$ m^{-2} s^{-1})	278	276	24.6	8.9	0.03	0.1	0.2
J_f (μmol e$^-$ m^{-2} s^{-1})	231	225	36.0	15.6	0.7	0.6	0.2
N_{mass} (mg g^{-1})	41	42.2	4.8	11.4	0.4	0.2	0.4
SPAD	46.2	50	2.2	4.5	≤0.001	≤0.001	0.6
V_{cmax25}/N_{area} (μmol m^{-2} s^{-1}(gN^{-1}))		69.7			0.35		

J_g: electron transport rate from gas exchange; J_f: electron transport rate from fluorescence

Table 3.8 Growing traits and yield components of CIMCOG set (Mex). The mean is calculated from 30 wheat genotypes and 3 repetitions. ANOVA-Lattice residual standard error (SE) with DF=29.

Traits	Mex	SE	P-value Gen
Growth Rate, GR (g m^{-2} per day)	19.3	5.1	0.05
Days to flowering (DTF)	86.5	1.3	≤0.001
Biomass at flowering, BMF (Mg ha^{-1})	9.4	1	≤0.001
Percentage Grain Filling, PGF (%)	33.1	1	≤0.001
Biomass at maturity, BMM (Mg ha^{-1})	14	0.069	0.003
Yield (Mg ha^{-1})	6.98	0.32	≤0.001
Harvest Index, HI	0.5	0.014	≤0.001

A correlated positively with g_s, C_i/C_a, V_{cmax25} and J_g (Table 3.9). From yield components, *A*, g_s and C_i/C_a had a positive correlation with percentage of grain filling (PGF), but negative correlation with biomass at flowering (BMF) and days to flowering (DTF), so genotypes with high photosynthetic rate, g_s and intercellular CO_2 had a longer period of time to fill the grain, faster flowering and less biomass at flowering. Interestingly, unlike *A*, V_{cmax25} was not influenced by flowering time as *A* did. Electron transport rate from gas exchange, J_g, correlated positively with growth rate (GR), but not electron transport rate from fluorescence, J_f. GR had a positive correlation between N_{mass}, so plants that grew faster before anthesis to anthesis accumulated more nitrogen. Yield did not correlate with any variable, but HI correlated positively with SPAD.

Table 3.9 Phenotypic correlation between traits from CB_ Mex and CA_Mex. Traits with significant correlations: ***P≤ 0.001; **P≤ 0.01; *P≤ 0.06. DF=28.

	g_s	C_i/C_a	V_{cmax25}	J_g	J_f	N_{mass}	SPAD
A	0.92***	0.79***	0.55**	0.47**	-0.02	-0.32	0.13
g_s	1.00	0.94***	0.26	0.18	0.03	-0.36*	0.19
C_i/C_a		1.00	0.03	-0.06	0.07	-0.38*	0.11
V_{cmax25}			1.00	0.82***	-0.31	-0.12	0.04
J_g				1.00	-0.14	0.20	0.12
J_f					1.00	-0.03	-0.17
N_{mass}						1.00	0.07
SPAD							1.00
Yield components							
	GR	**DTF**	**BMF**	**PGF**	**BMM**	**Yield**	**HI**
A	0.08	-0.76***	-0.61***	0.64***	-0.08	-0.10	-0.03
g_s	-0.13	-0.81***	-0.69***	0.75***	-0.07	-0.11	-0.07
C_i/C_a	-0.23	-0.77***	-0.60***	0.68***	-0.12	-0.26	-0.20
V_{cmax25}	0.34	0.18	-0.21	0.22	-0.09	0.10	0.24
J_g	0.46*	0.01	-0.23	0.08	-0.09	0.22	0.39
J_f	-0.18	0.08	-0.25	-0.18	0.05	0.01	0.05
N_{mass}	0.37*	0.49*	0.26	-0.33	0.15	0.26	0.17
SPAD	0.31	-0.28	-0.35	0.32	-0.15	0.18	0.40*

3.4.3.3.2 Comparison of CIMCOG genotypes measured in the field in Australia and in Mexico

Experiment **Aus3** and **Mex** provide an opportunity to assess the effect of geographical location on photosynthetic performance in wheat. The ANOVA table shows that the location and genotypes were significantly different for all traits. Genotypes were ranked using Tukey's HSD test (A13). A, V_{cmax25}, J, V_{cmax25}/N_{area} were higher in genotypes measured in Mexico (**CA_Mex**) than in genotypes measured in Australia (**CA_Aus3**). In contrast, N_{area}, SPAD and LMA were higher in **CA_Aus3**. The G × E interaction was significant for all traits except for N_{area} and SPAD (Table 3.10).

Table 3.10 CIMCOG set, experiments Aus3 and Mex. Mean from 20 wheat genotypes, 4 repetitions for Aus3 and 3 repetitions for Mex. ANOVA residual standard error (SE) with DF=19. Coefficient of variation (CV%).

Variable	Means				ANOVA *P-value*		
	Aus3	**Mex**	**SE**	**CV%**	**Genotype**	**Env**	**G × E**
A (µmol CO_2 m⁻² s⁻¹)	24	28	3.8	14.7	≤0.001	≤0.001	≤0.001
g_s (mol H_2O m⁻² s⁻¹)	0.39	0.38	0.1	27.9	≤0.001	0.04	≤0.001
C_i/C_a (µmol CO_2 mol air⁻¹)	0.67	0.64	0.05	7.4	≤0.001	≤0.001	≤0.001
V_{cmax25} (µmol CO_2 m⁻² s⁻¹)	148	188	20.7	12.7	≤0.001	≤0.001	0.02
J (µmol e⁻ m⁻² s⁻¹)	230	274	26.4	10.7	≤0.001	≤0.001	0.008
V_{cmax25}/N_{area} (µmol m⁻² s⁻¹(gN⁻¹))	43.5	68.8	6.9	13.1	≤0.001	≤0.001	0.003
N_{area} (N g m⁻²)	3.4	2.7	0.3	8.8	≤0.001	≤0.001	0.3
SPAD	55.8	49.8	2.6	4.9	≤0.001	≤0.001	0.7
LMA (g m⁻²)	75	65	4.3	6	≤0.001	≤0.001	0.006

G × E was significant for most of the traits, for this reason two phenotypic correlations were used to understand the relationship between traits in each location. The main differences found in the two locations were the correlations from LMA, N_{area}, V_{cmax25} and J. In **Mex**, LMA and N_{area} were negatively correlated with A and g_s but not significant in **Aus3**. LMA was positively correlated with SPAD in **Aus3** but not in **Mex**. V_{cmax25} and J had a positive correlation with g_s in **Aus3** but not in **Mex**, and the correlation between V_{cmax25} or J with A was stronger in **Aus3** than in **Mex** (Table 3.11).

Table 3.11 Phenotypic correlation between traits from CA_ Aus3 and CA_Mex. *P-value* ≤0.05.Traits with significant correlations: ***P≤ 0.001; **P≤ 0.01; *P≤ 0.06. DF=18.

	g_s	C_i/C_a	V_{cmax25}	J	N_{area}	SPAD	LMA
CA_Aus3							
A	0.91***	0.80***	0.84***	0.72***	-0.32	-0.13	-0.19
g_s	1.00	0.94***	0.61**	0.43*	-0.28	0.04	-0.06
C_i/C_a		1.00	0.38	0.20	-0.28	-0.03	-0.10
V_{cmax25}			1.00	0.91***	-0.18	-0.12	-0.21
J				1.00	-0.25	-0.31	-0.25
N_{area}					1.00	0.36	0.59**
SPAD						1.00	0.60**
CA_Mex							
	g_s	C_i/C_a	V_{cmax25}	J	N_{area}	SPAD	LMA
A	0.94***	0.79***	0.52*	0.55*	-0.45*	0.03	-0.53*
g_s	1.00	0.94***	0.34	0.33	-0.47*	-0.08	-0.56**
C_i/C_a		1.00	0.16	0.12	-0.41	-0.12	-0.54*
V_{cmax25}			1.00	0.92***	0.34	0.23	0.19
J				1.00	0.28	0.29	0.10
N_{area}					1.00	0.18	0.85***
SPAD						1.00	0.12

In summary, there was no significant G × E interaction for fertilizer treatment or for plant stage of development. However, there was G × E interaction when glasshouse *vs* field, and Australia *vs* Mexico were compared. Photosynthetic rate was correlated with short flowering time, a longer period of grain filling and reduced biomass at flowering in the CIMCOG set. There was variation for photosynthetic parameters in the Early Vigour, BUNYIP and CIMCOG sets measured in Australia, but there were not always highly significant differences between genotypes. There was no statistical difference across genotypes of the CIMCOG set for V_{cmax25} was measured in Mexico.

3.5 DISCUSSION

In general there was significant genetic variation for photosynthetic traits across the genotypes measured, parameters considering that all these genotypes are high yielding wheats. Since the main focus of this project was to analyse genotypic variation for photosynthetic capacity and efficiency, this discussion addresses: A. the mechanisms

responsible for the ranking of wheat genotypes; B. the bases for the small genotypic variation for V_{cmax25} in the Mexico experiments, C. the trends in photosynthetic efficiency measured in Australia and Mexico and finally D. a general reflection on how to scale up from low level traits to yield.

3.5.1 Factors that did not affect the ranking of genotypes for photosynthetic capacity and efficiency

Two external factors did not change the ranking of genotypes for the photosynthetic traits: The fertilizer treatments and the plant development stage.

There was no interaction between genotypes and fertilizer treatments for A, V_{cmax25}, J and V_{cmax25}/N_{area} (Table 3.4 and 3.5), despite the observation that nitrogen can strongly influence these traits. In this project +N increased A, V_{cmax25} and J and conversely –N reduced these values, which agrees with previous observations in wheat where A increases at higher nitrogen contents until a plateau is reached (Evans, 1983). Field experiments in the literature agree with the absence of genotype × nitrogen interaction observed here. It has been suggested that favourable nutrition, particularly nitrogen commonly applied during breeding, will indirectly apply a selection pressure for high photosynthesis and leaf area as a result of the maximum crop growth rate (Richards, 2000).

In this project, there was no interaction between genotypes and development stage (G × S) for A, V_{cmax25}, J and V_{cmax25}/N_{area} (Table 3.7). In measurements reported for A in the field at Tlaltizapán, Mexico, significant low G × S ($P \leq 0.02$) was observed in 16 wheat cultivars, and the interaction (G × S) did not affect the ranking of the genotypes (Reynolds *et al.*, 2000). In the current experiment A and V_{cmax25} were higher before anthesis, GS49-57 (**CB_Mex**) than after anthesis, GS60-69 (**CA_Mex**) (Table 3.7). Although measurements from the Tlaltizapán experiment were made at an earlier stage, A was also higher in booting (GS37-49) than in anthesis (GS55-70) (Reynolds *et al.*, 2000). Similar observations have been reported for wheat at the Yaqui Valley, Mexico where A tended to be higher before anthesis (GS39-62) than at anthesis (GS71-77) (Fischer *et al.*, 1998a). It is known that environmental conditions can influence plant energy conversion efficiency (Slattery *et al.*, 2013), and usually temperature is higher after anthesis than before anthesis during the growth cycle of wheat growing in the field. The maximum temperature when **CB_Mex** was measured was 29.7 C and for **CA_Mex** this was 32.1 C (Figure 3.1). However, C_i/C_a was similar in the two developmental stages (Table 3.7) and plants that showed low stomatal conductance were remove from the analysis. Solar irradiance was higher when **CA_Mex** was measured than when **CB_Mex** was measured (Figure 3.1), probably A and

V_{cmax25} were lower after anthesis than before anthesis because after anthesis the solar energy was dissipated into heat for photoprotection to maintain the photochemistry (Baker, 2008), J_g and J_f were not significant different by plant stage (Table 3.7), but CO_2 assimilation and Rubisco activity was compromised.

After anthesis wheat plants start to reallocate assimilates for the future grains, the plant is larger and requires more assimilates to continue growing spikes for other tillers, shoots and roots (Lupton, 1966; King *et al.*, 1967). Low *A* and V_{cmax25} after anthesis than before anthesis can be also due to the compromise of the source and sink relationship, translocation of sugars, hormones and other factors (Wardlaw and Moncur, 1976). Interestingly, there were not significant interaction between **CB_Mex** and **CA_Mex** and ranking of genotypes at both plant stages seem to be relatively similar.

These observations suggest that while attention needs to be paid to developmental stage and nutrition treatment of material when screening for photosynthetic traits, ranking may be relatively robust across a range of stages and nitrogen levels.

3.5.2 Factors that affected the ranking of genotypes for photosynthetic capacity and efficiency

There was significant G × E interaction for V_{cmax25}, *J* and V_{cmax25}/N_{area} when glasshouse *vs* field were compared (Table 3.6). However, when V_{cmax25}/N_{area} was plotted using the mean of both glasshouse and field measurements, it was possible to differentiate genotypes with higher and lower V_{cmax25}/N_{area} (Figure 3.4). One phenotypic correlation table could explain both environment conditions (A10). In this experiment, although some data from the glasshouse can be translated in to the field, it is still important to be aware that ranking of genotypes may change due to environment.

J and LMA were significantly different for G × E interaction (E: glasshouse *vs* field) and both traits were reduced when were measured in the glasshouse (Table 3.6). Possibly some genotypes were affected by the lower light intensity in the glasshouse which is generally lower than in the field due to light absorption, but also from being grown at a different time of the year. Sun leaves are thicker than shaded leaves (Terashima *et al.*, 2006) and LMA is commonly affected by growth irradiance. Plants grown in the field have more light which may lead to increased chloroplast surface area, chlorophyll and Rubisco content and consequently greater photosynthetic capacity (Nishio *et al.*, 1993; Evans *et al.*, 1999). When measuring different sets of genotypes to determine variation in electron transport rate and leaf structure, it is important to take into account such G × E interaction, because genetic

potential for J and LMA measured in the glasshouse could be underestimated and as mentioned before, more measurements in the field are required to understand plant physiology (Slattery *et al.*, 2013).

There was also G × E interaction for A, V_{cmax25}, J and V_{cmax25}/N_{area} when Australia *vs* Mexico were compared (Table 3.10). This is not surprising and literature reports on 13 wheat genotypes analysed for A showed significant variation between different locations (Sadras *et al.*, 2012). When the two phenotypic correlations (**CA_Aus3** and **CA_Mex**) were separated, it was possible to observe three main aspects: 1) A had a lower correlation with V_{cmax25} and J in Mexico than in Australia (Table 3.11). 2) In Mexico, V_{cmax25} measured in the CIMCOG set did not show diversity across wheat genotypes but there was diversity for A and J_g (Table 3.7). Moreover, there was genetic variation for V_{cmax25} for the CIMCOG Set in Australia. 3) In Mexico LMA and N_{area} were negatively correlated with A (Table 3.11, **CA_Mex**). This behaviour and the environmental drivers responsible of this variation are discussed in the next section.

3.5.3 Understanding photosynthetic performance measured at different geographical locations

In order to further explore the differences between A/V_{cmax25} correlation measured in Australia (0.84) and in Mexico (0.52) (Table 3.11), all data were re-plotted (Figure 3.8). Immediately, two factors become obvious which could underpin the poor correlation between A and V_{cmax25} for genotypes measured in Mexico.
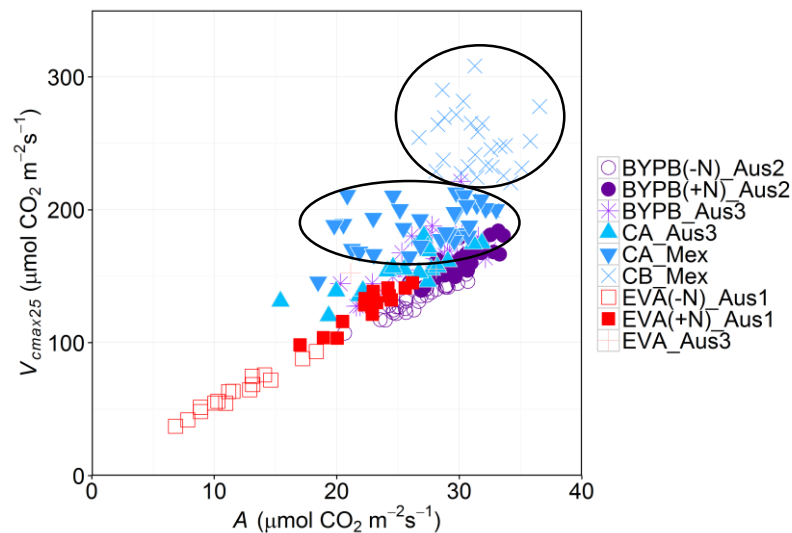
Figure 3.8 Assimilation rate (*A*) as a function of velocity of carboxylation (*V_{cmax25}*) for wheat genotypes grown in different environments and measured at different stages as described in Table 3.1. Symbols are the mean of the traits. Circles delimit the general behaviour of CB_Mex and CA_Mex wheat genotypes.

First, genotypes measured before anthesis (**CB_Mex**) had a higher variation in V_{cmax25} for a small range of A (Figure 3.8, symbol "×"). As suggested in the literature, A depends on stomatal sensitivity and this is the reason C_i/C_a has been used to select water-use efficient wheat genotypes (Condon *et al.*, 2004). The present study supports this relationship, where g_s was highly correlated with A in all experiments (Table 3.12). For experiments in Mexico, the mean of C_i/C_a was 0.6 (Table 3.7) and in general correlated positively with A (Table 3.12). In the plot (Figure 3.8) it can also be seen that some genotypes with low A had high V_{cmax25}. This could be explained by some genotypes displaying low A caused by stomatal closure, while in reality their Rubisco capacity was higher, as evidenced by high V_{cmax25}. This could explain the low correlation between A and V_{cmax25} for **CB, CA_Mex** (Table 3.12).

Table 3.12 Summary of phenotypic correlations with photosynthetic rate (A). Taken from genotypic means from Tables A6, A8, A10, 3.9 and A13.

	g_s	C_i/C_a	V_{cmax25}	J
Aus1	0.84***	-0.04	0.97***	0.92***
Aus2	0.64***	0.21	0.90***	0.79***
+NAus2 &Aus3	0.83***	0.4*	0.82***	0.87***
CA_Aus3	0.91***	0.80***	0.84***	0.72***
CA_Mex	0.94***	0.79***	0.52*	0.55*
CB, CA_Mex	0.92***	0.79***	0.55**	0.47**

Second, genotypes measured at anthesis (**CA_Mex**) had higher variation in A for a small range of V_{cmax25} (Figure 3.8). This leads to the same explanation from **CB_Mex**. Genotypes with low A closed their stomata, inferred from their low g_s, but it does not mean that these leaves had lower Rubisco capacity. This confirms that V_{cmax25} is not as sensitive to g_s as a simple measurement of A and it is a more robust trait to assess Rubisco capacity, as has been suggested decades ago (Farquhar and Sharkey, 1982). Probably this issue of stomatal limitation is more evident during anthesis than before anthesis because temperature was higher after anthesis (Figure 2.1), and even if the plants were grown under potential yield, measurements in the afternoon and high temperatures caused stomatal closure. The utility of V_{cmax25} as a metric for P_c is also supported by the strong correlation between V_{cmax25} and Rubisco measured *in vitro* (Figure 3.5). Perhaps the question that needs further attention is why V_{cmax25} and Rubisco *in vitro* have a curvilinear trend (Figure 3.5).

In Mexico, V_{cmax25} did not show significant diversity across wheat genotypes but there was diversity for J and A (Table 3.7). It is possible that the Mexican environment in which these lines were selected and then measured did not permit expression of genetic variation in V_{cmax25} or Rubisco levels. This could be to nitrogen leaching that has been reported in that region, because 75% of the nitrogen fertilizer is applied before planting that can be lost

in the first post-planting irrigation (Riley *et al.*, 2001). If there was not enough nitrogen in the soil for plant development, perhaps it was not enough nitrogen allocated to leaves, avoiding the maximum quantity of Rubisco protein into leaves and grain (Hawkesford 2013). However, under these conditions, it seems that there is scope for genetic variation in the electron transport rate (J_g) (Table 3.7).

A was also positively related with short flowering time and longer period of grain filling (Table 3.9), which could be related to sink strength. It has been shown that *A* changes relatively rapidly depending on the demand from grain filling, and *A* can drop when sink activity from vegetative growth shows before grains start to grow (King *et al.*, 1967; Evans and Dunstone, 1970; Evans, 1993). In these experiments (**CA_Aus** and **CA_Mex**) *A* was measured 7 to 10 days after anthesis. Some genotypes may have started grain filling earlier than others potentially leading to differences in *A* due to sink demand. Therefore, while *A* was representative of the photosynthetically active leaves in a given period from anthesis to grain filling, it may not represent the general genetic potential for photosynthetic capacity, as assessed by V_{cmax25}. Further research is needed to understand the relationship between V_{cmax25} and sink strength.

There was significant genetic variation for V_{cmax25} measured in the CIMCOG Set in Australia. The genotypes were not as vigorous as in Mexico, even if it was attempted to grow the plants under high yield potential conditions; during anthesis temperatures were high, conditions that limited the maximum plant development and could affect expression of maximum Rubisco carboxylation for all genotypes. In regard to potential environmental differences, Mexico belongs to wheat mega- environment 1 and Australia to wheat mega-environment 4 (Fischer *et al.*, 2014). Potentially, these genotypes may have reacted to differences in environmental factors such as photoperiod or light intensity (which are the main differences between the two geographical locations) giving more scope for expression of genotypic diversity in photosynthetic traits in Australia. Differences in photoperiod were observed during wheat selection to increase wheat yield from the middle of Mexico to the north of Mexico (Borlaug, 2007). Solar radiation was higher in Australia than in Mexico (Figure 3.1). Perhaps, such differences influenced changes in leaf size, thickness and leaf nitrogen content.

Interestingly N_{area}, LMA and SPAD were lower for genotypes grown in Mexico (**CA_Mex**) than in Australia (**CA_Aus3**). Probably different trade-off between leaf structure and photosynthetic traits occurred. For example, in some plants, electron transport is reduced under low irradiance, but it is compensated by investing of more nitrogen in pigment

protein complexes (Evans, 1989). Also in an experiment comparing a low and a high level of nitrogen nutrition in spinach, at the highest nitrogen level there was an increase of electron transport capacity despite maintaining the same proportion (24%) of thylakoid nitrogen compared to the low nitrogen treatment, and the excess of nitrogen from the high nitrogen treatment was allocated to the soluble protein (Terashima and Evans, 1988). Plants were bigger with larger leaf area evident in Mexico compared to Australia (unfortunately leaf size was not measured in both locations). Perhaps in Mexico, genotypes had a larger leaf area surface that compensated for a thinner leaf. Having a thin leaf may have limited the chlorophyll and nitrogen per unit leaf area basis. In contrast, plants in Australia increased chloroplast surface with higher LMA to compensate the reduction of leaf size, allowing higher N_{area}, but it was not enough to increase Rubisco activity.

3.5.4 Understanding photosynthetic efficiency

Photosynthetic efficiency, V_{cmax25}/N_{area}, was higher in Mexico than in Australia (Figure 3.9). As mention before, wheat genotypes grown in Mexico had a larger leaf area surface than those grown in Australia. Probably, environmental conditions (Figure 3.1) and management resulted in larger leaves and hence in less nitrogen and chlorophyll per leaf area (Table 3.10). Potentially, leaf plasticity may have reacted to environmental conditions and PY management that allowed higher V_{cmax25}/N_{area} in Mexico than in Australia.

These results showed that 20% reduction in N_{area} and 10% reduction in SPAD of **Mex** genotypes in relation to **Aus3** genotypes did not penalise photosynthetic capacity. Perhaps, bigger leaves which were more transparent allowed more light go through the canopy. Further experiments regarding photosynthetic capacity and efficiency in the canopy level would be necessary in the future to avoid the limitations of measuring a single organ of the plant, as has been shown in soybean. In soybean(*Glycine max* L.), a near-isogenic line Clark$_{y11}$ has approximately 30% lower chlorophyll content than the wild-type Clark but similar CO_2 assimilation rate per unit leaf area. It was suggested that canopy CO_2 assimilation rate was higher in Clark$_{y11}$ than Clark because photosynthetic photon flux could penetrate better in the canopy (Pettigrew *et al.*, 1989). However, the greater chlorophyll reduction will inevitably decrease A. Scaling of V_{cmax} and photosynthetic efficiency can be confounded by pleiotropic effects that will affect the conversion efficiency for biomass and yield (Slattery, 2014).
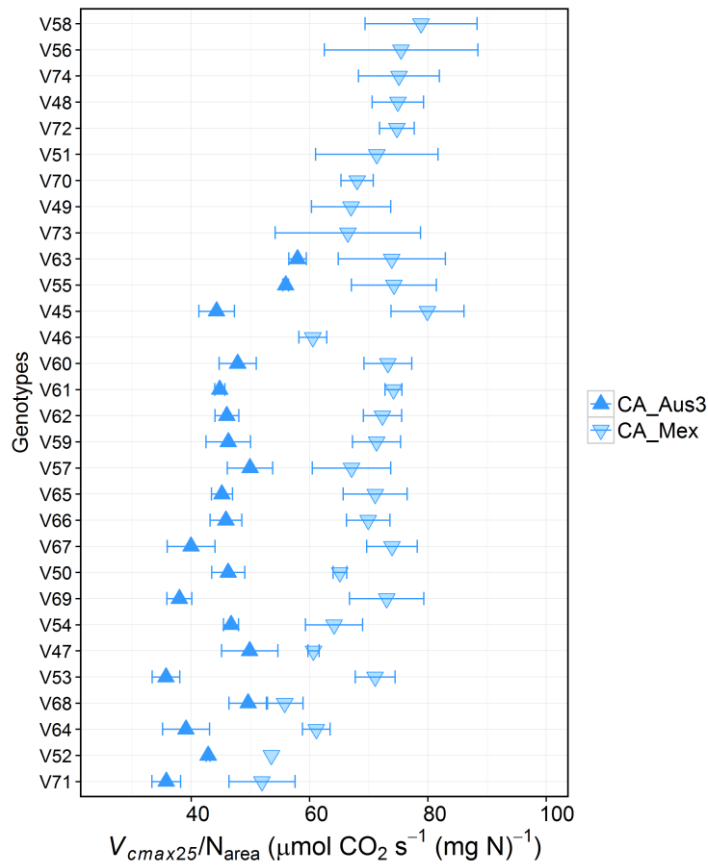
Figure 3.9 Diversity for photosynthetic efficiency (V_{cmax25}/N_{area}) from wheat genotypes of CIMCOG set measured at anthesis in Mexico (CA_Mex) and Australia (CA_Aus3). Symbols are the mean of the repetition, the error bar the standard error. Genotypes are ranked from the mean of each genotype including both environments (Aus3 and Mex).

Four *Triticum aestivum* and one of the *Triticale* genotypes from the BYPB set selected to cover a range of 46 genotypes for V_{cmax25}/N_{area} (Figure 3.4) showed similar catalytic turnover rate of Rubisco carboxylation (k_{cat}) (Figure 3.7). Perhaps variation was minimised because V_{cmax} was normalized to 25 °C. Genotypic variation was more apparent in different *Triticeae* species when measurements were done at 35 °C than 25 °C (Prins *et al.*, 2014).

The parameter V_{cmax25}/N_{area} was found to be a good way to evaluate carboxylation efficiency as was proposed previously (Evans and Seemann, 1984). It could facilitate the selection of plants with higher V_{cmax25} without requiring an increase in leaf nitrogen and also normalizes for leaf age related differences in N.

3.5.5 Scaling up from low level traits to yield

In this study, reversing the "reductionist" approach in order to scale up (Passioura, 2010) showed no correlation between photosynthetic traits and yield or HI (Table 3.9). This is similar to early research when *A* was compared with yield across modern high-yielding cultivars (Brinkman and Frey, 1978; Hart *et al.*, 1978; Murthy and Singh, 1979; Gifford and

Evans, 1981; Evans, 1993; Sadras *et al.*, 2012). Possible reasons why scaling up from flag leaf photosynthesis to yield seem to fail are:

1) Too few measurements. A correlated with yield when A was measured often (Reynolds *et al.*, 1994; Fischer *et al.*, 1998b; Gutierrez-Rodriguez *et al.*, 2000; Reynolds *et al.*, 2000). The A:C_i curves used to calculate V_{cmax25} and J take a long time to measure with gas exchange. Consequently, in this research only one or two measurements were done in the plant cycle. More frequent measurements in more leaves during the plant cycle are probably necessary to determine the accumulated assimilate and this should potentially be compared with plant biomass as a first approximation of assimilates use in the plant.

2) Time of measurements. Consideration should be given to the developmental stage when the measurement of V_{cmax25} and J are most likely to influence yield. For wheat grown under optimal conditions, photosynthesis may be more important from 10-15 days before flowering because this is the period when the steam is growing, the grain number is set and the most of the florets are growing (Fischer, 1985). Further analysis should be done for V_{cmax25} and J over a diurnal cycle, and over the course of longer periods during growth to see weather spot measurements can be related over a day, a week or weeks of measurements.

3) Canopy photosynthesis and remobilisation from other sinks (such as stems) were ignored. In this research, spot measurements were made in the upper most flag leaf. Thus, no account was made for photosynthesis from the spike, from lower leaves, for variation in leaf area, on leaf area duration or in canopy stature. It has been shown that wheat spikes make an important contribution to assimilate supply during grain filling (Sanchez-Bragado *et al.*, 2014) and that remobilisation of carbohydrates stored in the stem pre-anthesis also plays a key role in grain filling (Asseng and van Herwaarden, 2003).

4) Photosynthesis from source tissue could be used differently in each genotype. Photosynthesis is the sole source of energy to plants for growing roots, stems, leaves, spikes and grains (King *et al.*, 1967). However, each wheat genotype may have different sink demands and in this research it was unknown exactly how assimilates were used by the plant: i.e. in respiration, dissipation via heat, growth and development or temporary storage.

5) Yield is the product of LI, RUE and HI (Equation 1.1). Photosynthesis is related to RUE but LI and HI can also be major drivers of yield and were not uniform across all genotypes analysed here. HI, the ratio between grain and biomass, has been a

major breeding target for yield and even if there is increased availability of source carbon (i.e. biomass), but the grain sink is low, yield will not be correlated with photosynthetic capacity due to lack of optimisation of partitioning. Source-sink relationships need to be take into account since crops may be either source or sink limited across different developmental stages and during grain filling (Rawson *et al.*, 1976; Reynolds *et al.*, 2005).

3.6 CONCLUSIONS

V_{cmax25}, J and V_{cmax25}/N_{area} are shown here to be robust traits with which to assess genotypic variation in photosynthetic performance in wheat; they are not highly influenced by g_s or by sink strength during grain filling. V_{cmax25}/N_{area} can be used to select for photosynthetic efficiency, since V_{cmax25}/N_{area} normalizes Rubisco activity for leaf nitrogen content that can vary with leaf age and nitrogen availability and split the clustering observed when only V_{cmax25} is used.

While statistically significant differences across genotypes were not always found for photosynthetic traits, sufficient diversity in photosynthetic capacity and efficiency was found. In general, nitrogen applications and plant stage did not change the ranking of genotypes. However, environmental conditions can modify plant plasticity and photosynthetic traits.

Understanding and exploiting photosynthetic variation in plants is still challenging given our inability to currently monitor daily photosynthetic performance in plants during the whole plant cycle, in multiple leaves or in a complete canopy in field conditions. Rapid methods to assess photosynthetic parameters are still required.

CHAPTER 4

Can reflectance spectra be used to predict photosynthetic characters in wheat?

Centro Experimental Norman E. Borlaug, Cd. Obregón, Mexico. 2013.

4.1 ABSTRACT

This study investigates whether hyperspectral reflectance analysed with partial least squares regression (PLSR) or leaf reflectance at a smaller number of wavelengths could be used to predict V_{cmax25}. The **Aus1** experiment that comprises 16 wheat genotypes, three repetitions and two fertilizer levels was used to measure leaf reflectance and to test if discrete wavelengths or analysis of the full spectrum is required to predict V_{cmax25}. Results showed that V_{cmax25} could not be predicted from just a few wavelengths. However, it can be predicted from hyperspectral reflectance (400 to 2500 nm) analysed with the PLSR. This chapter describes a protocol for measuring leaf hyperspectral reflectance in wheat and describes the use of PLSR to predict V_{cmax25} from hyperspectral reflectance.

4.2 INTRODUCTION

Photosynthetic parameters such as maximum Rubisco activity at 25 ºC (V_{cmax25}) and electron transport rate (J) describe the underlying biochemical potential for photosynthesis of a leaf. However, V_{cmax25} and J are derived from CO_2 response curves which take at least 20 minutes to measure with the LI-COR. This is not suitable if one wishes to screen large populations. A tool that allows prediction of photosynthetic traits and other physiological parameters more rapidly and without destroying the leaf could enable selection of genotypes with improved photosynthetic performance. This chapter explores hyperspectral reflectance as a potential approach to facilitate physiological measurements in wheat populations.

There is a large body of historical knowledge that supports the idea that hyperspectral reflectance could be used to predict photosynthetic parameters. One of the first analyses of reflectance in leaves has been for determining chlorophyll and the subsequent development of a chlorophyll meter based on leaf reflectance (SPAD). This resulted in the development of the SPAD meter which uses transmittance and absorbance of red light at 560 nm and infrared light at 940 nm to predict leaf chlorophyll content (Benedict and Swidler, 1961; Inada, 1963, 1985; Mullan and Mullan, 2012). Furthermore, numerous indexes based on wavelengths in the visible and infrared part of the electromagnetic spectrum have been used in remote sensing to predict amounts of vegetation, biochemical leaf components and physiological traits. For example, vegetation index (VI), transformed vegetation index (TVI) and normalized difference vegetative index (NDVI) are used to monitor vegetation using red, infrared and near-infrared regions of the electromagnetic spectrum to measure relative greennes, foliage development, sencescence, biomass and chlorophyll content (Tucker, 1979). Water index (WI) is used to infer water content from reflectance at 900 and

970 nm (Peñuelas *et al.*, 1997). Photochemical reflectance index (PRI) is used to determine photosynthetic radiation-use efficiency using reflectance at 531 and 570 nm (Gamon *et al.*, 1992; Peñuelas *et al.*, 2011).

Since V_{cmax} and J have been widely adopted in ecophysiology and plant physiology to represent photosynthetic performance in trees and crops, some teams have predicted these parameters using either a small or broader region of the electromagnetic spectrum at leaf and canopy level. For instance, the index λRE taken from the red edge position of the spectra measured in tree leaves (*Quercus rubra* and *Betula papyrifera*) has been correlated with V_{cmax} and J (Dillen *et al.*, 2012). Sixteen wavelengths have been proposed to predict V_{cmax25} (Serbin *et al.*, 2012) but also using the full reflectance spectrum of 400 to 2500 nm and partial least square regression (PLSR) V_{cmax25} and J were accurately predicted in 159 species of tropical trees at canopy level, and in aspen, cotton and soybean at leaf level (Doughty *et al.*, 2011; Serbin *et al.*, 2012; Ainsworth *et al.*, 2014). Full length reflectance spectra and PLSR has also been used in wheat to predict nitrogen content and leaf mass dry area (LMA) (Ecarnot *et al.*, 2013). Consequently, measuring discrete wavelengths or combining hyperspectral reflectance spectra with PLSR to predict multiple traits seemed to be promising approach to accelerate the assessment of photosynthetic properties of wheat in the field.

One hyperspectral reflectance scan results in 2150 reflectance measurements, one for each wavelength from 350 to 2500 nm, that need to be correlated with one observation such as V_{cmax}. This means that there are 24650 variables and one observation and the observation can correlate with multiple variables. One method that can deal with these types of data and is highly used in chemometrics is PLSR. It has been used in multiple disciplines to solve the problem of dimensionality and multicollinearity such an approach has been used to predict the density of drawn poly(ethylene terephthalate) (PET) yarns from reflectance measured with Raman spectroscopy (Swierenga *et al.*, 1999), quality of olive oil and octanes from petrol (Kalivas, 1997; Mevik and Wehrens, 2007), soluble sugars and cell wall composition in *Sorghum bicolor* (Martin *et al.*, 2013). Consequently, this approach is explored in this chapter for its ability to predict photosynthetic traits in wheat leaves.

One objective of this chapter is to develop a method that accurately and reproducibly measures reflectance from wheat leaves. Since combining leaf reflectance with PLSR has already been used to predict photosynthetic traits in trees, cotton and soybean, the next objective was to evaluate the potential of using particular wavelengths versus hyperspectral reflectance with PLSR to predict V_{cmax25} in wheat.

4.3   MATERIALS AND METHODS

4.3.1   Plant Material and experiment conditions

In order to have a wide range of reflectance spectra, a gradient of leaf greenness was obtained by imposing two levels of fertilization on the early vigour set of wheat genotypes (EVA, +N, -N) described in Chapter 3, Experiment **Aus1**.

4.3.2   Traits measured

Gas exchange was measured with a LICOR LI-6400XT infrared gas analyser (LI-COR Inc., Lincoln, NE, USA) with the 6 cm^2 rectangular head. The flow rate in the CO_2 chamber of the Li-Cor was set at 500 µmol s^{-1}, irradiance at 1800 µmol quanta m^{-2} s^{-1}, and block temperature at 25 °C. Gas exchange was used to measure the photosynthetic rate at 400 µmol inlet CO_2 mol^{-1} (*A*). The CO_2 response curve was set to 400, then 50, 100, 250, 400, 800, 400 µmol inlet CO_2 mol^{-1}. The initial slope of the CO_2 response curve was used to calculate V_{cmax25} and *J* with the kinetic parameters obtained in Chapter 2 and the leaf biochemical model of photosynthesis (Farquhar *et al.*, 1980). Mesophyll conductance (g_m) was calculated with the formula $g_m = (0.55/25)*A_{260}$ (Equation 2.4, Chapter 2). Wheat flag leaves were measured with a SPAD-502 chlorophyll meter (Minolta Camera Co., Ltd, Japan) to provide a rapid estimate of chlorophyll content (Mullan and Mullan, 2012).

4.3.3   Hyperspectral reflectance

Reflectance spectra were measured with a FieldSpec® 3 (Analytical Spectral Devices, Boulder, CO, USA) spectroradiometer which measures visible and infrared portions of the spectrum (350-2500 nm) coupled via a fibre optic cable to the RTS-3ZC Integrating Sphere or to a leaf-clip device, all pieces from Analytical Spectral Devices, Inc., ASD.

The integrating sphere is coated with a highly reflective Zenith diffuse polymer such that light reflected from a sample is evenly diffused and can be measured at one point (www.asdi.com). To calibrate this experiment the light source was placed in the port 'A', the white reference was placed in ports 'B' and 'C', whilst the port 'D' remained closed. Then, the leaf was placed in port 'C' with the light trap behind to measure leaf reflectance (Figure 4.1).
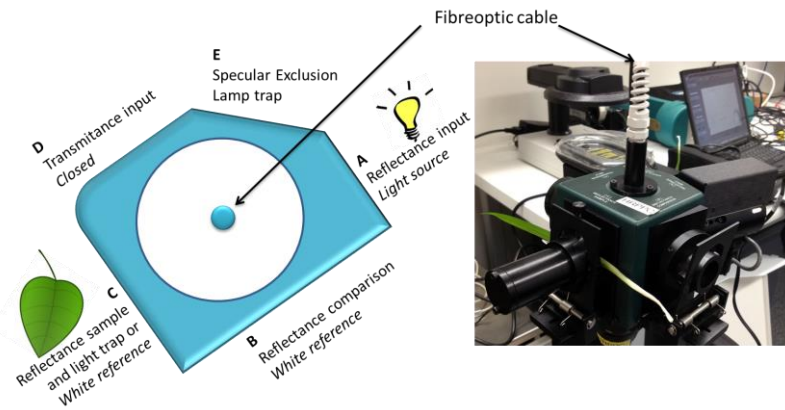
Figure 4.1 Diagram of the integrating sphere.

The leaf-clip looks like a gun with a trigger lock/release grip. It has a two-sided rotating plate that is behind the sample, one side is white and the other is black. A light source within the leaf-clip shines onto the sample and reflected light is collected by a fibre optic cable connected to the spectroradiometer (www.asdi.com). In this experiment the white side of the plate was always used to calibrate the instrument and when measuring transmittance and reflectance. The black side of the plate was used when measuring reflectance (Figure 4.2).

After gas exchange measurements in experiment **Aus1** (see Chapter 3), reflectance was measured with the leaf-clip twice. First, reflectance was measured from the same part of the leaf where gas exchange was measured, even if the window of the leaf-clip was not covered completely. Second, depending on the leaf length, a 3-5 cm long sector of the tip of the leaf was cut, and then the leaf pieces were held together with a homemade frame and clips to present leaf material covering all the window of the leaf-clip. If the leaf was too narrow a third section was used (see Results of this chapter).
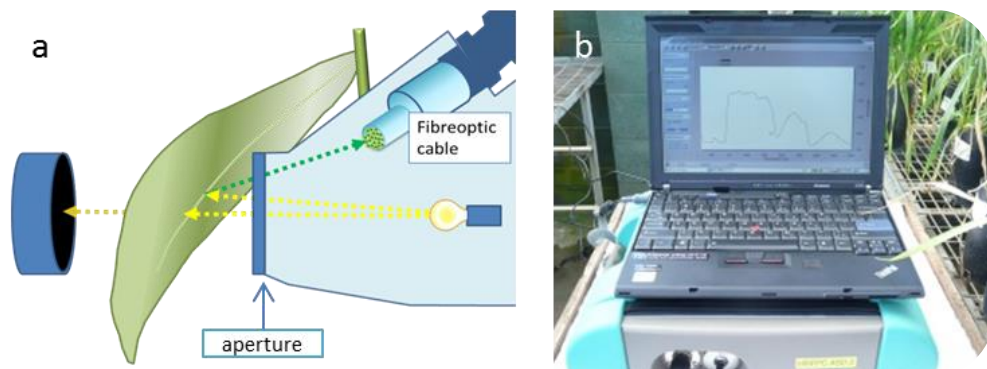
Figure 4.2 Reflectance measurement a) diagram of a leaf-clip showing the light reflected by the leaf into the fibreoptic cable, b) the ASD is below the computer which receives the reflected light through the fibre optic cable and then, transmits the signal to the laptop.

4.3.4 Main instructions used in the Partial Least Squares Regression

To build the calibration model, partial least squares regression fitted with the orthogonal scores algorithm was used in the script as follows:

pVc25 = plsr(V_{cmax25} ~ **Reflectance,** scale=F, **ncomp=30**, validation="LOO", data=**train data**)

where **pVc25** is the model that will predict the trait, **plsr** is the command to perform partial least squares regression, fitted with the orthogonal scores algorithm. V_{cmax25} is the trait observed (Y). **Reflectance** is the reflectance measured corresponding at each Y (X). **Scale** is used to standardise the variables. In our case this was not used, so FALSE was used in the script. **ncomp** is the number of components that will be run in the regression. The number 30 was used in the first instance because sometimes more than 20 components give the best predictions. **validation**="LOO" is a cross-validation called 'Leave-One-Out'. Details of the formula and options have been described by the 'pls' authors (Mevik and Wehrens, 2007).

Extraction of predicted data was done using this script:

predict(**pVc25**, newdata = test data, ncomp=5, type="response")

where **predict** is the command from plsr to predict the trait based in the information provided in the parenthesis, **pVc25** is the model generated before to predict V_{cmax25}, **newdata** directs the program to use the reflectance of the test data, **ncomp** is the number of component selected before with RMSEP in the cross validation, **type** can be either 'response', to extract the predicted trait, or 'scores' to extract the scores.

4.4 RESULTS

The ASD FieldSpec 3 spectroradiometer was tested as a means to quickly determine photosynthetic parameters, by comparing leaf reflectance data with gas exchange derived in wheat leaves. Given the long narrow leaves of wheat, we first evaluated the accessory devices available for the FieldSpec 3 and how these devices could be adapted to the narrow leaves of wheat. This information was used to develop a protocol suitable for wheat leaves that was reliable. Secondly, a range of PLSR methods were explored to obtain the best predictive algorithms to predict photosynthetic parameters.

4.4.1 Measuring hyperspectral reflectance in wheat leaves

The ASD FieldSpec 3 spectroradiometer has a fibre optic cable which collects the light reflected from the sample and focuses it on a detector. The optic fibre can be coupled to different devices that can be used to measure at leaf or canopy level. In this case we were interested in leaf level measurements and compared two accessory devices, an integrating sphere and a leaf-clip (Figure 4.1, 4.2 and 4.3).
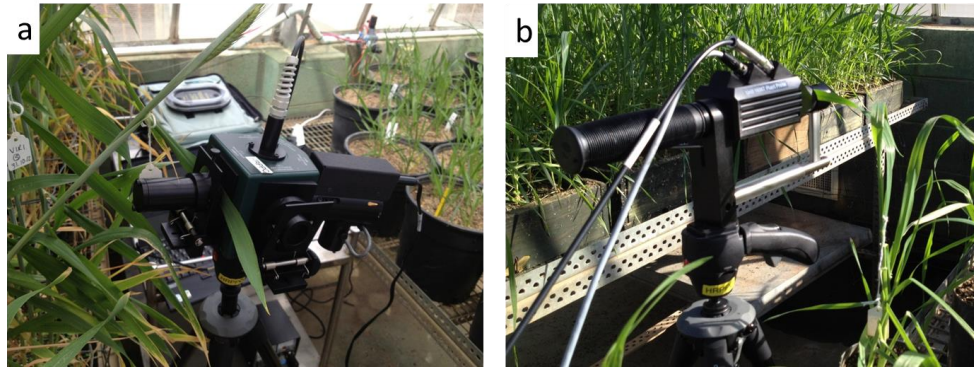
Figure 4.3 a) Integrating sphere, b) Leaf-clip. In both cases, one cable is the fibre optic that is conected to the spectroradiometer and the other is the power for the light source (see section 4.3).

4.4.1.1 Integrating sphere

The advantage of the sphere is that its small aperture (~ 5 mm diameter) allows measurements on just a small section of the wheat leaf blade between the leaf edge and mid-vein, avoiding the potentially problematic increased light scatter caused by the mid-vein (Figure 4.4). Two disadvantages were encountered with the sphere. Firstly, reflectance measurements in the short wave infrared 2 (SWIR2) band from 1900 to 2500 were poorly resolved (Figure 4.5); possible due to the coating used on the sphere's internal surface and a potential problem discussed later. Also, the set up and calibration of the sphere are complex and time consuming, making it less attractive for rapid field use.

Figure 4.4 Measuring reflectance with the ASD fieldspec 3 coupled to the integrating sphere in a flag leaf of wheat.
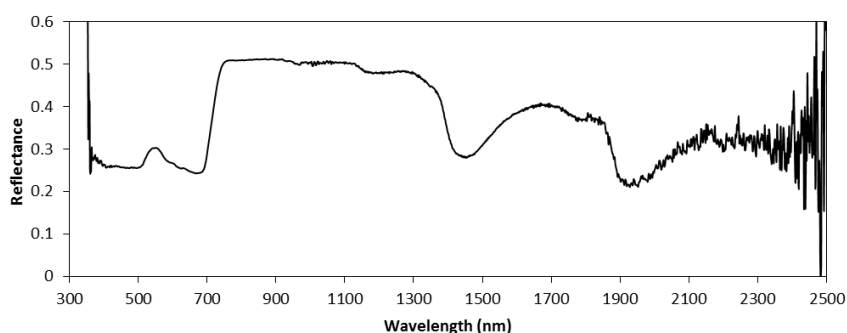
Figure 4.5 Reflectance measured in Figure 4.4. The short wave infrared 2 from 1900 to 2500 nm is the noisiest region.

4.4.1.2 Leaf-clip

When using the leaf-clip we found that there was much less noise in the reflectance measurements over the whole range of wavelengths (Figure 4.6.a). It was quicker and it was much easier to calibrate than the integrating sphere and easier to manage in the field than the sphere. The disadvantages were that the aperture is bigger than the width of most of the wheat leaves, which affects the reproducibility between leaves. Also, if more than 40 seconds was spent taking the measurement, heat from the light source could damage the leaf or can cause sufficient water to evaporate that it condense on the window, leading to greater variance in the reflectance measurements. Even though there was no apparent noise in the reflectance measurements, there was a discontinuity at 1000 nm and at 1800 nm because of the switch between the detectors used to measure the three wavebands. Given the ease of use of the leaf-clip in the field, it was decided to develop this measuring system further for wheat leaf measurements.

4.4.1.2.1 Aperture of the leaf-clip

Reflectance spectra were compared using one leaf partially covering the aperture of the leaf-clip and two pieces of leaf arranged so that they completely covered the window of the leaf-clip. Standard error was substantially higher for the former (Figure 4.6.b.), so a protocol was established that used two leaves for measurements.
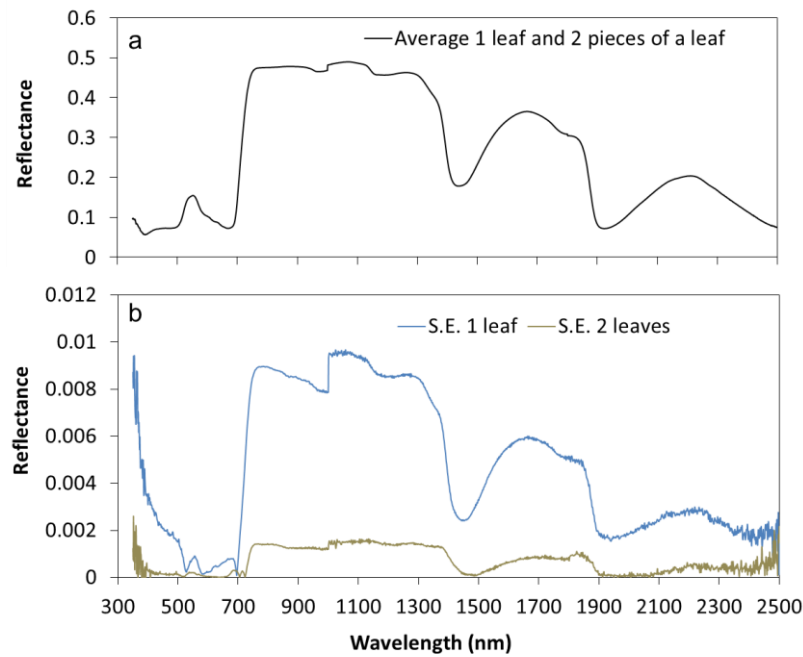
Figure 4.6 a) Average and b) standard error (S.E) of reflectance obtained using the leaf-clip when a single leaf did not completely cover the aperture and when two leaves were arranged to completely cover the aperture. S.E. from three measurements on the same leaf.

4.4.1.2.2 Background panel of the leaf-clip

Using the leaf-clip, there is an option to measure reflectance, with a black background, or transmittance, with a white background where light passes through the leaf and is reflected back to the detector by passing through the leaf again. In order to compare these spectra, two genotypes were chosen: genotype V8 (W020308) at low nitrogen with low A and SPAD, and genotype V3 (K1056) at high nitrogen, with high A and SPAD (Table 4.1). Two pieces of leaf were used to measure reflectance and transmittance because by covering the aperture, more consistent spectra were obtained. To achieve this, a section 4 – 5 cm from the tip of the leaf was cut and placed parallel with the rest of the leaf using a homemade frame and two clips (Figure 4.7).

Table 4.1 Rate of CO_2 assimilation (A) and SPAD from wheat genotypes V8 and V3.

Genotype	Experiment	Repetition	SPAD units	A (µmol CO_2 m^{-2} s^{-1})
V8	EVA(-N)_**Aus1**	1	21.0	9.80
		2	22.7	7.54
		3	16.8	5.22
V3	EVA(+N)_**Aus1**	1	47.3	28.18
		2	49.6	24.60
		3	46.8	25.35

V8   **V3**

Figure 4.7 Two pieces of a leaf from wheat genotypes V8 (EVA −N) and V3 (EVA +N).

Transmittance produced higher values than reflectance (Figure 4.8). In the case of reflectance, light collected by the fibre-optic cable, detected by the radiometer and recorded in the computer is only that reflected from the leaf, since transmitted light is absorbed by the black background (Figure 4.2). By contrast, a white background will reflect transmitted light that will pass back through the leaf again and emerge to combine with the reflected light. Both types of measurements, reflectance and transmittance, were tested to determine the potential to predict photosynthetic parameters (see Section 4.4.2.2).
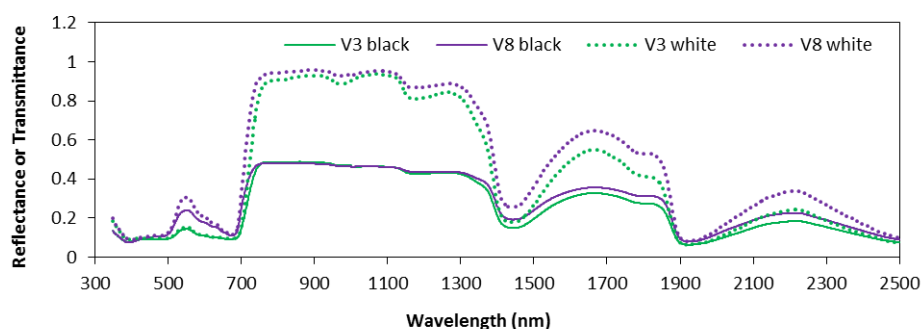
Figure 4.8 Reflectance (black background) in solid lines and transmittance (white blackground) in dots. Wheat genotype V3 (green) and wheat genotype V8 (purple).

4.4.1.2.3 Refining the reflectance measurements

Even though two pieces of leaf had been shown to work better than one in the leaf-clip, it takes a considerable time to put two leaves together to measure reflectance. To overcome this problem, a mask was built so that the field of view in the leaf-clip could be covered with a single piece of leaf. The aperture through the black mask was designed based on the field of view provided in the manual, using 1.15 cm drill entering at an angle. Thin foam gasket was placed on the mask to avoid damaging the leaf when closing the leaf-clip (Figure 4.9). By only needing to use a single leaf, the mask enabled measurements to be made faster.
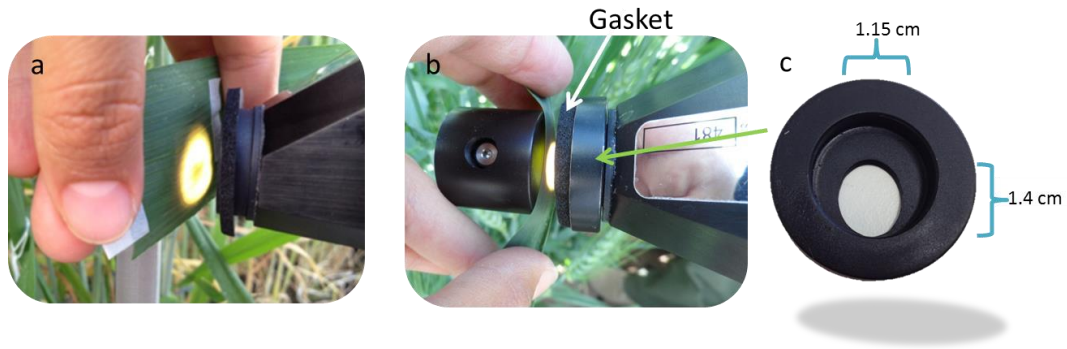
Figure 4.9 Measuring reflectance a) using two pieces of leaf, b) using one leaf, and c) the mask used to reduce the aperture size.

Reflectance spectra were compared using two pieces of leaf arranged to cover the window of the leaf-clip or using a single leaf measured with the mask adapted to the leaf-clip. It was found that using the mask reduced the standard error compared to when two pieces of leaf were used without the mask (Figure 4.10).
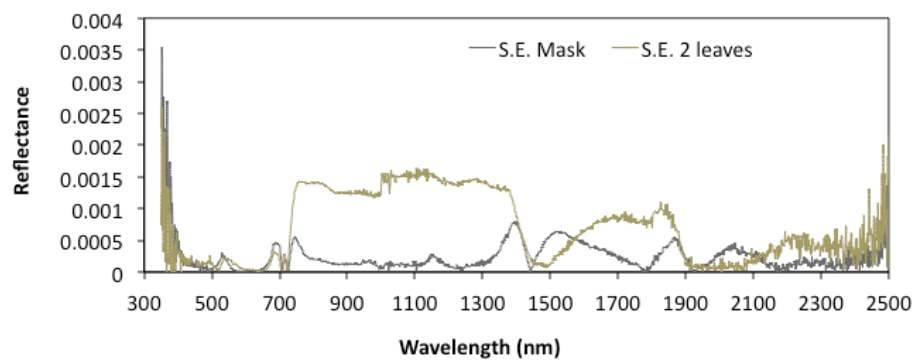
Figure 4.10 Standard error (S.E.) measuring one leaf of wheat with the leaf-clip and the mask and standard error measuring with two leaves without the mask. S.E. from three measurements in the same leaf.

4.4.1.2.4 Computer settings

In order to avoid damage to leaves caused by heat from the source light or error in the reflectance measurements caused by condensation in the leaf-clip, measurements time was set to 10 s. Over a 10 s period, one scan of 100 reflectance spectra averaged is captured. In the glasshouse experiment **Aus1**, the calibration and three scans (of 100 reflectance spectra averaged) measured in the same leaf took in total 55 s.

In the computer, in the section Control < Adjust Configuration < spectrum, dark current and white reference were set to 100 in **Aus1**. Later in the field experiments it was realised that the time could be reduced, hence dark current and white reference were subsequently set to 3s. The calibration and three scans (of 30 reflectance spectra averaged) measured in

the same leaf took 15 to 20 s (see Chapter 5 and 6). Reflectance was saved using the space bar of the lap top after three scans were completed.

4.4.2 Predicting photosynthetic parameters for wheat from hyperspectral reflectance

Up to this time, the best evidence for using reflectance spectrometry to predict photosynthetic parameters (V_{cmax} and J) with the ASD Field Spec leaf-clip had come from reflectance measurements in aspen and cotton using the partial least square regression (PLSR) calibration. Results from those experiments identified a certain number of wavelengths which were used to build equations to predict V_{cmax} and J (Serbin *et al.*, 2012). In this section both the analysis and a calibration set derived from wheat germplasm were tested to predict V_{cmax} in wheat.

4.4.2.1 Using reflectance wavelength to predict photosynthetic parameters

Serbin et al., 2012 identified 13 important wavelengths to predict V_{cmax} (Equation 4.1).

$$V_{cmax} = \begin{bmatrix} \left(\lambda_{495} \times 2512.75\right) + \left(\lambda_{610} \times -3804.89\right) + \left(\lambda_{680} \times -9121.73\right) + \left(\lambda_{695} \times 8114.26\right) \\ + \left(\lambda_{710} \times -1281.10\right) + \left(\lambda_{1510} \times 4284.40\right) + \left(\lambda_{1680} \times 6566.05\right) + \left(\lambda_{1755} \times -9975.12\right) \\ + \left(\lambda_{1890} \times -5262.65\right) + \left(\lambda_{1935} \times 8315.75\right) + \left(\lambda_{2210} \times 7361.03\right) + \left(\lambda_{2405} \times -14208.39\right) \\ + \left(\lambda_{2490} \times 7473.89\right) \end{bmatrix} -105.10$$

$$(4.1)$$

We tried to apply equation 4.1 to predict V_{cmax} using reflectance spectra data measured on wheat from the **Aus1** experiment using two pieces of leaf together. The predictions of V_{cmax} using equation 4.1 correlated negatively with V_{cmax} derived from CO_2 response curves, (Figure 4.11.b). From these results, it was concluded that the wavelengths identified for aspen were not suitable for wheat. Consequently, we returned to the initial procedure that the authors used to predict V_{cmax} in aspen, which involves partial least squares regression using the full reflectance spectrum (400 to 2400 nm).
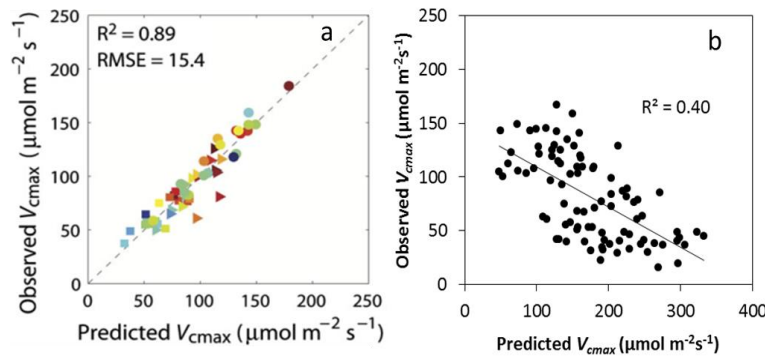
Figure 4.11 a) Predictions of V_{cmax} for aspen leaves from Serbin et al., 2012, and b) predictions of V_{cmax} for wheat using the wavelengths and Equation 4.2 and reflectance data from EVA_Aus1 experiment.

4.4.2.2 Using hyperspectral reflectance to predict photosynthetic parameters

In their work Serbin *et al.*, 2012 used PLSR to predict V_{cmax}, J, leaf mass per unit area and nitrogen in aspen and cotton leaves. Since equation 4.1 clearly did not work for wheat, it was decided to use PLSR to analyse reflectance spectra obtained from experiment **Aus1**. For the first attempt to understand PLSR, the four types of spectra explained before were used: One leaf partially covering the aperture of the leaf-clip or two pieces of leaf covering the aperture, in both cases two spectra were obtained using either the white or the black background panel (section 4.4.1.2.2).

The analysis was performed following the tutorial of the 'pls' package 'Principal Component and Partial Least Squares Regression in R' (Mevik and Wehrens, 2007) under R software version 2.15.0. Two repetitions from the **Aus1** experiment were used as a training set and one repetition was used as the test set.

Preliminary results showed good correlations predicting SPAD, V_{cmax} and J (Figure 4.12). V_{cmax} and J had higher R^2 when the two pieces of leaves were measured at the same time and their R^2 was similar when transmittance or reflectance was measured. This confirmed that measuring two leaves gave better results than measuring one leaf without the mask, and that the mask will be needed for future measurements. The correlations were similar regardless of whether a black or white background was used to obtain the spectra.
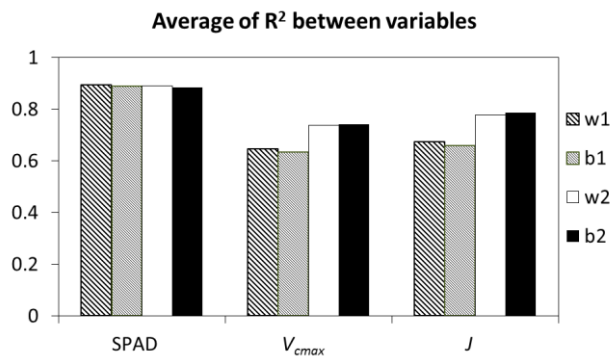
Figure 4.12 Correlations between observed and predicted SPAD, V_{cmax} and J from experiment Aus1. Two repetitions were used to train the PLSR and one repetition was predicted for comparison against the observed value. One leaf (1) and two pieces of leaf (2) were used to measure transmittance with the white background panel (w) and reflectance with the black background panel (b) of the leaf-clip.

Once PLSR showed positive results, the preliminary results predicting SPAD, V_{cmax} and J with the PLSR were used to optimize future measurements and to improve the method. From a review of the literature the black background is more commonly used (Serbin *et al.*, 2012; Ainsworth *et al.*, 2014), so it was decided to use the black background to measure leaf

reflectance. The next step was to clean the reflectance data to eliminate outliers that can result in inaccurate predictions.

The spectrum of the standard error of reflectance across the full spectral range plotted (Figure 4.6.b) from one leaf measured also previously clearly shows the jump that occurs at 1000 nm. Usually, the discontinuity at 1800 nm is less noticeable. In order to correct these discontinuities, a jump correction to re-align the spectrum was done at 1000 nm and 1800 nm with the software Spectral Analysis and Management System, version 3.2 from the University of California, Davis, USA.

Spectra with very low or high reflectance values could be potential outliers and give erroneous predictions, so the outliers were removed if reflectance was less than 0.35 and more than 0.6 at 800 nm. As well, to avoid potential noise from the edges of the spectra, only the band from 400 nm to 2400 nm was used (Figure 4.13). After cleaning the reflectance data with the jump correction and removing outliers, the reflectance data was ready to use in the PLSR.
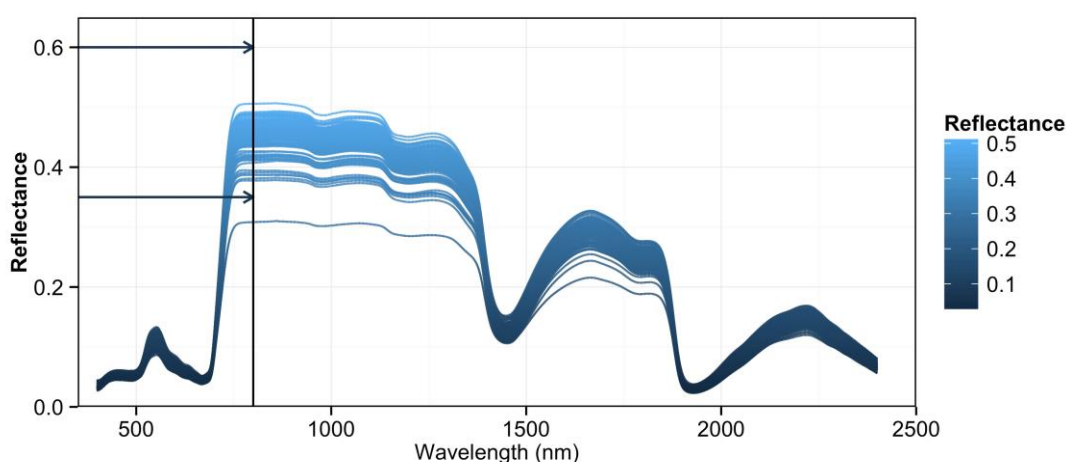
Figure 4.13 Detection of outliers in reflectance measurements. Arrows show the range 0.35 and 0.6 reflectance crossing at 800 nm. The spectrum out of this range was rejected.

4.4.2.3 Analysis of Aus1 experiments

Once the most evident outliers were eliminated, the reflectance spectra obtained in experiment **Aus1** showed substantial variation in shape (Figure 4.14). For example, in the visible range and from 2000 nm to 2500 nm, leaves from the –N treatment had higher reflectance than those from the +N treatment. Signal of noise in this region measured with the integrating sphere was unacceptably high (Figure 4.5) and is one of the reasons why the integrating sphere was deemed not be useful for predicting physiological traits with PLSR when using the full potential wavelength range of reflectance spectra.
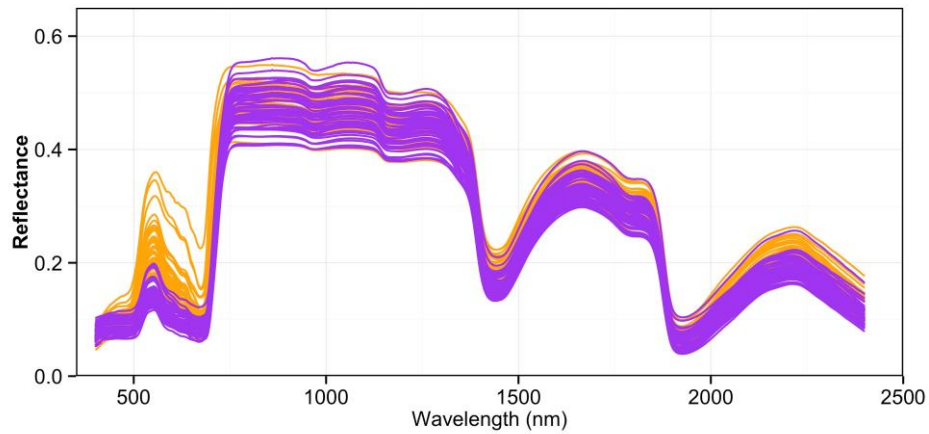
Figure 4.14 Reflectance measurements from Aus1 experiment EVA −N in yellow and EVA +N in purple.

To build a model with PLSR one needs a set of data to calibrate the fitting procedure, which is called the 'training data'. **'Training data'** comprises the observed values for the trait of interest (eg. V_{cmax25}), each with their respective reflectance spectrum. The trait value and reflectance spectra are used to calibrate the model for best fit. A second set of data, the test data, is used to validate the fit. **The test data** has two components: First, the model obtained from the training data is used to predict the trait from each reflectance spectrum. Then the predicted trait value is compared with the observed value to validate the model. In this case the training data used repetitions 1 and 2 from **Aus1** experiment. The test data came from repetition 3.

In this case the script was set to calculate 30 components because it gives more opportunity to find the model that best predicts the trait. In general, the number of components refers to the number of models generated with the PLSR (See section 4.3.4).

In order to choose the best number of components to be used in the predictions, the 'plsr' package creates a plot showing the Root Mean Square Error of Prediction (RMSEP) using two types of validation: cross-validation (CV) that is the ordinary CV estimate and adjCV which is a bias-corrected CV estimate. Both validations gave the same result (Mevik and Cederkvist, 2004; Mevik and Wehrens, 2007). The lowest error is associated with the best prediction and in this case 5 components had the lowest RMSEP (Figure 4.15) explaining 81.33% of the variance.
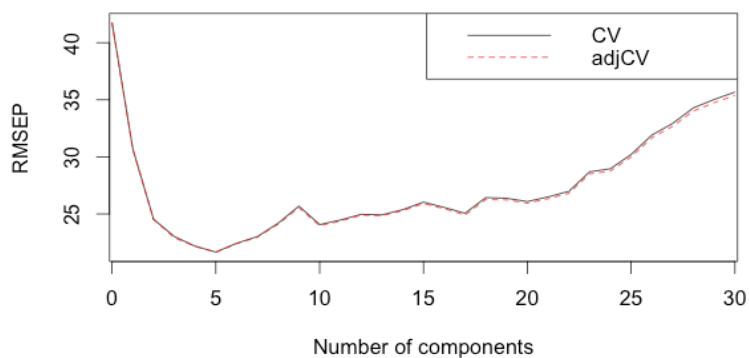
Figure 4.15 Root mean square error of prediction (RMSEP) of V_{cmax25} for 30 components or 30 models. CV is the cross-validation and adjCV is a bias-corrected CV estimate.

The fifth model (5 components) generates one loading for each wavelength (in this case 2000 loadings), which are used to generate scores for the new reflectance measurements. These scores are then used to generate new scores for the predicted trait (pV_{cmax25}). The latter scores and loadings are used to generate the predicted trait. The 'pls' package uses the loadings and scores to calculate the regression coefficients (Figure 4.16). By multiplying each regression coefficient by its reflectance value and summing these together with an intercept, the predicted trait value is obtained.
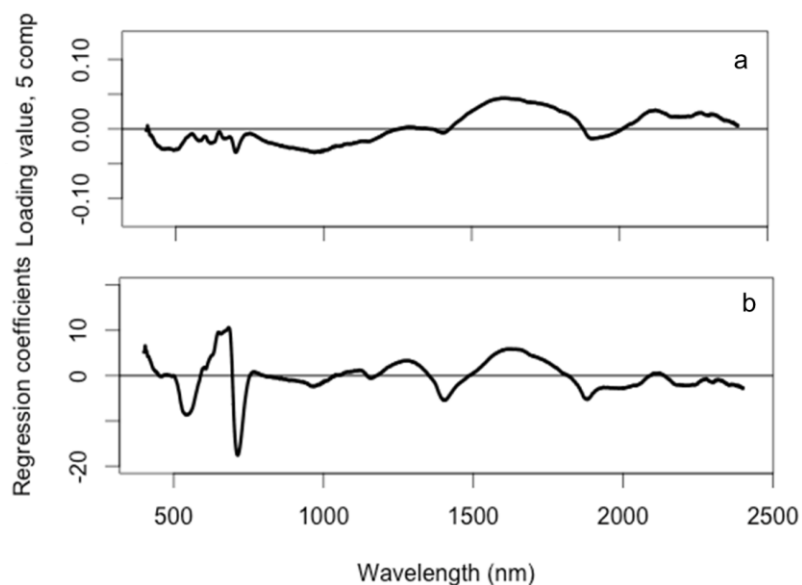
Figure 4.16 a) Loading value and b) regression coefficients from the PLSR model for V_{cmax25} using 5 components.

The PLSR generated 30 models, however the fifth model (5 components) had the lowest RMSEP (Figure 4.15), hence the model from 5 components was the best at predicting V_{cmax25}. The R^2 for the correlation between V_{cmax25} predicted and V_{cmax25} observed (calculated from the CO_2 response curves) using five components was 0.69 (Figure 4.17).

104
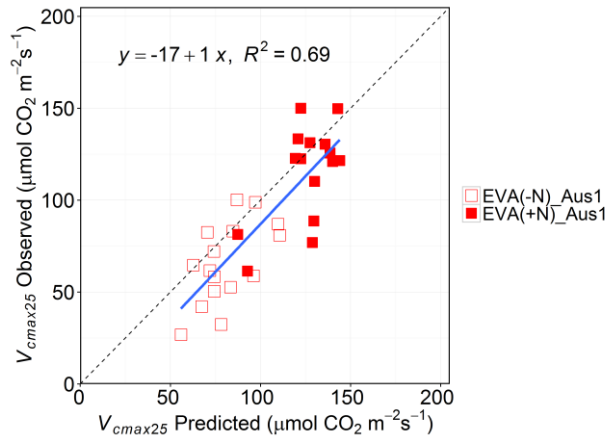
Figure 4.17 Validation of V_{cmax25} predictions using five components for Aus1 experiment, repetition 3, n=31.

Can the prediction from figure 4.17 be improved?. When the test data were used to calculate RMSEP and not the CV, the number of components changed. In this case it was reduced to three components (Figure 4.18). This means that actually the third model predicted V_{cmax25} better for this set of data. This was confirmed with a higher R^2 for the correlation between V_{cmax25} observed and V_{cmax25} predicted using three components (R^2 =0.77), than the model using five components (R^2 =0.69) (Figure 4.19).
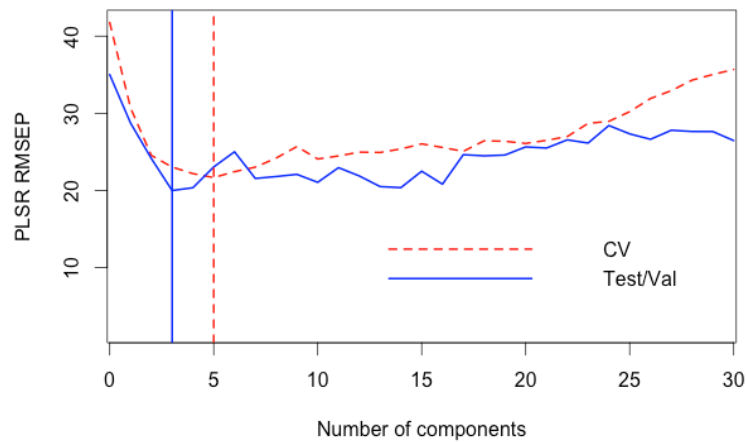
Figure 4.18 Root mean square error of prediction (RMSEP) of V_{cmax25} for 30 components. CV is the cross-validation and Test/Val are the test data.

These results suggest that the cross-validation assessment for predicting the test data was inaccurate because, another model predicted the test data better. It is probable that in this test data the model with 5 components did not generate the best predictions, however, the result was still reasonable.
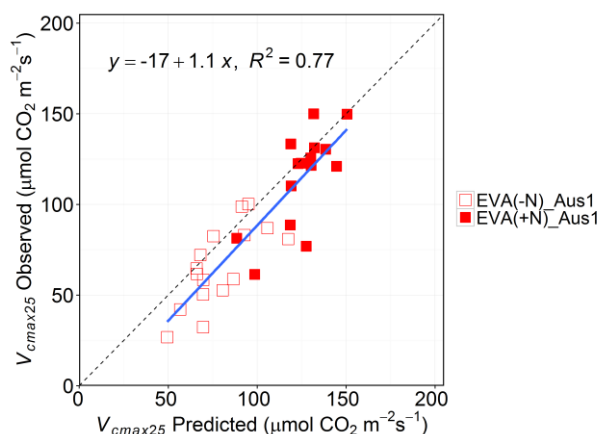
Figure 4.19 Validation of V_{cmax25} predictions using 3 components for Aus1 experiment, repetition three, n=31.

In the next chapter more number of data will be used to select the number of components of the models for V_{cmax25}, J, LMA, N_{area}, SPAD and chlorophyll.

4.5   DISCUSSION

4.5.1   Changes in reflectance

Even to the naked eye it was clear that nitrogen fertilizer treatment changed the leaf hue from green in +N plants to light green in –N plants (Figure 4.7). In addition to changes in the visible region and near infrared (IR) edge (400 nm to 740 nm), reflectance changed considerably in the short wave infrared region (SWIR) from 1400 to 2500 nm. These regions also changed considerably when reflectance was measured in dry and senescent leaves when nitrogen levels in the leaf were low (Ecarnot *et al.*, 2013). These changes of leaf hue agree with previous studies with cereals to determine important wavelengths to predict leaf chlorophyll. Reflectance at wavelengths from 500 to 650 nm decreased with increasing chlorophyll content per unit area (Inada, 1963, 1985). Nowadays, SPAD is in common use for this purpose and uses 940 nm and 650 nm wavelengths to predict chlorophyll content (Konica Minolta, 2009-2013), and chlorophylls are also estimated with reflectance indexes using wavelengths at 550, 675, 700 and 750 nm at CIMMYT (Pietragalla *et al.*, 2012). The Photochemical Reflectance Index (PRI) uses wavelengths at 531 and 570 nm and has been used to track stress in plants because it is related to the dissipation of excess absorbed energy by xanthophylls which is not used in photosynthesis and by consequence is negatively correlated with light use efficiency (Peñuelas *et al.*, 2011).

In this study using hyperspectral reflectance, the regression coefficients using 5 components for V_{cmax25} revealed outstanding peaks and regions at 400, 530, 650-700, 1240 and 1580 nm (Figure 4.13). Some of these wavelengths are located in the visible region but there is also an important region in the SWIR as has been detected in aspen, cotton and

106

soybean (Serbin *et al.*, 2012; Ainsworth *et al.*, 2014). It is possible that these discrete wavelengths may have predictive power in wheat and this will be examined in the following chapter.

4.5.2 Challenges selecting the model for predictions

PLSR can generate multiple models; for a given training set and one challenge remains in how to choose the best model. Selecting the model from PLSR was done using the lowest, Root Mean Square Error of the prediction (RMSEP) from leave one out-cross validation (LOO-CV). LOO-CV generates artificial data from the training data to try to predict the behaviour of the test data, and then RMSEP is used to choose the model that best predicted the best the new artificial data. In this project, these artificial data indicated that the model with 5 components was the best to predict V_{cmax25}. However, when the real test data were used, it was shown that 3 components fitted the test data better (Figure 4.18). There are two parts of the predictions that could be improved: the prediction of the artificial data from the LOO-CV and the method to choose the model or number of components to use (in this case RMSEP). Until this moment LOO-CV is the best option to use, since it uses a continuous iteration to create artificial test data. In fact, both LOO-CV and RMSEP are highly used in chemometrics, giving very accurate predictions (Kalivas, 1997; Swierenga *et al.*, 1999; Mevik and Wehrens, 2007; Martin *et al.*, 2013). Probably the quality of this prediction is due to measuring optically homogenous solutions such as oil, petrol or sugars which is much easier than measuring a leaf. The light reflected by a leaf can be scattered, absorbed and reflected from different depths within a leaf, depending on the leaf thickness (Markwell *et al.*, 1995; Jones and Vaughan, 2010), causing noise in the spectra. With leaves, a further challenge results from the leaf surface, which contains water, waxes, veins and trichomes.

In the literature, alternatives to RMSEP have been reported, for choosing the best model to use in PLSR predictions. The predicted residual sum of squares (PRESS) is an alternative algorithm that has been used to select a model or number of components generated from the PLSR LOO-CV from reflectance measured in plants (Feret *et al.*, 2011; Serbin *et al.*, 2012; Ainsworth *et al.*, 2014; Serbin *et al.*, 2014). PRESS uses the training data to predict new values; it takes each predictor aside sequentially and estimates the model each time with the error generated from the data point removed. PRESS is automatic, unlike RMSEP which requires that the user look for the lowest value. PRESS does this itself. Its orthogonal design makes it computationally affordable and efficient (Chen *et al.*,

2004). Thus, future models can be selected with both the RMSEP and PRESS minimized and they will be used in the next chapter to calibrate the traits.

4.6 CONCLUSIONS

Reflectance spectra can be used to predict photosynthetic traits in wheat. The protocol developed in this chapter proposes to use reflectance measurements from 400 to 2400 nm, since changes in reflectance occur in both at the visible and infrared regions of the electromagnetic spectrum and better results were obtained than using a smaller number of discrete wavelengths.

A measurement can be made in 3 s with a leaf-clip attached to the spectroradiometer. For narrow leaves it is recommended to use a mask that creates a small aperture thereby reducing the standard error across measurements. A foam gasket stuck to the mask avoided damaging the leaves when placed in the leaf clip as well as preventing stray light from interfering. A pre-treatment of the spectra also eliminated outliers due to low signal intensity. During the analysis of the reflectance spectra, it is recommended that both RMSEP and PRESS be used to select the number of components in the PLSR LOO-CV.

CHAPTER 5

Validation of reflectance spectra for predicting the main photosynthetic characters in wheat

Centro Experimental Norman E. Borlaug, Cd. Obregón, Mexico. 2013.

5.1 ABSTRACT

This study investigates whether having a larger number of observations helps to determine the best models to predict V_{cmax}, V_{cmax25}, J, N_{area}, SPAD, LMA and V_{cmax25}/N_{area} from hyperspectral reflectance and partial least square regression (PLSR). **Aus1**, **Aus2**, **Aus3** and **Mex** experiments were used to calibrate the model for each trait in the PLSR, and Root Mean Square Error of Prediction (RMSEP) and the Predicted Residual Sum of Squares (PRESS) were used to select the model for each trait. SPAD values were calibrated against direct measurements of chlorophyll content. Reflectance spectra were used to predict both SPAD and chlorophyll content. Using all experiments to calibrate the PLSR with RMSEP and PRESS improved the choice of a model to accurately predict each trait. In the validation, when observed data were compared against predictions from reflectance spectra, correlation coefficients (R^2 values) of 0.62 for V_{cmax25}, 0.71 (J), 0.82 (SPAD), 0.77 (Chlorophyll content), 0.89 (LMA) and 0.93 (N_{area}), were obtained. Potential regions of the spectra were identified to help mechanistically understand how the model predicts each trait.

5.2 INTRODUCTION

Screening large populations in the field for phenotypic variation is challenging when measuring photosynthetic parameters and traits requiring destructive harvesting. One conclusion from Chapter 3 is that an accurate detection of genetic variation for photosynthetic parameters requires multiple measurements between leaves of the same plant, between plants and during the plant life cycle. In order to detect and understand genetic variation in crops, it is important to develop reliable and fast phenotyping tools that act as a bridge between genomics, plant function and agricultural traits (Furbank and Tester, 2011).

Leaf chemical properties such as nitrogen, chlorophyll *a* and *b*, carotenoids and leaf mass per unit area (LMA) from trees and crops have successfully predicted from hyperspectral reflectance and the partial least square regression (PLSR) (Asner and Martin, 2008; Townsend *et al.*, 2008; Asner *et al.*, 2009; Asner *et al.*, 2011a; Asner *et al.*, 2011b; Doughty *et al.*, 2011; Ecarnot *et al.*, 2013). The same method has been used to predict photosynthetic parameters such as V_{cmax} and J, in tropical trees, aspen, cotton and soybean (Doughty *et al.*, 2011; Serbin *et al.*, 2012; Ainsworth *et al.*, 2014).

PLSR is a more robust analysis than the classical multiple regression and principal component regression model (Geladi and Kowalski, 1986). PLSR is a method that

correlates a variable with multiple measured values, in this case, reflectance values at many wavelengths. To deal with this dimensionality problem it uses a latent decomposition (components) of the response matrix and the predictor matrix. In this process, matrices including linear combinations (scores), loadings and random errors are created. Scores and loadings used to create the regression coefficients that basically represent the model that is used to predict the traits (Mevik and Wehrens, 2007). PLSR consists of two steps: calibration (training) and prediction (test). This chapter shows both steps for each trait measured.

It is possible to calculate many PLSR's because there are a number of possible solutions. However some models only describe noise, so for this reason the cross validation aproach "leave one out" (LOO-CV) is used with Square Error of Prediction (RMSEP) and the Predicted Residual Sum of Squares (PRESS). RMSEP and PRESS find the smaller error or residual across the number of components, which is a criteria that evaluates the predictive power of the model and permits the identification of the best model to predict the test data (Geladi and Kowalski, 1986).

There have been several attempts to detect key wavelengths involved in predicting the traits. In Chapter 4, sixteen wavelengths proposed in the literature review to predict V_{cmax} in aspen (Serbin *et al.*, 2012) were used unsuccessfully to predict V_{cmax} in wheat. Therefore, the models obtained in this study would need to be analysed further for their utility in other species.

The objective of this study was to calibrate and test predictions for V_{cmax}, V_{cmax25}, J, N_{area}, SPAD, Chlorophyll content, LMA and V_{cmax25}/N_{area} obtained from hyperspectral reflectance and PLSR analysis from measurements collected from wheat in four experiments (**Aus1**, **Aus2**, **Aus3** and **Mex**).

5.3 MATERIALS AND METHODS

5.3.1 Plant Material and experiment conditions

The germplasm and experiments used in this chapter have been described in detail in Chapter 3 (Tables 3.1, 3.2, 3.3). The first glasshouse experiment, **Aus1**, was designed to achieve a range in leaf colour with a drastic reduction of nitrogen levels in one treatment and high fertilizer in the other treatment. The second glasshouse experiment, **Aus2,** was also designed to vary nitrogen, but over a shorter treatment duration which resulted in smaller differences in leaf nitrogen content per unit leaf area and photosynthetic parameters. Field experiments **Aus3** and **Mex** were designed to test if reflectance can

differentiate between wheat genotypes grown under moderate fertilization and to evaluate if the ASD FieldSpec®3 can be used in the field to screen quickly for traits that could be important in breeding for improved photosynthetic performance.

In order to calibrate the SPAD chlorophyll meter against chlorophyll content, another experiment was performed. This experiment was called Sun and Shade (**S&S**). Experiment **S&S** was carried out in a glasshouse at CSIRO Black Mountain, Canberra (-35.271875, 149.113982), where temperature was controlled to 25/15 °C (day/night). Six seeds of each wheat genotype (Table 5.1) were sown in pots of 5 L with 50:50 loam:vermiculite soil mix containing basal fertilizer on December 22nd, 2011. The day of emergence (DAE) was on December 26th, and during the following week the plants were thinned to keep 3 plants per pot. The experiment was organized in a randomized block design, 4 blocks with 10 wheat genotypes, one genotype per pot. At 10 DAE, when the plants had 2.5 leaves, two blocks were kept under usual glasshouse sun conditions (900 to 1250 µmol quanta m^{-2} s^{-1}) and two blocks were shaded (230-300 µmol quanta m^{-2} s^{-1}).

Table 5.1 List of wheat genotypes used in the S&S experiment. Some genotypes are shared in experiments described in Chapter 3.

Names	Acronym	Characteristics
Sunstar	**V6** (Table 3.2)	Condon et al., 1990
Hartog (Pavon 76)	**V58** (Table 3.3)	CIMMYT Historic (Condon *et al.*, 1990)
Seri M82	**V61** (Table 3.3)	CIMMYT Historic
Siete Cerros 66	**V62** (Table 3.3)	CIMMYT Historic
Bd 912	**V77**	Bodallin + Semi-dwarf + Tin gene; Very high LMA
Bodallin	**V78**	Tall, low LMA
Chinese Spring	**V79**	Tall, low LMA
Red Egyptian	**V80**	Semi-dwarf, low LMA
Songlen	**V81**	Parent of DH crossed with Sundor
Sundor	**V82**	Condon et al., 1990

5.3.2   Traits evaluated

The traits measured have been described in Chapter 3 (Section 3.3.4 and Figure 3.2). The traits that will be used in this chapter are: the maximum Rubisco activity (V_{cmax}), the maximum Rubisco activity at 25 ºC (V_{cmax25}), the electron transport rate (J), nitrogen content per unit leaf area (N_{area}) , V_{cmax25}/N_{area}, leaf mass per unit area (LMA), SPAD (as surrogate of chlorophyll content) and reflectance. SPAD and reflectance were measured after the CO_2 response curves in the same region of the flag leaf. In the glasshouse (**Aus1**

and **Aus2**), immediately following measurements, the leaf was sampled for destructive analysis. In the field (**Aus3** and **Mex**), leaves were sampled in the afternoon after all measurements were finished to avoid plant dehydration.

5.3.3   Calibration of SPAD against extracted chlorophyll

Leaf transmittance with a SPAD-502 chlorophyll meter (Minolta Camera Co., Ltd, Japan) was measured in the middle of wheat leaves in the **S&S** experiment at three plant developmental stages: 1) At 33 DAE, GS39-41, measurements were performed in one block of each treatment in three different plants of each pot, in the fifth to eighth leaf of the main shoot. 2) At 61 DAE, around GS75, 13 days after anthesis, measurements were performed in one plant per plot in the four blocks using the flag leaf except for the genotype Chinese Spring that was around GS30 (its vegetative stage was longer than the rest of the genotypes). 3) At 74 DAE, around GS87 when plants were approaching maturity, measurements were made using the flag leaf of three wheat genotypes (Hartog, Sunstar and Bodallin). After SPAD measurements, four 1 cm lengths of leaf were cut, their width was measured, each fresh piece was weighed, wrapped in foil, put in liquid nitrogen and stored at -80 °C for later chlorophyll determination in the laboratory. For the chlorophyll extraction, 1mL of N,N-Dimethylformamide (DMF) was added to an eppendorf tube (1.5mL) to cover the 1 cm leaf sample. Tubes with resuspended samples were kept 2-4 days at 4°C under a foil cover and shaken in an orbital shaker during the last 24 h. When leaves were looking white-transparent, 800 µL of the solution was placed in a quartz cuvette and measured with a UV-VIS spectrophotometer V-650 (JASCO International Co., Ltd.) at 647 nm and 664 nm using fresh DMF as a blank. Chloropyll a and b were calculated with the following equations (Porra *et al.*, 1989): *Chl a = 12.00 A^{664} – 3.11 A^{647}. Chl b = 20.78 A^{647} – 4.88 A^{664}. Chls a+b= 17.67A^{647} + 7.12 A^{664}*, where A^{664} and A^{647} are the absorbance values at 664 and 647 nm respectively.

An exponential curve was fitted between the SPAD-502 chlorophyll meter (Minolta Camera Co., Ltd, Japan) values and chlorophyll content measured in the S&S experiment as suggested before (Markwell *et al.*, 1995). The fitting was made with the function nonlinear least squares (nls) in R (https://stat.ethz.ch/R-manual/R-devel/library/stats/html/nls.html) to estimate *a* and *b* of the exponential equation. After seven iterations *a* = 0.11964088 and *b* = 0.03551441 (Equation 5.1 and Figure 5.1).

$$Chl = 0.12\, e^{0.036x} \hspace{4cm} (5.1)$$

where *x* is the SPAD-502 chlorophyll meter value and Chl is the chlorophyll content per unit leaf area (mmol m^{-2}). This equation allows conversion of SPAD values measured in **Aus1**, **Aus2**, **Aus3** and **Mex** experiments into chlorophyll content.
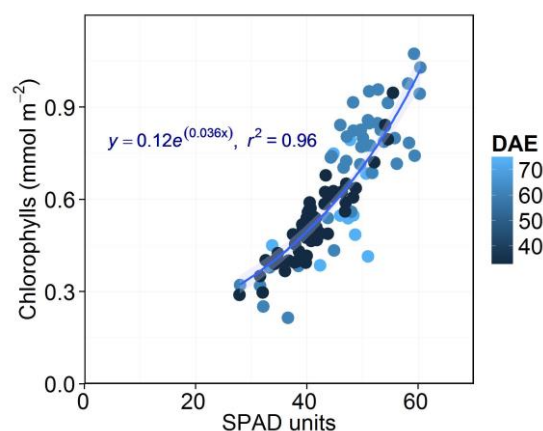
Figure 5.1 Correlation between leaf chlorophyll content (Chl) and SPAD-502 meter values measured with wheat at different days after emergence (DAE) (Equation 5.1).

5.3.4 Reflectance measurements and statistical analysis

Reflectance spectra were measured with FieldSpec®3 (Analytical Spectral Devices, Boulder, CO, USA) spectroradiometer full length (350-2500 nm) coupled via the fibre optic cable to a leaf clip with an internal light source and with two panels, a white panel used for instrument calibration and a black panel used for measurements (Analytical Spectral Devices, Boulder, CO, USA). A mask was used to reduce the leaf-clip aperture to an elliptic area of 1.264 cm^2 (1.1 × 1.4 cm) suitable for wheat leaves, a circular gasket of 2 cm diameter edge to edge and 3 mm thick was pasted to the mask to avoid leaf damage and to eliminate potential for external light to enter through the edges. The calibration and three scans (of 100 reflectance spectra averaged) measured in the same leaf took 55 s in **Aus1** experiment. In **Aus2**, **Aus3** and **Mex** experiments the calibration and three scans (of 30 reflectance spectra averaged) measured in the same leaf took 15 to 20 s. In **Aus1** reflectance was measured without the mask using two pieces of leaf measured in the horizontal position without the mask (perpendicular to the clip of the leaf –clip). In **Aus2**, **Aus3** and **Mex** each leaf was placed vertically (parallel to the clip of the leaf-clip), which helped to speed the measurements in the field. In all experiments, 3 readings from SPAD were averaged per leaf lamina. In experiments **Aus1** and **Mex** one reflectance measurement was made per leaf lamina, two in **Aus2**, and three in **Aus3,** which were averaged. The leaf lamina repetitions are independent from the experimental design repetitions.

For pre-treatment of the spectra, first, two different jump corrections were applied to the reflectance measurements because two different ASD FieldSpec®3 spectroradiometer were

used, one in Australia and the other in Mexico. Reflectance measured with the FieldSpec in Australia was corrected at 1000 nm and 1800 nm. Reflectance measured with the FieldSpec in Mexico was corrected at 1000 nm and 1830 nm. Spectra with reflectance lower than 0.35 and higher than 0.6 at 800 nm were removed because an earlier analysis had shown these to be outliers.

Analysis of the reflectance data was performed using the 'pls' package 'Principal Component and Partial Least Squares Regression in R' (Mevik and Wehrens, 2007) under R software version 2.15.0. The training data and the test data were split between repetitions of experiments (Table 5.2). The number of components used in the regression model fitted to the reflectance data was based in the smaller root mean square error (RMSEP) and the smaller predicted residual sum of squares (PRESS).

Table 5.2 Training data and test data from experiments used in the PLSR model. Glasshouse (GH). Fertilized plants (+N), not fertilized (-N). Repetition (Rep). Number of genotypes used (Gen). Experiment (Exp).

Exp (Gen)	Training data	Test data
Aus1 (16)	GH(+N) Rep 1 & 2	GH(+N) Rep 3
	GH(-N) Rep 1 & 2	GH(-N) Rep 3
Aus2 (30)	GH(+N) Rep 1	GH(+N) Rep 2
	GH(-N) Rep 1	GH(-N) Rep 2
Aus3 (2)	Field EVA Rep 1 & 2	Field EVA Rep 3 & 4
Aus3 (26)	Field BYPB Rep 1 & 2	Field BYPB Rep 3 & 4
Aus3 (20)	Field CA Rep 1 & 2	Field CA Rep 3 & 4
Mex (30)	Field CA Rep 1 & 2	Field CA Rep 3
Mex (30)*	Field CB Rep 1 & 2*	Field CB Rep 3*

*__CB_Mex__ measurements were only used for SPAD and chlorophyll content predictions and validations. LMA and N_{area} were not measured. As V_{cmax25} and J were calculated from only a few points in the CO_2 curve it was decided not to include these data.

5.4   RESULTS

In Chapter 4, experiment **Aus1** was used to evaluate prediction of V_{cmax25}. The results obtained helped to refine the method used in the subsequent experiments. In **Aus1**, it was shown that two models to predict V_{cmax25} could be successfully applied (3 and 5 components), so the same analysis was repeated here using **Aus1**, **Aus2**, **Aus3** and **Mex** experiments (Table 5.2). These results are discussed in this chapter in order to determine

the best model to predict each trait: V_{cmax}, V_{cmax25}, J, LMA, N_{area}, V_{cmax25}/N_{area}, SPAD and chlorophyll content. As LMA and N_{area} were not measured in **CB_Mex** experiment they were only predicted.

5.4.1 New model for V_{cmax25}

In Chapter 4, experiment **Aus1** was used to predict V_{cmax25}. A model using 5 components chosen with the lowest Root Mean Square Error of Prediction (RMSEP) from cross-validation leaf-one-out (LOO-CV) data was not the best model for predicting the test data. A better fit of the test data was obtained using 3 components (Figure 4.18). In this chapter it was expected that more data would help determine how to choose the best model. Therefore, data from **Aus1**, **Aus2**, **Aus3** and **Mex** experiments have been used to re-calibrate the model to predict V_{cmax25} (Table 5.2).

Cross validation (LOO-CV) generates an 'artificial test data' based on the training data. The LOO-CV data were used to choose the best model from 30 generated with PLSR to predict V_{cmax25} using the RMSEP. RMSEP was lowest in the model with 18 components, which means that this model will give the best prediction of V_{cmax25}. If the original data were tested with RMSEP instead of the 'artificial test data' the result was the same with the model generated with 18 components giving the best prediction. Perhaps the larger amount of data helped to generate a more accurate LOO-CV data from which to choose the best model to predict the original data.

In chapter 4, it was suggested that the Predicted Residual Sum of Squares (PRESS) could be an alternative method to RMSEP. Therefore, both methods were tested to predict V_{cmax25}. The result showed that both RMSEP and PRESS selected the same model to predict V_{cmax25} and both methods showed that 18 components gave the highest R^2 (Figure 5.2).

For each of the other traits evaluated, the test data RMSEP was minimal with a different number of components, although their impact in the coefficient of determination was minimal. For example: 18 components were selected from LOO-CV data to predict J, reaching $R^2=0.71$, whereas 19 components were selected using the original test data reaching $R^2=0.7$.
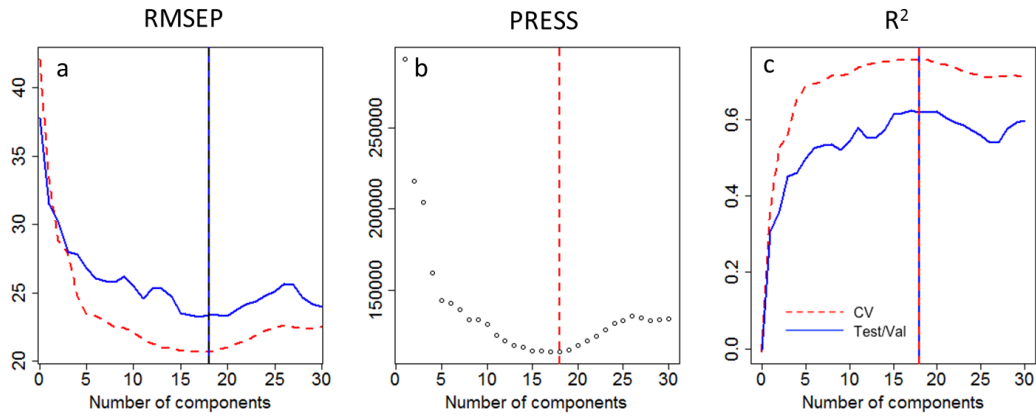
Figure 5.2 Root Mean Square Error of Prediction (RMSEP), Predicted Residual Sum of Squares (PRESS) and the coefficient of determination of V_{cmax25} for up to 30 components. CV is the cross-validation data and Test/Val are the test data to validate the model.

PLSR generates loadings used to create scores for each wavelength. Both loadings and scores are used to generate a group of regression coefficients for each model. These will be different in a model with one component compared to a model with 18 components. The loading and the regression coefficients for V_{cmax25} from the model using 18 components resulted in more peaks with higher value coefficients (Figure 5.3) than those generated in experiment **Aus1** for the same trait (Figure 4.16).

PLSR was applied for other traits, and one model from the initial 30 models was selected from LOO-CV data with both RMSEP and PRESS. The number of components was different for each trait: V_{cmax} (23 components), V_{cmax25} (18 components), J (18 components), LMA (21 components), N_{area} (21 components), V_{cmax25}/N_{area} (13 components), and SPAD (16 components). Therefore, each trait had its own model with its own loadings and scores to generate the regression coefficients.

Regression coefficients to predict each trait were calculated from the training data for that trait (Table 5.2). The regression coefficients and the intercept are the most useful results, because these specify the model for predicting each trait from each reflectance spectrum. Given a reflectance spectrum (400 to 2400 nm) for a leaf, it is possible to predict any trait that has been calibrated. The predicted value for a given trait is calculated from the sum of the products of factors by reflectance value for each wavelength plus the intercept.
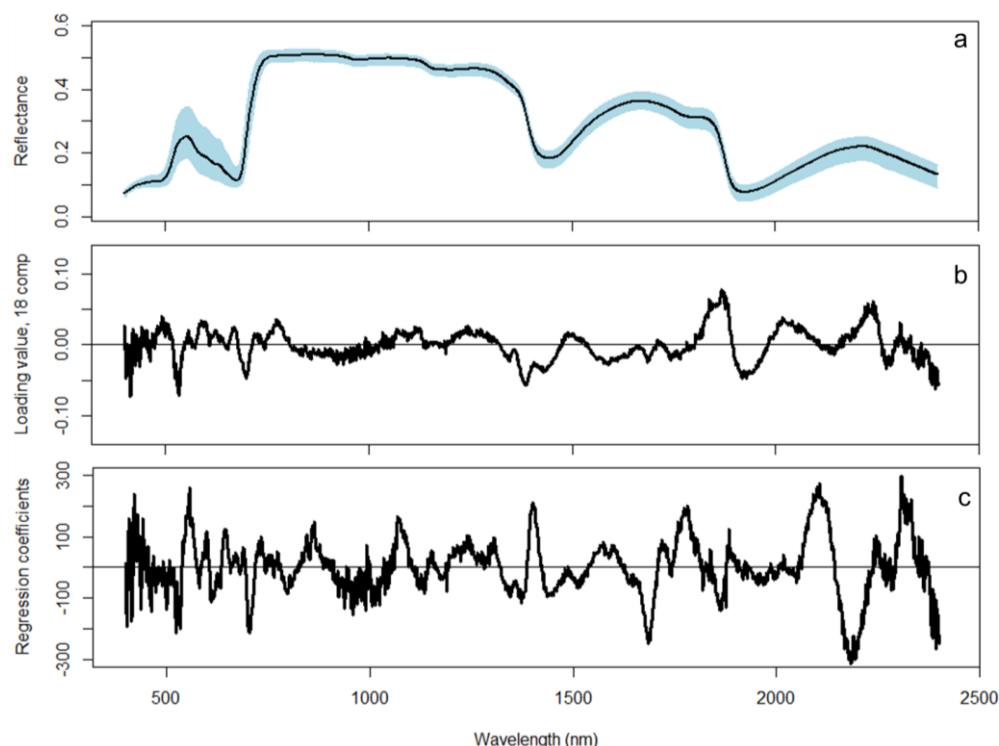
Figure 5.3 a) Reflectance from Aus1, Aus2, Aus3 and CB_Mex experiments. The solid line is the mean and the range is given by the blue shading. b) Loadings and c) regression coefficients of the model for V_{cmax25} with 18 components.

5.4.2   Predictions and validation of traits

The models chosen for each trait from the training data was validated against the test data. One or two repetitions were used for the training data and the remaining repetitions were used as the test data (Table 5.2).

Predictions for V_{cmax} had a higher coefficient of determination than V_{cmax25} (Figure 5.4). This could be associated with the fact that the range in V_{cmax} (25 to 400 µmol CO_2 m^{-2} s^{-1}) was greater than for V_{cmax25} (23 to 280 µmol CO_2 m^{-2} s^{-1}), but both predictions fall about the 1:1 line. The residuals between observed data and predictions were larger for V_{cmax} than V_{cmax25}. For V_{cmax25} there was a positive trend in the residuals, within each experimental group, while for V_{cmax} the residuals were more uniformly dispersed. Positive trends in the residuals show bias, by contrast a null plot (with no particular pattern apparent) means unbiased data and that the model used is adequate (Fox and Weisberg, 2011).

In the case of *J*, predictions fell about the 1:1 line and the coefficient of determination was higher (R^2=0.71) than for V_{cmax} and V_{cmax25} (Figure 5.4). Again there was a positive trend evident in the residuals within several of the experimental groups.

Predictions for N_{area}, LMA and SPAD had higher coefficients of determination than for the photosynthetic parameters and observations were aligned to the 1:1 line (Figure 5.5). For these traits, the residuals were smaller and showed no underlying trends.
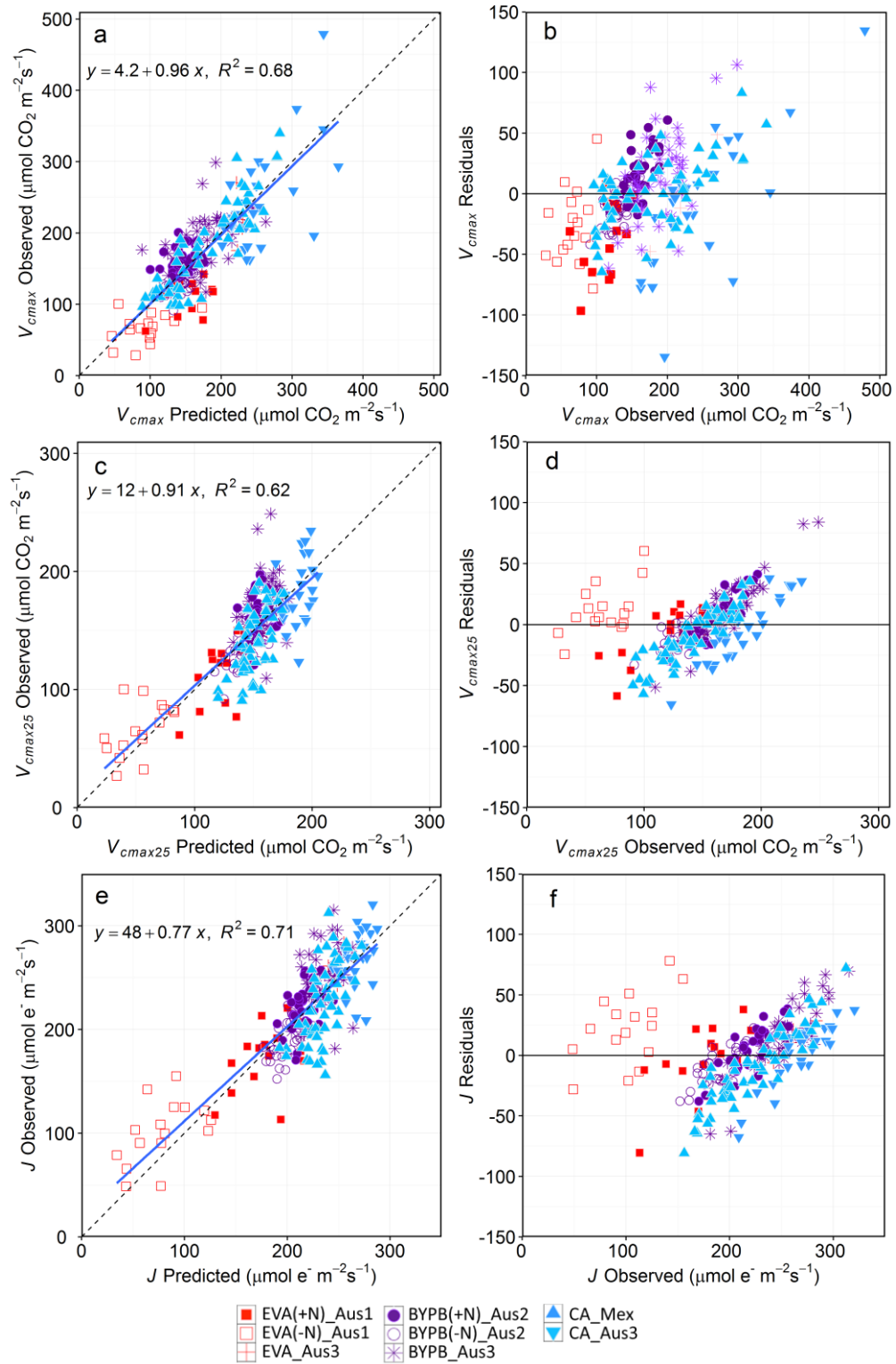
Figure 5.4 Validation of predictions and residuals for a), b) V_{cmax} **(23 components, RMSEP=27.8), c), d)** V_{cmax25} **(18 components, RMSEP=18.3) and e), f)** J **(18 components, RMSEP=20.3).**
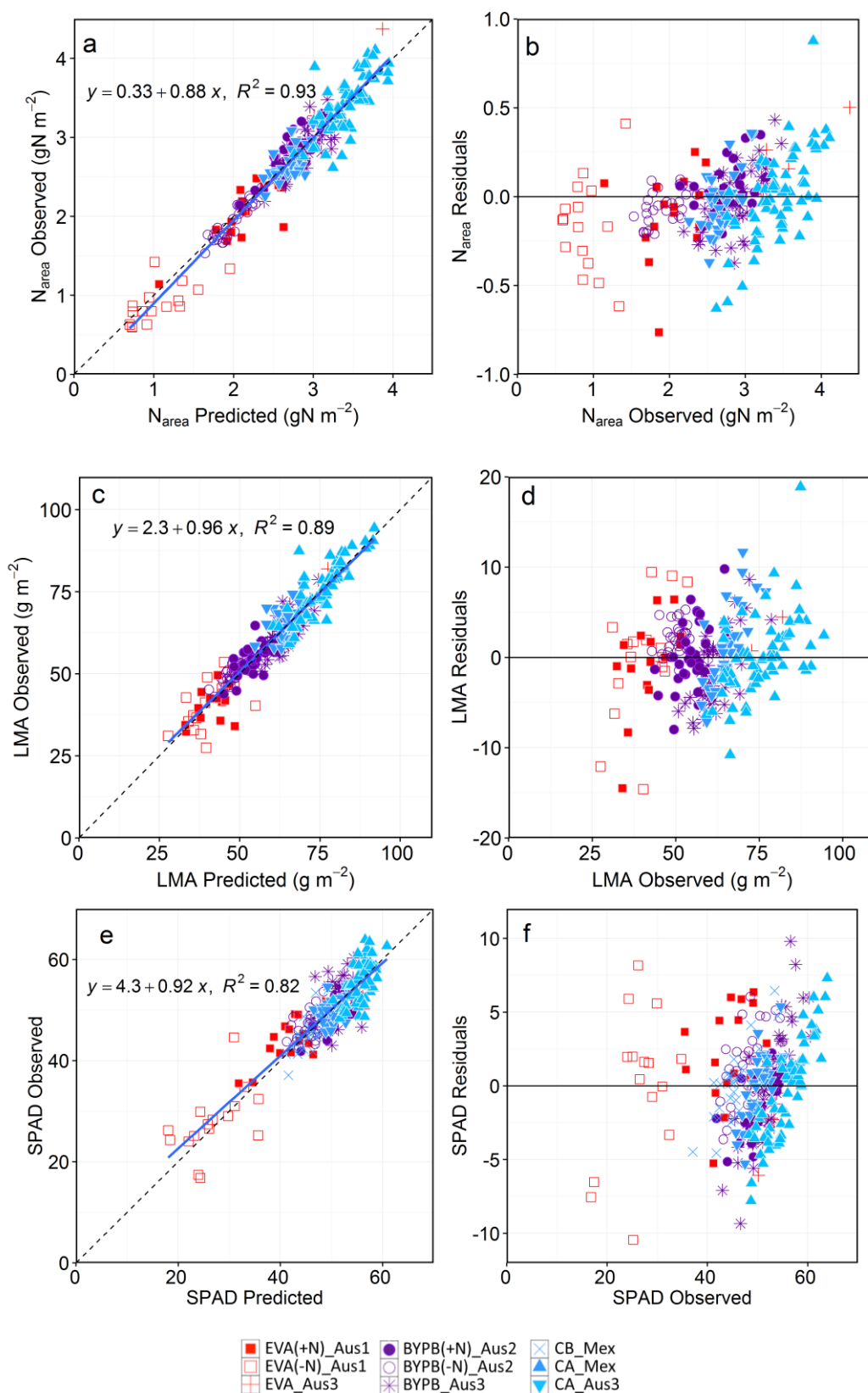
Figure 5.5 Validation of predictions and residuals for a), b) N_area (21 components, RMSEP=0.18), c), d) LMA (21 components, RMSEP=3.4) and e), f) SPAD (16 components, RMSEP=2.8). Note: SPAD was predicted using CB_Mex too.

Each SPAD value was used to calculate a chlorophyll content from which a PLSR model was generated to predict chlorophyll content rather than SPAD value from reflectance spectra measured in **Aus1**, **Aus2**, **Aus3** and **Mex** experiments. The chlorophyll content calculated from SPAD was predicted and validated with PLSR (Figure 5.6). The coefficient of determination was slightly less that obtained for the SPAD model ($R^2=0.77$ vs $R^2=0.82$). The residuals were relatively evenly dispersed. Consequently, with this model it is possible to also predict the actual chlorophyll content from the reflectance spectrum.

V_{cmax25}/N_{area} was used in Chapter 3 to analyse photosynthetic efficiency. The ratio itself could be predicted with points falling about the 1:1 line (Figure 5.7). Curiously, the coefficient of determination was higher ($R^2=0.49$) than when the ratio was calculated using a ratio of values of V_{cmax25} and N_{area} ($R^2=0.13$) predicted separately (Figures 5.4.c and 5.5.a). However, as the residuals showed a distinct positive trend within each experiment (Figure 5.7.b), this indicated that the method struggles to completely capture this parameter.
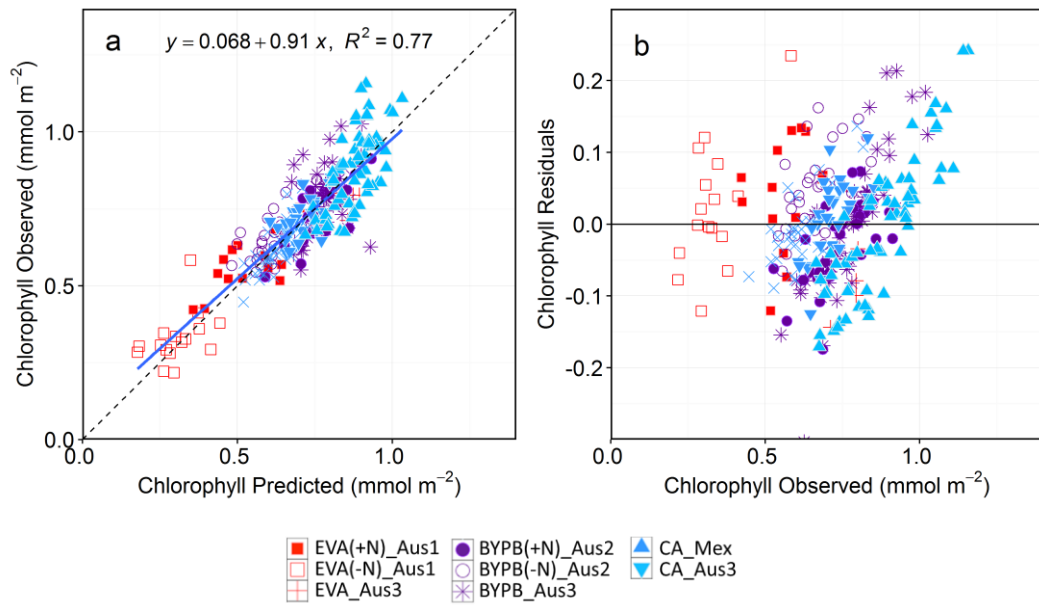
Figure 5.6 a) Validation of predictions and b) residuals for chlorophyll content (19 components, RMSEP=0.08). The legend is in Figure 5.5.
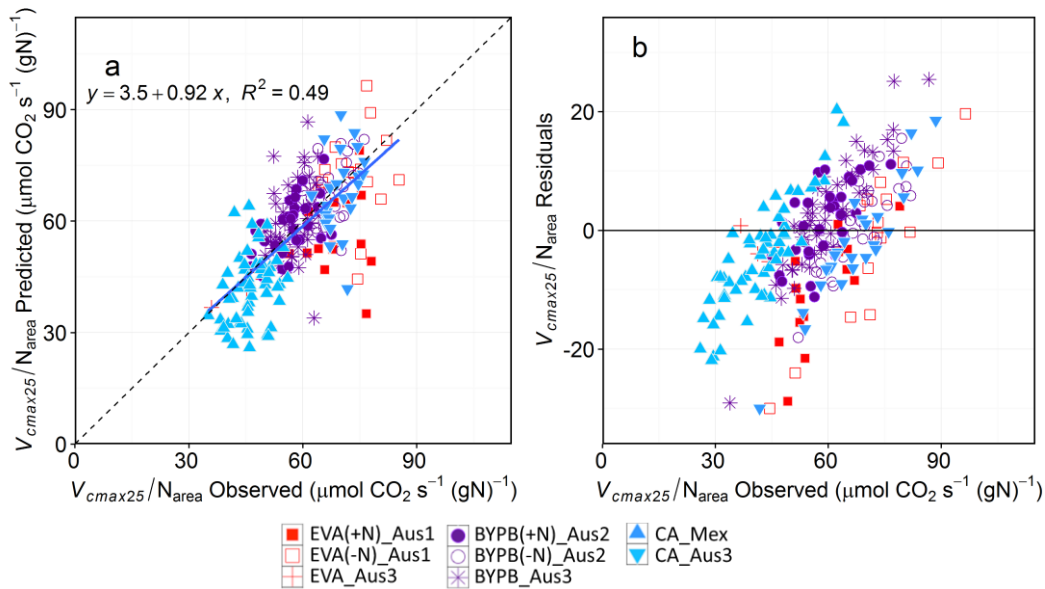
Figure 5.7 a) Validation of predictions and b) residuals for V_{cmax25}/N_{area} (13 components, RMSEP=9.2).

Even if different models had the same number of components, this does not mean that these models are identical since they were trained with different data. For example, the models predicting LMA and N_{area} were both chosen using 21 components but each one predicts a different trait value.

Another way to compare the range of observed and predicted data is with box plots. In general, the range from predictions was similar to or slightly less than the range for observed data. For instance, N_{area} **Aus1** (+N) showed a smaller distribution in the predicted data than in the observed data, even though the mean was similar (Figure 5.8).

Hyperspectral reflectance was measured in all experiments, and one big advantage is that multiple traits can be predicted in retrospect, having the model for those traits. Leaf area was not measured in **CB_Mex** experiment, so LMA and N_{area} were missing. Nevertheless, using the reflectance measured in **CB_Mex** experiment and the model generated previously with the other experiments, LMA and N_{area} were predicted for the genotypes of **CB_Mex** experiment.

Exp	Env	Gen			
Aus1	GH(+N)	EVA(16)	Predicted		
	GH(+N)	EVA(16)	Observed		
	GH(-N)	EVA(16)	Predicted		
	GH(-N)	EVA(16)	Observed		
Aus2	GH(+N)	BYPB(30)	Predicted		
	GH(+N)	BYPB(30)	Observed		
	GH(-N)	BYPB(30)	Predicted		
	GH(-N)	BYPB(30)	Observed		
Aus3	Field	EVA(2)	Predicted		
	Field	EVA(2)	Observed		
	Field	BYPB(28)	Predicted		
	Field	BYPB(28)	Observed		
	Field	CA(20)	Predicted		
	Field	CA(20)	Observed		
Mex	Field	CA(30)	Predicted		
	Field	CA(30	Observed		
	Field	CB(30)	Predicted		
	Field	CB(30	Observed		

Figure 5.8 Summary of the ranges in LMA and N$_{area}$ between genotypes in each experiment. Ranges were either predicted for each trait from reflectance spectra or represent the true range observed. As LMA was not measured in CB_Mex, N$_{area}$ can only be predicted for these genotypes using a reflectance model.

5.4.3 Regression coefficients

The models used to predict each trait are described as the regression coefficient for each wavelength and an intercept. A high value for the regression coefficient occurs when that wavelength strongly influences the model. Raw regression coefficients used for the predictions and validations (Figures 5.4, 5.5 and 5.7) are shown to reveal important peaks (Figure 5.9). The patterns in the regression coefficients varied between traits, and it was difficult to detect significant regions. Interesting regions were highlighted based on the size of the peak and when differing between traits (Figure 5.9):

- V_{cmax} 400-460, 1390-1430, 1870-1910, 2263-2333 nm
- V_{cmax25} 400-460, ~550, ~700, ~1067, ~1130, 1390-1430, 1680-1880, 2040-2380 nm
- J ~405, 537-570, ~700, ~1067, 1390-1430, 1680-1880, 2040-2380 nm
- N$_{area}$ 400-430, 1600-1700, 2050-2380 nm
- LMA   400-430, 1600-1700, 1870-1930, 2240-2500 nm
- SPAD 400-1750, 1320-1400, 1750-1900, 2050-2380 nm
- V_{cmax25}/N$_{area}$ 500-730, 1300-1400, 1670-1760 nm

The green waveband in figure 5.9 (900 to 1100 nm) is highlighted because the coefficients within that region have small values but they vary from being negative for V_{cmax25}, J and V_{cmax25}/N$_{area}$ to being positive for N$_{area}$, LMA and SPAD.
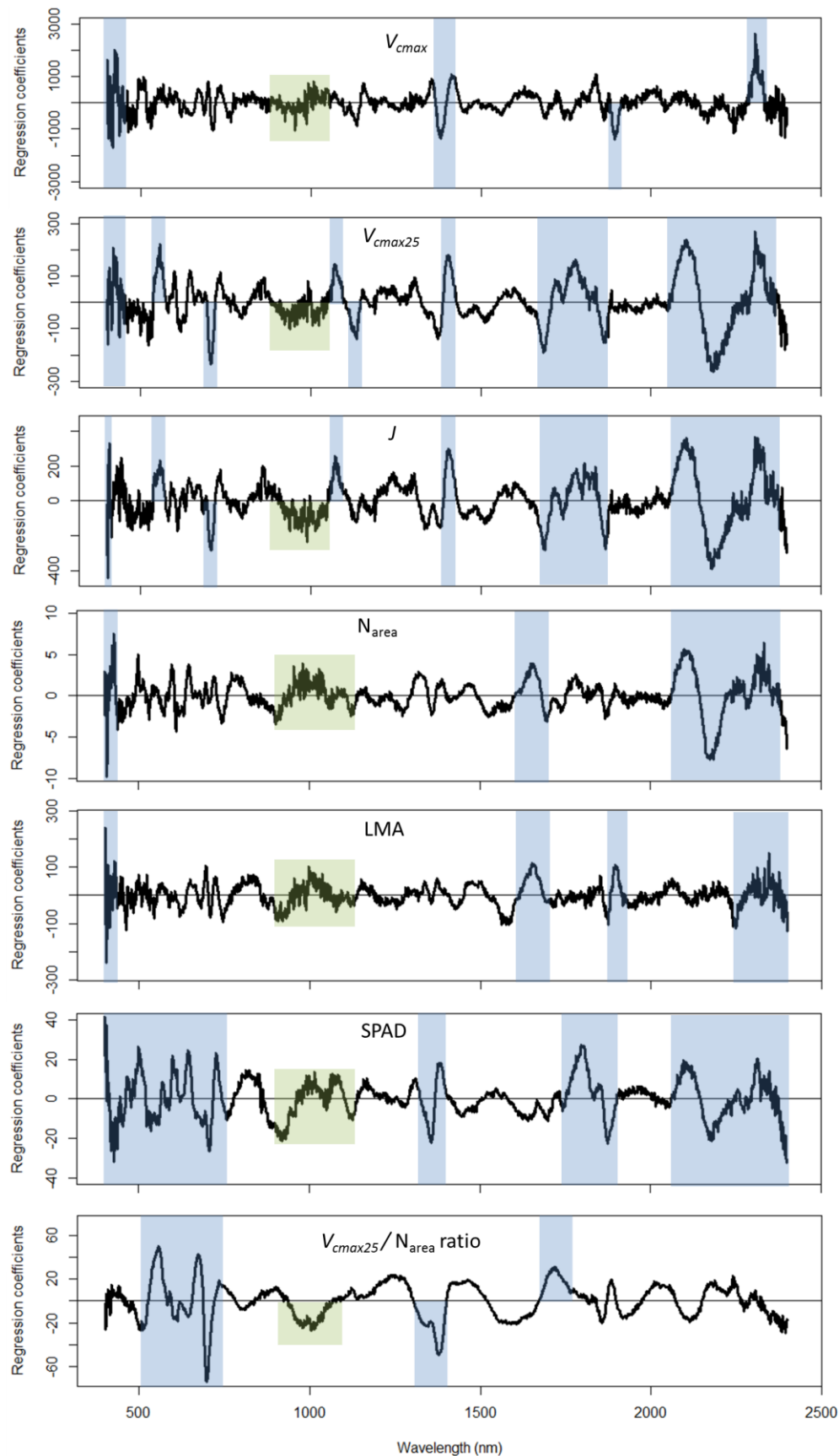
Figure 5.9 Regression coefficients for V_{cmax}, V_{cmax25}, J, N_{area}, LMA, SPAD and V_{cmax25}/N_{area}.
Blue bands represent outstanding peaks while values in the green band differ between
photosynthetic and morphological traits.

5.5   DISCUSSION

5.5.1   Important wavelength points in the spectra

From the literature some regions of the electromagnetic spectrum have been correlated with important plant physiological traits. Therefore, the spectral regions which were highly weighted in this study for prediction of LMA, N_{area}, V_{cmax} and J were compared with the regions determined in other studies.

Some experiments indicate that the visible region (VIS, 400-700 nm) (Doughty *et al.*, 2011; Serbin *et al.*, 2012) or the region from 400-1450 are important for predicting LMA (Ecarnot *et al.*, 2013). From the current work with wheat, while those regions are important, the short wave infrared (SWIR) region seems to be more important (Figure 5.9, LMA). Perhaps, reflectance is integrating the information of cellulose, proteins, starch and nitrogen that have been located before in leaves in the SWIR region (Curran, 1989).

The VIS region and the red edge (RE, 690-740 nm 700-740 nm) have been found to be important in predicting nitrogen content (Dillen *et al.*, 2012) and nitrogen concentration (Doughty *et al.*, 2011; Serbin *et al.*, 2012; Ecarnot *et al.*, 2013). The VIS-RE region was confirmed here as important, but again the SWIR region looks to be more important (Figure 5.9, N_{area}). The SWIR region has also been identified in other studies (Serbin *et al.*, 2012; Ecarnot *et al.*, 2013).

Fewer regions were associated with V_{cmax} in this project than for V_{cmax25}. Some regions overlapped: 400-460 nm, 1390-1430 nm and 2263-2333 nm. Some regions associated with V_{cmax25} in this study are similar to regions detected in soybean and aspen (Ainsworth *et al.*, 2014): 550, 700-750, 1400-1430 and 2200 in soybean and 2210 in aspen (Serbin *et al.*, 2012). These regions could be important for predicting V_{cmax25} across species. The advantage of identifying fewer and specific wavelengths for a given trait is that it may enable the construction of a lighter, cheaper spectroradiometer specific for measuring V_{cmax25}.

Regression coefficients for J from measurements in aspen and cotton indicated 44 important wavelengths across the whole spectrum (Serbin *et al.*, 2012). This large number increases the probability of matching wavelengths selected in this study and makes it more difficult to establish a trend. The best conclusion from this comparison is that the whole spectrum, including the SWIR, region is required to predict J (Table 5.3). Interestingly, comparing predictions of J with predictions of V_{cmax25} revealed similar regions except for the negative peak around 1130 nm for V_{cmax25}, which was not relevant to aspen (Serbin *et al.*, 2012).

Table 5.3 Summary of the coefficients of determination for each model and important spectral regions for each trait.

Plant material and source	[1]V_{cmax} [2]V_{cmax25} [3]V_{cmax30}	J	LMA	N_{mass} (%)	N_{area}	[4]Chl *a, b* [5]SPAD [6]Chl NDI
159 tropical plants (Doughty *et al.*, 2011)	[1]0.39	0.52	0.9 ~750, ~2250	0.83 ~750, ~2250		[4]0.66-0.67 ~750, ~2250
Aspen, Cotton (Serbin *et al.*, 2012)	0.89 495-710 1510-1935 2210, 2405, 2490	0.93 465-710 >1095	0.95 545 705-955 >1245	0.89 505-855 1690-1995 2115, 2470, 2480		
Red oak, paper birch (Dillen *et al.*, 2012)	[1]0.76 λRE 692-740	0.57 λRE			0.67 λRE	[6]0.87 λRE
Wheat (Ecarnot *et al.*, 2013)			0.94 400-1450	0.94 450-780 1180-1280 >1700		
Soybean (Ainsworth *et al.*, 2014)	[2]0.88 ~550 640-670 ~750 1400-2200					
9 Food crops e.g. Avocado, oat, grape (Serbin *et al.*, 2015)	[3]0.94 400-700 743 1150-1300 >1300					
This study Wheat/Triticale	[1]0.62 [2]0.68 See text	0.71	0.89		0.93	[5]0.82

Regression coefficients for V_{cmax25}/N_{area} showed less noise than the coefficients from other traits and interestingly, the larger correlations were found in the visible region and the red edge (Figure 5.9, V_{cmax25}/N_{area}), and from 1300 to 1400 nm, similar to SPAD. The regression coefficients for V_{cmax25}/N_{area} showed a significant contribution near ~1700 nm which was also heavily weighted for the models of both V_{cmax25} and N_{area}. Further analysis of the coefficients predicting V_{cmax25}, N_{area} and V_{cmax25}/N_{area} is needed to understand which features in reflectance spectra are most important.

5.5.2 Validation of predictions and future application of reflectance spectra

Results from the validation performed in this study (Figures 5.4 and 5.5) showed coefficients of determination within the ranges from other published predictions using reflectance (Table 5.3).

Stronger correlations were obtained for N_{area} and LMA compared to photosynthetic traits, which agree with measurements collected from multiple environments, nitrogen levels and different wheat species by Ecarnot et al. (2013). The results from this study are important since the plants evaluated were high yielding wheat and triticale many of which are currently used by farmers around the world. Moreover, even if low nitrogen treatments are removed from the correlation, it remains high (N_{area} R^2=0.8, LMA R^2=0.87). This means that hyperspectral leaf reflectance can act as rapid surrogate method suitable for use in the field which can replace destructive analyses. It was able to differentiate subtle differences between genotypes in leaf nitrogen and leaf thickness/density present in plants growing under high yield conditions.

The correlations between model predictions from reflectance and both SPAD and chlorophyll content were high (R^2=0.82 and 0.77), in agreement biochemical extraction (Doughty *et al.*, 2011) or from Chlorophyll Normalized Difference Index (Chl NDI) (Dillen *et al.*, 2012). In this study SPAD was calibrated against chlorophyll content quantified in leaf extracts and extrapolated to all experiments using an exponential equation as proposed before (Markwell *et al.*, 1995). Reflectance predictions for SPAD showed that reflectance can successfully be used to predict chlorophylls and probably other pigments as has been done for carotenoids (Asner *et al.*, 2011a; Doughty *et al.*, 2011).

V_{cmax} had a higher coefficient of determination than V_{cmax25} (R^2=0.68 *vs* 0.62) (Figure 5.4). The simplest explanation for this is that the dispersion of V_{cmax} was bigger than for V_{cmax25} due to variability of temperature during the measurements. Reflectance should represent the composition of the material rather than the rate of a reaction. Consequently, one might expect that V_{cmax25} should be the more valid model than that predicting V_{cmax}. In Chapter 2, V_{cmax} was normalized to 25 °C (V_{cmax25}), which reduced the dispersion of the data and probably the smaller range made it harder to predict this trait in fertilized plants. The residuals showed a positive trend which indicates bias in the predictions. However, the results do indicate that leaf reflectance could be used to select tails for V_{cmax25} from large populations and then small numbers of genotypes could be measured in detail by gas exchange or other low throughput approaches. Moreover, reflectance measurements will facilitate making more measurements during the plant life cycle and on more leaves within

plants, which can reduce error assessing genotypic variation of V_{cmax25} and J. In addition, reflectance using imaging spectroscopy has also shown potential for predicting V_{cmax} at the canopy level (Serbin *et al.*, 2015), which would provide an opportunity for even further collection on large numbers of leaves.

Predictions of J showed a high coefficient of determination (Figure 5.4). Part of this may be associated with the fact that J was not corrected for variation in leaf temperature. In Chapter 2 it was shown that J did not vary as much as V_{cmax} with temperature, so perhaps correction for temperature is not essential over the range encountered here. J also showed a positive trend in residuals, but similar to V_{cmax25} its prediction from reflectance measurements will help to obtain multiple measurements in a faster way to select tails that can be analysed with more accurate tools.

Interestingly, V_{cmax25}/N_{area} was predicted with a higher coefficient of determination directly than predicting each trait separately and then calculating the ratio. It may be that the N_{area} and V_{cmax25} had an additive effect in training the model more accurately. The coefficient of determination was not too high, but it should be considered that V_{cmax25} was normalized for temperature and now for leaf nitrogen, so even with an R^2 of 0.49 (Figure 5.7), the prediction of this ratio has potential to determine photosynthetic efficiency.

Reflectance spectroscopy at leaf and canopy level appears to have great potential in predicting leaf chemistry and other traits such as carotenoids, water, phosphorus (Asner and Martin, 2008; Doughty *et al.*, 2011) carbon content, $\delta^{15}N$, lignin (acid-digestible lignin), fibre (acid-digestible fibre) and cellulose (Serbin *et al.*, 2014). SPAD has been used in numerous experiments as chlorophyll surrogate (Giunta *et al.*, 2002; Lopes and Reynolds, 2012; Hamblin *et al.*, 2014)

5.6 CONCLUSIONS

In summary, it is demonstrated that hyperspectral reflectance has the power to predict V_{cmax}, V_{cmax25}, J, N_{area}, SPAD, LMA and V_{cmax25}/N_{area} in leaves of plants grown in the glasshouse or field, in Mexico and in Australia. The strongest predictions were obtained for N_{area} and LMA.

Potential regions of the spectra were identified to help understand how the model predicts each trait. However, further refinements of the models may be possible.

Hyperspectral reflectance has the potential to predict more variables underpinning photosynthesis, such as carotenoids or photoprotection.

Hyperspectral reflectance provides an opportunity to screen for genotypic variability in breeding programs and it may be possible to apply the method at the scale of the canopy level with hyperspectral imaging. The method could contribute towards efforts to monitor how crop physiology deals with climate change.

CHAPTER 6

Applying reflectance spectra to screen and select genotypes in a new set of wheat genotypes

Centro Experimental Norman E. Borlaug, Cd. Obregón, Mexico. 2013.

6.1   ABSTRACT

This study investigates if the models predicting V_{cmax}, V_{cmax25}, J, N_{area}, SPAD, LMA and V_{cmax25}/N_{area} with hyperspectral reflectance and partial least square regression (PLSR) can be used in different elite wheat populations and wheat landraces other than those used to train the model. Two new sets of genotypes were measured twice. The first set consisted of duplicated measures of 216 wheat genotypes that are candidates for CIMCOG II. Reflectance and SPAD were measured on the first occasion from which twelve genotypes were chosen for more detailed measurement. Reflectance, SPAD and J_{800} were obtained from the second measurement. The second set of genotypes consisted of 230 wheat landraces and 5 elite wheat genotypes. Again reflectance and SPAD were measured in the first survey. From this, 21 wheat landraces and 2 elite wheat genotypes were measured for reflectance, SPAD, J_{800}, LMA and N_{area} during a second survey. Previously constructed models using hyperspectral reflectance were able to make useful predictions for J_{800} and more accurate predictions for SPAD, LMA and N_{area}.

6.2   INTRODUCTION

Precision agriculture uses images from satellites to optimize crop management in the field; this technology helps to predict yield, trace soil components and detect nutrient deficiencies in plants. This can have a huge impact controlling and adding management of inputs during the crop cycle. Most of the image analysis uses the normalized difference vegetation index (NDVI). NDVI is based on specific wavelengths from the visible part of the electromagnetic spectrum (400 to 700 nm) normalised to the near infrared part of the spectrum (700 to 1100 nm). It has been used to assess leaf area index, ground cover and plant responses to photosynthetically active radiation (Lee *et al.*, 2010; Mulla, 2013). Instruments able to measure a wider spectrum (350 to 2500 nm) have the potential to contribute to precision agriculture and breeding programs, not only for stress or nutrient deficiency, but also predicting other physiological and biochemical traits in plants, in order to explore genotypic variation.

In Chapter 4, we adapted the ASD FieldSpec 3 spectroradiometer to measure hyperspectral reflectance of wheat leaves. In Chapter 5, the statistical model and algorithm for predicting several parameters from the spectra were established. We validated 6 models to predict 6 traits: three photosynthetic traits, Rubisco activity (V_{cmax25}), electron transport rate (J) and V_{cmax25}/N_{area}, and three traits to evaluate leaf structure and composition, leaf mass per unit area (LMA), chlorophyll (SPAD) and leaf nitrogen content per unit area (N_{area}).

The models based on hyperspectral reflectance were validated in Chapter 5. Because other teams have been able to predict photosynthetic parameters in tropical trees, aspen, cotton and soybean (Doughty *et al.*, 2011; Serbin *et al.*, 2012; Ainsworth *et al.*, 2014), and nitrogen content and LMA in wheat (Ecarnot *et al.*, 2013), we expect that these models can be applied to diverse wheat genotypes measured in the field. In this chapter, we explore whether the models generated in Chapter 5 work with genotypes that did not contribute to their development. We also trialled using hyperspectral reflectance to rapidly screen plants in order to select a subset of wheat genotypes for more detailed gas exchange analysis.

6.3   MATERIALS AND METHODS

6.3.1   Plant material

Two new sets of wheat genotypes were used in this chapter: **1)** Candidates of CIMCOG II (**CC**). This set comprised 216 elite wheat genotypes plus seven wheat genotypes from CIMCOG Subset II (**Mex** experiment) in total giving 223 wheat genotypes (A14). They were sown in 2012-2013 winter-spring cycle to select a new set of elite wheat genotypes in CIMMYT. **2)** Wheat landraces (**L**) from the CIMMYT's 'Spikes Germplasm Bank'. 230 wheat landraces (Figure 6.1), plus five elite wheat genotypes including two from the **Mex** experiment, giving 235 wheat genotypes in total (A15).
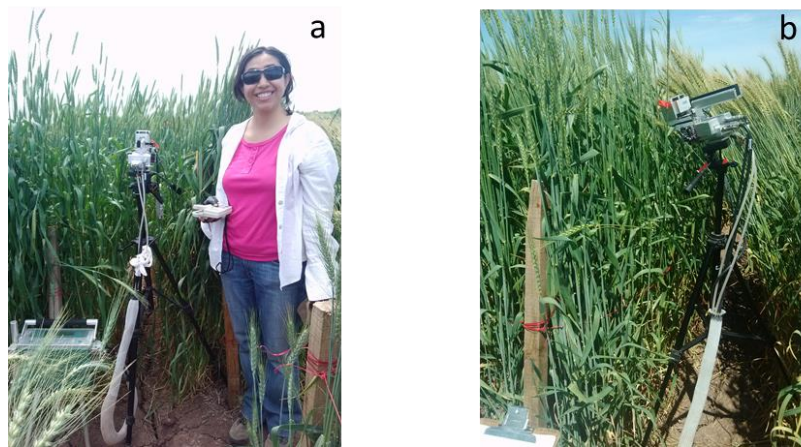
Figure 6.1 a) Some wheat landraces can be taller than me (1.60 m), b) Tall landraces are susceptible to lodging, so they were supported with wooden sticks in the field plots.

6.3.2   Experiment conditions

CC and **L** genotypes were sown near the plots from the **Mex** experiment (Chapter 3). These new sets of wheat were grown in the field at *Centro Experimental Norman E. Borlaug* (CENEB) research station, located in the Yaqui Valley, Sonora, Mexico (27.370837, -109.930362) for a winter-spring cycle. The sowing was on November 23rd, 2012 and plant

emergence was on 2nd December 2012. From 1 to 138 DAE, the average maximum temperature was 26 °C and the minimum 8.3 °C, with an accumulative thermal time of 2,364.6 °C and 15.38 mm of rainfall. Plots in both sets of wheat genotypes were 2 m long × 1.6 m, each one contained two beds arranged in the 24-56 system (24 cm distance between rows on a bed and 56 cm is the distance between rows across a furrow width).

CC plants were arranged in the field in 20 × 22 plots plus 6 plots in the 23rd row of plots to give 446 plots in total, the whole experiment comprised two randomized blocks.

L plants were sown in a band of 5 × 54 plots. From these 270 plots, 230 plots contained single landrace wheat genotypes and 40 plots contained elite wheats (checks), placed after every ten landrace plots. The checks were V522 × 10, V65 × 5, V68 × 5, V290 × 10 and V291 × 10 repetitions.

In general, plants were grown under optimal management in the field. The first fertilization was at soil preparation with 50 kg ha^{-1} of N and 50 kg ha^{-1} of P and a second fertilization in the first irrigation of 150 kg ha^{-1} of N. However, during the measurements (110 to 117 DAE) some plants showed water stress due to high temperatures, 28±2 °C (Figure 3.1).

6.3.3 Measurements

The experiment of this chapter is called **Mex2**, and the measurements were done in two main steps:

1) Survey: CC and **L** flag leaves were measured for reflectance and SPAD on all plots including repetitions and checks. For **CC** (n=440) plants were from 101 to 103 DAE, which was 15 days after anthesis on average. For **L** plants (n=270) plants were 110 to 111 DAE, which for 22 genotypes was the period from 7 days before anthesis to anthesis, with the remainder of the genotypes being from 1 to 36 days after anthesis.

2) Second measurement (S): After the survey, 12 CC genotypes and 23 L genotypes were selected and measured a second time (details of the selection will be described in Results). The measurements were done on different plants of the same genotype. In the second measurement, **CCS** genotypes were measured at 114 DAE (12 genotypes with four repetitions, two plants per plot) and **LS** at 117 DAE (21 genotypes with two repetitions, the checks V177 with six repetitions and V523 with four repetitions, two plants per plot) for reflectance, SPAD and photosynthetic rate at 400 and 800 inlet μmol CO_2 mol^{-1}. LS genotypes were also sampled to calculate leaf mass area (LMA) and leaf nitrogen content

per unit leaf area (N_{area}). The additional 'S' to CC and L refers to the second time of measurements.

6.3.4 Traits

Reflectance spectra (350-2500 nm) were measured with a FieldSpec®3 spectroradiometer (Analytical Spectral Devices, Boulder, CO, USA) coupled to a leaf-clip with an internal light source by a fibre optic cable. The leaf-clip had two panels, a white panel used for instrument calibration and a black panel used for measurements (Analytical Spectral Devices, Boulder, CO, USA). A mask was used to reduce the leaf-clip aperture to an elliptic area of 1.264 cm^2 (1.1 × 1.4 cm), a circular gasket of 2 cm diameter edge to edge and 3 mm thick was pasted to the mask to prevent leaf damage and entrance of external light through the edges. Each measurement lasted 9 to 12 s, with the leaf placed vertically (parallel to the handle of the leaf-clip). For each leaf, three readings from a SPAD-502 chlorophyll meter (Minolta Camera Co., Ltd, Japan) were averaged per leaf lamina and one reflectance measurement was made.

In this survey, we wanted to screen the maximum number of genotypes, so no gas exchange measurements were made. Having identified a subset of genotypes, gas exchange was subsequently measured at two CO_2 concentrations in a 2 cm^2 leaf area enclosed within a LI-6400XT instrument (LI-COR Inc., Lincoln, NE, USA) with the fluorescence head (Li-6400-40; LI-COR Inc.). The airflow rate in the system was 400 µmol s^{-1} with an irradiance of 1800 µmol quanta m^{-2} s^{-1}. Gas exchange was used to measure the photosynthetic rate (*A*) at 400 and 800 inlet µmol CO_2 mol^{-1}. Electron transport rate (*J*) was calculated with equation 6.1 and gas exchange measurements, which assumes RuBP (ribulose-1,5-bisphosphate) regeneration rate is limiting (von Caemmerer, 2000). In this case, we were interested in fast measurements, so only one high CO_2 concentration was used for the calculation of *J* and mitochondrial respiration was ignored.

$$J = \frac{A_{800}(4C_{c,800}+8\Gamma_*)}{C_{c,800}-\Gamma_*} \tag{6.1}$$

where $\boldsymbol{A_{800}}$ is the CO_2 assimilation rate measured at 800 inlet µmol CO_2 mol^{-1}. $\boldsymbol{C_{c,800}}$ is the chloroplastic CO_2 partial pressure calculated from measurements made with an inlet CO_2 concentration of 800 µmol CO_2 mol^{-1}.

The chloroplastic CO_2 partial pressure (Equation 6.2) and the chloroplastic CO_2 partial pressure at which the rate of carboxylation equals the rate of photorespiratory CO_2 release

was adjusted to leaf temperature using the Arrhenius equation (Equation 6.3). Information about activation energy and values at 25 °C used are described in Chapter 2.

$$C_{c,800} = C_{i,800} - \frac{A_{800}}{g_m} \tag{6.2}$$

$C_{i,800}$ is the intercellular CO_2 partial pressure, μbar, when measured with an inlet CO_2 concentration of 800 μmol CO_2 mol^{-1} and mesophyll conductance at 25 °C (g_m) was assumed to be 0.55 mol m^{-2} s^{-1} bar^{-1}.

$$\Gamma_* = \Gamma_{*25} \frac{O}{210} e^{\left(\frac{E(T-25)}{R298.15(T+273.15)}\right)} \tag{6.3}$$

Γ_* is the chloroplastic CO_2 partial pressure at which the rate of carboxylation equals the rate of photorespiratory CO_2 release, at 25 °C, $\Gamma_{*25}=37.74$ μbar (Table 2.2, Chapter 2). E is the activation energy of Γ_*, 24.42 kJ mol^{-1}. T is the leaf temperature. In this case the average T of all measured leaves was used, 31.42 °C for CCS genotypes and 32.8 °C for LS genotypes. R is the gas constant 8.314 J mol^{-1} K^{-1} and O is the O_2 partial pressure, which at sea level and standard pressure is 210 mbar.

There was not enough time to measure CO_2 response curves, so J calculated from gas exchange (J_g) was compared with that calculated from chlorophyll fluorescence (J_f) (Equation 6.4).

$$J_f = \left(\frac{F_m'-F'}{F_m'}\right) fI \propto_{leaf} \tag{6.4}$$

where F_m' is the maximal fluorescence in the light and F' is the steady state of fluorescence in the light, prime (') is used because the fluorescence parameters are determined on leaves that have experienced actinic light, f is the fraction of absorbed quanta that is used by photosystem II, assumed to be 0.5. I is the incident flux density, 1800 μmol quanta m^{-2} s^{-1} and α_{leaf} is leaf absorbance, assumed to be 0.85 (LI-COR, 2011).

Electron transport rate (J_f) was calculated from fluorescence measurements at 800 inlet μmol CO_2 mol^{-1}. Stomatal conductance (g_s) was low; therefore data with g_s lower than 0.1 mol H_2O m^{-2} s^{-1} were removed. g_s of LS and CCS varied from 0.1 to 0.55 mol H_2O m^{-2} s^{-1}. J_g and J_f showed a good relationship ($R^2=0.76$) (Figure 6.2). J_g is used here to differentiate from J_f calculated from fluorescence otherwise J_g will be called J.
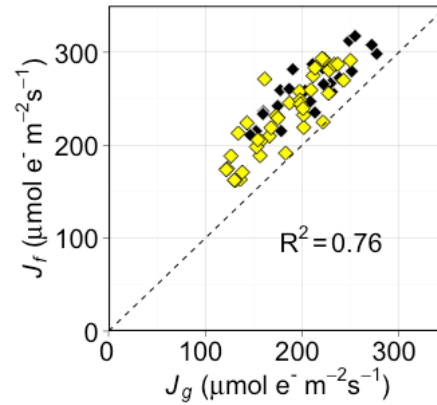
Figure 6.2 Comparison between two methods to calculate electron transport rate in wheat. J_f calculated from fluorescence as function of J_g calculated from gas exchange measurements and equation 6.1 for CCS (yellow diamond) and LS (black diamond) wheat genotypes. Dashed line represents the 1:1.

Leaf area was measured on a complete flag leaf using a leaf area meter (LI3050A/4; LICOR, Lincoln, NE). Then, the samples were dried for 48h at 70°C and weighed to obtain leaf mass per unit area (LMA, g m^{-2}). Nitrogen concentration, N_{mass} (mgN g^{-1}) was determined at CIMMYT Batan, Mexico, where samples were digested and analysed with a Technicon AutoAnalyzer (Galicia *et al.*, 2008). N_{mass} and LMA were used to calculate nitrogen per leaf area N_{area} (gN m^{-2}).

6.3.5   Statistical analysis of predictions using reflectance

The selection of CCS and LS from the survey was done predicting SPAD and *J* with the partial least square regression (PLSR) following the tutorial of the 'pls' package 'Principal Component and Partial Least Squares Regression in R' (Mevik and Wehrens, 2007). The selection of a subset of genotypes was done rapidly so as to be able to return to the field to make more detailed measurements.

The training model in March 2013 was constructed from one repetition of the glasshouse measurements in Australia (**Aus2**, Chapter 3) because they were the data available at that time. Subsequently, the reflectance spectra measured for CC, CCS, L and LS were reanalysed in 2015 to predict SPAD, *J*, Rubisco activity (V_{cmax25}), LMA, N_{area} and V_{cmax25}/N_{area}. This prediction followed the steps of the validation of the models in Chapter 5. First, jump corrections at 1000 and 1830 nm were made and spectra with reflectance lower than 0.35 and higher than 0.6 at 800 nm were removed. Then the 'pls' package 'Principal Component and Partial Least Squares Regression in R' (Mevik and Wehrens, 2007) under R software version 3.1.3 was run. The training data from Chapter 5 (Table 5.2)

were used to generate the same model. The same number of components were used to generate the same coefficients from Chapter 5, V_{cmax25} (18), J (18), N_{area} (21), LMA (21) and SPAD (16). None of the spectra measured in **Mex2** were used to train the model. Seven wheat genotypes from **Mex** experiment (V45, V48, V53, V65, V68, V72, V74) were repeated, but the plots of **Mex2** experiment were different and specific for the **Mex2** experiment.

6.4 RESULTS

First, reflectance was measured in a survey of 458 elite wheat genotypes and landraces to predict the traits. After that, for a subset of landraces and elite wheat genotypes, reflectance was measured a second time together with other traits using established methods to validate the predictions.

6.4.1 Elite wheats

The set of elite wheat genotypes, Candidates to CIMCOG II (**CC_Mex2**) were surveyed for reflectance and SPAD. Predictions of SPAD overlapped the range observed in experiments from Chapter 5 (Figure 6.3.a). From these results, 12 genotypes were chosen to measure a second time which encompassed the full range of SPAD values (Figure 6.3.b).
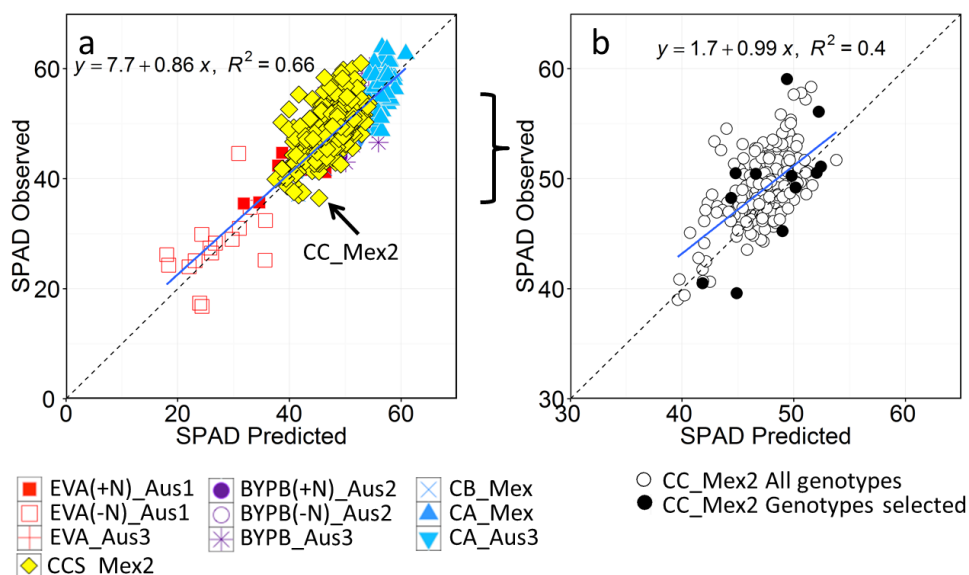
Figure 6.3 Comparison of SPAD predicted from reflectance using the model developed in Chapter 5 and actual SPAD measurements. a) Observations from experiments of chapter 5 and CC_Mex2, the R² includes all the points of the plot, b) 12 genotypes selected to measure a second time (solid points), each dot is the mean of two repetitions for the 223 genotypes.

In the second measurement (**CCS_Mex2**), predictions of electron transport rate (*J*) overlapped the range observed in Chapter 5 (Figure 6.4).

These measurements (**CC** and **CCS**) were the first attempt in the project to use reflectance to screen many genotypes and then select some of them for further analysis. This gave an indication of the number of genotypes that could be measured in a survey. Having this information, we planned a second experiment to screen wheat landraces and validate the hyperspectral reflectance by measuring more traits.
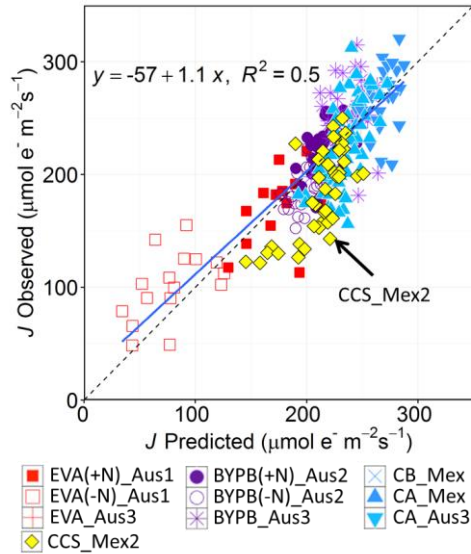
Figure 6.4 Comparison of electron transport rate (*J*) predicted from reflectance using the model developed in Chapter 5 and *J* observed for CCS_Mex2 genotypes. The R² include all the points of the plot. The dashed line represents the 1:1.

6.4.2   Landrace wheats

Wheat Landraces (**L_Mex2**) are domesticated wheats but not selected intensively for high yield. This set also included five elite wheats to add diversity and provide checks. First, 235 **L_Mex2** wheat genotypes were screened in a survey for reflectance and SPAD. Predictions of SPAD also overlapped the range observed in experiments from Chapter 5, and the correlation was slightly better for **L_Mex2** ($R^2=0.74$) compared to **CC_Mex2** ($R^2=0.66$) genotypes (Figure 6.5 and 6.3.a).
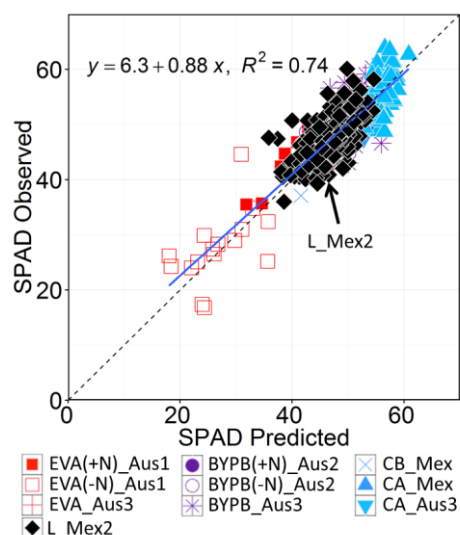
Figure 6.5 Comparison of SPAD predicted from reflectance using the model developed in Chapter 5 and actual SPAD measurements for the wheat landraces set (L_Mex2), the R² include all the points of the plot. The dashed line represents the 1:1.

At the time the reflectance survey of 235 wheat landraces was made, their phenological development ranged from seven days before to 36 days after flowering (Figure 6.6.a). Consequently, it was decided to select plants between six and nine days after flowering because the spike reaches its maximum dry weight around seven days after anthesis, the grain weight is insignificant and the water soluble carbohydrate reserves in stem are at their peak (Pask, 2012). The observed SPAD reading measured during the survey was compared against *J* predicted from reflectance model. 29 wheat genotypes between six and nine days after anthesis were dispersed within the whole range of measurements. From these 29, 21 wheat landraces and two elite wheats (checks) were chosen for more detailed measurements (Figure 6.6.b.).
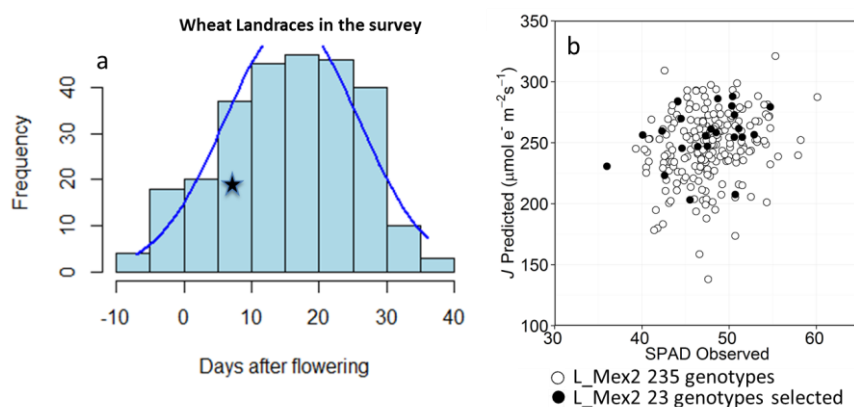
Figure 6.6 a) Histogram of the days after flowering (DAF) when the landraces were surveyed for reflectance, the star marks 5-10 DAF b) predicted *J* from the model derived in Chapter 5 shown in relation to observed SPAD. A subset of 23 wheat genotypes were selected based on their flowering time (6-9 DAF) from 235 wheat genotypes measured in the first survey.

The plot of observed SPAD versus predicted *J* for the subset of **L_Mex2** genotypes measured in the survey and again six days after the survey, **LS_Mex2** are shown in Figure 6.7. Comparing the first and second measurements, we observed that in general landrace wheats had increased SPAD and *J* in the second measurement, while the elite genotypes maintained SPAD values and reduced *J* (V523 and V177). The changes between the first and the second measurement show that trait values for genotypes can vary a lot in a few days. The spread in values for each check genotype indicates the number of replicates needed to achieve a given precision. It is also interesting that the correlation between *J* and SPAD is not high.
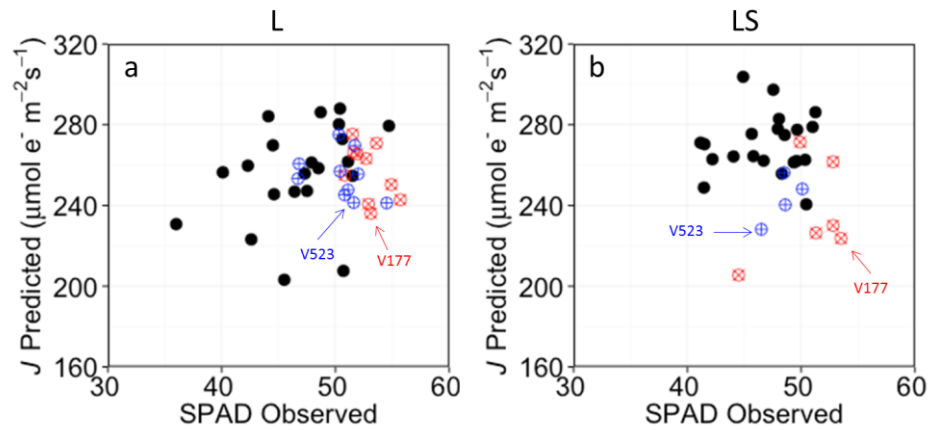
Figure 6.7 Relationship between *J* predicted and SPAD for a subset of 21 wheat landraces and 2 elite genotypes a) measured in the first survey (L), each dot is one repetition, genotypes V177 and V523 are elite genotypes with 10 repetitions each, b) six days after the survey (LS), black dots represent the mean of two repetitions while 6 and 4 repetitions are shown for V177 and V523, respectively.

When predicted *J* was compared against observed *J*, there was a tendency for predicted *J* to exceed observed *J* (Figure 6.8). Predicted and observed values of *J* fall largely within the range observed from Chapter 5 for fertilized plants. The model predicted *J* less well for landraces (**LS_Mex2**, R^2=0.4, Figure 6.8) compared to elite genotypes (**CCS_Mex2**, R^2=0.5, Figure 6.4). LMA and N_{area} predicted from reflectance models developed in Chapter 5 both correlated strongly with observed values (Figure 6.9).
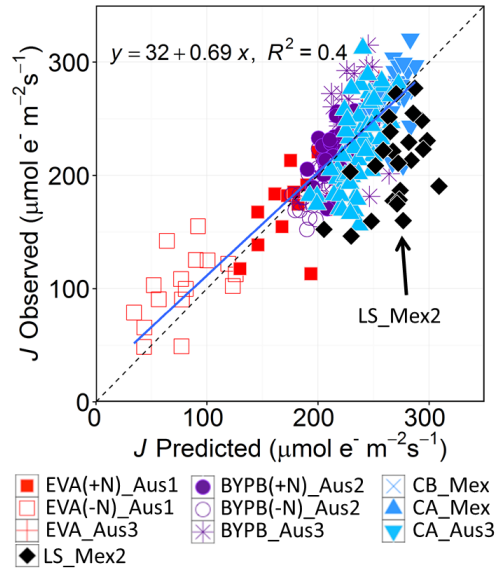
Figure 6.8 *J* **predicted from reflectance measurements as function of** *J* **calculated from gas exchange and equation 6.1. Black diamonds represent LS_Mex2 superimposed over the data used to validate the model in Chapter 5.**
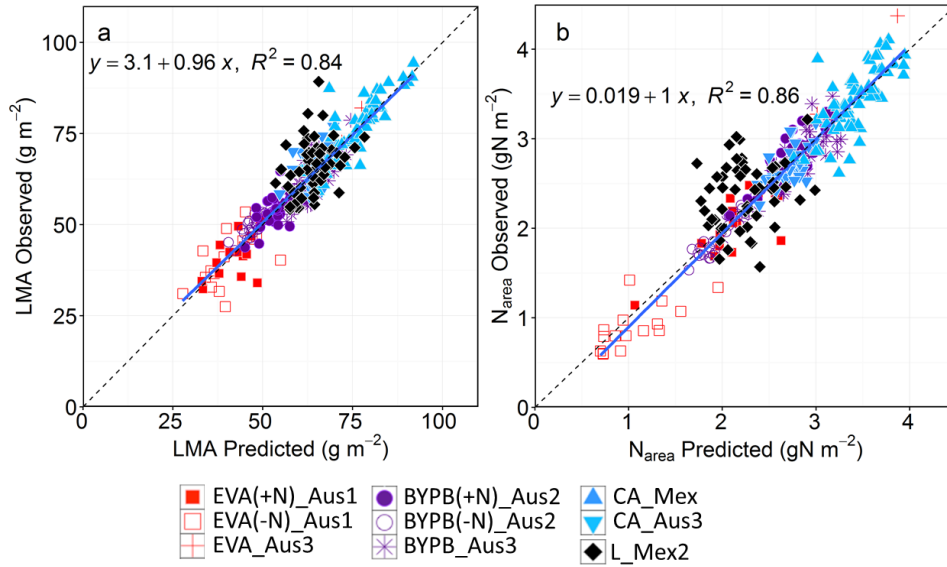
Figure 6.9 Validation of predictions using reflectance with the models derived in Chapter 5 against observed data for wheat a) LMA and b) N$_{area}$ (21 genotypes with two repetitions, check V177 with six repetitions and V523 with four repetitions for LS). There were 295 observations in total for LMA and N$_{area}$.

6.4.3 Predicting all traits

Reflectance spectra were also used to predict V_{cmax25} and V_{cmax25}/N$_{area}$. The genotypic range for each character is compared against data collected from the **Mex** experiments elite wheat genotypes from CIMCOG Subset II before anthesis (**CB_Mex**) and after anthesis (**CA_Mex**), see Chapters 3 and 5. The **L_Mex2** set of wheat genotypes showed the biggest variation in all traits. For V_{cmax25}, *J* and V_{cmax25}/N$_{area}$, the **Mex** experiments showed less variation than the **Mex2** experiments. All sets of wheat genotypes had similar ranges for

142

LMA and different ranges for N_{area} and SPAD. Also shown are the ranges for the selected subsets **LS_Mex2** and **CCS_Mex2**. Mean values for V_{cmax25}, J and V_{cmax25}/N_{area} all increased while the range narrowed for LS compared to L. By contrast, mean values for V_{cmax25}, J and N_{area} all decreased for CCS compared to CC.

J increased in the second measurement, **LS_Mex2** (Figure 6.7), and the predictions reveal that for most of these genotypes, V_{cmax25}, J and V_{cmax25}/N_{area} also increased, while LMA, N_{area} and SPAD remained similar in both measurements (Figure 6.10).

Elite genotypes from **LS_Mex2** showed a decrease in J (Figure 6.7.b), which agrees with predictions from **CCS_Mex2**. These elite genotypes reduced V_{cmax25} and J in the second measurement, and interestingly V_{cmax25}/N_{area} remained similar between occasions. N_{area} was also lower in the second measurement, but LMA and SPAD increased (Figure 6.10).
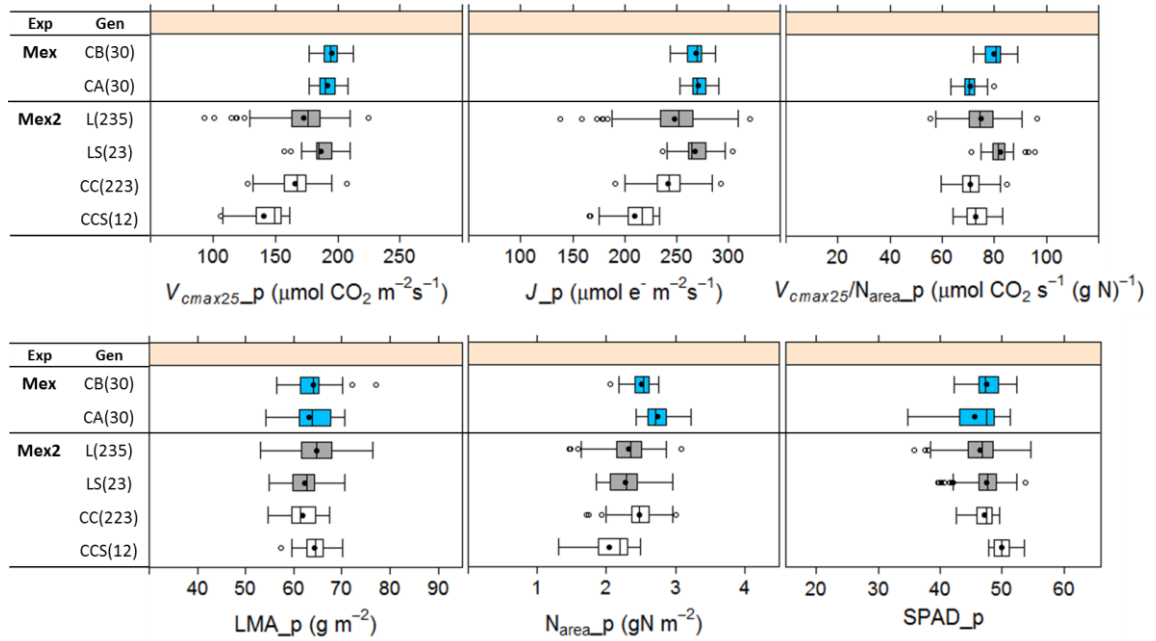
Figure 6.10 Ranges of V_{cmax25}, J, V_{cmax25}/N_{area}, LMA, N_{area} and SPAD predicted from reflectance measurements and the models generated in Chapter 5 for 6 different groups of wheat genotypes (CB, CA, L, LS, CC, CCS).

6.5 DISCUSSION

This chapter demonstrates that hyperspectral reflectance can be used in the field to rapidly screen for photosynthetic, leaf structure and composition traits. Importantly, the models generated in Chapter 5 were able to predict traits for novel genotypes that were not used in their construction. This screening method allowed us to rapidly select genotypes in the

same season in which they were measured, while biochemical analysis and gas exchange can take much longer and require many more resources to produce similar results.

6.5.1 Predicting traits for novel wheat genotypes that were not used for model derivation

Models derived from a combination of several sets of wheat genotypes were tested on genotypes which had not been used to develop the models in Chapter 5. Results revealed that it is possible to screen for V_{cmax25}, J, V_{cmax25}/N_{area}, LMA, N_{area} and SPAD using reflectance. The best predictions were obtained for LMA and N_{area}. Interestingly, models derived from aspen and cotton were able to predict leaf nitrogen concentration and LMA from reflectance measured on soybean (Ainsworth *et al.*, 2014). It would be useful to compare the models derived here for wheat with those derived from aspen and cotton.

It is still difficult to define the size and composition of the germplasm training set required to build a robust model with 2,000 wavelengths while balancing good prediction against 'over fitting'. In this project with wheat, 282 measurements were used to build the model to predict LMA, N_{area} and SPAD, and 262 measurements to predict V_{cmax25}, J, V_{cmax25}/N_{area}. These models performed well at predicting traits in 223 novel elite wheat genotypes and 235 novel wheat landraces. In another experiment with wheat, Ecarnot et al., (2013) used reflectance to predict LMA and N_{area}, using a calibration obtained from a diverse collection of wheats measured under multiple conditions and environments (Ecarnot *et al.*, 2013). By contrast, it seems that the calibration for aspen required fewer observations (Serbin *et al.*, 2012). However, in this study a strong driver of variation was environmental treatment rather than genetic variation. Further analysis comparing different sizes of training sets to construct the models is required.

In the second measurement, gas exchange was used to validate predictions of *J*. The correlation between observed *J* and predicted *J* in **Mex2** was relatively poor with R^2=0.4-0.5 (Figure 6.4 and 6.8). During the second measurement, mean leaf temperature was 32 ºC and many plants showed low g_s (average of 0.23 mol H_2O m^{-2} s^{-1}) suggesting that plants were stressed on the day of measurements. Both of these factors could influence calculations of *J* with gas exchange. There is likely to be genetic variation for g_m between elite wheats and wheat landraces as found by Jahan et al., 2014 or between leaves with different photosynthetic capacity (von Caemmerer and Evans, 1991). We assumed a constant g_m of 0.55 mol m^{-2} s^{-1} bar^{-1} for all wheat genotypes in these surveys, but because the measurements were made at high ambient CO_2 concentrations (800 ppm), the error introduced by this assumption was thought to be small. While *J* could also be estimated

from chlorophyll fluorescence, the need to surround the leaf with a high CO_2 concentration would mean that each measurement was more complicated and time consuming. Wheat landraces are a source of diversity that needs to be explored more intensively in the future.

At present we are satisfied with the calibration of the models, which provide adequate estimates for six different traits from a single hyperspectral reflectance measurement. Other instruments target only one trait such as SPAD for chlorophylls (Konica Minolta, 2009-2013) or FluorPen to estimate electron transport rate from chlorophyll fluorescence. However, choosing the best method to screen genotypes for photosynthetic traits will depend on the objectives of the experiment, and whether the data is used simply to rank genotypes or provide more precise quantitative data.

6.5.2 Leaf spectroscopy

Spectroscopy has been used widely to quantify particular molecules. For example the wavelengths 647 nm and 664 nm are routinely used to calculate chloropyll *a* and *b* in N,N-Dimethylformamide as the aqueous solvent (Porra *et al.*, 1989). Extractions of leaf tissue for lab-based spectroscopy is much more time consuming than measuring hyperspectral reflectance *in vivo*.

Leaf spectroscopy is easy to use in the field because it is quick and it is a non-destructive method. For instance, the SPAD-502, uses absorbance measurements at 660 and 940 nm, and has been widely used in the field to assess chlorophyll content and leaf nitrogen in wheat (Giunta *et al.*, 2002; Sadras *et al.*, 2012; Hamblin *et al.*, 2014). The CCM-200 hand-held chlorophyll meter from Opti-Sciences, based on absorbance at 650 and 940 nm, has also been used to estimate chlorophyll content in *Quercus* and sugar maple leaves (Cate and Perkins, 2003; Silla *et al.*, 2010). Comparisons between SPAD meter, CCM meter, reflectance indexes such as first derivative of the reflectance spectrum at 730 nm (D_{730}) and reflectance integral index (NII) have all shown good correlations with chlorophyll content (Richardson *et al.*, 2002) meaning that leaf spectroscopy has a huge potential for measuring in the field. Now, using hyperspectral reflectance as done in this project with the FieldSpec®3 spectroradiometer, more physiological plant features can be assessed in the field and correlated with the actual value of the trait. This technique has been applied in aspen, cotton and soybean (Serbin *et al.*, 2012; Ainsworth *et al.*, 2014) so the method clearly has widespread potential for use in other crops and trees. It is possible that the models generated in this project can be applied to similar grasses and crops such as rice and barley.

Reflectance is already utilised in precision agriculture. For example, Green Seeker™ (NTech Industries, Ukiah. CA, USA) is a commercial sensor that determines the normalized difference vegetation index (NDVI) from canopy reflectance in the visible and near infra-red part of the spectrum. It is used extensively in first world farming and even by farmers in Africa to determine when to apply fertilizer (Kim K, 2015). New technology allows measurements from a wider spectral band that can potentially capture the signature of more leaf traits and predict their values. As more teams explore hyperspectral reflectance for crop management, ecosystems management and landscape ecology (Jones and Vaughan, 2010), predictive power will improve as demonstrated by the estimation of nitrogen in forest canopies (Smith *et al.*, 2003).

Leaf biochemistry based reflectance measurements definitely have great potential for agricultural use in breeding programs to select for genetic diversity, and for this reason more research is needed in this field to improve the power of the technique and instrument affordability.

6.6   CONCLUSIONS

Hyperspectral reflectance modelling of wheat leaves accurately predicted V_{cmax25}, J, LMA, N_{area}, SPAD and V_{cmax25}/N_{area} in previously uncharacterised wheat germplasm. This method predicts multiple variables related to photosynthetic performance with one measurement, giving high accuracy for SPAD, LMA and N_{area}. This method is faster and cheaper than sending samples for biochemical analysis in laboratories, and shows promise for future application in crop breeding, agronomy and in crop physiology research.

CHAPTER 7

General discussion and future prospects

CSIRO Experimental Station at Ginninderra, Australia. 2013.

7.1 OVERVIEW OF THE THESIS

Improving photosynthesis has the potential to increase biomass and yield in wheat (Reynolds *et al.*, 2012b; Evans, 2013; Furbank *et al.*, 2015). One way to improve photosynthetic traits is exploiting existing photosynthetic diversity (Parry *et al.*, 2011). The major objective of this study was to identify if there is photosynthetic diversity in wheat, particularly in the context of whether enough diversity exist to support breeding strategies for crop improvement. The biochemical model of leaf photosynthesis was optimised for wheat, which permitted calculation of important photosynthetic components such as Rubisco activity and electron transport rate. Photosynthetic diversity was assessed with conventional methods in 67 wheat and 9 triticale genotypes where V_{cmax25}, J and V_{cmax25}/N_{area} were important traits describing photosynthetic capacity and efficiency. Since it is known that assessing photosynthetic traits with conventional methods can be slow, the next major objective was to explore a promising technique, hyperspectral leaf reflectance, to screen photosynthetic capacity and efficiency in wheat. Measurements of reflectance are faster than conventional methods such as gas exchange or leaf nitrogen. The method was able to predict V_{cmax25}, J, LMA, N_{area}, V_{cmax25}/N_{area} and SPAD from one reflectance measurement. The models generated to predict these traits were used to screen 223 elite and 235 landrace wheat genotypes. Hyperspectral leaf reflectance has a future to measure physiological and biochemical leaf traits in high throughput and the method can still be improved.

7.2 UNDERSTANDING PHOTOSYNTHETIC DIVERSITY

Phenotyping has become relevant to correlate with markers in recombinant inbreed populations to detect quantitative trait loci (QTLs) or for marker assisted selection (MAS). Thus, detection of photosynthetic diversity can help breeding programs to select genotypes with higher photosynthetic capacity and efficiency and detect QTLs. This study revealed genetic variation for photosynthetic traits in wheat; however, assessing photosynthesis in plants is complex. The leaf *per ser* is complex and it is vulnerable to environmental factors.

The leaf is the organ used by plants to harvest sunlight and where the photosynthetic process takes place. The leaf dry mass per unit area (LMA) is a trait that reflects the carbon cost of constructing leaf surface. It relates to the overall structure that contains the different photosynthetic components such as chloroplasts and Rubisco protein. Rubisco is the main enzyme of the photosynthetic process in the Calvin Cycle and accounts for a significant proportion of leaf nitrogen. Thus, LMA may set an upper limit to the quantity of photosynthetic machinery and nitrogen in a given leaf area. Leaf structure also

influences diffusion of CO_2 from stomata to Rubisco. Consequently, stomatal conductance (g_s) and mesophyll conductance (g_m) are important traits when assessing photosynthetic capacity. Rubisco activity and activation state are important for understanding Rubisco carboxylation, and they change with radiation, CO_2 concentration and temperature. Not only CO_2 limits Rubisco carboxylation. RuBP is the other substrate of Rubisco and RuBP regeneration in the Calvin Cycle requires the electron transport chain to convert light into chemical energy. Thylakoid composition and the Calvin cycle enzymes are both influenced by radiation and leaf nitrogen. Limitations in the photosynthetic machinery can vary across wheat genotypes making it difficult to correlate directly with harvest index and yield. However, there is no doubt that leaves are the essential plant organ that produces sugars which are used for growth and yield (Figure 7.1).
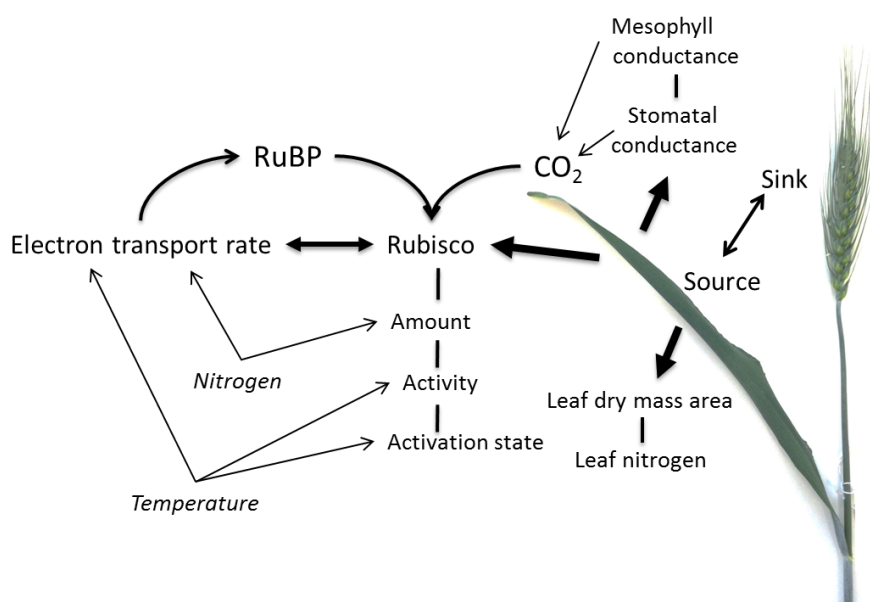
Figure 7.1 Diagram showing relationships between key photosynthetic attributes. Leaves are the main photosynthetic organ in wheat that provides sugars to the grain.

7.3   ASSESSING PHOTOSYNTHETIC DIVERSITY

The first question is to determine the traits that can be used to assess photosynthesis in plants. Photosynthetic rate (A) has been a trait commonly measured in wheat (Fischer *et al.*, 1998b; Gutierrez-Rodriguez *et al.*, 2000; Reynolds *et al.*, 2000). However, it is highly dependent on g_s (Condon *et al.*, 2004). The velocity of carboxylation (V_{cmax25}) and the electron transport rate (J) calculated from A at different CO_2 concentrations at saturated light can be determined independently from g_s and thus potentially provide robust traits to assess photosynthetic diversity (Wong *et al.*, 1979; Farquhar and Sharkey, 1982).

Results from this study showed that V_{cmax25} and Rubisco measured *in vitro* were positively correlated (Figure 3.4). However, the R^2 of the linear relationship between Rubisco *in vitro* and V_{cmax25} was relatively low ($R^2=0.52$). Similarly, in previous studies, the initial slope of A/C_i curves were positively related to Rubisco measured *in vitro* in *Phaseolus vulgaris* and wheat (von Caemmerer and Farquhar, 1981; von Caemmerer and Evans, 1991). It has been suggested that this relationship may be curvilinear. An extreme example of this was observed for an unbranching apple (Cheng and Fuchigami, 2000). This curvilinear relationship may be related to g_m and Rubisco activation state. This is documented below.

7.4   MESOPHYLL CONDUCTANCE IS IMPORTANT TO ASSESS V_{cmax25}

Mesophyll conductance, previously called CO_2 transfer conductance, is the conductance to CO_2 diffusion from intercellular airspaces to the sites of CO_2 fixation in the chloroplast stroma and influences the estimation of V_{cmax25} (Evans and von Caemmerer, 1996; Scafaro *et al.*, 2011; Evans and von Caemmerer, 2013). In this thesis, g_m has been scaled in direct proportion to assimilation rate at a given C_i (details in Chapter 2). Perhaps, the relationship between V_{cmax25} and Rubisco *in vitro* would be linear if the g_m of each genotype would be measured. It has been reported that g_m varies between plant species (von Caemmerer and Evans, 2015) and in wheat can vary from 0.2 to 0.6 mol m^{-2} s^{-1} bar^{-1} (von Caemmerer and Evans, 1991; Jahan *et al.*, 2014), which can influence V_{cmax25} specially when g_m is lower than 0.3 mol m^{-2} s^{-1} bar^{-1} (Figure 7.2). In a recent experiment, genetic diversity for V_{cmax} and J was observed between eleven wheat genotypes when g_m was used in the calculations (Jahan *et al.*, 2014). Greater variability in V_{cmax25} may have been found in this study if it had been possible to also measure g_m.
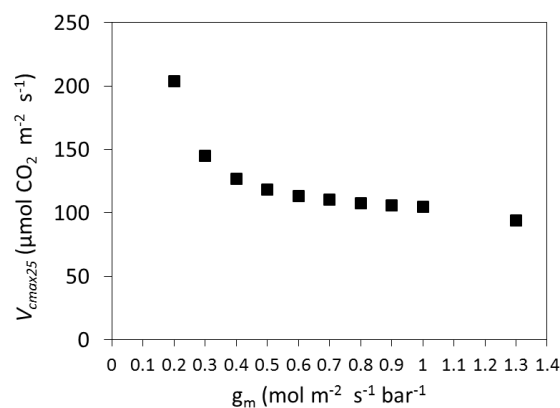
Figure 7.2 Velocity of carboxylation at 25 °C (V_{cmax25}) as a function of assumed mesophyll conductance (g_m) from an $A{:}C_c$ curve measured in *Triticum aestivum* cv. Mace.

For some species such as tobacco, g_m is very responsive to temperature, increasing three fold from 10 to 40 °C. By contrast, g_m for wheat was rather unresponsive to leaf temperature (von Caemmerer and Evans, 2015). It has been shown that g_m also changes depending on leaf nitrogen (von Caemmerer and Evans, 1991), but the underlying mechanism has yet to be conclusively explained. Mesophyll conductance has been related to the surface area of chloroplasts exposed to intercellular airspace (Evans *et al.*, 1994) and aquaporins have been implicated (Kaldenhoff and Fischer, 2006; Uehlein *et al.*, 2008).

In wheat, g_m seems to be more affected by leaf nitrogen content than by leaf temperature, which could be relevant analysing photosynthetic performance in the field. In this study genotypes measured in the field in Mexico had lower leaf nitrogen than genotypes in Australia (Figure 3.1). A deeper experiment regarding leaf nitrogen in different wheat varieties including elite and landraces genotypes would help to understand the effect of g_m on wheat photosynthetic performance.

7.5 IS CHANGING RUBISCO ACTIVATION CONTRIBUTING TO THE OBSERVED TEMPERATURE RESPONSE?

Rubisco activity varies with temperature and could be due to either E (activation energies) involved in the carboxylation and oxygenation process and/or changing Rubisco activation state. The relationship between V_{cmax25} and leaf nitrogen (Figure 3.2) could be confounded by changing activation state.

A curvilinear relationship was observed between V_{cmax25} and Rubisco measured *in vitro* (Figure 3.4). It was assumed that Rubisco was fully activated when deriving V_{cmax25} from gas exchange. However, since Rubisco activation state changes depending on environmental factors such as radiation, CO_2, temperature and leaf nitrogen availability, the assumption of full activation may be invalid in some instances. This could easily be tested by appropriate sampling and assay in future work.

In this study, measurements were taken in 1800 µmol quanta m^{-2} s^{-1} which is in the light saturated region for wheat. However, it is known that Rubisco activation state varies with irradiance. Initial Rubisco activity increases considerably when the light is turned on to 300 or 600 µmol quanta m^{-2} s^{-1} (Parry *et al.*, 1997; Parry *et al.*, 2013). Maximal Rubisco activity can also be reduced at high light intensity. Therefore, measuring after acclimation to different environments is likely to result in variability in Rubisco activation. To understand the impact of irradiance on apparent photosynthetic capacity in different wheat genotypes

growing in different environments, such as Mexico *versus* Australia, further experiments need to be undertaken.

Rubisco activity also changes depending on CO_2 concentration. CO_2 assimilation (A) also rises curvilinearly at increasing CO_2 concentrations, A increases faster up to ~380 µbar intercellular CO_2 partial pressure then it increases slightly as shown in the A:C_i curves (see von Caemmerer 2000). In sweet potato, Rubisco activation state reached a maximum of ~90% of full activation at 140 µbar intercellular CO_2 partial pressure at 25 °C. It then decreased to ~75% of Rubisco activation state at 500 µbar intercellular CO_2 partial pressure showing a higher RuBP consumption than RuBP regeneration (Sage and Kubien, 2007). Atmospheric CO_2 is relatively stable compared to irradiance or temperature the wheat growing environments, but it should be considered when determining photosynthetic capacity in wheat for future climates because CO_2 concentrations continue to increase.

A curvilinear relationship between the initial slope of the A:C_i curve as function of leaf nitrogen has previously been observed for wheat, reflecting a range of values for the initial slope at given leaf nitrogen (Evans and Seemann, 1984). It has also been suggested that Rubisco activation state can be reduced in at high leaf nitrogen content in wheat (Machler *et al.*, 1988). This could be related to the lower V_{cmax25} and higher N_{area} measured in Australia (**CA_Aus3**) than genotypes measured in Mexico (**CA_Mex**) (Figure 3.3). Further experiments evaluating Rubisco activity and Rubisco state at different leaf nitrogen levels are required in wheat.

Rubisco activation state is the ratio of initial Rubisco activity to total Rubisco activity. Rubisco activase is one type of chaperone involved in the catalytic activity of Rubisco (Portis, 2003). It has been shown that Rubisco activation state and Rubisco activase activity change with changes in temperature. In general, Rubisco activation state, Rubisco activase activity and CO_2 assimilation rise slightly at increasing temperatures and then decrease drastically from 30 to 40 °C depending on the species, their native growing environment and water status (Crafts-Brandner and Salvucci, 2000; Yamori *et al.*, 2006; Carmo-Silva and Salvucci, 2011, 2012; Parry *et al.*, 2013). In this project, activation energies for V_c, K_c and K_o were modified to assess V_{cmax} at 25 °C inferred from measurements at different temperatures (Chapter 2). The newly derived activation energies helped to improve the fitting at different temperatures. However, it is possible that instead of activation energy being incorrect, the assumption of full Rubisco activation state could be wrong at temperatures greater than 30 °C. Further analysis of Rubisco kinetics in wheat at different

temperatures is required to validate the assumption made here. To improve photosynthesis modelling, a better understanding of how Rubisco activation state changes with temperature is needed (Salvucci and Crafts-Brandner, 2004). Temperature and photosynthesis are key factors for future research related to climate change.

The current study provides an adjustment in the calculations of V_{cmax25} that can be used with other physiological traits (J, LMA, N_{area}, SPAD) in selection of wheat genotypes with high photosynthetic capacity and efficiency. However, understanding the main enzyme of photosynthesis, Rubisco, in different environments is complex because Rubisco activity changes with irradiance, CO_2 concentration, leaf nitrogen content and temperature. For this reason more experiments are required to understand the effect of these traits on photosynthetic capacity in wheat to improve the accuracy and value of screens for photosynthetic traits.

7.6 HYPERSPECTRAL REFLECTANCE PREDICTING MULTIPLE PHYSIOLOGICAL AND BIOCHEMICAL TRAITS

Hyperspectral leaf reflectance combined with partial least square regression (PLSR) modelling was able to predict the following traits: V_{cmax25}, J, LMA, N_{area} and SPAD (Chapter 5). The method is fast and multiple variables can be predicted from one reflectance measurement. In addition, the method is not static; it can be improved for future measurements and applied to other crops.

Firstly, in evaluating the advantages and disadvantages of this method, it would have been better to have a lighter instrument. This may be possible if a narrower part of the spectrum or a reduced number of wavelengths is needed because it would be possible to design a light weight, cheaper instrument with a fixed, more restricted number of wavelengths.

Using the full length spectrum (350 to 2500 nm) has proven to give good predictions for V_{cmax25}, J, LMA, N_{area}, leaf transpiration, carotenes, chlorophylls (Asner *et al.*, 2011a; Asner *et al.*, 2011b; Serbin *et al.*, 2012; Ainsworth *et al.*, 2014; Wang and Jin, 2015), and specific regions have been proposed to predict this traits. More recently, it has been proposed to combine tree regression models, PLSR, Random Forest (RFR) and Support Vector Machine regression (SVMR), to detect spectral bands. This multi-method ensemble was shown to be robust selecting spectral bands for chlorophyll, dry matter and water (Feilhauer *et al.*, 2015). Thus, it will be interesting to apply the multi-method ensembles to the data obtained in this study for wheat in order to select the most important bands and wavelengths for V_{cmax25}, J, LMA, N_{area} and SPAD. As well, bands selected for chlorophylls

calculated from SPAD could be compared with the bands obtained by Feilhauer et al., 2015 from 1267 data sets from numerous species, mainly trees.

In order to better understand leaf reflectance, it would be interesting to explore more broadly spectroscopy in leaves. A relevant technique for such analyses is infrared absorption and Raman scattering. This method has been used to track molecular vibrations that give accurate information on actual chemical structures. Raman spectroscopy and Raman imaging have been used in plants to relate cell wall components, metabolites, organic and inorganic substances with bands of the electromagnetic spectra. Infrared and Raman spectroscopy have been used to characterise plant cuticles for polysaccharides, phenols, water, etc (Gierlinger and Schwanninger, 2007; Gierlinger *et al.*, 2012; Heredia-Guerrero *et al.*, 2014). In tomato a portable spectrometer coupled to a micro-videocamera and a confocal Raman microscope was used *in vivo* to detect lycopenes and carotenoids (Trebolazabala *et al.*, 2013). Since Rubisco protein is present at high levels present in plant leaves, it will be interesting to explore if Rubisco protein can be quantified with Raman spectroscopy. Perhaps, in the future interesting peaks for Rubisco content or V_{cmax25} detected with hyperspectral reflectance and PLSR can be tested with Raman spectroscopy to more accurately quantify Rubisco protein.

Hyperspectral reflectance and PLSR has been widely applied in ecology with success. Therefore, this method can also been applied in agriculture and pre-breeding selection for biochemical and physiological traits in other crops. It has been shown that a model for leaf nitrogen generated from aspen trees reflectance measurements could be applied in soybean (Ainsworth and Long, 2005). It would be interesting to test the models obtained in this study (Chapter 5) in other Graminae such as rice or barley to see if the models or some models work with similar leaf anatomy, and in other crops with different leaf anatomy and photosynthetic pathways such as sorghum.

Hyperspectral reflectance and PLSR will enable larger populations to be screened for photosynthetic characters which can be combined with molecular markers to find regions in the plant genome related to the phenotypic character (QTLs, quantitative trait loci). Subsequently a smaller part of the genome can be studied with fine mapping to identify smaller regions of interest or genes (Collard *et al.*, 2005). The hyperspectral reflectance approach is also starting to be implemented in imaging spectroscopy to predict photosynthetic traits, leaf nitrogen and leaf dry mass area in forest and crops (Serbin *et al.*, 2014; Serbin *et al.*, 2015). Therefore, this method has a future to rapidly screen for

phenotypes that can be used to find QTLs and in marker assisted selection (Collard and Mackill, 2008).

7.7 CONCLUDING REMARKS

This thesis analysed photosynthesis from biochemistry to leaf physiology. It provides the bases to understand photosynthetic diversity in wheat at the leaf level, but further experiments at the canopy level are required to provide the link to crop biomass production.

Reflectance is a technique that can be used to measure photosynthetic and other leaf traits in the field. The next step is to evaluate V_{cmax25} and J in segregating populations to determine the variability and heritability of the traits and to identify markers that would enable their selection. This would then enable exploration of the relationships between the traits and biomass and yield with the aim of ultimately providing a new objective for incorporation into breeding programs.

References

Ainsworth EA, Long SP. 2005. What have we learned from 15 years of free-air CO_2 enrichment (FACE)? A meta-analytic review of the responses of photosynthesis, canopy. New Phytologist **165**, 351-371.

Ainsworth EA, Serbin SP, Skoneczka JA, Townsend PA. 2014. Using leaf optical properties to detect ozone effects on foliar biochemistry. Photosynthesis Research **119**, 65-76.

Asner GP, Martin RE. 2008. Spectral and chemical analysis of tropical forests: Scaling from leaf to canopy levels. Remote Sensing of Environment **112**, 3958-3970.

Asner GP, Martin RE, Ford AJ, Metcalfe DJ, Liddell MJ. 2009. Leaf chemical and spectral diversity in Australian tropical forests. Ecological Applications **19**, 236-253.

Asner GP, Martin RE, Knapp DE, Tupayachi R, Anderson C, Carranza L, Martinez P, Houcheime M, Sinca F, Weiss P. 2011a. Spectroscopy of canopy chemicals in humid tropical forests. Remote Sensing of Environment **115**, 3587-3598.

Asner GP, Martin RE, Tupayachi R, Emerson R, Martinez P, Sinca F, Powell GVN, Wright SJ, Lugo AE. 2011b. Taxonomy and remote sensing of leaf mass per area (LMA) in humid tropical forests. Ecological Applications **21**, 85-98.

Asseng S, van Herwaarden AF. 2003. Analysis of the benefits to wheat yield from assimilates stored prior to grain filling in a range of environments. Plant and Soil **256**, 217-229.

Atkin OK, Tjoelker MG. 2003. Thermal acclimation and the dynamic response of plant respiration to temperature. Trends in Plant Science **8**, 343-351.

Austin RB, Bingham J, Blackwell RD, Evans LT, Ford MA, Morgan CL, Taylor M. 1980. Genetic Improvements in Winter-Wheat Yields since 1900 and Associated Physiological-Changes. Journal of Agricultural Science **94**, 675-689.

Badger MR, Collatz GJ. 1977. Studies on the kinetic mechanism of ribulose-1,5-bisphosphate carboxylase and oxygenase reactions, with particular reference to the effect of temperature on kinetic parameters. Carnegie Institution of Washington Year Book **76**, 355-361.

Baker NR. 2008. Chlorophyll fluorescence: A probe of photosynthesis in vivo. Annual Review of Plant Biology **59**, 89-113.

Benedict HM, Swidler R. 1961. Nondestructive method for estimating chlorophyll content of leaves. Science **133**, 2015-&.

Bernacchi CJ, Portis AR, Nakano H, von Caemmerer S, Long SP. 2002. Temperature response of mesophyll conductance. Implications for the determination of Rubisco enzyme kinetics and for limitations to photosynthesis in vivo. Plant physiology **130**, 1992-1998.

Bernacchi CJ, Singsaas EL, Pimentel C, Portis AR, Long SP. 2001. Improved temperature response functions for models of Rubisco-limited photosynthesis. Plant Cell and Environment **24**, 253-259.

Berry PM, Sylvester-Bradley R, Berry S. 2006. Ideotype design for lodging-resistant wheat. Euphytica **154**, 165-179.

Borlaug NE. 2007. Sixty-two years of fighting hunger: personal recollections. Euphytica **157**, 287-297.

Borrás L, Slafer GA, Otegui MaE. 2004. Seed dry weight response to source–sink manipulations in wheat, maize and soybean: a quantitative reappraisal. Field Crops Research **86**, 131-146.

Brinkman MA, Frey KJ. 1978. Flag leaf physiological analysis of oat isolines that differ in grain-yield from their recurrent parents. Crop Science **18**, 69-73.

References

Carmo-Silva AE, Keys AJ, Andralojc PJ, Powers SJ, Arrabaca MC, Parry MAJ. 2010. Rubisco activities, properties, and regulation in three different C-4 grasses under drought. Journal of Experimental Botany **61**, 2355-2366.

Carmo-Silva AE, Salvucci ME. 2011. The activity of Rubisco's molecular chaperone, Rubisco activase, in leaf extracts. Photosynthesis Research **108**, 143-155.

Carmo-Silva AE, Salvucci ME. 2012. The temperature response of CO_2 assimilation, photochemical activities and Rubisco activation in *Camelina sativa*, a potential bioenergy crop with limited capacity for acclimation to heat stress. Planta **236**, 1433-1445.

Cate TM, Perkins TD. 2003. Chlorophyll content monitoring in sugar maple (*Acer saccharum*). Tree Physiology **23**, 1077-1079.

Chen M, Blankenship RE. 2011. Expanding the solar spectrum used by photosynthesis. Trends in Plant Science **16**, 427-431.

Chen S, Hong X, Harris CJ, Sharkey PM. 2004. Sparse modeling using orthogonal forward regression with PRESS statistic and regularization. Trans. Sys. Man Cyber. Part B **34**, 898-911.

Cheng LL, Fuchigami LH. 2000. Rubisco activation state decreases with increasing nitrogen content in apple leaves. Journal of Experimental Botany **51**, 1687-1694.

Collard BCY, Jahufer MZZ, Brouwer JB, Pang ECK. 2005. An introduction to markers, quantitative trait loci (QTL) mapping and marker-assisted selection for crop improvement: The basic concepts. Euphytica **142**, 169-196.

Collard BCY, Mackill DJ. 2008. Marker-assisted selection: an approach for precision plant breeding in the twenty-first century. Philosophical Transactions of the Royal Society of London B: Biological Sciences **363**, 557-572.

Condon AG, Farquhar GD, Richards RA. 1990. Genotypic variation in carbon isotope discrimination and transpiration efficiency in wheat. Leaf gas exchange and whole plant studies. Functional Plant Biology **17**, 9-22.

Condon AG, Richards RA, Farquhar GD. 1987. Carbon Isotope Discrimination is Positively Correlated with Grain Yield and Dry Matter Production in Field-Grown Wheat1. Crop Science **27**.

Condon AG, Richards RA, Rebetzke GJ, Farquhar GD. 2002. Improving Intrinsic Water-Use Efficiency and Crop Yield. Crop Sci **42**, 122-131.

Condon AG, Richards RA, Rebetzke GJ, Farquhar GD. 2004. Breeding for high water-use efficiency. Journal of Experimental Botany **55**, 2447-2460.

Cousins AB, Ghannoum O, von Caemmerer S, Badger MR. 2010. Simultaneous determination of Rubisco carboxylase and oxygenase kinetic parameters in *Triticum aestivum* and *Zea mays* using membrane inlet mass spectrometry. Plant Cell and Environment **33**, 444-452.

Crafts-Brandner SJ, Salvucci ME. 2000. Rubisco activase constrains the photosynthetic potential of leaves at high temperature and CO_2. Proceedings of the National Academy of Sciences of the United States of America **97**, 13430-13435.

Curran PJ. 1989. Remote sensing of foliar chemistry. Remote Sensing of Environment **30**, 271-278.

de Mendiburu F. 2015. Package 'agricolae'. Version 1.2-1. CRAN.R, 153.

Deery D, Jimenez-Berni J, Jones H, Sirault X, Furbank R. 2014. Proximal Remote Sensing Buggies and Potential Applications for Field-Based Phenotyping. Agronomy **4**, 349.

Denison RF. 2009. Chapter 9 - Darwinian Agriculture: Real, Imaginary and Complex Trade-offs as Constraints and Opportunities A2 - Sadras, Victor. In: Calderini D, ed. *Crop Physiology*. San Diego: Academic Press, 214-234.

Derkx AP, Orford S, Griffiths S, Foulkes MJ, Hawkesford MJ. 2012. Identification of Differentially Senescing Mutants of Wheat and Impacts on Yield, Biomass and Nitrogen Partitioning. Journal of Integrative Plant Biology **54**, 555-566.

Dillen SY, Op de Beeck M, Hufkens K, Buonanduci M, Phillips NG. 2012. Seasonal patterns of foliar reflectance in relation to photosynthetic capacity and color index in two co-occurring tree species, Quercus rubra and Betula papyrifera. Agricultural and Forest Meteorology **160**, 60-68.

Doughty CE, Asner GP, Martin RE. 2011. Predicting tropical plant physiology from leaf and canopy spectroscopy. Oecologia **165**, 289-299.

Driever SM, Lawson T, Andralojc PJ, Raines CA, Parry MA. 2014. Natural variation in photosynthetic capacity, growth, and yield in 64 field-grown wheat genotypes. Journal of Experimental Botany.

Ecarnot M, Compan F, Roumet P. 2013. Assessing leaf nitrogen content and leaf mass per unit area of wheat in the field throughout plant cycle with a portable spectrometer. Field Crops Research **140**, 44-50.

Evans J, Wells C, Hood K. 1999. A possible effect of different light sources on pregnancy rates following gamete intra-Fallopian transfer. Human Reproduction **14**, 80-82.

Evans JR. 1983. Nitrogen and photosynthesis in the flag leaf of wheat (*Triticum aestivum* L.). Plant Physiology **72**, 297-302.

Evans JR. 1986. The relationship between carbon-dioxide-limited photosynthetic rate and ribulose-1,5-bisphosphate-carboxylase content in two nuclear-cytoplasm substitution lines of wheat, and the coordination of ribulose-bisphosphate-carboxylation and electron-transport capacities. Planta **167**, 351-358.

Evans JR. 1989. Photosynthesis and nitrogen relationships in leaves of C_3 Plants. Oecologia **78**, 9-19.

Evans JR. 2013. Improving Photosynthesis. Plant Physiology **162**, 1780-1793.

Evans JR, Seemann JR. 1984. Differences between Wheat Genotypes in Specific Activity of Ribulose-1,5-bisphosphate Carboxylase and the Relationship to Photosynthesis. Plant Physiology **74**, 759-765.

Evans JR, Seemann JR. 1989. The allocation of protein nitrogen in the photosynthetic apparatus: costs, consequences and control. In: W.R.Brigs, ed. *Photosynthesis*. New York: Alan R. Liss, 183–205.

Evans JR, von Caemmerer S. 1996. Carbon dioxide diffusion inside leaves. Plant Physiology **110**, 339-346.

Evans JR, von Caemmerer S. 2013. Temperature response of carbon isotope discrimination and mesophyll conductance in tobacco. Plant Cell and Environment **36**, 745-756.

Evans JR, von Caemmerer S, Setchell BA, Hudson GS. 1994. The Relationship between CO_2 Transfer Conductance and Leaf Anatomy in Transgenic Tobacco with a Reduced Content of Rubisco. Australian Journal of Plant Physiology **21**, 475-495.

Evans LT. 1993. *Crop evolution, adaptation and yield*. Cambridge: Cambridge University Press.

Evans LT, Dunstone RL. 1970. Some Physiological Aspects of Evolution in Wheat. Australian Journal of Biological Sciences **23**, 725-&.

FAO. 2010. *FAOSTAT 2010* Available at http://faostat.fao.org/site/368/DesktopDefault.aspx?PageID=368#ancor, update 02 June 2010., Vol. 2012: Food and Agriculture Organization of the United Nations.

Farquhar GD, Sharkey TD. 1982. Stomatal Conductance and Photosynthesis. Annual Review of Plant Physiology and Plant Molecular Biology **33**, 317-345.

Farquhar GD, von Caemmerer S, Berry JA. 1980. A biochemical model of photosynthetic CO_2 assimilation in leaves of C_3 species Planta **149**, 78-90.

Feilhauer H, Asner GP, Martin RE. 2015. Multi-method ensemble selection of spectral bands related to leaf biochemistry. Remote Sensing of Environment **164**, 57-65.

Feret JB, Francois C, Gitelson A, Asner GP, Barry KM, Panigada C, Richardson AD, Jacquemoud S. 2011. Optimizing spectral indices and chemometric analysis of leaf chemical properties using radiative transfer modeling. Remote Sensing of Environment **115**, 2742-2750.

References

Fischer RA. 1985. Number of kernels in wheat crops and the influence of solar-radiation and temperature. Journal of Agricultural Science **105**, 447-461.

Fischer RA, Byerlee D, Edmeades GO. 2014. Crop yields and global food security: will yield increase continue to feed the world? Canberra: Australian Centre for International Agricultural Research, 634.

Fischer RA, Rees D, Sayre KD, Lu Z-M, Condon AG, Saavedra AL. 1998a. Wheat Yield Progress Associated with Higher Stomatal Conductance and Photosynthetic Rate, and Cooler Canopies. Crop Science **38**, 1467-1475.

Fischer RA, Rees D, Sayre KD, Lu ZM, Condon AG, Saavedra AL. 1998b. Wheat yield progress associated with higher stomatal conductance and photosynthetic rate, and cooler canopies. Crop Science **38**, 1467-1475.

Foulkes MJ, Slafer GA, Davies WJ, Berry PM, Sylvester-Bradley R, Martre P, Calderini DF, Griffiths S, Reynolds MP. 2011. Raising yield potential of wheat. III. Optimizing partitioning to grain while maintaining lodging resistance. Journal of Experimental Botany **62**, 469-486.

Fox J, Weisberg S. 2011. *An R companion to applied regression*. Los Angeles Calif. ; London: SAGE.

Furbank RT, Quick WP, Sirault XRR. 2015. Improving photosynthesis and yield potential in cereal crops by targeted genetic manipulation: Prospects, progress and challenges. Field Crops Research **182**, 19-29.

Furbank RT, Tester M. 2011. Phenomics - technologies to relieve the phenotyping bottleneck. Trends in Plant Science **16**, 635-644.

Galicia L, Nurit E, Rosales A, Palacios-Rojas N, eds. 2008. *Maize nutrition quality and plant tissue analysis laboratory. Laboratory protocols 2008*. Mexico City: CIMMYT.

Galmés J, Kapralov MV, Andralojc PJ, Conesa MA, Keys AJ, Parry MAJ, Flexas J. 2014. Expanding knowledge of the Rubisco kinetics variability in plant species: environmental and evolutionary trends. Plant Cell and Environment **37**, 1989-2001.

Galmes J, Kapralov MV, Copolovici LO, Hermida-Carrera C, Niinemets U. 2015. Temperature responses of the Rubisco maximum carboxylase activity across domains of life: phylogenetic signals, trade-offs, and importance for carbon gain. Photosynthesis Research **123**, 183-201.

Gamon JA, Peñuelas J, Field CB. 1992. A narrow-waveband spectral index that tracks diurnal changes in photosynthetic efficiency. Remote Sensing of Environment **41**, 35-44.

Geladi P, Kowalski BR. 1986. Partial Least-Squares Regression - a Tutorial. Analytica Chimica Acta **185**, 1-17.

Gierlinger N, Keplinger T, Harrington M. 2012. Imaging of plant cell walls by confocal Raman microscopy. Nature Protocols **7**, 1694-1708.

Gierlinger N, Schwanninger M. 2007. The potential of Raman microscopy and Raman imaging in plant research. Spectroscopy-an International Journal **21**, 69-89.

Gifford RM, Evans LT. 1981. Photosynthesis, Carbon Partitioning, and Yield. Annual review of plant physiology and plant molecular biology **32**, 485-509.

Gillon D, Houssard C, Joffre R. 1999. Using near-infrared reflectance spectroscopy to predict carbon, nitrogen and phosphorus content in heterogeneous plant material. Oecologia **118**, 173-182.

Giunta F, Motzo R, Deidda M. 2002. SPAD readings and associated leaf traits in durum wheat, barley and triticale cultivars. Euphytica **125**, 197-205.

Grace J, Nichol C, Disney M, Lewis P, Quaife T, Bowyer P. 2007. Can we measure terrestrial photosynthesis from space directly, using spectral reflectance and fluorescence? Global Change Biology **13**, 1484-1497.

Gutierrez-Rodriguez M, Reynolds MP, Larque-Saavedra A. 2000. Photosynthesis of wheat in a warm, irrigated environment - II. Traits associated with genetic gains in yield. Field Crops Research **66**, 51-62.

Haake V, Geiger M, Walch-Liu P, Of Engels C, Zrenner R, Stitt M. 1999. Changes in aldolase activity in wild-type potato plants are important for acclimation to growth irradiance and carbon dioxide concentration, because plastid aldolase exerts control over the ambient rate of photosynthesis across a range of growth conditions. The Plant Journal **17**, 479-489.

Hamblin J, Stefanova K, Angessa TT. 2014. Variation in chlorophyll content per unit leaf area in spring wheat and implications for selection in segregating material. PLoS One **9**.

Hart RH, Pearce RB, Chatterton NJ, Carlson GE, Barnes DK, Hanson CH. 1978. Alfalfa yield, specific leaf weight, CO_2 exchange-rate, and morphology. Crop Science **18**, 649-653.

Hay RKM. 1995. Harvest index: a review of its use in plant breeding and crop physiology. Annals of Applied Biology **126**, 197-216.

Heredia-Guerrero JA, Benitez JJ, Dominguez E, Bayer IS, Cingolani R, Athanassiou A, Heredia A. 2014. Infrared and Raman spectroscopic features of plant cuticles: a review. Frontiers in Plant Science **5**.

Horie T, Matsuura S, Takai T, Kuwasaki K, Ohsumi A, Shiraiwa T. 2006. Genotypic difference in canopy diffusive conductance measured by a new remote-sensing method and its association with the difference in rice yield potential. Plant Cell Environ **29**, 653-660.

Inada K. 1963. Studies on a method for determining the deepness of green and color chlorophyll content of intact crop leaves and its practical aplications. Proceedings of the Crop Science Society of Japan **32**, 157-162.

Inada K. 1985. Spectral ratio of reflectance for estimating chlorophyll content of leaf. Japanese Journal of Crop Science **54**, 261-265.

Ingle JD, Crouch SR. 1988. *Spectrochemical analysis*. Englewood Cliffs: Prentice-Hall.

Isidro J, Knox R, Clarke F, Singh A, DePauw R, Clarke J, Somers D. 2012. Quantitative genetic analysis and mapping of leaf angle in durum wheat. Planta **236**, 1713-1723.

Jahan E, Amthor JS, Farquhar GD, Trethowan R, Barbour MM. 2014. Variation in mesophyll conductance among Australian wheat genotypes. Functional Plant Biology **41**, 568-580.

Jin J, Liu X, Wang G, Mi L, Shen Z, Chen X, Herbert SJ. 2010. Agronomic and physiological contributions to the yield improvement of soybean cultivars released from 1950 to 2006 in Northeast China. Field Crops Research **115**, 116-123.

Jones HG, Vaughan RA. 2010. *Remote sensing of vegetation : principles, techniques, and applications*. Oxford ; New York: Oxford University Press.

Kaldenhoff R, Fischer M. 2006. Aquaporins in plants. Acta Physiologica **187**, 169-176.

Kalivas JH. 1997. Two data sets of near infrared spectra. Chemometrics and Intelligent Laboratory Systems **37**, 255-259.

Kim K H. 2015. Pocket sensors for precision agriculture to reach Ethiopian farmers. . *http://blog.cimmyt.org/pocket-sensors-for-precision-agriculture-to-reach-ethiopian-farmers/*, Vol. 2015: Blog CIMMYT.

King RW, Wardlaw IF, Evans LT. 1967. Effect of assimilate utilization on photosynthetic rate in wheat. Planta **77**, 261-&.

Konica Minolta I. 2009-2013.) Chlorophyl Meter SPAD-502Plus. Instruction Manual.

Kumar A, Li C, Portis A, Jr. 2009. *Arabidopsis thaliana* expressing a thermostable chimeric Rubisco activase exhibits enhanced growth and higher rates of photosynthesis at moderately high temperatures. Photosynthesis Research **100**, 143-153.

Lee WS, Alchanatis V, Yang C, Hirafuji M, Moshou D, Li C. 2010. Sensing technologies for precision specialty crop production. Computers and Electronics in Agriculture **74**, 2-33.

Lefebvre S, Lawson T, Zakhleniuk OV, Lloyd JC, Raines CA. 2005. Increased Sedoheptulose-1,7-Bisphosphatase Activity in Transgenic Tobacco Plants Stimulates

Photosynthesis and Growth from an Early Stage in Development. Plant Physiology **138**, 451-460.

LI-COR, ed. 2011. *Using the LI-6400 / LI-6400XT Portable Photosynthesis System. Version 6.* Nebraska: LI-COR Biosciences.

Long SP, Farage PK, Garcia RL. 1996. Measurement of leaf and canopy photosynthetic CO_2 exchange in the field. Journal of Experimental Botany **47**, 1629-1642.

Lopes MS, Reynolds MP. 2012. Stay-green in spring wheat can be determined by spectral reflectance measurements (normalized difference vegetation index) independently from phenology. Journal of Experimental Botany **63**, 3789-3798.

Lupton FGH. 1966. Translocation of photosynthetic assimilates in wheat. Annals of Applied Biology **57**, 355-&.

Machler F, Oberson A, Grub A, Nosberger J. 1988. Regulation of photosynthesis in nitrogen deficient wheat seedlings. Plant Physiology **87**, 46-49.

Makino A, Mae T, Ohira K. 1988. Differences between wheat and rice in the enzymic properties of Ribulose-1,5-bisphosphate carboxylase oxygenase and the relationship to photosynthetic gas-exchange. Planta **174**, 30-38.

Markwell J, Osterman JC, Mitchell JL. 1995. Calibration of the Minolta SPAD-502 leaf chlorophyll meter. Photosynthesis Research **46**, 467-472.

Martin AP, Palmer WM, Byrt CS, Furbank RT, Grof CPL. 2013. A holistic high-throughput screening framework for biofuel feedstock assessment that characterises variations in soluble sugars and cell wall composition in *Sorghum bicolor*. Biotechnology for Biofuels **6**.

Maurino VG, Peterhansel C. 2010. Photorespiration: current status and approaches for metabolic engineering. Current Opinion in Plant Biology **13**, 248-255.

McCree KJ. 1971. The action spectrum, absorptance and quantum yield of photosynthesis in crop plants. Agricultural Meteorology **9**, 191-216.

Mevik B-H, Cederkvist HR. 2004. Mean squared error of prediction (MSEP) estimates for principal component regression (PCR) and partial least squares regression (PLSR). Journal of Chemometrics **18**, 422-429.

Mevik BH, Wehrens R. 2007. The pls package: Principal component and partial least squares regression in R. Journal of Statistical Software **18**.

Monteith JL. 1977. Climate and efficiency of crop production in britain. Philosophical Transactions of the Royal Society of London Series B-Biological Sciences **281**, 277-294.

Morrison MJ, Voldeng HD, Cober ER. 1999. Physiological Changes from 58 Years of Genetic Improvement of Short-Season Soybean Cultivars in Canada ECORC contribution no. 971204. Agronomy Journal **91**.

Mulla DJ. 2013. Twenty five years of remote sensing in precision agriculture: Key advances and remaining knowledge gaps. Biosystems Engineering **114**, 358-371.

Mullan D, Mullan D. 2012. Chlorphyll content. In: Pask AJD, Pietragalla J, Mullan DM, Reynolds MP, eds. *Physiological Breeding II: A Field Guied to Wheat Phenotyping*. Mexico, D.F.: CIMMYT, 41-43.

Munns R, Rebetzke GJ, Husain S, James RA, Hare RA. 2003. Genetic control of sodium exclusion in durum wheat. Australian Journal of Agricultural Research **54**, 627-635.

Munns R, Tester M. 2008. Mechanisms of salinity tolerance. Annu Rev Plant Biol **59**, 651-681.

Murthy ASP, Ramu MNV, Yadav JSP. 1979. Effect of Saline Water Irrigation on Sodium and Potassium Uptake in up-301 Wheat (Triticum-Aestivum L). Annals of Arid Zone **18**, 62-67.

Murthy KK, Singh M. 1979. Photosynthesis, chlorophyll content and ribulose diphosphate carboxylase activity in relation to yield in wheat genotypes. Journal of Agricultural Science **93**, 7-11.

Nishio JN, Sun JD, Vogelmann TC. 1993. Carbon fixation gradients across spinach leaves do not follow internal light gradients. Plant Cell **5**, 953-961.

162

Niyogi KK, Grossman AR, Björkman O. 1998. Arabidopsis mutants define a central role for the xanthophyll cycle in the regulation of photosynthetic energy conversion. The Plant Cell **10**, 1121-1134.

Olivier DJ. 1998. Photorespiration and the C_2 cycle. In: Raghavendra AS, ed. *Photosynthesis : a comprehensive treatise*. Cambridge: Cambridge University Press, xviii, 376 p.

Ort DR, Merchant SS, Alric J, Barkan A, Blankenship RE, Bock R, Croce R, Hanson MR, Hibberd JM, Long SP, Moore TA, Moroney J, Niyogi KK, Parry MAJ, Peralta-Yahya PP, Prince RC, Redding KE, Spalding MH, van Wijk KJ, Vermaas WFJ, von Caemmerer S, Weber APM, Yeates TO, Yuan JS, Zhu XG. 2015. Redesigning photosynthesis to sustainably meet global food and bioenergy demand. Proceedings of the National Academy of Sciences **112**, 8529-8536.

Parry MA, Reynolds M, Salvucci ME, Raines C, Andralojc PJ, Zhu XG, Price GD, Condon AG, Furbank RT. 2011. Raising yield potential of wheat. II. Increasing photosynthetic capacity and efficiency. Journal of Experimental Botany **62**, 453-467.

Parry MAJ, Andralojc PJ, Parmar S, Keys AJ, Habash D, Paul MJ, Alred R, Quick WP, Servaites JC. 1997. Regulation of Rubisco by inhibitors in the light. Plant Cell and Environment **20**, 528-534.

Parry MAJ, Andralojc PJ, Scales JC, Salvucci ME, Carmo-Silva AE, Alonso H, Whitney SM. 2013. Rubisco activity and regulation as targets for crop improvement. Journal of Experimental Botany **64**, 717-730.

Parry MAJ, Keys AJ, Gutteridge S. 1989. Variation in the specificity factor of C_3 higher plant Rubiscos determined by the total consumption of Ribulose-P_2. Journal of Experimental Botany **40**, 317-320.

Pask AJD. 2012. Determining key developmental stages. In: Pask AJD, Pietragalla J, Mullan DM, Reynolds MP, eds. *Physiological Breeding II: A Field Guied to Wheat Phenotyping*. Mexico City: CIMMYT, 72-77.

Passioura JB. 1979. Accountability, philosophy and plant physiology. Search **10**, 347-350.

Passioura JB. 2010. Scaling up: the essence of effective agricultural research. Functional Plant Biology **37**, 585-591.

Patrick JW, Offler CE. 2001. Compartmentation of transport and transfer events in developing seeds. Journal of Experimental Botany **52**, 551-564.

Peñuelas J, Filella I. 1998. Visible and near-infrared reflectance techniques for diagnosing plant physiological status. Trends in Plant Science **3**, 151-156.

Peñuelas J, Garbulsky MF, Filella I. 2011. Photochemical reflectance index (PRI) and remote sensing of plant CO_2 uptake. New Phytologist **191**, 596-599.

Peñuelas J, Pinol J, Ogaya R, Filella I. 1997. Estimation of plant water concentration by the reflectance water index WI (R900/R970). International Journal of Remote Sensing **18**, 2869-2875.

Peterhansel C, Blume C, Offermann S. 2012. Photorespiratory bypasses: how can they work? Journal of Experimental Botany.

Peterhansel C, Maurino VG. 2011. Photorespiration redesigned. Plant Physiology **155**, 49-55.

Pettigrew WT, Hesketh JD, Peters DB, Woolley JT. 1989. Characterization of canopy photosynthesis of chlorophyll-deficient soybean isolines. Crop Science **29**.

Pietragalla J, Mullan D, Sereno-Mendoza R. 2012. Spectral reflectance. In: Pask AJD, Pietragalla J, Mullan DM, Reynolds MP, eds. *Physiological Breeding II: A Field Guied to Wheat Phenotyping*. Mexico, D.F.: CIMMYT, 41-43.

Pietragalla J, Pask AJD. 2012. Grain yield and yield components. In: Pask AJD, Pietragalla J, Mullan DM, Reynolds MP, eds. *Physiological Breeding II: A Field Guied to Wheat Phenotyping*. Mexico City: CIMMYT, 95-103.

Poorter H, Niinemets U, Poorter L, Wright IJ, Villar R. 2009. Causes and consequences of variation in leaf mass per area (LMA): a meta-analysis. New Phytologist **182**, 565-588.

References

Porra RJ, Thompson WA, Kriedemann PE. 1989. Determination of accurate extinction coefficients and simultaneous equations for assaying chlorophylls a and b extracted with four different solvents: verification of the concentration of chlorophyll standards by atomic absorption spectroscopy. Biochimica et Biophysica Acta (BBA) - Bioenergetics **975**, 384-394.

Porter JR, Gawith M. 1999. Temperatures and the growth and development of wheat: a review. European Journal of Agronomy **10**, 23-36.

Portis A, Jr. 2003. Rubisco activase – Rubisco's catalytic chaperone. Photosynthesis Research **75**, 11-27.

Price GD, Badger MR, von Caemmerer S. 2011. The prospect of using Cyanobacterial bicarbonate transporters to improve leaf photosynthesis in C_3 crop plants. Plant Physiology **155**, 20-26.

Prins A, Andralojc PJ, Carmo-Silva AE, Reynolds MP, Parry M. 2014. Determining Rubisco kinetic data from diverse Triticeae species. In: Reynolds MP, Molero G, Quilligan E, Listman M, Braun H, eds. *Proceedings of the 4th International Workshop of the Wheat Yield Consortium*. CENEB, CIMMYT, Cd. Obregón, Sonora, Mexico, 24-25 March 2014. Mexico: DF.:CIMMYT, 195.

Prins A, Orr DJ, Andralojc PJ, Reynolds MP, Carmo-Silva E, Parry MAJ. 2016. Rubisco catalytic properties of wild and domesticated relatives provide scope for improving wheat photosynthesis. Journal of Experimental Botany **67**, 1827-1838.

Rawson HM, Gifford RM, Bremner PM. 1976. Carbon dioxide exchange in relation to sink demand in wheat. Planta **132**, 19-23.

Reynolds M, Bonnett D, Chapman SC, Furbank RT, Manes Y, Mather DE, Parry MA. 2011a. Raising yield potential of wheat. I. Overview of a consortium approach and breeding strategies. Journal of Experimental Botany **62**, 439-452.

Reynolds M, Braun H, Quilligan E. 2012a. *Proceedings of the 2nd International Workshop of the Wheat Yield Consortium*. CENEB, CIMMYT, Cd. Obregón, Sonora, Mexico, 12-15 March 2012. Mexico: DF.: CIMMYT.

Reynolds M, Foulkes J, Furbank R, Griffiths S, King J, Murchie E, Parry M, Slafer G. 2012b. Achieving yield gains in wheat. Plant Cell and Environment **35**, 1799-1823.

Reynolds M, Foulkes MJ, Slafer GA, Berry P, Parry MAJ, Snape JW, Angus WJ. 2009. Raising yield potential in wheat. Journal of Experimental Botany **60**, 1899-1918.

Reynolds M, Gemma M, Julie M, Braun H. 2015. *Proceedings of the International TRIGO (Wheat) Yield Potential Workshop 2015*. CENEB, CIMMYT, Cd. Obregón, Sonora, Mexico, 24-26 March 2015. Mexico: DF.: CIMMYT.

Reynolds M, Mullan D, Braun H. 2011b. Proceedings of the 1st International Workshop of the Wheat Yield Consortium. CENEB, CIMMYT, Cd. Obregón, Sonora, Mexico, 1-3 March 2011. Mexico: Mexico, DF.: CIMMYT., 40.

Reynolds MP, ed. 2011. *Climate change & crop production*. Croydon: CABI.

Reynolds MP, Balota M, Delgado MIB, Amani I, Fischer RA. 1994. Physiological and morphological traits associated with spring wheat yield under hot, irrigated conditions. Australian Journal of Plant Physiology **21**, 717-730.

Reynolds MP, Braun H. 2013. *Proceedings of the 3rd International Workshop of the Wheat Yield Consortium*. CENEB, CIMMYT, Cd. Obregón, Sonora, Mexico, 5-7 March 2013. Mexico: DF.:CIMMYT.

Reynolds MP, Delgado MI, Gutierrez-Rodriguez M, Larque-Saavedra A. 2000. Photosynthesis of wheat in a warm, irrigated environment - I: Genetic diversity and crop productivity. Field Crops Research **66**, 37-50.

Reynolds MP, Molero G, Quilligan E, Listman M, Braun H. 2014. *Proceedings of the 4th International Workshop of the Wheat Yield Consortium*. CENEB, CIMMYT, Cd. Obregón, Sonora, Mexico, 24-25 March 2014. Mexico: DF.:CIMMYT.

Reynolds MP, Pellegrineschi A, Skovmand B. 2005. Sink-limitation to yield and biomass: a summary of some investigations in spring wheat. Annals of Applied Biology **146**, 39-49.

Richards RA. 2000. Selectable traits to increase crop photosynthesis and yield of grain crops. Journal of Experimental Botany **51**, 447-458.

Richardson AD, Duigan SP, Berlyn GP. 2002. An evaluation of noninvasive methods to estimate foliar chlorophyll content. New Phytologist **153**, 185-194.

Riley WJ, Ortiz-Monasterio I, Matson PA. 2001. Nitrogen leaching and soil nitrate, nitrite, and ammonium levels under irrigated wheat in Northern Mexico. Nutrient Cycling in Agroecosystems **61**, 223-236.

Sadras VO, Lawson C. 2011. Genetic gain in yield and associated changes in phenotype, trait plasticity and competitive ability of South Australian wheat varieties released between 1958 and 2007. Crop & Pasture Science **62**, 533-549.

Sadras VO, Lawson C, Montoro A. 2012. Photosynthetic traits in Australian wheat varieties released between 1958 and 2007. Field Crops Research **134**, 19-29.

Sadras VO, Richards RA. 2014. Improvement of crop yield in dry environments: benchmarks, levels of organisation and the role of nitrogen. Journal of Experimental Botany **65**, 1981-1995.

Sage RF. 2002. Variation in the k_{cat} of Rubisco in C_3 and C_4 plants and some implications for photosynthetic performance at high and low temperature. Journal of Experimental Botany **53**, 609-620.

Sage RF, Kubien DS. 2007. The temperature response of C_3 and C_4 photosynthesis. Plant, Cell & Environment **30**, 1086-1106.

Salvucci ME, Crafts-Brandner SJ. 2004. Inhibition of photosynthesis by heat stress: the activation state of Rubisco as a limiting factor in photosynthesis. Physiologia Plantarum **120**, 179-186.

Sanchez-Bragado R, Molero G, Reynolds MP, Araus JL. 2014. Relative contribution of shoot and ear photosynthesis to grain filling in wheat under good agronomical conditions assessed by differential organ δ13C. Journal of Experimental Botany **65**, 5401-5413.

Sayre KD, Rajaram S, Fischer RA. 1997. Yield potential progress in short bread wheats in northwest Mexico. Crop Science **37**, 36-42.

Scafaro AP, Von Caemmerer S, Evans JR, Atwell BJ. 2011. Temperature response of mesophyll conductance in cultivated and wild *Oryza* species with contrasting mesophyll cell wall thickness. Plant Cell and Environment **34**, 1999-2008.

Scafaro AP, Yamori W, Carmo-Silva AE, Salvucci ME, von Caemmerer S, Atwell BJ. 2012. Rubisco activity is associated with photosynthetic thermotolerance in a wild rice (*Oryza meridionalis*). Physiologia Plantarum **146**, 99-109.

Serbin SP, Dillaway DN, Kruger EL, Townsend PA. 2012. Leaf optical properties reflect variation in photosynthetic metabolism and its sensitivity to temperature. Journal of Experimental Botany **63**, 489-502.

Serbin SP, Singh A, Desai AR, Dubois SG, Jablonski AD, Kingdon CC, Kruger EL, Townsend PA. 2015. Remotely estimating photosynthetic capacity, and its response to temperature, in vegetation canopies using imaging spectroscopy. Remote Sensing of Environment.

Serbin SP, Singh A, McNeil BE, Kingdon CC, Townsend PA. 2014. Spectroscopic determination of leaf morphological and biochemical traits for northern temperate and boreal tree species. Ecological Applications **24**, 1651-1669.

Sharkey TD, Bernacchi CJ, Farquhar GD, Singsaas EL. 2007. Fitting photosynthetic carbon dioxide response curves for C_3 leaves. Plant Cell Environ **30**, 1035-1040.

Shearman VJ, Sylvester-Bradley R, Scott RK, Foulkes MJ. 2005. Physiological processes associated with wheat yield progress in the UK. Crop Science **45**, 175-185.

Shimshi D, Ephrat J. 1975. Stomatal Behavior of Wheat Cultivars in Relation to Their Transpiration, Photosynthesis, and Yield1. Agronomy Journal **67**.

References

Silla F, González-Gil A, González-Molina ME, Mediavilla S, Escudero A. 2010. Estimation of chlorophyll in Quercus leaves using a portable chlorophyll meter: effects of species and leaf age. Ann. For. Sci. **67**, 108.

Sinclair TR, Purcell LC, Sneller CH. 2004. Crop transformation and the challenge to increase yield potential. Trends in Plant Science **9**, 70-75.

Slattery RA. 2014. Analyzing variation in plant canopy conversion efficiency and assessing canopy and leaf photosynthetic efficiency in soybean with reduced chlorophyll content, University of Illinois at Urbana-Champaign, 159.

Slattery RA, Ainsworth EA, Ort DR. 2013. A meta-analysis of responses of canopy photosynthetic conversion efficiency to environmental factors reveals major causes of yield gap. Journal of Experimental Botany **64**, 3723-3733.

Smith ML, Martin ME, Plourde L, Ollinger SV. 2003. Analysis of hyperspectral data for estimation of temperate forest canopy nitrogen concentration: comparison between an airborne (AVIRIS) and a spaceborne (Hyperion) sensor. Geoscience and Remote Sensing, IEEE Transactions on **41**, 1332-1337.

Swierenga H, de Weijer AP, van Wijk RJ, Buydens LMC. 1999. Strategy for constructing robust multivariate calibration models. Chemometrics and Intelligent Laboratory Systems **49**, 1-17.

Takai T, Matsuura S, Nishio T, Ohsumi A, Shiraiwa T, Horie T. 2006. Rice yield potential is closely related to crop growth rate during late reproductive period. Field Crops Research **96**, 328-335.

Tazoe Y, von Caemmerer S, Estavillo GM, Evans JR. 2011. Using tunable diode laser spectroscopy to measure carbon isotope discrimination and mesophyll conductance to CO_2 diffusion dynamically at different CO_2 concentrations. Plant Cell and Environment **34**, 580-591.

Terashima I, Evans JR. 1988. Effects of light and nitrogen nutrition on the organization of the photosynthetic apparatus in Spinach. Plant and Cell Physiology **29**, 143-155.

Terashima I, Hanba YT, Tazoe Y, Vyas P, Yano S. 2006. Irradiance and phenotype: comparative eco-development of sun and shade leaves in relation to photosynthetic CO2 diffusion. Journal of Experimental Botany **57**, 343-354.

Townsend AR, Asner GP, Cleveland CC. 2008. The biogeochemical heterogeneity of tropical forests. Trends in ecology & evolution **23**, 424-431.

Trebolazabala J, Maguregui M, Morillas H, de Diego A, Madariaga JM. 2013. Use of portable devices and confocal Raman spectrometers at different wavelength to obtain the spectral information of the main organic components in tomato (*Solanum lycopersicum*) fruits. Spectrochimica Acta Part a-Molecular and Biomolecular Spectroscopy **105**, 391-399.

Tucker CJ. 1979. Red and photographic infrared linear combinations for monitoring vegetation. Remote Sensing of Environment **8**, 127-150.

U.N. 2015. World population prospects. The 2015 revision. Key findings and advance tables. United Nations Department of Economic and Social Affairs/Population Division, 59.

Uehlein N, Otto B, Hanson DT, Fischer M, McDowell N, Kaldenhoff R. 2008. Function of Nicotiana tabacum Aquaporins as Chloroplast Gas Pores Challenges the Concept of Membrane CO_2 Permeability. The Plant Cell **20**, 648-657.

von Caemmerer S. 2000. *Biochemical Models of Leaf Photosynthesis*. Collingwood: CSIRO.

von Caemmerer S, Evans J, Hudson G, Andrews TJ. 1994. The kinetics of ribulose-1,5-bisphosphate carboxylase/oxygenase in vivo inferred from measurements of photosynthesis in leaves of transgenic tobacco. Planta **195**, 88-97.

von Caemmerer S, Evans JR. 1991. Determination of the average partial-pressure of CO_2 in chloroplasts from leaves of several C_3 plants. Australian Journal of Plant Physiology **18**, 287-305.

von Caemmerer S, Evans JR. 2014. Temperature responses of mesophyll conductance differ greatly between species. Plant, Cell & Environment, n/a-n/a.
166

von Caemmerer S, Evans JR. 2015. Temperature responses of mesophyll conductance differ greatly between species. Plant Cell and Environment **38**, 629-637.

von Caemmerer S, Farquhar GD. 1981. Some Relationships between the Biochemistry of Photosynthesis and the Gas-Exchange of Leaves. Planta **153**, 376-387.

von Caemmerer S, Quick WP, Furbank RT. 2012. The Development of C_4 Rice: Current Progress and Future Challenges. Science **336**, 1671-1672.

Wang Q, Jin J. 2015. Leaf transpiration of drought tolerant plant can be captured by hyperspectral reflectance using PLSR analysis. iForest - Biogeosciences and Forestry **0**, 1093-1100.

Wardlaw IF, Moncur L. 1976. Source, sink and hormonal-control of translocation in wheat. Planta **128**, 93-100.

Watanabe N, Evans JR, Chow WS. 1994. Changes in the photosynthetic properties of australian wheat cultivars over the last century. Australian Journal of Plant Physiology **21**, 169-183.

Whitney SM, Birch R, Kelso C, Beck JL, Kapralov MV. 2015. Improving recombinant Rubisco biogenesis, plant photosynthesis and growth by coexpressing its ancillary RAF1 chaperone. Proceedings of the National Academy of Sciences **112**, 3564-3569.

Whitney SM, Kane HJ, Houtz RL, Sharwood RE. 2009. Rubisco oligomers composed of linked small and large subunits assemble in tobacco plastids and have higher affinities for CO_2 and O_2. Plant Physiology **149**, 1887-1895.

Wong SC, Cowan IR, Farquhar GD. 1979. Stomatal conductance correlates with photosynthetic capacity. Nature **282**, 424-426.

Yamori W, Kondo E, Sugiura D, Terashima I, Suzuki Y, Makino A. 2016. Enhanced leaf photosynthesis as a target to increase grain yield: insights from transgenic rice lines with variable Rieske FeS protein content in the cytochrome b6/f complex. Plant, Cell & Environment **39**, 80-87.

Yamori W, Noguchi K, Terashima I. 2005. Temperature acclimation of photosynthesis in spinach leaves: analyses of photosynthetic components and temperature dependencies of photosynthetic partial reactions. Plant Cell and Environment **28**, 536-547.

Yamori W, Suzuki K, Noguchi K, Nakai M, Terashima I. 2006. Effects of Rubisco kinetics and Rubisco activation state on the temperature dependence of the photosynthetic rate in spinach leaves from contrasting growth temperatures. Plant Cell and Environment **29**, 1659-1670.

Zadoks JC, Chang TT, Konzak CF. 1974. Decimal code for growth stages of cereals. Weed Research **14**, 415-421.

Zarco-Tejada PJ, Miller JR, Noland TL, Mohammed GH, Sampson PH. 2001. Scaling-up and model inversion methods with narrowband optical indices for chlorophyll content estimation in closed forest canopies with hyperspectral data. Geoscience and Remote Sensing, IEEE Transactions on **39**, 1491-1507.

Zhu XG, Long SP, Ort DR. 2010. Improving photosynthetic efficiency for greater yield. Annual Review of Plant Biology, Vol 61 **61**, 235-261.

References

Appendix

Table Chapter 2

A 1 Protocol followed to measure temperature CO_2 response curves in the field.

Genotype	Rep/Plant	LI-COR	Time	Field Temp °C	Leaf Temp °C	Block Temp °C
Curves at 26 °C						
V45	1	#3	09:00	21.9	24.6	25
	2	#3	09:28	-	25.8	25
	3	#3	09:53	-	25.7	25
V62	1	#4	09:09	22.3	24.4	25
	2	#4	09:36	-	25.7	25
	3	#4	09:59	-	26.1	25
V57	1	#4	10:24	-	26.5	25
	2	#4	10:45	-	26.8	25
	3	#4	11:10	-	27.1	25
V66	1	#3	10:14	-	26.3	25
	2	#3	10:37	-	26.6	25
	3	#3	11:02	-	26.9	25
Curves at 28 °C						
V45	1	#3	11:38	25.9	27.4	25
	2	#3	12:17	-	27.5	25
	3	#3	12:37	-	27.9	25
V62	1	#4	12:01	-	27.2	25
	2	#4	12:23	-	27.3	25
	3	#4	12:44	-	28.0	25
V57	1	#4	13:09	-	28.4	25
	2	#4	13:29	-	28.2	25
V66	1	#3	12:57	-	28.2	25
	2	#3	13:22	-	29.0	26
Curves at 30 °C						
V45	1	#3	13:51	28.3	29.6	28
	2	#3	14:10	-	31.1	28
	3	#3	14:29	-	29.9	28
V62	1	#4	13:58	27.7	29.9	28
	2	#4	14:16	-	29.7	28
	3	#4	14:36	-	29.8	28
V57	1	#4	15:00	29.6	30.3	28
	2	#4	15:22	-	30.1	28
V66	1	#3	14:57	29.4	30.4	28
	2	#3	15:16	-	30.4	28
Curves at 32 °C						
V45	1	#3	15:37	30.8	31.6	30
	2	#3	15:59	-	33.3	30
	3	#3	16:18	-	32.3	30
V62	1	#4	15:44	29.7	31.5	30

Figures Chapter 3
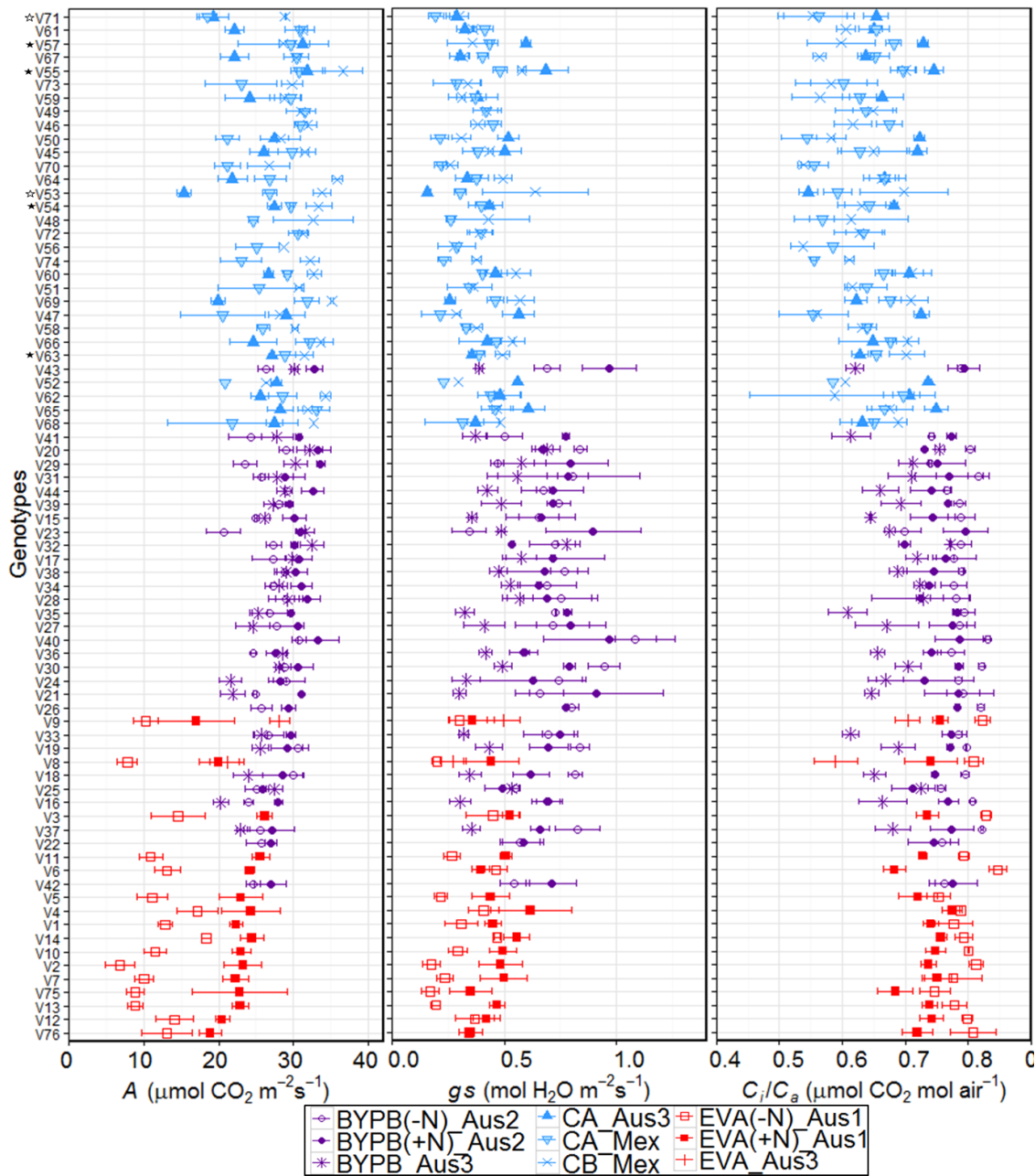
A 2 **Variation in Assimilation rate (A_{380}), stomatal conductance (g_s) and of intercellular to ambient CO_2 partial pressure (C_i/C_a) for BUNYIP set in glasshouse (circles), 30 genotypes, 2 repetitions; BUNYIP set in the field (asterisks), 28 genotypes, 4 repetitions; CIMCOG set in Australia (closed triangles), 20 genotypes, 2-8 repetitions; CIMCOG set in Mexico (open triangles), 30 genotypes, 1-3 repetitions; Early vigour set in glasshouse (squares), 16 genotypes, 3 repetitions; Early vigour in the field (plus sign), 2 genotypes, 4 repetitions. Symbols are the average of the repetitions, and error bars represent the standard error from the same repetitions.**
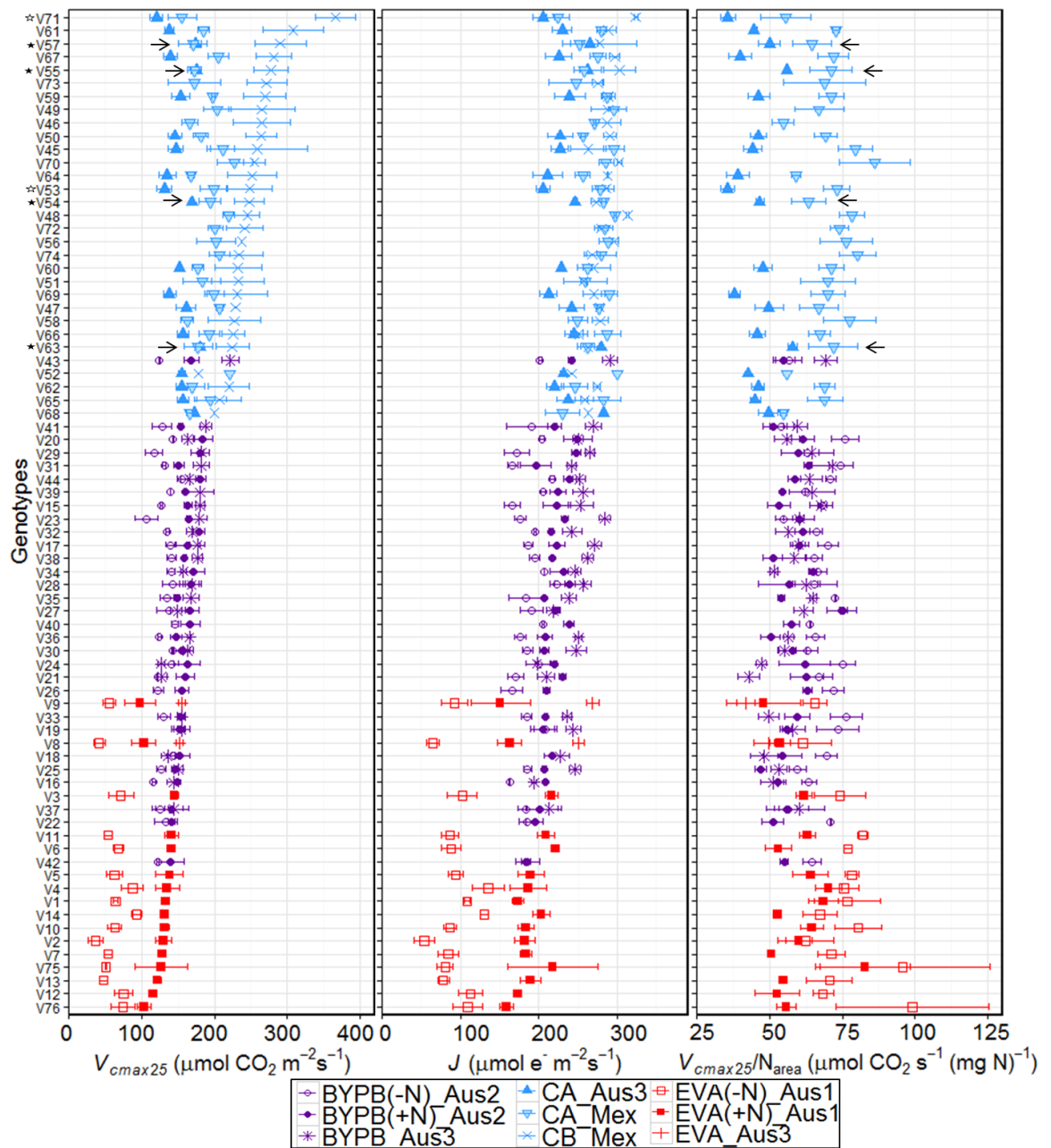
A 3 Variation in velocity of carboxylation (V_{cmax}) at 25 °C, electron transport rate from gas exchange (J), and V_{cmax} at 25 °C N_{area}^{-1} for BUNYIP set in glasshouse (circles), 30 genotypes, 2 repetitions; BUNYIP set in the field (asterisks), 28 genotypes, 4 repetitions; CIMCOG set in Australia (closed triangles), 20 genotypes, 2-8 repetitions; CIMCOG set in Mexico (open triangles), 30 genotypes, 1-3 repetitions; Early vigour set in glasshouse (squares), 16 genotypes, 3 repetitions; Early vigour in the field (plus sign), 2 genotypes, 4 repetitions. Symbols are the average of the repetitions, and error bars represent the standard error from the same repetitions.
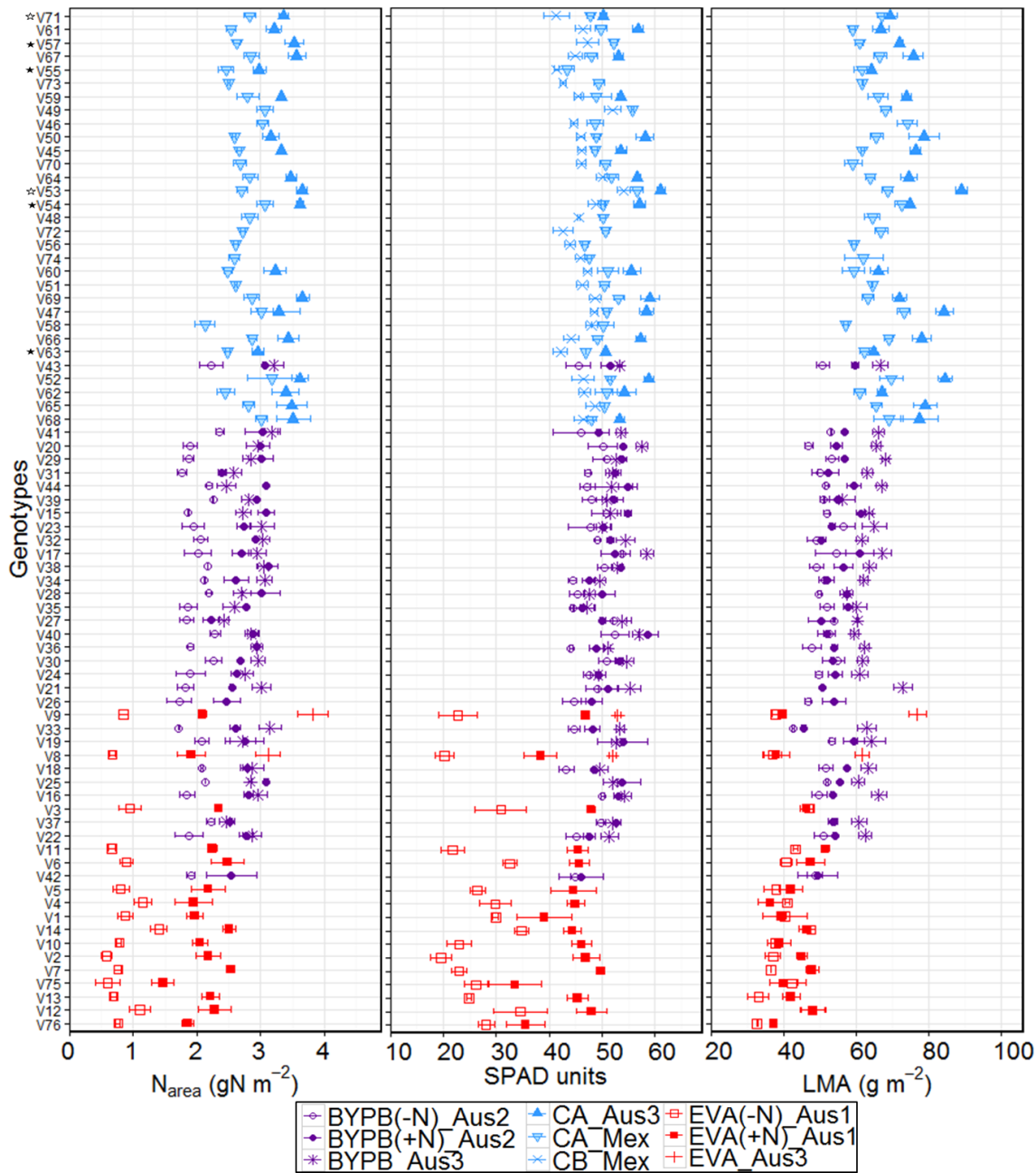
A 4 Variation in Nitrogen (N$_{area}$), chlorophylls content (SPAD units) and leaf dry mass per area (LMA) for BUNYIP set in glasshouse (circles), 30 genotypes, 2 repetitions; BUNYIP set in the field (asterisks), 28 genotypes, 4 repetitions; CIMCOG set in Australia (closed triangles), 20 genotypes, 2-8 repetitions; CIMCOG set in Mexico (open triangles), 30 genotypes, 1-3 repetitions; Early vigour set in glasshouse (squares), 16 genotypes, 3 repetitions; Early vigour in the field (plus sign), 2 genotypes, 4 repetitions. Symbols are the average of the repetitions, and error bars represent the standard error from the same repetitions.

Tables Chapter 3

A 5 Genotypes, means and Tukey's HSD test (P<0.08) for traits that showed *P-value* ≤0.06 between genotypes in the ANOVA test of the experiment EVA (±N)_Aus1, n=6. Means with the same letter are not significantly different. Honest Significant Difference (HSD).

	A			C_i/C_a			V_{cmax25}			J	
V14	22.0	a	V9	0.80	a	V14	116.7	a	V14	173.7	a
V4	20.7	ab	V6	0.78	ab	V4	111.6	ab	V75	163.0	ab
V3	20.4	ab	V3	0.78	ab	V3	108.5	ab	V4	160.8	ab
V11	18.3	abc	V4	0.78	ab	V5	101.0	ab	V3	159.4	ab
V1	17.6	abc	V2	0.77	ab	V1	98.9	ab	V11	147.9	ab
V6	17.5	abc	V8	0.77	ab	V11	97.9	ab	V12	143.0	ab
V12	17.3	abc	V10	0.77	ab	V10	97.6	ab	V5	141.7	ab
V10	17.3	abc	V14	0.77	ab	V6	97.6	ab	V6	141.5	ab
V75	17.2	abc	V12	0.77	ab	V75	96.9	ab	V1	140.9	ab
V5	17.1	abc	V7	0.76	ab	V12	95.9	ab	V76	139.0	ab
V76	16.6	abc	V11	0.76	ab	V76	92.1	ab	V10	134.9	ab
V7	16.2	bc	V1	0.76	ab	V7	91.5	ab	V7	134.1	ab
V13	15.9	bc	V13	0.76	ab	V13	84.8	ab	V13	133.9	ab
V2	15.0	c	V76	0.75	ab	V2	83.7	ab	V2	117.9	ab
V8	13.9	c	V5	0.74	ab	V9	73.0	ab	V9	115.8	ab
V9	13.0	c	V75	0.71	b	V8	72.8	b	V8	113.9	b

	V_{cmax25}/N_{area}			N_{area}			SPAD	
V75	88.08	a	V14	2.06	a	V12	41.30	a
V76	73.12	ab	V12	1.69	ab	V14	40.56	ab
V4	72.92	ab	V7	1.65	abc	V3	39.38	ab
V1	72.65	ab	V3	1.65	abc	V6	38.26	abc
V10	72.59	ab	V6	1.61	abc	V4	37.42	abc
V11	72.55	ab	V4	1.55	abc	V7	36.40	abc
V5	71.23	ab	V5	1.49	bc	V5	35.52	abc
V3	68.04	ab	V11	1.45	bc	V13	35.08	abc
V6	67.36	ab	V13	1.45	bc	V10	34.53	abc
V13	62.74	ab	V76	1.42	bc	V1	34.47	abc
V2	61.30	b	V1	1.42	bc	V11	33.60	abc
V7	61.02	b	V10	1.41	bc	V2	33.27	abc
V12	60.51	b	V2	1.38	bc	V76	32.56	abc
V14	58.67	b	V9	1.34	bc	V9	32.40	abc
V9	58.54	b	V8	1.29	bc	V75	30.60	bc
V8	57.63	b	V75	1.12	c	V8	29.28	c

A 6 Phenotypic correlation between traits from experiment Aus1. Traits with significant correlations: ***P≤ 0.001; **P≤ 0.01; *P≤ 0.055. DF=14.

	g_s	C_i/C_a	V_{cmax25}	J	N_{area}	SPAD	LMA
A	0.84***	-0.04	0.97***	0.92***	0.65**	0.67***	0.53*
g_s	1.00	0.49*	0.77***	0.63**	0.78***	0.77***	0.49*
C_i/C_a		1.00	-0.14	-0.32*	0.37	0.32	0.11
V_{cmax25}			1.00	0.91***	0.61**	0.68*	0.49*
J				1.00	0.49*	0.54*	0.49*
N_{area}					1.00	0.87***	0.61*
SPAD						1.00	0.67**

A 7 Genotypes, means and Tukey's HSD test (P<0.05) for traits that showed P-value ≤0.05 between genotypes in the ANOVA test of the experiment BYP(±N)_Aus2, n=4. Means with the same letter are not significantly different.

	A			V_{cmax25} (P<0.09)			J			V_{cmax25}/N_{area}	
V40	32.0	a	V44	168.38	a	V28	231	a	V27	75.1	a
V20	31.1	ab	V20	163.69	ab	V44	228	ab	V31	68.9	ab
V44	30.9	ab	V32	157.35	ab	V20	226	abc	V20	68.8	ab
V28	30.4	ab	V40	156.35	ab	V40	222	abcd	V24	68.6	ab
V19	29.8	ab	V34	155.47	ab	V43	221	abcd	V33	68.0	abc
V30	29.7	ab	V28	155.43	ab	V34	219	abcd	V26	67.5	abc
V38	29.6	ab	V19	152.68	ab	V18	217	abcd	V34	65.8	abc
V43	29.6	ab	V27	152.38	ab	V39	214	abcd	V17	65.2	abc
V34	29.2	ab	V24	152.13	ab	V29	210	abcd	V21	64.9	abc
V18	29.2	ab	V17	151.68	ab	V24	209	abcd	V44	64.8	abc
V27	29.1	ab	V38	150.34	ab	V19	207	abcd	V19	64.8	abc
V17	29.0	ab	V39	150.02	ab	V38	206	abcd	V32	63.7	abc
V39	28.8	ab	V29	148.95	ab	V27	206	abcd	V35	63.3	abc
V32	28.7	ab	V30	148.59	ab	V41	205	abcd	V18	62.0	abc
V24	28.6	ab	V18	148.04	ab	V32	205	abcd	V29	61.7	abc
V29	28.6	ab	V43	146.51	ab	V23	205	abcd	V28	61.2	abc
V35	28.3	ab	V15	145.23	ab	V17	204	abcd	V22	61.1	abc
V33	28.2	ab	V33	142.76	ab	V21	200	abcd	V40	60.8	abc
V21	27.9	ab	V35	142.34	ab	V33	197	abcd	V15	60.7	abc
V26	27.5	ab	V41	141.18	ab	V25	196	abcd	V30	60.5	abc
V41	27.5	ab	V31	141.06	ab	V30	196	abcd	V42	59.8	abc
V15	27.5	ab	V21	140.89	ab	V35	195	abcd	V39	58.3	bc
V31	27.2	ab	V26	139.14	ab	V15	195	abcd	V16	58.3	bc
V37	26.4	ab	V22	137.30	ab	V37	193	abcd	V38	58.2	bc
V22	26.3	ab	V23	136.20	ab	V36	192	abcd	V36	58.1	bc
V36	26.1	ab	V25	136.14	ab	V22	190	abcd	V23	57.7	bc
V16	26.0	ab	V36	136.12	ab	V26	187	bcd	V37	56.3	bc
V23	25.8	ab	V37	133.81	ab	V16	185	cd	V43	55.8	bc
V42	25.8	ab	V16	132.77	ab	V42	185	cd	V25	53.4	bc
V25	25.5	b	V42	130.97	b	V31	181	d	V41	52.7	c

	N_{area}			SPAD			LMA		
V41	2.69	a	V40	55.5	a	V17	57.8	a	
V38	2.64	ab	V19	53.8	ab	V15	56.6	ab	
V44	2.64	ab	V25	53.3	abc	V19	56.3	ab	
V43	2.64	ab	V17	53.1	abc	V44	55.5	ab	
V25	2.61	abc	V15	52.8	abcd	V43	55.2	ab	
V28	2.60	abc	V29	52.3	abcd	V29	55.1	ab	
V39	2.60	abc	V20	52.1	abcd	V41	54.9	ab	
V40	2.59	abcd	V30	52.1	abcd	V35	54.8	ab	
V32	2.49	abcde	V38	52.0	abcd	V23	54.8	ab	
V30	2.47	abcde	V16	51.6	abcd	V18	54.5	ab	
V15	2.47	abcde	V37	51.3	abcd	V30	54.2	ab	
V20	2.44	abcde	V27	51.1	abcd	V25	53.7	ab	
V29	2.44	abcde	V44	51.0	abcd	V37	53.7	ab	
V18	2.43	abcde	V32	50.4	abcd	V28	53.5	ab	
V36	2.41	abcde	V39	50.2	abcd	V39	52.9	ab	
V19	2.41	abcde	V21	50.2	abcd	V38	52.7	ab	
V37	2.37	abcde	V31	49.9	abcd	V22	52.6	ab	
V34	2.36	abcde	V23	49.0	abcd	V40	52.2	ab	
V17	2.35	abcde	V43	48.6	abcd	V27	52.1	ab	
V23	2.34	abcde	V24	48.4	abcd	V24	51.9	abc	
V16	2.32	abcde	V28	47.7	bcd	V16	51.6	abc	
V22	2.32	abcde	V41	47.6	bcd	V34	51.5	abc	
V35	2.31	abcde	V36	46.5	bcd	V31	51.1	abc	
V24	2.26	abcde	V26	46.4	bcd	V36	50.9	abc	
V42	2.22	abcde	V33	46.4	bcd	V20	50.7	abc	
V21	2.19	abcde	V22	46.4	bcd	V21	50.6	abc	
V33	2.16	bcde	V34	46.0	cd	V26	50.3	abc	
V26	2.09	cde	V18	45.9	cd	V32	49.7	bc	
V31	2.07	de	V42	45.5	d	V42	48.9	bc	
V27	2.02	e	V35	45.4	d	V33	44.1	c	

A 8 Phenotypic correlation between traits from experiment Aus2. Traits with significant correlations: ***P≤ 0.001; **P≤ 0.01; *P≤ 0.04. DF=28

	g_s	C_i/C_a	V_{cmax25}	J	N_{area}	SPAD	LMA
A	0.64***	0.21	0.90***	0.79***	0.34	0.33	0.16
g_s	1.00	0.84***	0.32	0.24	-0.05	0.31	-0.01
C_i/C_a		1.00	-0.13	-0.22	-0.31	0.14	-0.10
V_{cmax25}			1.00	0.81***	0.35	0.33	0.18
J				1.00	0.56 **	0.17	0.26
N_{area}					1.00	0.30	0.47**
SPAD						1.00	0.38*

A 9 Genotypes, means and Tukey's HSD test (P<0.05) for traits that showed P-value ≤0.05 between genotypes in the ANOVA test of the experiment BYP(+N)_Aus2 and BYP_Aus3, n=26. Means with the same letter are not significantly different.

	A			V_{cmax25}			J			V_{cmax25}/N_{area}	
V20	32.5	a	V43	204	a	V43	274	a	V31	68.8	a
V32	31.6	ab	V29	182	ab	V23	267	ab	V27	66.3	ab
V29	31.4	ab	V41	177	abc	V29	259	abc	V43	64.6	abc
V23	31.3	ab	V23	175	abcd	V17	255	abcd	V29	63.0	abc
V43	31.0	abc	V39	174	abcd	V41	253	abcde	V15	62.0	abc
V44	30.3	abcd	V15	174	abcde	V28	251	abcde	V44	61.6	abc
V17	30.2	abcd	V32	173	abcde	V20	250	abcde	V35	61.3	abc
V28	30.1	abcd	V17	172	abcde	V38	247	abcdef	V39	61.2	abc
V38	29.4	abcd	V44	172	abcde	V44	246	abcdefg	V28	60.7	abc
V34	29.1	abcde	V31	172	abcde	V39	245	abcdefg	V23	60.3	abc
V30	28.9	abcde	V38	171	abcde	V34	241	abcdefg	V17	60.2	abc
V41	28.7	abcde	V20	171	abcde	V15	241	abcdefgh	V37	58.5	abc
V36	28.2	abcde	V28	168	bcde	V36	236	bcdefgh	V32	58.1	abc
V31	28.1	abcde	V34	162	bcde	V30	234	bcdefgh	V20	57.8	abc
V39	28.0	abcde	V35	162	bcde	V32	233	bcdefgh	V19	57.3	abc
V15	27.7	abcde	V30	161	bcde	V19	231	bcdefgh	V41	56.8	abc
V33	27.0	abcde	V36	160	bcde	V25	231	bcdefgh	V30	56.1	abc
V25	26.8	abcde	V27	155	bcde	V35	228	cdefgh	V34	56.1	abc
V35	26.8	bcde	V33	155	bcde	V33	227	cdefgh	V38	56.1	abc
V19	26.7	bcde	V19	155	bcde	V31	226	cdefgh	V36	54.5	abc
V27	26.6	bcde	V25	149	bcde	V18	224	cdefgh	V24	53.2	abc
V18	25.5	cde	V16	146	bcde	V27	220	defgh	V33	53.0	bc
V21	24.9	de	V37	144	cde	V21	216	efgh	V16	52.0	bc
V37	24.6	de	V24	142	cde	V37	208	fgh	V25	50.8	bc
V24	24.2	de	V18	141	de	V24	206	gh	V18	50.3	c
V16	23.4	e	V21	138	e	V16	200	h	V21	49.6	c

	N_{area}			SPAD			LMA	
V43	3.16	a	V17	56.5	a	V21	65.3	a
V41	3.12	a	V20	56.4	a	V17	65.1	ab
V38	3.07	a	V44	55.3	ab	V43	64.3	abc
V32	3.00	ab	V30	54.2	abc	V29	64.3	abc
V20	2.97	ab	V21	53.9	abc	V44	64.2	abc
V33	2.96	ab	V25	53.9	abc	V15	63.3	abcd
V36	2.93	ab	V32	53.5	abc	V41	62.9	abcd
V25	2.93	abc	V38	53.2	abc	V19	62.5	abcd
V23	2.92	abc	V16	53.1	abc	V20	61.9	abcd
V34	2.91	abc	V19	53.0	abc	V18	61.3	abcd
V29	2.90	abc	V29	53.0	abc	V38	61.2	abcd
V30	2.87	abc	V37	52.8	abcd	V23	61.1	abcd
V17	2.86	abc	V43	52.7	abcd	V16	60.1	abcd
V39	2.86	abc	V15	52.6	abcd	V36	59.6	abcd
V21	2.85	abc	V27	52.5	abcd	V25	59.5	abcd
V18	2.84	abc	V41	52.2	abcd	V31	59.4	abcd
V15	2.84	abc	V31	52.1	abcd	V35	59.3	abcd
V16	2.82	abc	V33	51.7	abcd	V30	59.0	abcd
V28	2.81	abc	V39	51.4	abcd	V34	58.6	abcd
V44	2.80	abc	V36	50.4	bcd	V32	57.8	abcd
V19	2.73	abc	V23	50.2	bcd	V28	57.3	abcd
V24	2.68	abc	V24	49.3	bcd	V37	57.3	abcd
V35	2.65	abc	V18	49.3	bcd	V33	57.0	bcd
V31	2.51	bc	V34	48.9	cd	V27	57.0	cd
V37	2.47	bc	V28	48.4	cd	V24	56.8	cd
V27	2.35	c	V35	46.9	d	V39	55.7	d

A 10 Phenotypic correlation between traits from experiment BYPB(+N)_Aus2 and BYPB_Aus3. Traits with significant correlations: ***P≤ 0.001; **P≤ 0.01; *P≤ 0.05. DF=24.

	g_s	C_i/C_a	V_{cmax25}	J	N_{area}	SPAD	LMA
A	0.83***	0.40*	0.82***	0.87***	0.50**	0.27	0.29
g_s	1.00	0.76***	0.62***	0.58**	0.20	0.37	0.12
C_i/C_a		1.00	0.09	0.10	-0.11	0.38	-0.15
V_{cmax25}			1.00	0.87***	0.46*	0.16	0.33
J				1.00	0.60**	0.13	0.44*
N_{area}					1.00	0.17	0.39*
SPAD						1.00	0.48*

A 11 Genotypes, means and Tukey's HSD test (P<0.06) for some traits of experiments CB_ Mex and CA_Mex, n=7. Means with the same letter are not significantly different.

	A			g_s			*C_i/C_a*			*J_g*	
V69	33.10	a	V55	0.52	a	V55	0.70	a	V48	304.84	a
V55	33.06	a	V69	0.50	a	V66	0.69	a	V49	296.45	a
V66	32.89	a	V66	0.50	a	V69	0.69	a	V56	293.21	ab
V65	32.45	ab	V60	0.48	ab	V60	0.69	a	V59	292.03	ab
V54	31.50	ab	V53	0.47	ab	V63	0.68	ab	V61	288.92	ab
V49	31.21	ab	V65	0.46	ab	V65	0.67	ab	V67	288.49	ab
V46	31.18	ab	V62	0.46	ab	V64	0.66	ab	V70	287.87	ab
V61	31.05	ab	V63	0.44	ab	V68	0.66	ab	V69	285.96	ab
V72	30.95	ab	V64	0.43	ab	V62	0.65	ab	V72	285.22	ab
V60	30.92	ab	V49	0.42	ab	V53	0.65	ab	V53	284.74	ab
V62	30.78	ab	V54	0.41	ab	V49	0.64	ab	V46	284.44	ab
V45	30.63	ab	V45	0.41	ab	V46	0.64	ab	V45	281.82	ab
V64	30.43	ab	V46	0.40	ab	V57	0.64	ab	V54	281.32	ab
V67	30.37	ab	V57	0.40	ab	V45	0.64	ab	V55	279.53	ab
V53	30.29	ab	V72	0.39	ab	V54	0.64	ab	V50	276.57	abc
V63	30.17	ab	V61	0.39	ab	V58	0.64	ab	V74	273.71	abc
V59	29.20	ab	V68	0.37	ab	V72	0.63	ab	V65	273.68	abc
V57	29.11	ab	V67	0.36	ab	V51	0.63	ab	V66	272.86	abc
V58	28.05	abc	V58	0.35	ab	V61	0.63	ab	V64	272.65	abc
V48	27.79	abc	V51	0.35	ab	V67	0.61	ab	V52	272.36	abc
V74	27.58	abc	V59	0.34	ab	V59	0.60	ab	V47	271.71	abc
V51	27.56	abc	V48	0.33	ab	V52	0.59	ab	V60	269.77	abc
V73	26.39	abc	V73	0.31	ab	V73	0.59	ab	V57	267.78	abc
V56	26.33	abc	V74	0.30	ab	V48	0.59	ab	V58	267.36	abc
V68	25.46	abc	V56	0.29	ab	V74	0.58	ab	V63	265.92	abc
V50	25.46	abc	V50	0.27	ab	V56	0.57	ab	V73	262.84	abc
V52	23.60	abc	V52	0.26	ab	V50	0.57	ab	V62	260.81	abc
V70	23.25	bc	V47	0.24	ab	V71	0.56	ab	V51	260.63	abc
V47	23.06	bc	V70	0.23	b	V47	0.56	ab	V68	243.91	bc
V71	18.47	c	V71	0.20	b	V70	0.54	b	V71	225.72	c

	SPAD			BMF			PGF			DTF	
V53	55.33	a	**V47**	12.1	a	V60	40.5	a	**V47**	100	a
V49	53.88	ab	V74	12.0	a	V57	38.1	ab	**V70**	95	ab
V64	51.56	abc	V50	11.8	ab	**V55**	37.5	abc	V56	95	abc
V69	51.00	abcd	V73	11.5	ab	**V53**	37.4	abc	V50	94	bc
V47	49.80	abcde	V52	11.2	abc	V54	35.3	bcd	V52	94	bc
V57	49.73	bcde	**V70**	10.6	abc	V62	35.2	bcd	V48	93	bc
V65	49.58	bcde	V68	10.5	abc	V49	35.1	bcd	V74	93	bc
V54	49.55	bcde	V56	10.5	abc	V64	34.2	cde	V68	92	bcd
V62	49.48	bcde	V63	10.0	abc	V59	34.0	def	V73	91	cde
V60	49.17	cde	V58	10.0	abc	**V69**	34.0	def	**V71**	90	cdef
V58	49.07	cde	V67	9.8	abc	V72	33.5	defg	**V65**	87	defg
V51	48.40	cde	V72	9.5	abc	**V66**	33.2	defgh	V61	87	efg
V48	48.36	cde	**V71**	9.4	abc	**V65**	33.0	defgh	V51	87	fg
V61	48.03	cde	V64	9.4	abc	V61	32.9	defgh	V58	87	fg
V70	47.83	cde	V48	9.3	abc	V51	32.8	defgh	V63	86	fg
V71	47.73	cdef	V51	9.2	abc	V45	32.6	defghi	V45	86	g
V45	47.37	cdef	V45	9.1	abc	V63	32.6	defghi	V46	86	g
V59	47.23	cdef	**V66**	9.1	abc	V67	31.7	efghij	V67	86	g
V50	47.00	cdef	V54	9.1	abc	V46	31.7	efghij	V72	86	g
V52	46.90	cdef	**V69**	9.0	abc	V73	31.4	efghij	V59	85	gh
V74	46.78	cdef	**V65**	9.0	abc	V58	31.4	efghij	V64	85	gh
V66	46.65	def	V57	8.7	abc	V52	30.9	efghijk	**V66**	84	gh
V72	46.65	def	V61	8.5	abc	V48	30.9	fghijk	V54	84	ghi
V68	46.47	def	V46	8.5	abc	V74	30.5	ghijk	**V69**	84	ghi
V67	46.45	def	V59	8.4	abc	**V71**	30.5	ghijk	V49	81	hi
V46	46.18	def	V60	8.3	bc	V50	30.1	ghijk	**V53**	81	hi
V73	46.03	ef	V62	8.3	bc	V56	29.6	hijk	**V55**	80	i
V56	44.83	ef	V49	8.1	bc	V68	29.0	ijk	V57	80	i
V63	44.52	ef	**V55**	8.0	c	**V70**	28.9	jk	V62	80	i
V55	42.36	f	**V53**	7.0	c	**V47**	27.5	k	V60	73	j

A 12 Genotypes, means and Tukey's HSD test (P<0.05) for some traits of experiments CB_ Mex and CA_Mex, n=7. Means with the same letter are not significantly different.

Yield			HI			BMM		
V53	7.9	a	V53	0.55	a	V74	15.0	a
V73	7.4	ab	V61	0.53	ab	V64	14.9	a
V64	7.4	ab	V60	0.52	abc	V73	14.9	ab
V56	7.4	ab	V48	0.52	abc	V54	14.7	abc
V74	7.3	ab	V46	0.52	abc	V56	14.6	abc
V65	7.3	ab	V59	0.52	abc	V45	14.5	abc
V60	7.3	ab	V52	0.52	abcd	V68	14.5	abc
V54	7.2	ab	V51	0.51	abcd	V65	14.5	abc
V47	7.2	ab	V49	0.51	abcd	V47	14.4	abc
V48	7.1	ab	V69	0.51	bcd	V67	14.4	abc
V59	7.1	ab	V56	0.50	bcd	V72	14.3	abc
V50	7.1	ab	V65	0.50	bcd	V53	14.3	abc
V70	7.1	ab	V70	0.50	bcd	V50	14.3	abc
V67	7.0	ab	V50	0.50	bcd	V71	14.2	abc
V71	7.0	ab	V73	0.50	bcd	V55	14.2	abc
V72	7.0	ab	V47	0.50	bcd	V70	14.1	abc
V55	7.0	ab	V71	0.49	bcd	V60	14.0	abc
V46	6.9	ab	V64	0.49	bcd	V63	14.0	abc
V68	6.9	abc	V55	0.49	bcd	V57	13.9	abc
V69	6.9	abc	V54	0.49	bcd	V48	13.8	abc
V45	6.8	bc	V67	0.49	bcd	V59	13.7	abc
V49	6.8	bc	V72	0.49	bcd	V66	13.6	abc
V52	6.8	bc	V74	0.49	bcd	V69	13.5	abc
V51	6.7	bc	V66	0.49	bcd	V46	13.5	abc
V57	6.7	bc	V57	0.48	cd	V62	13.4	abc
V61	6.7	bc	V62	0.48	cd	V49	13.3	abc
V66	6.6	bc	V68	0.48	cd	V51	13.2	abc
V62	6.5	bc	V45	0.47	d	V52	13.2	abc
V63	6.4	bc	V58	0.47	d	V58	12.7	bc
V58	5.9	c	V63	0.46	d	V61	12.6	c

A 13 Genotypes, means and Tukey's HSD test (P<0.05) for traits that showed *P*-value ≤0.05 between genotypes in the ANOVA test of the experiment CA_Aus3 and CA_Mex, n=7. Means with the same letter are not significantly different.

	A			g_s			C_i/C_a	
V55	31.2	a	V55	0.56	a	V55	0.72	a
V57	30.5	a	V65	0.54	a	V65	0.71	a
V65	30.3	a	V57	0.53	a	V57	0.71	a
V54	28.4	ab	V52	0.49	ab	V52	0.71	a
V63	28.2	ab	V62	0.46	ab	V62	0.70	a
V66	27.8	ab	V45	0.45	abc	V60	0.69	a
V60	27.8	ab	V47	0.45	abc	V45	0.68	a
V45	27.6	ab	V66	0.44	abc	V47	0.67	a
V62	26.8	ab	V60	0.44	abc	V64	0.67	a
V59	26.5	ab	V54	0.42	abc	V54	0.67	a
V52	26.3	abc	V50	0.42	abc	V50	0.66	a
V47	26.2	abc	V59	0.38	abcd	V66	0.66	a
V68	25.6	abc	V63	0.37	abcd	V61	0.65	a
V50	25.4	abcd	V61	0.35	abcd	V59	0.65	a
V61	25.0	abcd	V64	0.35	abcd	V63	0.64	ab
V67	24.4	abcd	V68	0.35	abcd	V67	0.64	ab
V64	23.7	abcd	V67	0.33	bcd	V68	0.64	ab
V69	23.2	bcd	V69	0.31	bcd	V69	0.64	ab
V71	19.1	cd	V71	0.26	cd	V71	0.63	ab
V53	18.5	d	V53	0.20	d	V53	0.56	b
	V_{cmax25}			J			V_{cmax25}/N_{area}	
V63	181.88	a	V63	273.115	a	V63	67.52	a
V54	180.75	a	V68	266.27	a	V55	66.95	a
V55	178.26	a	V66	265.65	a	V45	59.57	ab
V66	175.74	a	V54	264.75	a	V60	58.74	ab
V65	175.61	a	V59	263.39	a	V57	57.30	abc
V57	175.49	a	V55	263.18	a	V62	57.30	abc
V45	175.13	a	V57	261.98	a	V59	57.01	abc
V59	172.86	a	V65	259.90	a	V65	56.30	abc
V68	170.78	a	V45	258.51	a	V66	56.18	abc
V47	170.59	a	V47	250.41	ab	V61	54.62	abc
V52	166.09	ab	V61	249.74	ab	V54	54.20	abc
V60	165.27	ab	V60	246.35	ab	V47	53.48	abc
V62	164.87	ab	V52	245.54	ab	V50	52.55	abcd
V67	158.76	ab	V67	240.38	ab	V68	51.70	bcd
V69	157.56	ab	V50	236.45	ab	V67	49.25	bcd
V61	155.14	ab	V69	235.02	ab	V69	47.57	bcd
V50	154.17	ab	V62	233.93	ab	V64	47.39	bcd
V64	149.37	ab	V64	230.61	ab	V53	45.38	cd
V53	148.00	ab	V53	226.67	ab	V52	45.01	cd
V71	127.18	b	V71	211.38	b	V71	40.20	d
	N_{area}			**SPAD**			**LMA**	
V52	3.7	a	V53	59.9	a	V53	83.4	a
V69	3.4	ab	V69	57.4	ab	V52	82.7	ab
V53	3.4	abc	V52	57.2	abc	V47	81.0	abc
V54	3.4	abcd	V47	55.9	abcd	V68	75.2	bcd
V67	3.4	abcd	V50	54.9	bcd	V66	74.2	bcd
V68	3.4	abcd	V61	54.5	bcd	V50	73.9	bcd
V64	3.2	abcde	V64	54.4	bcd	V54	73.7	bcd
V47	3.2	abcde	V54	54.1	bcde	V65	73.2	cd
V71	3.2	abcde	V66	53.8	bcde	V67	73.1	cd
V65	3.2	abcde	V60	53.7	bcde	V64	72.3	de
V66	3.2	abcde	V57	53.6	bcde	V59	70.4	def
V57	3.1	abcde	V65	53.4	bcde	V45	70.0	defg
V59	3.1	abcde	V62	52.7	cde	V69	69.6	defg
V45	3.0	bcde	V67	51.7	de	V71	68.8	defg
V62	3.0	bcde	V59	51.5	de	V57	67.2	defg
V50	3.0	bcde	V45	51.5	de	V62	64.4	efg
V60	2.9	cde	V68	51.4	de	V60	63.2	fg
V61	2.9	de	V71	49.6	ef	V63	62.8	fg
V63	2.7	e	V63	48.6	ef	V55	62.7	fg
V55	2.7	e	V55	44.7	f	V61	62.2	g

Tables Chapter 6

A 14 List of wheat genotypes used for Candidates to CIMCOG II (CC), CCS marked with *.

No	Gen	CROSS NAME
1	V77	BABAX/LR42//BABAX/3/ER2000
2	V78	SOKOLL/3/PASTOR//HXL7573/2*BAU
3	V79	PASTOR//HXL7573/2*BAU/3/SOKOLL/WBLL1
4	V80	CHEN/AEGILOPS SQUARROSA (TAUS)//BCN/3/BAV92/4/BERKUT
5	V81	CHRZ//BOW/CROW/3/WBLL1/4/CROC_1/AE.SQUARROSA (213)//PGO
6	V82	SOKOLL//SUNCO/2*PASTOR
7	V83	MTRWA92.161/PRINIA/5/SERI*3//RL6010/4*YR/3/PASTOR/4/BAV92
8	V84	PSN/BOW//MILAN/3/2*BERKUT
9	V85	GK ARON/AG SECO 7846//2180/4/2*MILAN/KAUZ//PRINIA/3/BAV92
10	V86	WBLL1*2/BRAMBLING
11	V87	FRET2*2/BRAMBLING
12	V88	PRL/2*PASTOR/4/CHOIX/STAR/3/HE1/3*CNO79//2*SERI
13	V89	CHEWINK #1
14	V90	CHYAKHURA
15	V91	WHEAR/KUKUNA/3/C80.1/3*BATAVIA//2*WBLL1
16	V92	SAAR/WBLL1
17	V93	TRCH*2/3/C80.1/3*QT4118//3*PASTOR
18	V94	SHA7/VEE#5/5/VEE#8//JUP/BJY/3/F3.71/TRM/4/2*WEAVER/6/SKAUZ/PARUS//PARUS
19	V95	QUAIU
20	V96	CNDO/R143//ENTE/MEXI_2/3/AEGILOPS SQUARROSA (TAUS)/4/WEAVER/5/PICUS/6/TROST/7/TACUPETO F2001
21	V97	PBW343*2/KUKUNA*2//YANAC
22	V98	MUNAL #1
23	V99	WHEAR//INQALAB 91*2/TUKURU
24	V100	CNDO/R143//ENTE/MEXI_2/3/AEGILOPS SQUARROSA (TAUS)/4/WEAVER/5/2*PASTOR/6/SKAUZ/PARUS//PARUS
25	V101	PICAFLOR #2
26	V102	NELOKI
27	V103	ATTILA*2/PBW65/6/PVN//CAR422/ANA/5/BOW/CROW//BUC/PVN/3/YR/4/TRAP#1/7/ATTILA/2*PASTOR
28	V104	WHEAR//2*PRL/2*PASTOR
29	V105	WAXWING/6/PVN//CAR422/ANA/5/BOW/CROW//BUC/PVN/3/YR/4/TRAP#1
30	V106	WBLL1/KUKUNA//TACUPETO F2001/3/BAJ #1
31	V107	FRET2*2/4/SNI/TRAP#1/3/KAUZ*2/TRAP//KAUZ/5/PFAU/WEAVER//BRAMBLING
32	V108	KACHU/SAUAL
33	V109	ATTILA/3*BCN//BAV92/3/TILHI/5/BAV92/3/PRL/SARA//TSI/VEE#5/4/CROC_1/AE.SQUARROSA (224)//2*OPATA
34	V110	FRET2*2/4/SNI/TRAP#1/3/KAUZ*2/TRAP//KAUZ/5/PARUS/6/FRET2*2/KUKUNA
35	V111	TRCH/SRTU//KACHU
36	V112	SERI.1B//KAUZ/HEVO/3/AMAD*2/4/KIRITATI
37	V113	PBW343*2/KUKUNA//SRTU/3/PBW343*2/KHVAKI
38	V114	BABAX/LR42//BABAX/3/BABAX/LR42//BABAX/4/T.DICOCCON PI94625/AE.SQUARROSA (372)//3*PASTOR/5/T.DICOCCON PI94625/AE.SQUARROSA (372)//3*PASTOR
39	V115	FRET2*2/4/SNI/TRAP#1/3/KAUZ*2/TRAP//KAUZ/5/ONIX

No	Gen	CROSS NAME
40	V116	ONIX/4/MILAN/KAUZ//PRINIA/3/BAV92
41	V117	ACHTAR/4/MILAN/KAUZ//PRINIA/3/BAV92
42	V118	MILAN/KAUZ//PRINIA/3/BAV92/4/ATTILA/BAV92//PASTOR/5/CNO79//PF70354/MUS/3/PASTOR/4/BAV92
43	*V119	GK ARON/AG SECO 7846//2180/4/2*MILAN/KAUZ//PRINIA/3/BAV92
44	V120	SOKOLL/ROLF07
45	V121	BOW/VEE/5/ND/VG9144//KAL/BB/3/YACO/4/CHIL/6/CASKOR/3/CROC_1/AE.SQUARROSA (224)//OPATA/7/PASTOR//MILAN/KAUZ/3/BAV92
46	V122	ATTILA*2/PBW65*2//KACHU
47	V123	KACHU #1/KIRITATI//KACHU
48	V124	SAUAL/YANAC//SAUAL
49	V125	ATTILA*2/PBW65*2//MURGA
50	*V126	ATTILA*2/PBW65*2/4/BOW/NKT//CBRD/3/CBRD
51	V127	PAURAQ/SUP152
52	V128	WBLL1*2/BRAMBLING/5/BABAX/LR42//BABAX*2/4/SNI/TRAP#1/3/KAUZ*2/TRAP//KAUZ
53	V129	ALTAR 84/AE.SQUARROSA (221)//3*BORL95/3/URES/JUN//KAUZ/4/WBLL1/5/MUTUS
54	V130	TRCH/HUIRIVIS #1
55	V131	SUP152/HUIRIVIS #1
56	V132	WAXBILL
57	*V133	KFA/2*KACHU
58	V134	UP2338*2/4/SNI/TRAP#1/3/KAUZ*2/TRAP//KAUZ/5/MILAN/KAUZ//CHIL/CHUM18/6/UP2338*2/4/SNI/TRAP#1/3/KAUZ*2/TRAP//KAUZ
59	V135	NAC/TH.AC//3*PVN/3/MIRLO/BUC/4/2*PASTOR/5/KACHU/6/KACHU
60	*V136	FRANCOLIN #1/WBLL1
61	V137	TECUE #1/2*WAXWING
62	V138	KANZ*4/KS85-8-4//KUKUNA/3/KANZ
63	*V139	REEDLING #1
64	V140	PRL/2*PASTOR*2//FH6-1-7
65	V141	ATTILA*2/PBW65*2//MURGA
66	V142	ROLF07*2/5/FCT/3/GOV/AZ//MUS/4/DOVE/BUC
67	V143	BAJ #1/3/KIRITATI//ATTILA*2/PASTOR
68	V144	ALTAR 84/AE.SQUARROSA (221)//3*BORL95/3/URES/JUN//KAUZ/4/WBLL1/5/KACHU/6/KIRITATI//PBW65/2*SERI.1B
69	V145	BECARD/QUAIU #1
70	V146	BLOUK #1
71	V147	LOCAL CHECK
72	V148	BCN/RIALTO//ROLF07
73	V149	BCN/RIALTO//ROLF07
74	V150	BCN/WBLL1//ROLF07
75	V151	BCN/WBLL1//ROLF07
76	V152	BECARD(CGSS01B00063T-099Y-099M-099M-099Y-099M-45Y-0B)
77	V153	C80.1/3*QT4118//KAUZ/RAYON/3/2*TRCH/7/CMH79A.955/4/AGA/3/4*SN64/CNO67//INIA66/5/NAC/6/RIALTO
78	V154	C80.1/3*QT4118//KAUZ/RAYON/3/2*TRCH/7/CMH79A.955/4/AGA/3/4*SN64/CNO67//INIA66/5/NAC/6/RIALTO/8/WBLL1*2/KURUKU
79	*V155	C80.1/3*QT4118//KAUZ/RAYON/3/2*TRCH/7/CMH79A.955/4/AGA/3/4*SN64/CNO67//INIA66/5/NAC/6/RIALTO/8/WBLL1*2/KURUKU
80	V156	C80.1/3*QT4118//KAUZ/RAYON/3/2*TRCH/7/CMH79A.955/4/AGA/3/4*SN64/CNO67//INIA66/5/NAC/6/RIALTO/8/WBLL1*2/KURUKU
81	V157	C80.1/3*QT4118//KAUZ/RAYON/3/2*TRCH/7/CMH79A.955/4/AGA/3/4*SN64/CNO67//INIA66/5/NAC/6/RIALTO/8/WBLL1*2/KURUKU

No	Gen	CROSS NAME
82	V158	C80.1/3*QT4118//KAUZ/RAYON/3/2*TRCH/7/CMH79A.955/4/AGA/3/4*SN64/CNO67//INIA66/5/NAC/6/RIALTO/8/WBLL1*2/KURUKU
83	V159	C80.1/3*QT4118//KAUZ/RAYON/3/2*TRCH/7/CMH79A.955/4/AGA/3/4*SN64/CNO67//INIA66/5/NAC/6/RIALTO/8/WBLL1*2/KURUKU
84	V160	C80.1/3*QT4118//KAUZ/RAYON/3/2*TRCH/7/CMH79A.955/4/AGA/3/4*SN64/CNO67//INIA66/5/NAC/6/RIALTO/8/WBLL1*2/KURUKU
85	V161	CMH79A.955/4/AGA/3/4*SN64/CNO67//INIA66/5/NAC/6/RIALTO/7/BCN/WBLL1/8/C80.1/3*QT4118//KAUZ/RAYON/3/2*TRCH
86	V162	CMH79A.955/4/AGA/3/4*SN64/CNO67//INIA66/5/NAC/6/RIALTO/7/BCN/WBLL1/8/C80.1/3*QT4118//KAUZ/RAYON/3/2*TRCH
87	V163	CMH79A.955/4/AGA/3/4*SN64/CNO67//INIA66/5/NAC/6/RIALTO/7/ROLF07
88	V164	CMH79A.955/4/AGA/3/4*SN64/CNO67//INIA66/5/NAC/6/RIALTO/7/ROLF07
89	V165	CMH79A.955/4/AGA/3/4*SN64/CNO67//INIA66/5/NAC/6/RIALTO/7/ROLF07
90	V166	NL623/W-78//ROLF07
91	V167	QUAIU
92	V168	SERI/BAV92/7/CMH79A.955/4/AGA/3/4*SN64/CNO67//INIA66/5/NAC/6/RIALTO/8/WBLL1*2/KURUKU
93	V169	SERI/BAV92/7/CMH79A.955/4/AGA/3/4*SN64/CNO67//INIA66/5/NAC/6/RIALTO/8/WBLL1*2/KURUKU
94	V170	SERI/BAV92/7/CMH79A.955/4/AGA/3/4*SN64/CNO67//INIA66/5/NAC/6/RIALTO/8/WBLL1*2/KURUKU
95	V171	WBLL1*2/KUKUNA
96	V172	LOCAL CHECK
97	V173	WBLL1//YANGLING SHAANXI/ESDA/3/ROLF07
98	V174	WBLL1//YANGLING SHAANXI/ESDA/3/ROLF07
99	V175	BCN/WBLL1
100	V176	WHEAR/KUKUNA/3/C80.1/3*BATAVIA//2*WBLL1
101	V177	SOKOLL
102	V178	VARIS
103	V179	THELIN#2//ATTILA*2/PASTOR/3/PRL/2*PASTOR
104	V180	THELIN/2*WBLL1
105	V181	WBLL1*2/BRAMBLING
106	V182	PLATA_6/GREEN_17//SNITAN/4/YAZI_1/AKAKI_4//SOMAT_3/3/AUK/GUIL//GREEN
107	V183	YAV79/4/ARMENT//SRN_3/NIGRIS_4/3/CANELO_9.1/5/MINIMUS/COMB DUCK_2//CHAM_3/3/GREEN_19
108	V184	BABAX/KS93U76//BABAX/3/ATTILA/3*BCN/'TOBA97/4/WBLL1*2/KURUKU
109	*V185	SILK_3/DIPPER_6/3/ACO89/DUKEM_4//5*ACO89/4/PLATA_7/ILBOR_1//SOMAT_3
110	V186	TADIZ/9/USDA595/3/D67.3/RABI//CRA/4/ALO/5/HUI/YAV_1/6/ARDENTE/7/HUI/YAV79/8/POD_9
111	V187	CNDO/VEE//CELTA/3/PATA_2/6/ARAM_7//CREX/ALLA/5/ENTE/MEXI_2//HUI/4/YAV_1/3/LD357E/2*TC60//JO69/9/USDA595/3/D67.3/RABI//CRA/4/ALO/5/HUI/YAV_1/6/ARDENTE/7/HUI/YAV79/8/POD_9
112	V188	GEMA C2004*2/ACO89
113	V189	SNITAN*2/RBC
114	V190	TACUPETO F2001/BRAMBLING*2//KACHU
115	V191	KACHU #1/3/C80.1/3*BATAVIA//2*WBLL1/4/KACHU
116	V192	SAUAL/WHEAR//SAUAL
117	V193	KACHU #1/4/CROC_1/AE.SQUARROSA (205)//KAUZ/3/SASIA/5/KACHU
118	V194	TACUPETO F2001/SAUAL//BLOUK #1
119	V195	TACUPETO F2001/6/CNDO/R143//ENTE/MEXI_2/3/AEGILOPS SQUARROSA (TAUS)/4/WEAVER/5/PASTOR/7/ROLF07
120	V196	KACHU/3/PRINIA/PASTOR//HUITES
121	V197	WBLL1*2/4/SNI/TRAP#1/3/KAUZ*2/TRAP//KAUZ/5/KACHU #1
122	V198	TRCH/5/REH/HARE//2*BCN/3/CROC_1/AE.SQUARROSA (213)//PGO/4/HUITES

No	Gen	CROSS NAME
123	*V199	ALD/COC//URES/5/VEE/LIRA//BOW/3/BCN/4/KAUZ/6/SAUAL
124	V200	ALD/CEP75630//CEP75234/PT7219/3/BUC/BJY/4/CBRD/5/TNMU/PF85487/6/PBW343*2/KUKUNA/7/CNO79//PF70354/MUS/3/PASTOR/4/BAV92
125	V201	ATTILA*2//CHIL/BUC*2/3/KUKUNA
126	V202	PARSI
127	V203	SIVAND
128	V204	PISHTAZ
129	V205	M-88-3
130	V206	M-88-5
131	V207	M-88-6
132	V208	M-88-13
133	V209	M-89-6
134	V210	S-78-11
135	V211	S-89-8
136	V212	S-89-12
137	V213	S-89-14
138	V214	S-87-7
139	V215	S-87-5
140	V216	S-87-6
141	V217	ATTILA//ARVAND 1/GLEN
142	V218	N-85-5
143	V219	MILAN//KA/BEZ1/3/TAJAN
144	V220	N-88-5
145	V221	N-88-20
146	*V222	N-89-6
147	V223	N-89-4
148	V224	VL 804
149	V225	HS 507
150	*V226	VL 892
151	V227	HS 490
152	V228	VL 829
153	V229	HPW 251
154	V230	HS 375
155	V231	UP 2338
156	V232	WH 542
157	V233	HD2687
158	V234	PBW343
159	V235	DBW 17
160	V236	PBW 502
161	V237	PBW 550
162	V238	HD 2967
163	V239	DPW 621-50
164	V240	PDW 291
165	V241	PDW 314
166	*V242	WHD 943
167	V243	PBW-373

No	Gen	CROSS NAME
168	*V244	RAJ3765
169	V245	UP2425
170	V246	DBW 16
171	V247	WH 1021
172	V248	PBW 590
173	V249	WH 1080
174	V250	K 9107
175	V251	HUW468
176	V252	HD2733
177	V253	CBW 38
178	V254	K 0307
179	V255	DBW 39
180	V256	HUW 234
181	V257	NW 2036
182	V258	HW2045
183	V259	DBW 14
184	V260	HD 2985
185	V261	HD 2888
186	V262	HI 1544
187	V263	GW 322
188	V264	GW 366
189	V265	LOK 1
190	V266	MPO 1215
191	V267	GW 173
192	V268	HD 2864
193	V269	HD 2932
194	V270	MP 4010
195	V271	HI 1500
196	V272	HI 1531
197	V273	HW2004
198	V274	HD 4672
199	V275	RAJ 4037
200	V276	MACS 6222
201	V277	NIDW 295
202	V278	RAJ 4083
203	V279	NIAW34
204	V280	HD 2781
205	V281	AKDW 2997-16
206	V282	HD 2987
207	V283	COW (W) 1
208	V284	RAJ 3077
209	V285	KRL 210
210	V286	KRL 19
211	V287	DDK 1009
212	V288	DDK 1029
213	V289	MACS 2971

No	Gen	CROSS NAME
214	V290	MACS 2496
215	V291	MACS 2846
216	V292	ROELFS F2007
217	V72	BECARD(CGSS01B00063T-099Y-099M-099M-099Y-099M-9Y-0B)
218	V48	BECARD/KACHU
219	V45	BABAX/LR42//BABAX/3/VORB
220	V74	WBLL1*2/4/BABAX/LR42//BABAX/3/BABAX/LR42//BABAX
221	V65	TACUPETO F2001/BRAMBLING*2//KACHU
222	V53	CIRNO C 2008
223	V68	UP2338*2/4/SNI/TRAP#1/3/KAUZ*2/TRAP//KAUZ/5/MILAN/KAUZ//CHIL/CHUM18/6/UP2338*2/4/SNI/TRAP#1/3/KAUZ*2/TRAP//KAUZ

A 15 List of wheat genotypes used for wheat landraces (L). LS marked with *.

No	Gen	CROSS NAME	No	Gen	CROSS NAME
1	V293	MEX94.10.47	46	V338	HGO94.11.2.26
2	V294	PBL94.14.66	47	V339	HGO94.11.2.43
3	*V295	HGO94.5.34	48	V340	HGO94.12.1.102
4	*V296	HGO94.3.13	49	V341	MEX94.1.6
5	*V297	MEX94.30.11	50	V342	MEX94.1.9
6	V298	MEX94.28.17	51	V343	HGO94.12.2.5
7	V299	MEX94.27.2.47	52	V344	HGO94.12.2.7
8	V300	MEX94.27.1.5	53	*V345	MEX94.1.28
9	V301	PUB94.16.87	54	V346	MEX94.2.32
10	V302	PUB94.16.49	55	V347	MEX94.7.49
11	V303	PUB94.15.1.18	56	*V348	MEX94.10.50
12	V304	MEX94.25.113	57	V349	MEX94.7.71
13	V305	CHIH95.3.52	58	V350	MEX94.9.11
14	V306	CHIH95.5.29	59	V351	MEX94.11.53
15	V307	MEX94.19.109	60	V352	MEX94.12.1.131
16	V308	MICH89.4.18	61	V353	MEX94.12.2.40
17	V309	QRO95.3.28	62	V354	MEX94.12.2.52
18	V310	QRO95.4.55	63	V355	MEX94.13.1.70
19	V311	MEX95.9.27	64	V356	MEX94.13.1.134
20	V312	MEX95.9.49	65	V357	MEX94.15.36
21	V313	MEX95.9.95	66	V358	MEX94.19.47
22	V314	MICH95.3.1.12	67	V359	MEX94.18.42
23	V315	MICH95.5.3	68	V360	MEX94.20.1.84
24	V316	QRO95.1.59	69	V361	MEX94.21.16
25	V317	PBL94.12.2.2	70	V362	MEX94.22.18
26	V318	PBL94.12.7	71	V363	MEX94.22.27
27	V319	PBL94.12.12.2	72	V364	MEX94.22.32
28	V320	PBL94.12.15.3	73	V365	MEX94.22.48
29	V321	PBL94.14.23	74	V366	MEX94.22.64
30	V322	QRO94.2.109	75	V367	MEX94.22.93
31	V323	HGO94.1.18	76	V368	MEX94.22.109
32	V324	HGO94.3.67	77	V369	MEX94.23.35
33	V325	GTO94.1.6	78	V370	MEX94.23.39
34	V326	HGO94.4.1	79	V371	MEX94.23.41
35	V327	HGO94.5.75	80	V372	MEX94.23.53
36	V328	HGO94.7.1.4	81	V373	MEX94.23.75
37	V329	HGO94.8.74	82	V374	MEX94.23.92
38	V330	HGO94.8.114	83	*V375	MEX94.24.18
39	V331	HGO94.8.119	84	*V376	MEX94.24.25
40	V332	HGO94.8.123	85	V377	MEX94.25.42
41	V333	HGO94.8.126	86	V378	MEX94.25.50
42	V334	HGO94.9.1.23	87	V379	MEX94.25.70
43	V335	HGO94.9.2.13	88	V380	PUB94.16.37
44	V336	HGO94.11.1.46	89	V381	PUB94.16.53
45	V337	HGO94.11.1.15	90	V382	PUB94.16.82

No	Gen	CROSS NAME	No	Gen	CROSS NAME
91	V383	PUB94.16.119	138	*V430	COAH94.8.21
92	V384	PUB94.16.132	139	V431	MICH89.1.4
93	*V385	PUB94.16.201	140	V432	MICH89.1.7
94	V386	MEX94.26.138	141	V433	MEX92.1.1.64
95	*V387	MEX94.27.2.54	142	V434	CHIH96.4
96	*V388	MEX94.29.60	143	V435	CHIH96.4
97	V389	GTO95.1.29	144	V436	CHIH96.4
98	V390	GTO95.1.38	145	V437	CHIH96.4
99	V391	GTO95.1.8	146	V438	CHIH96.4
100	V392	MICH95.6.40	147	V439	CHIH96.4
101	V393	CHIH95.1.18	148	V440	CHIH96.4
102	*V394	CHIH95.3.9	149	V441	CHIH96.4
103	V395	CHIH95.4.11	150	V442	CHIH96.7
104	V396	CHIH95.5.24	151	V443	CHIH96.4
105	V397	CHIH95.4.28	152	V444	CHIH96.4
106	V398	CHIH95.9.31	153	*V445	CHIH96.7
107	V399	CHIH95.9.66	154	V446	CHIH96.7
108	V400	CHIH95.10.42	155	V447	CHIH96.7
109	V401	CHIH95.10.82	156	V448	CHIH96.7
110	V402	TXL92.1.1.3	157	V449	CHIH96.7
111	V403	TXL92.6.1.8	158	*V450	CHIH96.7
112	V404	MEX92.1.1.12	159	V451	CHIH96.7
113	V405	OAX93.6.1	160	V452	OAX96.1
114	V406	OAX93.6.35	161	V453	IWA 8600940
115	V407	OAX93.6.74	162	V454	IWA 8614151
116	V408	TOL93.2.4	163	V455	IWA 8607291
117	V409	OAX93.17.7	164	*V456	IWA 8607721
118	V410	OAX93.16.19	165	V457	IWA8608280
119	V411	OAX93.16.23	166	V458	IWA 8608839
120	V412	OAX93.17.4	167	*V459	IWA8608858
121	V413	OAX93.21.22	168	V460	IWA 8608910
122	V414	OAX93.20.12	169	V461	IWA8613344
123	V415	OAX93.21.55	170	V462	IWA8613464
124	V416	OAX93.22.24	171	V463	IWA8613552
125	V417	OAX93.25.40	172	V464	IWA8603061
126	V418	OAX93.25.12	173	V465	IWA8604640
127	V419	OAX94.22	174	V466	IWA8606995
128	V420	PUE94.5	175	*V467	IWA8608862
129	V421	PUE94.7	176	V468	IWA8609366
130	*V422	PUE94.8	177	*V469	IWA8612352
131	V423	COAH94.1.48	178	V470	IWA8613272
132	V424	COAH94.1.107	179	V471	IWA8613600
133	V425	COAH94.1.181	180	V472	CM-64239
134	*V426	COAH94.2.38	181	V473	CHU MEH 3
135	V427	COAH94.6.92	182	*V474	HONG HUA MAI
136	V428	COAH94.7.31	183	V475	LAHN

No	Gen	CROSS NAME	No	Gen	CROSS NAME
137	V429	COAH94.6.96	184	V476	W38
185	V477	HGO94.9.1.37	230	V520	LANDRACE BV12 236
186	V478	GLENLEA	231	V521	LANDRACE BV12 237
187	V479	MONDEGO	232	V522	LANDRACE BV12 238
188	V480	SRMA/TUI//PASTOR	233	*V523	WEEBIL 1
189	V481	HGO94.9.1.10	234	*V177	SOKOLL
190	V482	ROELFS F2007	235	V292	ROELFS
191	V483	CHIH95.5.37			
192	V484	MEX94.19.88			
193	V485	CHIH95.10.61			
194	V486	CHIH95.10.67			
195	V487	QRO95.1.80			
196	V488	LARGO DURO_CWI53571			
197	V489	CItr 9107			
198	V490	COAH94.2.50			
199	V491	COAH94.5.34			
200	V492	COAH94.6.10			
201	V493	MEX94.12.2.64			
202	V494	LANDRACE BV12 210			
203	V495	MEX94.25.32			
204	V496	LANDRACE BV12 212			
205	V497	LANDRACE BV12 213			
206	V498	LANDRACE BV12 214			
207	V499	LANDRACE BV12 215			
208	V500	LANDRACE BV12 216			
209	V501	LANDRACE BV12 217			
210	V502	LANDRACE BV12 218			
211	V503	LANDRACE BV12 219			
212	V504	LANDRACE BV12 220			
213	V505	LANDRACE BV12 221			
214	V506	LANDRACE BV12 222			
215	V507	LANDRACE BV12 223			
216	V508	LANDRACE BV12 224			
217	V509	LANDRACE BV12 225			
218	V510	LANDRACE BV12 226			
219	V511	LANDRACE BV12 227			
220	V512	LANDRACE BV12 228			
221	V513	LANDRACE BV12 229			
222	V514	LANDRACE BV12 230			
223	V515	LANDRACE BV12 231			
224	V516	LANDRACE BV12 232			
225	V517	LANDRACE BV12 233			
226	V518	LANDRACE BV12 234			
227	V519	LANDRACE BV12 235			
228	V65	TACUPETO F2001/BRAMBLING*2//KACHU			
229	V68	UP2338*2/4/SNI/TRAP#1/3/KAUZ*2/TRAP//KAUZ/5/MILAN /KAUZ//CHIL/CHUM18/6/UP2338*2/4/SNI/TRAP#1/3/KAUZ*2/TRAP//KAUZ			